1-1-2011

Synthesis of peptide-ligand conjugates and their applications

Nitinkumar Dilipkumar Jabre
Wayne State University,

SYNTHESIS OF PEPTIDE-LIGAND CONJUGATES AND THEIR APPLICATIONS

by

NITINKUMAR DILIPKUMAR JABRE

DISSERTATION

Submitted to the Graduate School

of Wayne State University,

Detroit, Michigan

in partial fulfillment of the requirements

for the degree of

DOCTOR OF PHILOSOPHY

2011

MAJOR: CHEMISTRY (Organic)

Approved by:

_____

Advisor Date

_____

_____

_____

DEDICATION

"Selfless giving is love in action." I dedicate this dissertation to those loved ones who made many scarifies in making me who I am today, my parents Alka and Dilipkumar Jabre. They have nurtured the value of education since my childhood and despite all the challenges they have supported me financially as well as mentally. Dear Mom and Dad, I could achieve this only because of your blessings, training and the freedom you gave me to make my own decisions. I bow my head to you because thank you is just not enough for all that you have done for me.

ACKNOWLEDGEMENTS

First I would like to thank God, who gave me the strength and courage to achieve my goals. Next I would like to thank my parents, who are next to God for me and supported me in all my decisions. I extend my thanks to my sister, Priti and brother, Chirag for their love and support. I would also like to thank my wife Apeksha for her love and motivation, who stood by my side during all those tough days. My friends have contributed significantly in my achievements. I take this opportunity to thank them, especially my best friend Kapil Karki whose help and advice have made significant impact in my scholastic as well as personal accomplishments.

I would like to thank all my friends and colleagues at Wayne State University, particularly those from the Kodanko group. Dr. Anil Ekkati, a post-doctoral fellow in the Kodanko group, helped me with learning basic research skills during my initial months in the lab. I would like to thank two of my labmates, Dr. Ashley Campanali and Dr. Ahmed Abouelatta for their help and sharing light moments out side the lab. I would also like to thank Tomasz Respondek and Selma Ulku for excellent cooperation during our divergent strategy project that earned us the JOC paper. I would also like to thank Alyssa Yousif and Nadiya Pavlov for their significant contributions during undergraduate research projects. In addition, I also thank rest of the former and present coworkers of the Kodanko group for their help and support.

I would like to take this opportunity to thank all my professors at Wayne State University for the excellent training that helped become a good chemist. I would also like to thank my committee members, Dr. Brock, Dr. Guo and Dr. Firestine for their helpful suggestions, time and help. I express my thanks Dr. Hryhorczuk, Dr. Shay, Dr. Ksebati and

other CIF members as well as all other non-teaching staff members of the Wayne State University for their help and support.

Last but not least, I would like to express my sincere gratitude to my advisor Dr. Jeremy Kodanko for all the efforts he has put in training me. He has been inspirational and motivated to the research as well as in training his students. Apart from the traditional training, I will always remember a lesson of "*never to give up*" that I learnt as his student. His training was not limited in making us good researchers but he trained us to become a good mentor. Thank you very much Jeremy for choosing me as your graduate student and turning me from an ordinary student to an independent researcher. You are an awesome mentor and I will always remember the lessons learnt from you as well as cherish the time I spent as your student.

I acknowledge the philosophy of my life, which is the key behind my success and keeps me motivated. *"One has the power to act only, not to influence the results. Therefore one must act without the anticipation of the result, without succumbing to inaction. — Bhagavad Gita"*

TABLE OF CONTENTS

LIST OF TABLES

LIST OF FIGURES

LIST OF SCHEMES

Chapter 1: Introduction

Metal complex-peptide conjugates have been extensively explored in bioorganic chemistry, catalysis and *de novo* peptide and protein design. Metal complex-peptide conjugates are often used as radiopharmaceuticals[1,2], imaging agents[3-5], DNA/protein inactivating agents[6-10] as well as anticancer and antibacterial agents.[11] In such examples peptide motifs often serve as delivery vectors and carry the metal complexes to biological targets. With the advent of *de novo* designed metallopeptides, applications of metal complex-peptide conjugates have advanced beyond the biomedicine regime. The metal-assisted stabilization of peptide-microstructure is now being used in molecular recognition motifs, catalysis, light harvesting systems and material science.[12,13]

Considering the plethora of applications for metal complex-peptide conjugates, methods for their syntheses have been widely investigated. Methods for the synthesis of metal complex-peptide conjugates can be divided into two categories. The first method is called *pre-conjugation*, in which metals are coordinated to ligands prior to their incorporation into peptide chains. In the second method, metals are coordinated to ligands after they have been conjugated to peptide chains, hence this is called the *post-conjugation* method. Among these methods, the post-conjugation method is more frequently used since it allows the incorporation of sensitive/reactive metal complexes into the peptide during the final steps of the synthesis. Indeed several ligands containing *N*-, *O*-, *P*- and *S*-donor atoms have been successfully appended into the peptide chain at various positions. Using these peptide-ligand conjugates, sensitive, reactive or toxic metal complexes such as those used in

radiopharmaceutical, imaging and catalysis applications have been incorporated into peptide chains.

Despite all of the applications of peptide-ligand conjugates, methods for incorporating polydentate nitrogen-rich ligands into peptides are limited. In particular, divergent methods, where libraries of these chelators are built on a peptide scaffold were not known. Given the utility of such ligands in biology and bioinorganic chemistry, this was an area of research that needed to be explored. For example, high valent iron-oxo complexes, also called ferryl complexes, can be built from such ligands and have been thoroughly investigated as oxidants and enzyme models.[14,15] The Kodanko group has recently demonstrated the application of non-heme ligands and their ferryl complexes in cancer cell cytotoxicity[16] and protein inactivation.[17] Considering these results, incorporation of such non-heme ligands into peptides and understanding the chemistry of ferryl-peptide conjugates would be very critical for their applications as site selective anticancer agents. In addition this knowledge would be beneficial for the synthesis of artificial oxygenases. Unfortunately there is no divergent strategy available for the incorporation of non-heme ligands that support ferryl complexes into peptides. Moreover chemistry of ferryl-peptide conjugates is unexplored. This lack of information motivated us to develop a divergent strategy for the synthesis of non-heme ligand-peptide conjugates and explore its applications.

This dissertation will discuss my contribution towards efforts in the Kodanko group to explore the applications of non-heme transition metal complexes in targeting proteins, in metal-chelators mediated cancer therapy and in *de novo* protein design for artificial oxygenases as well as in intracellular localization of metal complexes. The first chapter will provide an overview of the research pertaining to my work in the Kodanko group. The first

section of this chapter will survey the existing strategies for the synthesis of peptide-ligand conjugates and discuss where our strategy fits with respect to other methods in the literature. The second section will include the applications of metal complex-ligand conjugates derived from peptide-ligand conjugates. In the subsequent section the chemistry of ferryls will be discussed in the context of the development of ferryl-peptide conjugates. The chapter will end with the thesis statement where the research goals and their importance will be discussed.

1.1 Synthesis Strategies for Peptide-Ligand Conjugates

In this section the strategies for the synthesis of peptide-ligand conjugates are described. This section has been limited to only post-conjugation labeling methods. Ligands have been incorporated into peptides via *N*- and/or *C*-terminus conjugation, within the backbone or through a side chain. Therefore these synthetic strategies are discussed according to these three major categories (Figure 1.1).

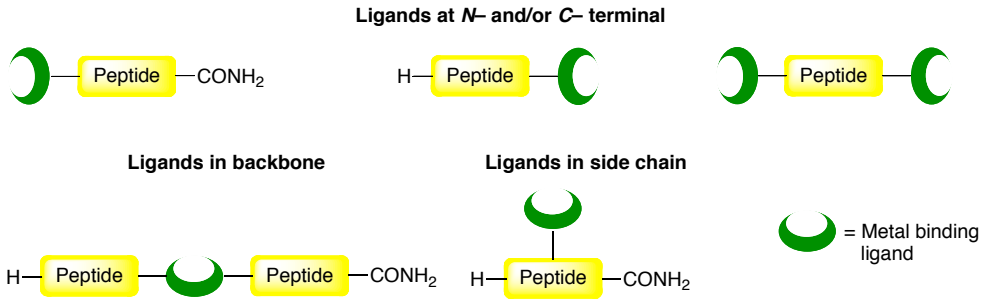

Figure 1.1: Types of peptide-ligand conjugates

1.1.1 Ligands at *N*- and/or *C*-termini of peptides

1.1.1.1 Ligand conjugation at the *N*-terminus

Since peptide synthesis is usually performed from *C*- to *N*-terminus via solid-phase peptide synthesis (SPPS), the most simple, convenient and widely used method to construct peptide-ligand conjugates is to attach ligands at the *N*-terminus.[18-32] For conjugation at the *N*-terminus, it is a common practice to include a linker between the metal-binding moiety and the peptide chain. In several instances, these spacers are found to be very critical to maintain the biological activity of the resulting metal complex-peptide conjugates.[32,33] Typical procedures include the synthesis of a desired peptide sequence followed by the attachment of linkers at the *N*-terminus through an amide bond formation. Upon cleavage of the Fmoc group from the linker, the amine functionality is exposed through which the ligands are attached (Figure 1.2, Mode A).[27,34] Alternatively, such linkers can be coupled first to ligands via solution phase synthesis, which can then be tethered at the *N*-terminus of the peptide chain (Figure 1.2, Mode B).[18-20,25,26] In addition to the traditional amide bond formation, ligands bearing activated esters and isocyanates groups could also be used as a mode of conjugation.[35,36]

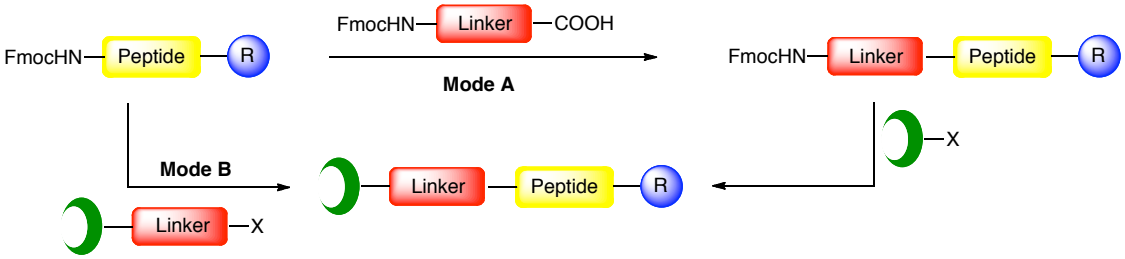

Figure 1.2: Modes of ligand conjugation at the *N*-terminus of peptides

Alternative to the standard coupling methods, click chemistry has also been used to construct peptide-ligand conjugates. For instance, the azide linker has been appended at the *N*-terminus of somatostatin **2** and a click reaction has been used to tether the alkyne-bearing

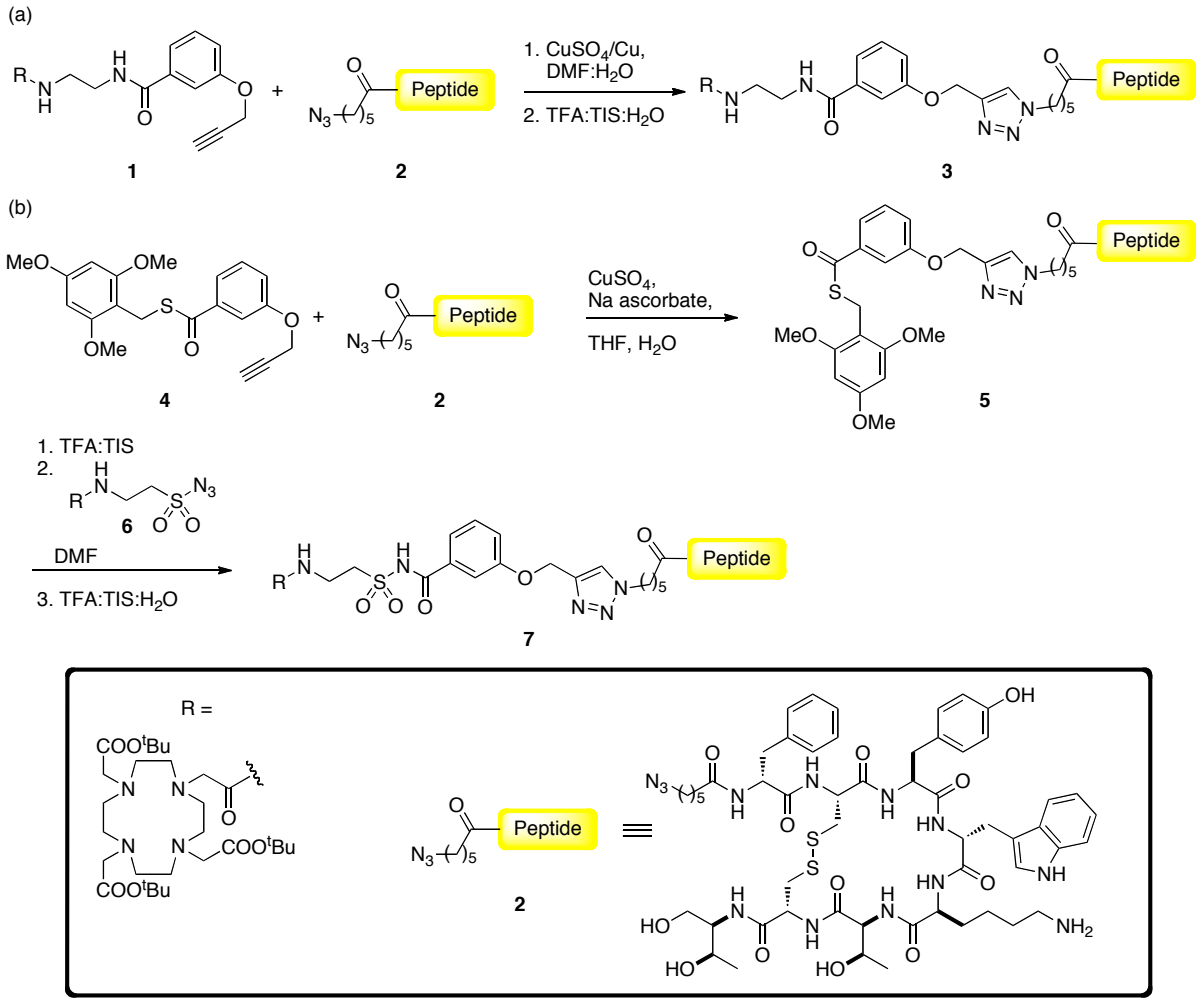

Scheme 1.1: Conjugation of DOTA at the *N*-terminus of octreotide via (a) copper catalyzed click reaction and (b) copper free click reaction

DOTA **1** with peptide **2** (Scheme 1.1a).[34] The use of an unprotected peptide demonstrates the remarkable chemoselectivity of this method. Despite such remarkable functional group compatibility, copper accumulation within the resulting peptide-ligand conjugates **3** limited the use of this strategy. To overcome this drawback, a sulfo-click reaction was developed in which alkyne containing thioester **4** was conjugated to the azido somatostatin analogue **2** via a traditional copper catalyzed click reaction (Scheme 1.1b).[37] Acidolytic cleavage of the

resulting thioester **5** unmasked the corresponding thioacid, which upon reaction with the DOTA bearing sulfonyl azide **6** furnished a sulfonamide linkage that conjugates DOTA with somatostatin. Mechanistic investigation suggested that the reaction proceeds via formation of a thiatriazoline and not via acyl substitution.[38,39] This is important since the later mechanism would not be chemoselective due to the presence of nucleophilic side chains in the unprotected peptide.

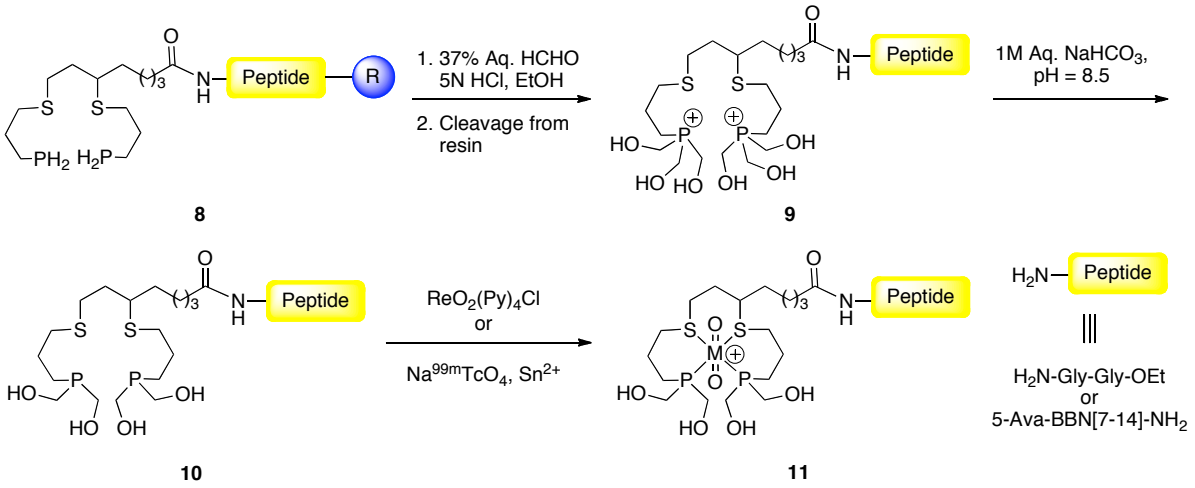

Scheme 1.2: Dithia-bisphosphine (P_2S_2) chelating agents at the *N*-terminus of the bombesin analogue

Although phosphine ligands are extensively used in organometallic complexes, their incorporation into peptides has been challenging due to the oxidation prone nature of alkyl phosphines, particularly in acidolytic cleavage conditions that are used to cleave peptides from resin. Such phosphine-ligand conjugates have been constructed in a stepwise fashion via solution as well as solid phase synthesis as described in Scheme 1.2.[40] Unlike alkyl phosphines, phosphorous hydrides (PH_2) have remarkable stability towards oxidation and other chemical reactions. Hence a straightforward incorporation into peptides was possible.

After conjugation of $(PH_2)_2S_2$-ligand at the *N*-terminus of the BBN analogue, the formylation of the phosphorous hydride moiety of **8** and cleavage of the peptide from resin yielded oxidatively stable phosphonium salt **9**. Treatment of the resulting phosphinium salt with 1M $NaHCO_3$ exposed the reactive bis(hydroxymethyl) phosphine **10** *in situ*, which was eventually transformed into the corresponding metal complexes. Using this method, P_2S_2-ligands were also incorporated at the N_ε-lysine of the LHRH analogue.

The stepwise ligand synthesis method has also been applied to the synthesis of *N*- and *O*-donor ligands. As shown in Scheme 1.3, NOTA-Aoc-BBN[6-14] (Where NOTA = 1,4,7-triazacyclononane-*N*,*N'*,*N''*-triacetic acid) was synthesized on NovaSyn TGR resin.[41] Upon synthesis of the desired peptide sequence **12**, α-bromo acetic acid was coupled at the *N*-terminus to obtain **13**. A two-step *N*-alkylation sequence followed by cleavage from resin gave the NOTA-peptide conjugate **15**. It is important to note that only one peptide was coupled per molecule of 1,4,7-triazacyclononane in the first alkylation (**13** to **14**). The NOTA ligand has also been attached to N_ε-amino of lysine using this strategy (*vide infra*).

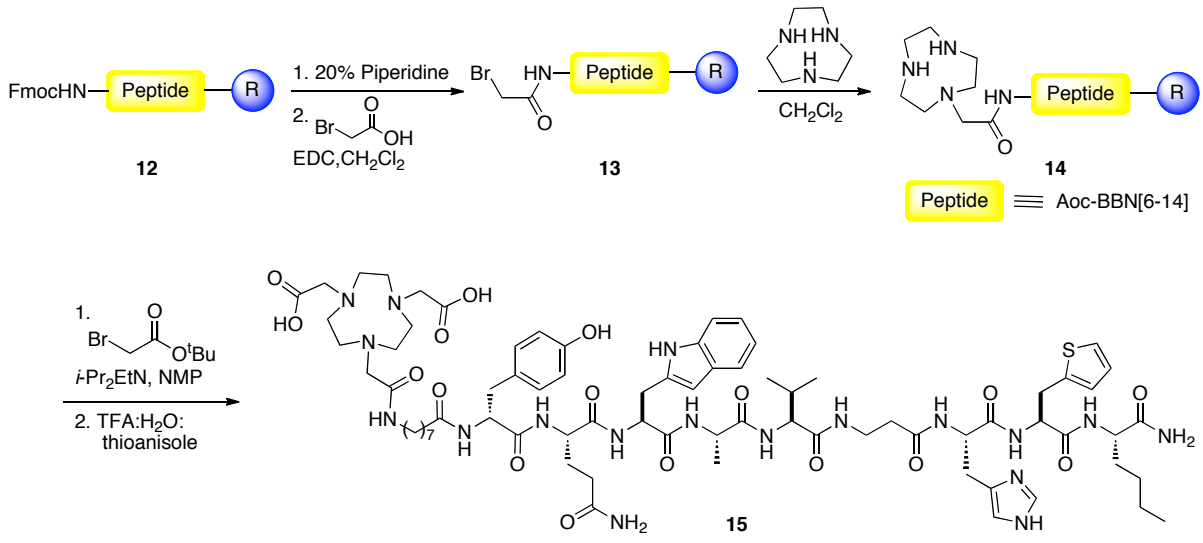

Scheme 1.3: Stepwise synthesis of NOTA on peptide bound resin

1.1.1.2 Ligand conjugation at the *C*-terminus

Ligand conjugation at the *C*-terminus of a peptide is the most challenging since peptides are usually synthesized via SPPS where *C*-terminus is attached to the solid support and a peptide chain is elongated from *C*- to *N*-terminus. An obvious method to conjugate ligands at the *C*-terminus is to attach ligands directly to the resin through a reactive functionality of a ligand (**16**) prior to elongation of the peptide chain (Scheme 1.4).[42] Finally the conjugate is cleaved from resin in a separate step or through *in situ* cleavage followed by complex formation (**18** to **19**). Unlike the example shown in Scheme 1.4, if a ligand has amino acid functionality it could be directly attached to the resin prior to the incorporation of the first amino acid residue in SPPS.[43]

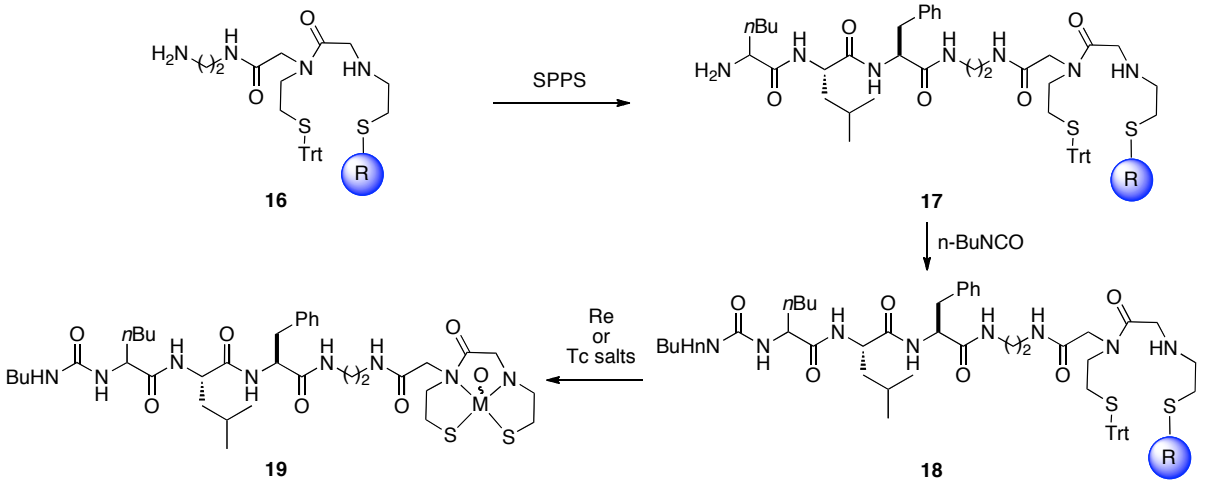

Scheme 1.4: Incorporation of monoamide monoamine (MAMA) ligands at the *C*-terminus of the peptide chain

A creative approach for ligand conjugation at the *C*-terminus involves the use of safety-catch linkers. A representative example is shown in Scheme 1.5 where a peptide **20** was built on the resin **19** containing a sulfonamide linker.[44] Upon completion of the desired

sequence, alkylation of the *N*-acylsulfonamide with iodoacetonitrile generated a highly reactive *N*,*N*-cyanomethyl-acylsulfonamide **21**. Displacement of the activated linker by nucleophilic propargyl amine furnished the peptide-ligand conjugate **22** where propargyl amine was tethered to the *C*-terminus. The alkyne moiety served as a ligand in the formation of hexacarbonyl cobalt complex. In another example, hydrazyl amide linker was used as a safety-catch linker in SPPS (vide infra).

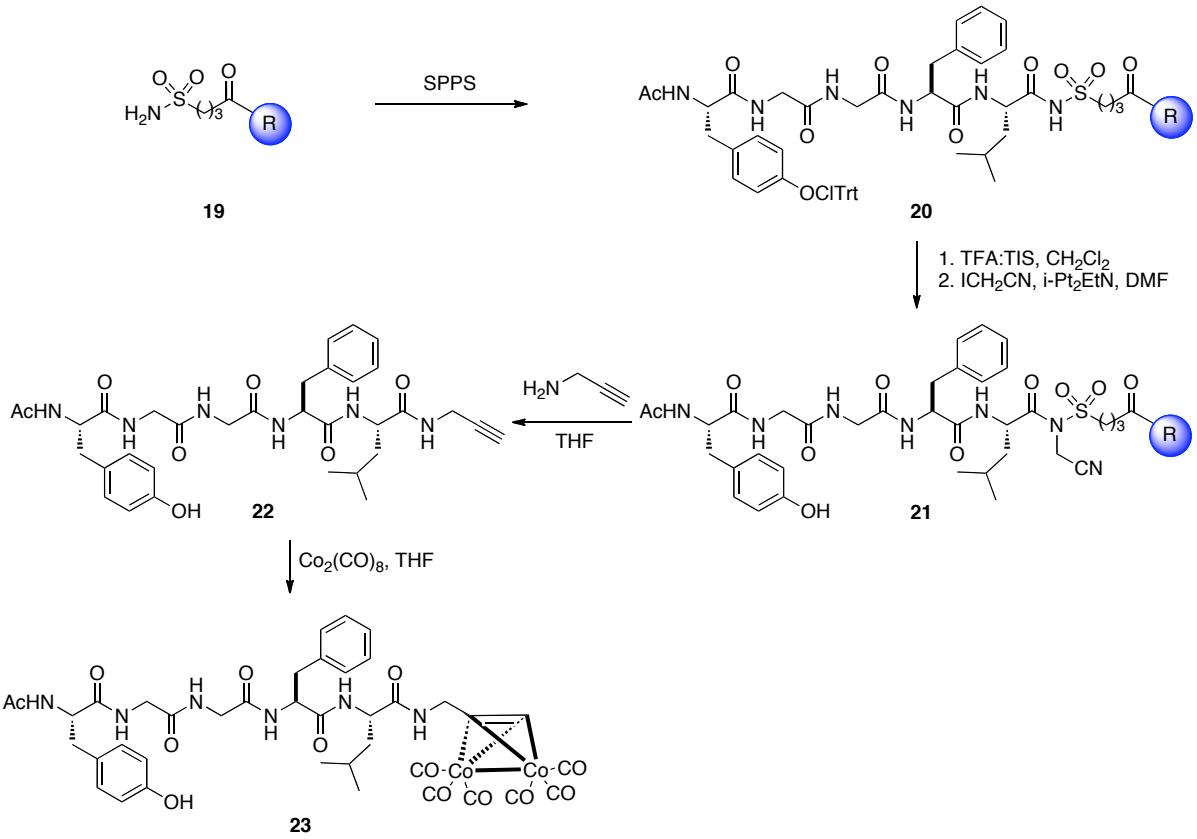

Scheme 1.5: Use of safety catch linker for incorporation of dicobalthexacarbonyl-alkyne at the *C*-terminal of enkephaline

1.1.1.3 Ligand conjugation at both termini

An obvious method to adjoin ligands at both termini involves the ligand conjugation at the *N*-terminus using standard methods, followed by cleave the peptide-ligand conjugate

from resin and attachment of the ligand at the *C*-terminus via solution phase synthesis.[45] As shown in Scheme 1.6, a substitution reaction between ligands carrying the benzyl halide linker and a *C*-terminus acid could be used as a conjugation method (**24** to **25**). Although no side chain protecting groups were present in the example shown here, the use of Sasrin resin is noteworthy because the side chain protecting groups of a peptide are retained when it is cleaved from Sasrin. This is important since the peptide side chains are expected to remain protected during the subsequent solution phase reaction. An apparent drawback of this method is that the final step has to be performed via solution phase synthesis, which is usually associated with insolubility and purification issues. In addition, if side chain protecting groups are present on the final conjugate, then a separate deprotection step is necessary.

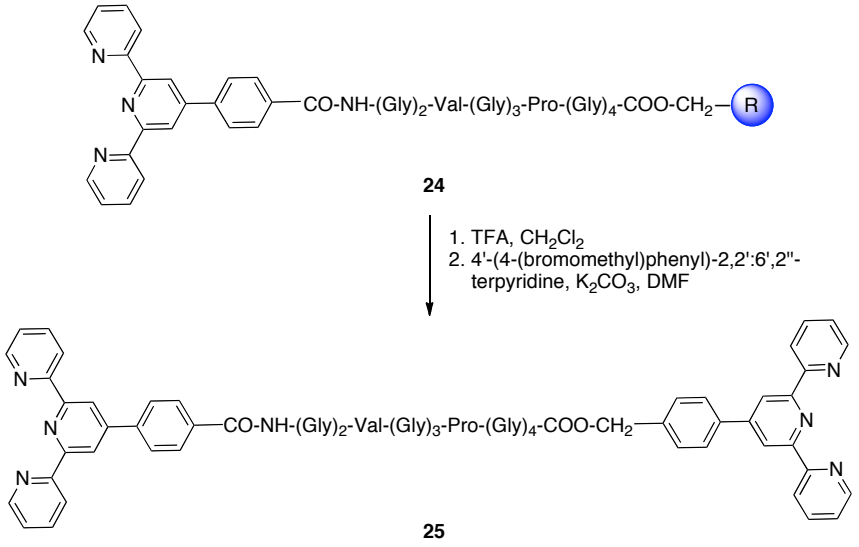

Scheme 1.6: Terpyridine conjugation at both the termini of a peptide for metal-assisted assembly of cyclometallopeptides

As described previously, safety catch linkers are also useful in incorporating ligands at both termini of peptides (Scheme 1.7).[46] A peptide was synthesized via SPPS using a safety catch linker and after ligand conjugation at the *N*-terminus, concomitant copper (II) acetate mediated oxidation of hydrazyl amide linker followed by nucleophilic displacement provided peptide-ligand conjugates in which ligands are present at both termini of the peptide. In the following example an unusual Lewis acid mediated cleavage condition was required to cleave methyl ether protecting groups on the catechol side chains.

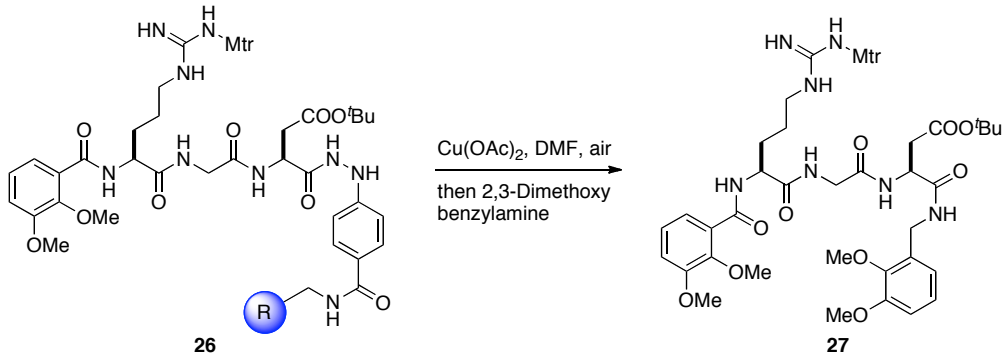

Scheme 1.7: RGD-bridged catechol ligands for metallomacrocycles

Apart from ligand conjugation at both termini, synthetic methods that allow selective incorporation of ligands at either *N*- or *C*-terminus from the same precursor are certainly interesting. In the following example, a threonine building block **28** was synthesized so that the side chain was attached to the acid labile dihydropyran resin, while *N*- and *C*-terminus were protected as Fmoc- and allyl groups, respectively (Scheme 1.8).[47] For conjugation of ligands at the *N*-terminus, DOTA or HYNIC ligands were incorporated into the peptide using traditional *N*-terminus ligand conjugation methods, except that a palladium-catalyzed allyl deprotection was performed prior to the cleavage of peptide from resin (**28** to **29** to **30**). For ligand conjugation at the *C*-terminus, the peptide chain was synthesized using SPPS and a

N_α-Boc protected amino acid was incorporated at the end of the sequence. Palladium-catalyzed conditions facilitated orthogonal cleavage of the allyl group, and the exposed *C*-terminus was coupled with Fmoc-protected ethylenediamine. Fmoc cleavage of the ethylenediamine moiety followed by coupling of the resulting amine with ligands bearing carboxylic acids provided ligand conjugation at the *C*-terminus (**28** to **31** to **32**). In either mode of conjugation, an acidolytic cleavage released the peptide from resin with concomitant deprotection of the side chain protecting groups. Although not discussed in this work, this method could potentially be used to conjugate two structurally different ligands at the *C*- and *N*-terminus of a peptide chain.

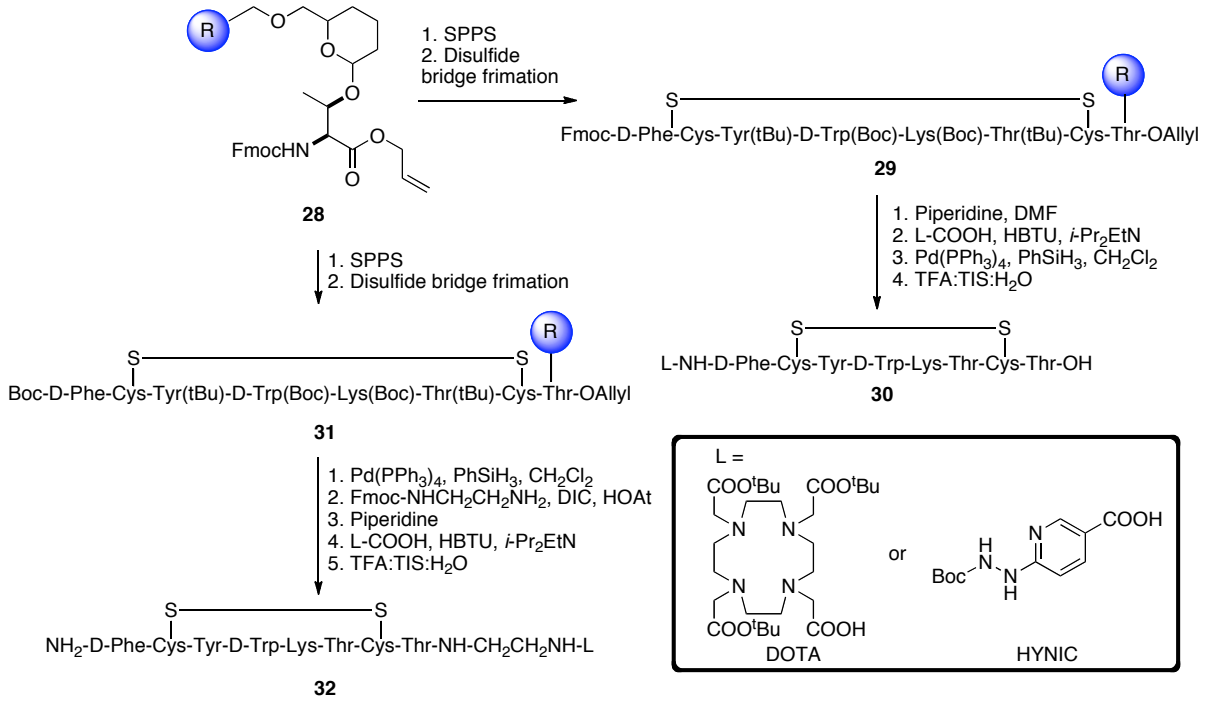

Scheme 1.8: General method for *C*- or *N*-terminal functionalization of Tyr^3-octreotate

1.1.2 Ligand incorporation within the backbone of peptides

The presence of metal-binding sites within the backbone is expected to have a significant influence on the peptide folding. Hence, peptide-ligand conjugates that contain ligands within their backbones have numerous applications in metal-assisted stabilization of peptide-microstructures (Section 1.2.4).[12] To incorporate the ligands within the backbone, ligand building blocks bearing amino acid functionalities were synthesized and used during peptide synthesis as artificial amino acid building blocks. Many of the commonly used ligand building blocks are comprised of 2,2'-bipyridine (Bpy) and some representative examples are shown in Figure 1.3.[48]

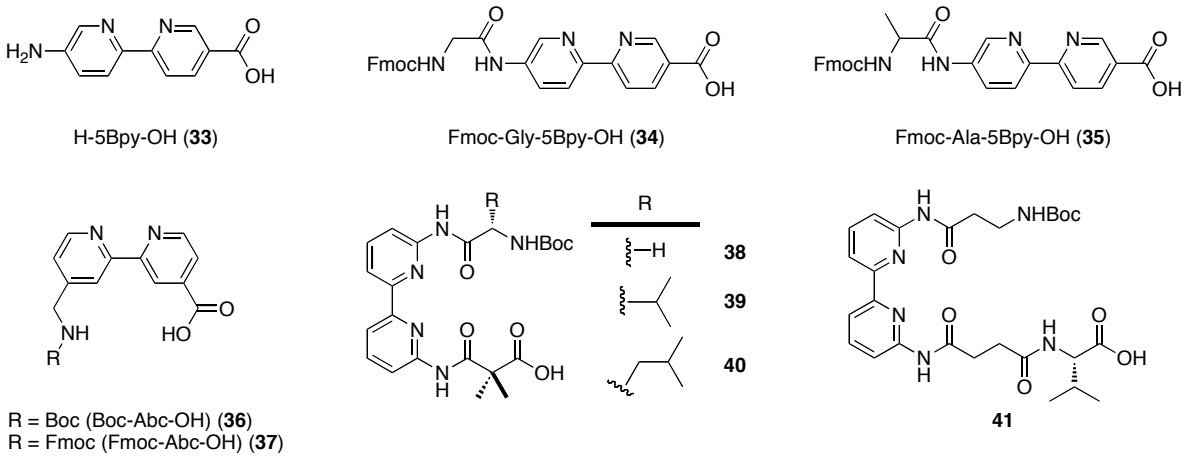

Figure 1.3: Examples of 2,2'-bipyridine derivatives for ligand incorporation into the backbone of peptides

Incorporation of amino groups directly into bipyridine, as in case of H-5Bpy-OH (**33**), is a straightforward modification of Bpy, however poor nucleophilicity of the resulting aromatic amine in Fmoc-protection of **33** restricted its use in SPPS. As a solution to this, pseudodipeptide derivatives **34** and **35** were synthesized via solution phase synthesis and efficiently incorporated into the peptide backbone.[48] Alternatively, a methylene group could be introduced between the amine and the pyridine ring to obtain **36**-**37**.[49] Other derivatives

were synthesized from (2,2'-bipyridine)-6,6'-diamine in such a way that Bpy could be incorporated into the peptide backbone via 6,6'-substitutions (**38-41**).[50] Peptide-ligand conjugates containing **38-41** have been shown to induce β-sheet formation upon metal coordination and hence have found applications in *de novo* β-sheet inducing metallopeptides.

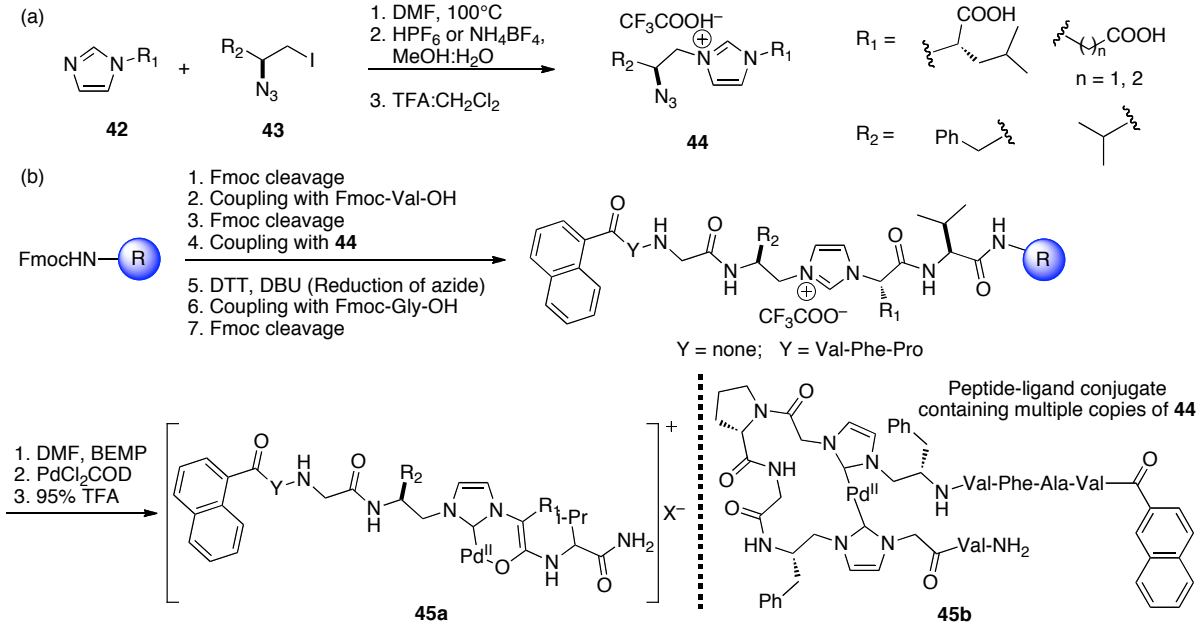

Scheme 1.9: Synthesis of imidazolium building blocks (a) and their utility in synthesis of carbene-peptide conjugates (b)

Carbenes are an important ligand for transition metal complexes, thus their incorporation into peptide chains has been envisioned as a potential method for synthesis of chiral metal complexes. For synthesis of carbene-peptide conjugates, imidazolium ion building blocks **44**, containing a carboxylic acid moiety and a dormant amine protected as an azide group, were synthesized by S_N2 displacement of iodides **43** with imidazoles **42** (Scheme 1.9a).[51] Building blocks **44** were coupled to the N_α-amino group of a growing peptide chain. Then, additional amino acids were incorporated after unmasking the latent

amino group via a DTT/DBU mediated azide reduction (Scheme 1.9b). Finally these conjugates were cleaved from resin and *N*-heterocyclic carbenes (NHC) were generated *in situ* by reaction with 2-(tert-butylimino)-2-(diethylamino)-1,3-dimethylperhydro-1,3,2-diazaphosphorine (BEMP), which were eventually trapped with $[Pd(Cl)_2(COD)]$. When peptide-ligand conjugates containing only one unit of **44** were reacted with BEMP, a *β*-enolate is generated that was found to coordinate the palladium center. Interestingly, when two units of **44** were incorporated into a peptide chain, their palladium complexes did not involve a *β*-enolate coordination.

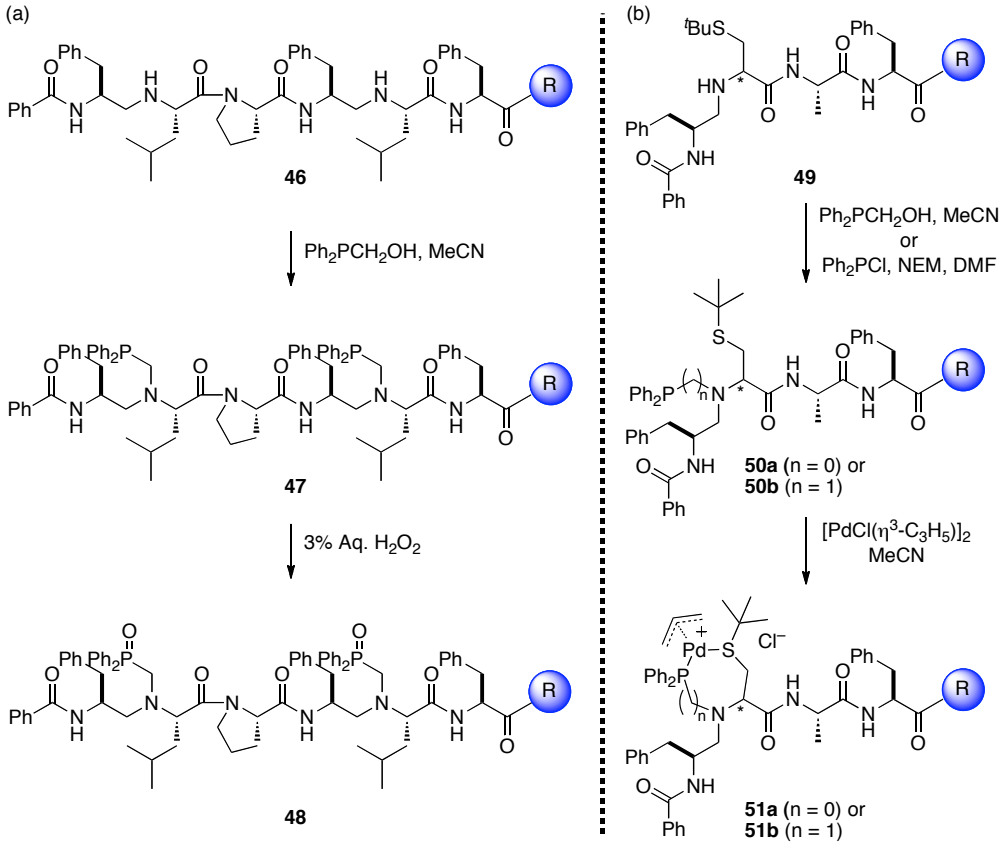

Scheme 1.10: Method for incorporation of phosphine ligands into the peptide backbone

Ligands can also be incorporated within the backbone of peptides that contain one or more reduced peptide bond(s), which provide a reactive secondary amine functionality for the ligand conjugation (Scheme 1.10).[52,53] These secondary amine functionalities of **46** and **49** were phosphinomethylated to obtain the phosphine-peptide conjugates **47** and **50b** respectively. Incorporation of cysteine into the peptide chain prior to the reduced double bond produced P,S-ligands **50**. In addition, reaction of **49** with diphenylphosphine chloride produced a P,S-ligand **50a** where phosphorous was directly attached to the backbone nitrogen. Palladium complexes were prepared from resin-bound conjugates and used as a solid supported catalyst for organic transformations. For ease in characterization, phosphine-ligand conjugates were oxidized prior to their cleavage from resin (**47** to **48**).

1.1.3 Ligands incorporation into the side chain of peptides

Among all the modes of ligand conjugations, ligand incorporation into the side chains is the most advantageous since the ligand can be introduced site-specifically at any position of the peptide chain. For incorporation of ligands into side chains, single amino acid chelates (SAAC) can be synthesized by appending ligands on the side chain of natural or unnatural amino acids. These SAAC could then be directly incorporated into peptides as if they were natural amino acid building blocks. Alternatively, ligands can be tethered to the side chains via use of on-resin orthogonal protecting group methods. In this method, a natural or unnatural amino acid bearing an orthogonal protecting group is introduced during peptide synthesis. After constructing the peptide, the orthogonal protecting group can be selectively removed in presence of other side chain protecting groups and ligands can be appended selectively at this position.

1.1.3.1 Ligand incorporation via SAAC

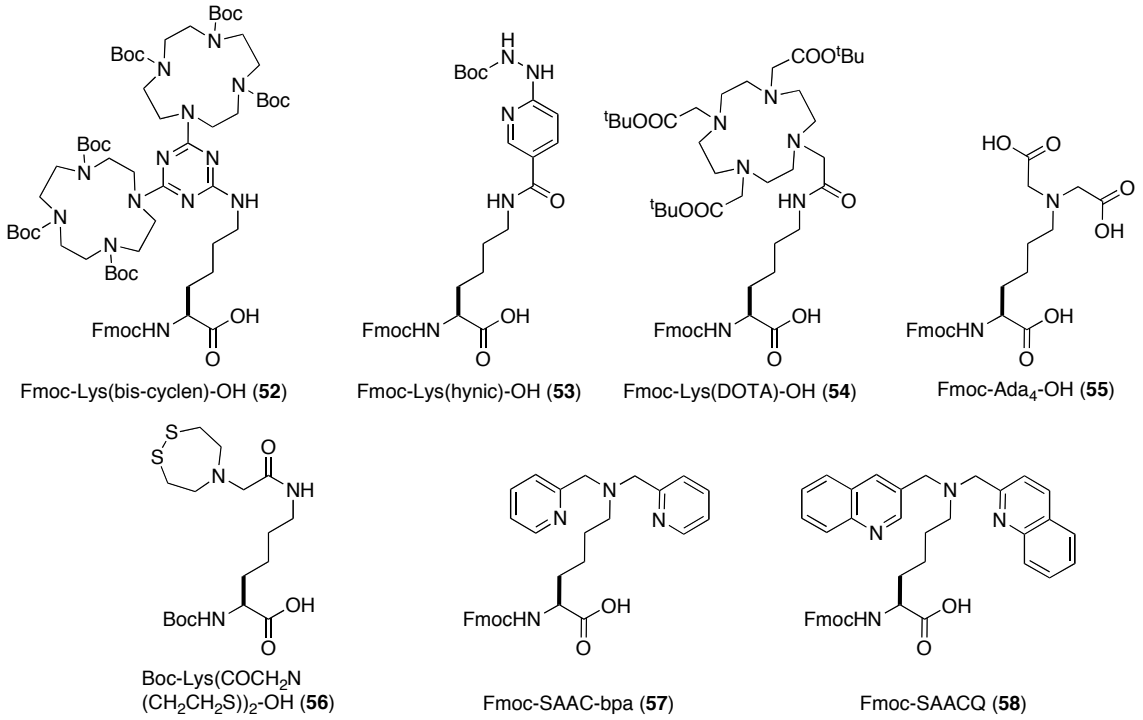

Figure 1.4: Examples of SAAC derived from lysine

Single amino acid chelates can be prepared by appending ligands on the side chains of natural or unnatural amino acids. Among all the natural amino acids, lysine is the most commonly used amino acid for the synthesis of SAAC's. Indeed SAAC's containing *N*- or *O*-donor ligands such as cyclen (**52**)[54], HYNIC (**53**)[55], DOTA (**54**)[56], Ada (**55**)[57-59] as well as the *S*-donor ligand **56**[60] were readily prepared (Figure 1.4). In addition, *N*-heterocyclic tridentate ligands, pertaining to this dissertation, were also incorporated into lysine derivatives (**57**-**58**).[61-64] In this method, reactive functionalities present on SAAC are usually protected with an acid labile protecting group so they can be unmasked during the final acidolytic cleavage from resin. In the case of peptides derived from **56**, a separate reduction step was needed to generate the reduced thiol groups for coordination to metal centers.[60] It is

important to note that *N*-heterocyclic ligands (**57** & **58**) do not require any protection and were well tolerated with SPPS conditions.[61-64] Most of the SAAC's were straightforward to incorporate into peptide chains except **52** and **53**. Bis-cyclen containing **52** suffered from poor coupling efficiency due to the bulkiness of the ligand and required specific coupling conditions[54], while HYNIC derivative **53** was found to be unstable in the oxidative conditions used for S-S bond formation and required an additional Boc protecting group.[55]

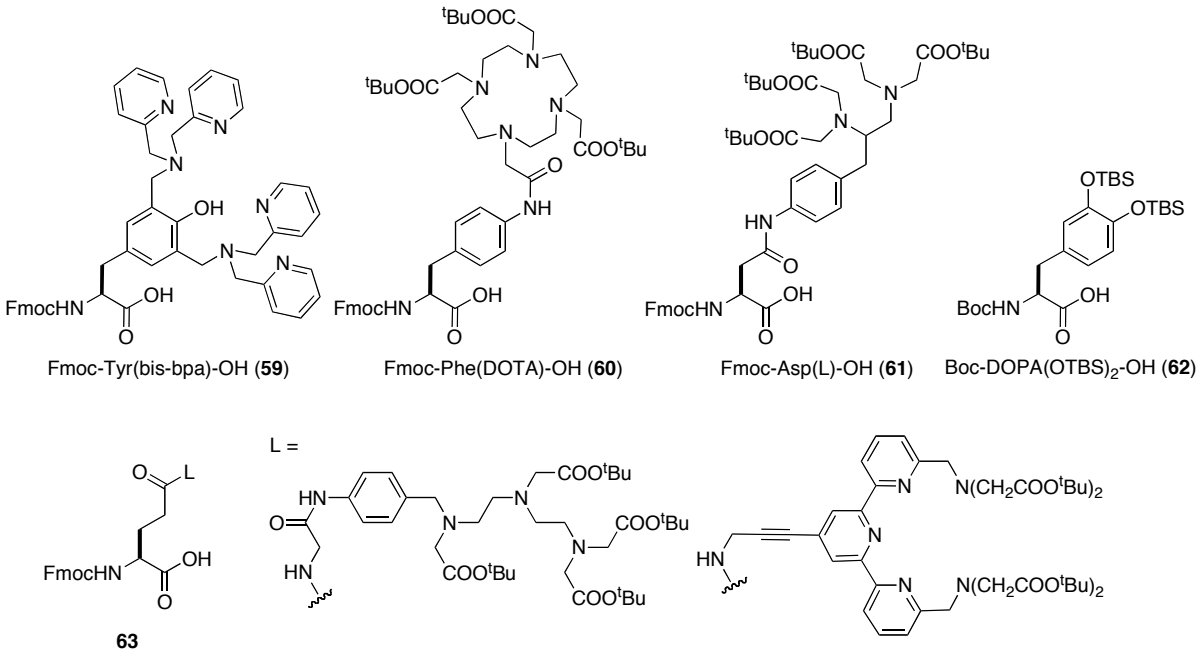

Figure 1.5: Examples of SAAC derived from tyrosine, phenylalanine, aspartic acid, tyrosine and glutamic acid

Apart form lysine, other natural amino acids such as tyrosine, phenylalanine, aspartic acid and glutamic acid have also been used for the synthesis of SAAC's where ligands such as bis-bpa, DOTA and EDTA were attached to the side chain (Figure 1.5).[56,65-70] In the case of phenylalanine, which does not have any reactive functionality on the side chain, a *p*-amino substitution was introduced for ligand conjugation (**60**).[56,65] Synthesis of Fmoc-Tyr(bis-bpa)-

OH (**59**) via a Mannich reaction[66,67] and Boc-DOPA(OTBS)$_2$-OH (**62**) via oxidation of tyrosine derivatives furnished SAAC's with improved metal-binding affinities.[68] Incorporation of these SAAC derivatives in SPPS was straightforward except for Fmoc-Phe(DOTA)-OH (**60**). In this instance, due to the bulkiness of DOTA, chain termination was observed after the incorporation of **60**. This issue was easily resolved by using pentafluorophenyl ester derivatives of the Fmoc amino acids following the incorporation of **60**.[56]

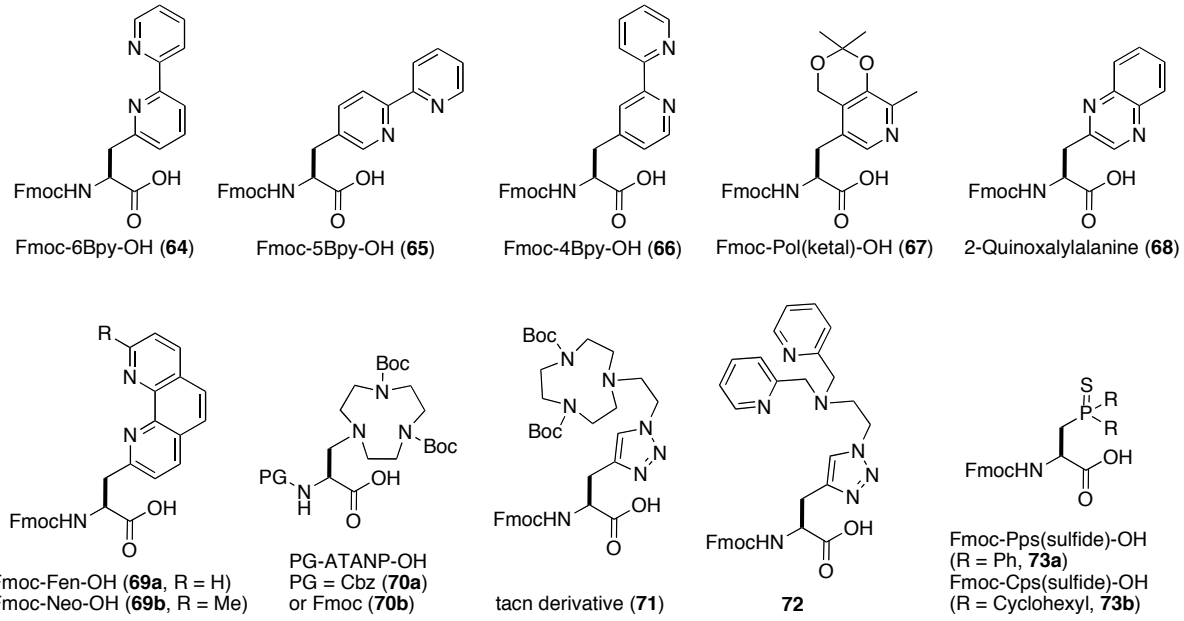

Figure 1.6: Examples of unnatural amino acids as SAAC

The synthesis of SAAC's are not limited to natural amino acids as demonstrated by the synthesis of unnatural amino acids where metal-binding moieties are directly attached to the amino acid skeleton. Representative examples of this class of SAAC's are shown in Figure 1.6. [71-82] Several pyridine-[71-76], quinoxaline-[77] and phenanthroline-[75] based mono- and bidentate SAAC were synthesized (**64**-**69**), most commonly using the asymmetric alkylation

method.[83,84] Click chemistry has also been used to synthesize SAAC derivatives where NOTA (**71**) and bpa (**72**) were attached to the amino acid skeleton via formation of 1,2,3-triazole.[80] To study the chemistry of rhodium-peptide conjugates, synthesis of phosphine-containing SAAC **73** was also developed.[78,79] In this example, an oxidation-prone phosphine was protected as a phosphine sulfide, which could be easily removed via reduction prior to complex formation.

1.1.3.2 Ligand incorporation directly onto peptides

Among all the methods discussed thus far, ligand incorporation directly onto the pre-synthesized peptide is the most convenient for the library synthesis of peptide-ligand conjugates. The only requirement for this method is the availability of an orthogonally protected functional group on one of the amino acids in a peptide chain. This group can be selectively cleaved and the unveiled reactive functionality can be used for ligand conjugation. Similar to SAAC derivatives, lysine is a well-known amino acid for ligand conjugation via this method. The enamine-based protecting group Dde (1-[(4,4-dimethyl-2,6-dioxocyclohex-1-ylidine)ethyl]) or its hindered version ivDde are often used to orthogonally protect N_{ε}-lysine (Scheme 1.11).[85,86] In a typical procedure, Fmoc-Lys(Dde)-OH or Fmoc-Lys(ivDde)-OH building blocks are used during SPPS. After completion of the desired peptide sequence, treatment of the peptide with 2-10% hydrazine selectively cleaves Dde or ivDde group in the presence of other acid-labile protecting groups. Next, a ligand is attached to the N_{ε}-amino group, typically through amide bond formation or by exploiting the reactivity of amines towards isocyanates or acyl substitution.

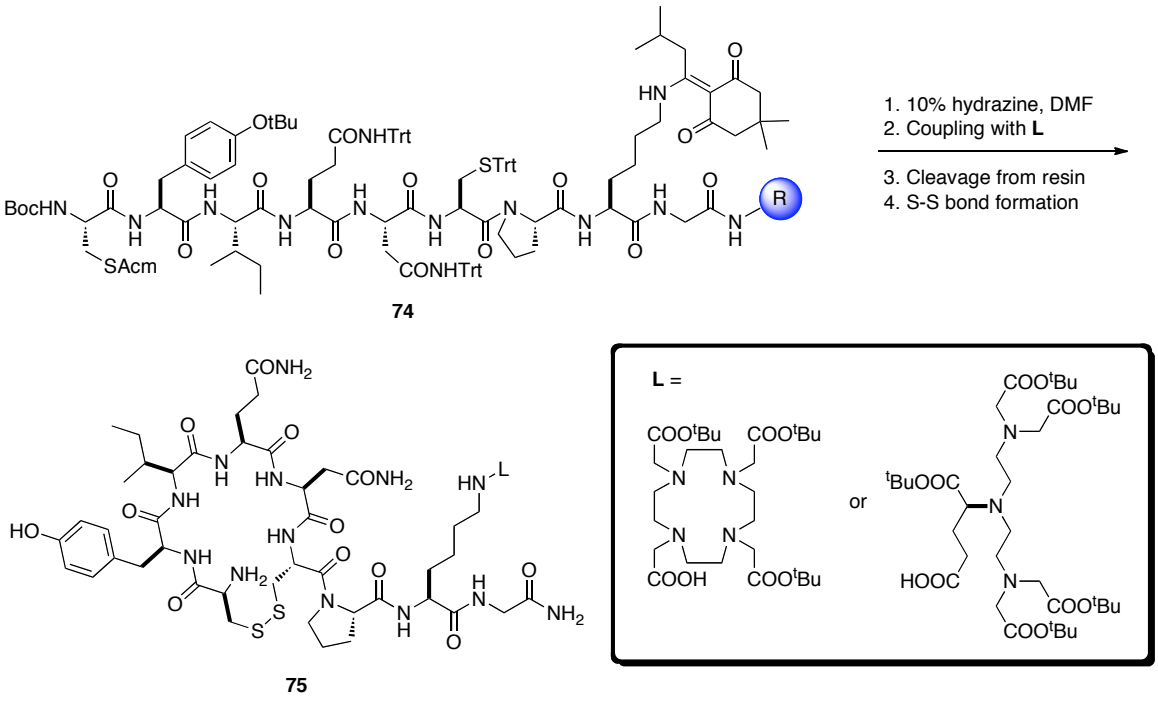

Scheme 1.11: Incorporation of DOTA and DTPA into the side chain of oxytocin analogues via orthogonally protected lysine

A rather unique method was developed where a lysine ε-amino group of somatostatin analogue **76** was chemoselectively transformed into azide (**77**, Scheme 1.12).[87] This azide was subsequently used as a handle to incorporate a DOTA group bearing an alkyne into somatostatin analogues via a click reaction. This method allows for the synthesis of dendrimeric structures by tethering multiple somatostatin analogues to the single ligand if a ligand with multiple alkynes is used. A highlight of this method is the use of protecting group free peptides in diazo-transfer as well as click reactions, which underscores the chemoselectivity of these reactions. Copper accumulation was a challenge in this example. Hence treatment with sodium sulfide (Na_2S) was incorporated into the workup but in several instances these conditions were detrimental to the resulting bioconjugates. More recently, an

alkyne linker named monofluoro-substituted cyclooctyne (MFCO) has been synthesized which reacts with an azide moiety under copper-free conditions due to presence of the strained alkyne moiety.[88]

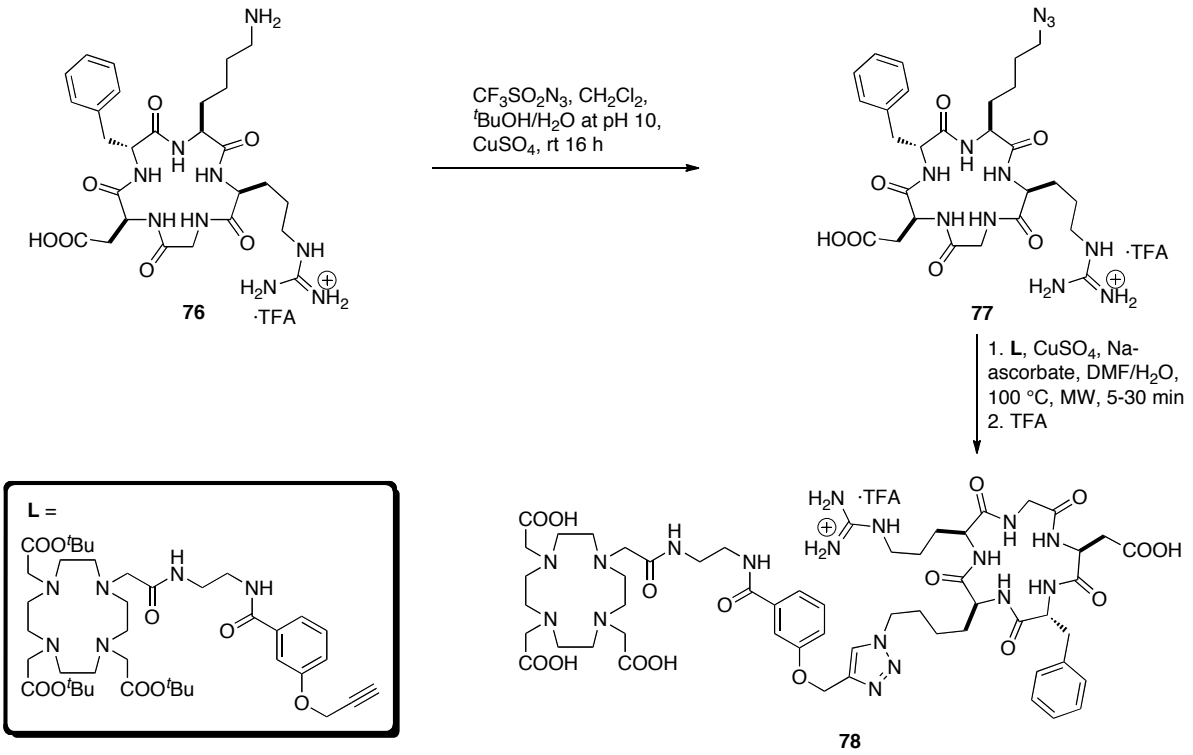

Scheme 1.12: Synthesis of N_{ε}-azido peptide from N_{ε}-lysine of cyclic RGD peptide and its utility in ligand incorporation via click reaction

Another chemoselective method for protecting group free peptides utilized a 6π-azaelectrocyclization reaction between reactive amine groups of a peptide and a pendent aldehyde group of a ligand.[89] An electron-deficient aldehyde linker **79** was designed, which selectively reacted with the amine group of a peptide to form 1-azatriene **80** *in situ* (Scheme 1.13). Subsequent intramolecular 6π-azaelectrocyclization resulted in the formation of 1,2-dihydropyridine. A key feature of this method includes shorter reaction time (less then 30 min), functional group compatibility and its applicability to short peptides as well as proteins.

In addition, although proteins contain multiple amino groups, the ratio of DOTA to protein could be controlled by optimization of the reaction conditions.

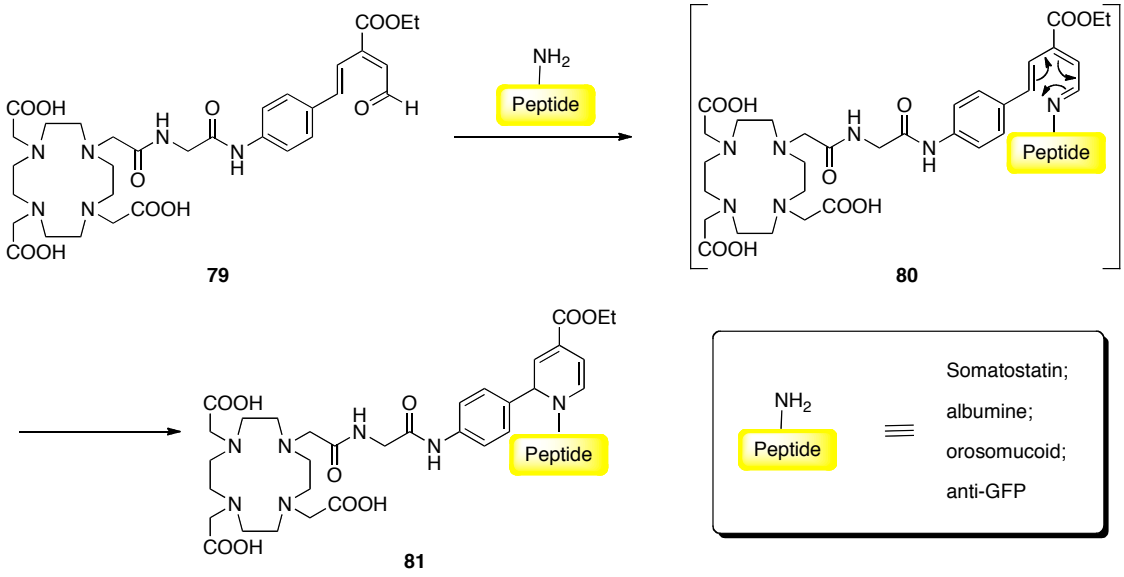

Scheme 1.13: 6π-Azaelectrocyclization for conjugation of ligands at the lysine side chain or *N*-terminus amino functionality of peptides and proteins

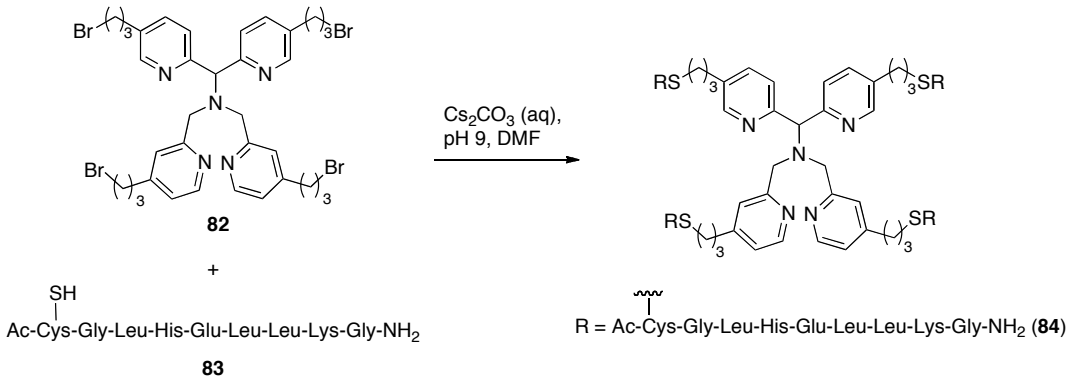

Scheme 1.14: Synthesis of a four-helix bundle N4Py derivative through ligation to a cysteine side chain

A simple alkylation of an electrophilic functional group on the ligand can be used for ligand conjugation (Scheme 1.14).[90] In this instance, the nucleophilicity of cysteine was

exploited and four electrophilic bromides on the tetradentate N4Py ligand were efficiently displaced to produce the ligand with four helixes attached. In this example, a three-carbon spacer between the bromide and the pyridine ring was essential for the stability of the bromide. Note that even an unprotected lysine was tolerated under those conditions.

Those unnatural amino acids that do not have highly reactive side chains such as glutamic acid, phenylalanine, tyrosine, serine and threonine have also been used for direct ligand incorporation into peptides (Scheme 1.15). For example, terpyridine ligands were incorporated into the side chain of glutamic acid residues of **85**, which employed a benzyl ester moiety as an orthogonal protecting group (Scheme 1.15a).[91] For incorporation of the ligand into the phenylalanine side chain, a *p*-nitro-phenylalanine derivative was introduced during peptide synthesis (e.g. **87**), which was found to be compatible with SPPS conditions (Scheme 1.15b).[92] Next, the nitro group of **87** was reduced orthogonally to expose an amine **88** through which terpyridine or bpa was attached to peptide nucleic acid (PNA) conjugates. DOPA is a derivative of tyrosine and could be obtained by *ortho*-hydroxylation of a phenol ring of the tyrosine. IBX oxidation of tyrosine containing peptide **90** was developed in which the tyrosine residue was selectively oxidized to generate DOPA-peptides **91** (Scheme 1.15c).[93] Alternatively, tyrosine of peptide **90** was also transformed into phosphine ligands upon reaction with dialkyl or diaryl chlorophosphines to obtain corresponding phosphine ligands **92a-c**.[94] This method is not limited to tyrosine and has also been applied to serine and threonine. In one instance, the tyrosine side chain of **93** was transformed into a phosphine ligand via a palladium catalyzed cross coupling reaction (Scheme 1.15d).[95]

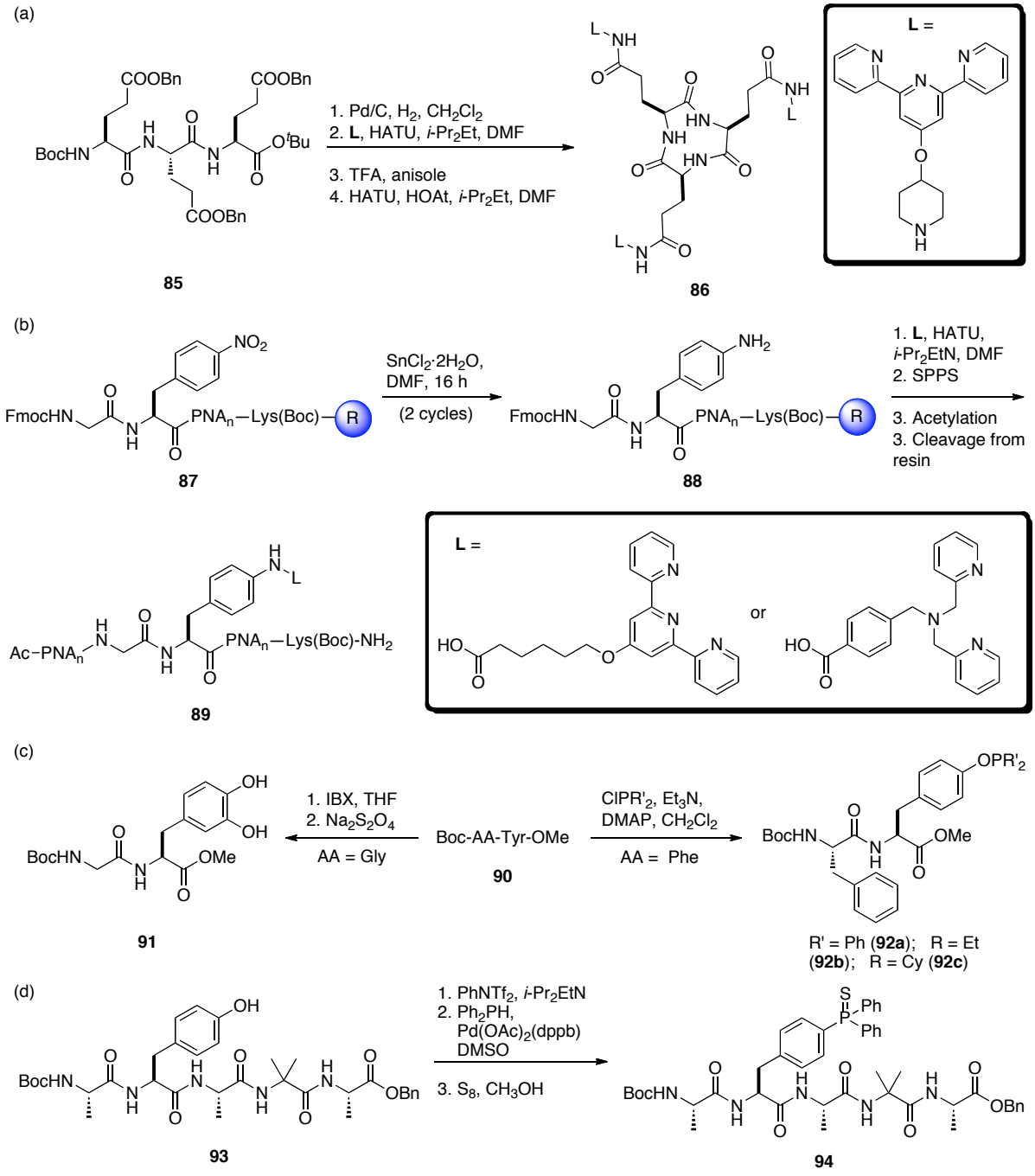

Scheme 1.15: Transformation of glutamic acid (a), phenylalanine (b), and tyrosine (c) side chains into various ligands

A method shown in Scheme 1.16 was not intended for the synthesis of peptide ligand conjugates, however it is still included in this section since DOTA has been attached to phosphopeptides using this method.[96] Elimination of phosphorylated serine or threonine furnished dehydroalanyl peptide **96** that was eventually trapped via 1,4-addition of DOTA bound thiols. In this chemical tagging method the rate of reaction decreases upon changing the substrate from phosphoserine to phosphothreonine.

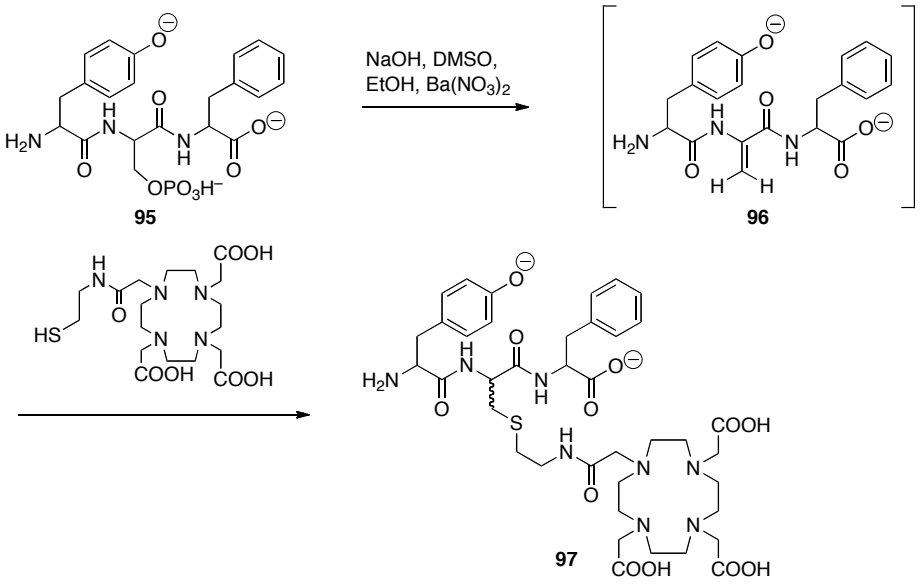

Scheme 1.16: Derivatization of phosphopeptides with DOTA through phosphate elimination and Michael addition

Unlike natural amino acids there are very few examples where a side chain of an unnatural amino acid could be used to append ligands. One method includes the synthesis of peptide **99** containing a propargyl glycine[44] or α,α-dialkyne[97] substituted unnatural amino acids **98**, which upon click reaction could furnish 1,2,3-triazole or di-1,2,3-triazole functionalities that serve as metal chelating groups (Scheme 1.17). In this method, the use of azide-containing ligands instead of azidoacetic acid could allow a rapid synthesis of a library

of peptide-ligand conjugates, however such work has not been established yet. In addition, alkynes could be directly used as ligands in the synthesis of cobalt hexacarbonyl complexes.

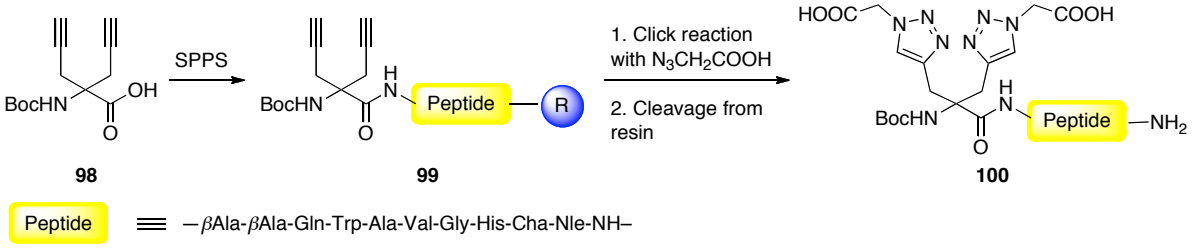

Scheme 1.17: Use of propargyl glycine derivatives for construction of 1,2,3-triazole chelates on bombesin analogue

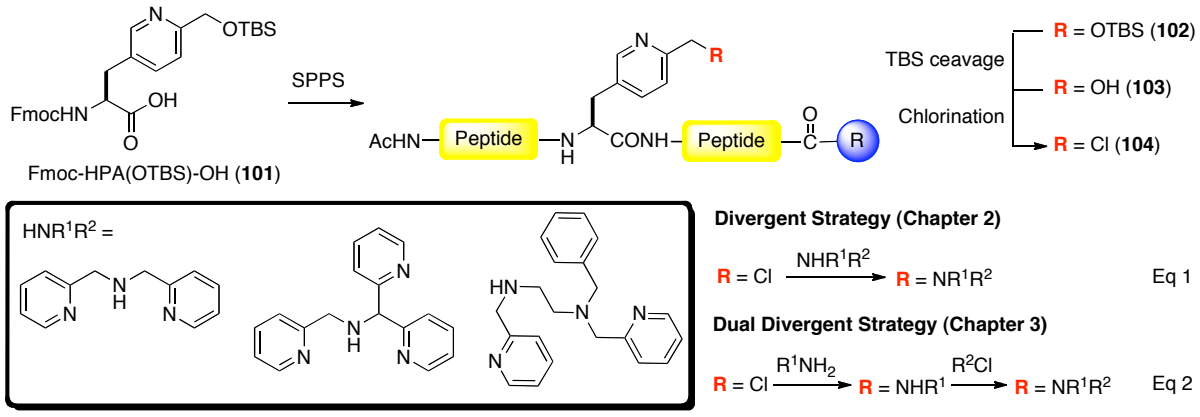

Scheme 1.18: Divergent and dual divergent strategies for synthesis of non-heme ligand-peptide conjugates

Two synthetic strategies have been developed by our group, named divergent and dual divergent strategies, which constitutes Chapters 2 and 3 of this dissertation. In short, unnatural amino acid **101** was synthesized and incorporated into a peptide chain to obtain **102** (Scheme 1.18). Next, the cleavage of the silyloxy ether followed by chlorination gave peptide **104**, which contains an electrophilic center on the side chain of a peptide. Finally, the ligand structure was elaborated by a one-step displacement of chloride with a variety of

secondary amines (Scheme 1.18, Eq 1, Divergent Strategy)[98] or stepwise alkylation with primary amines and chlorides (Scheme 1.18, Eq 2, Dual Divergent Strategy).[99] The functional group compatibility and the scope of these strategies were also explored.

1.2 Applications of Metal Complex-peptide Conjugates

Metal complexes derived from the peptide-ligand conjugates have numerous applications in biomedicinal chemistry, catalysis and *de novo* designed metallopeptides. This section will briefly discuss each of these applications.

1.2.1 Biomedical applications

One of the most challenging tasks in medicinal chemistry is to achieve the site-selective delivery of a medicinally active molecule to targeted locations. A *magic bullet* approach, originally introduced by Paul Ehrlich in the late 19th century, was considered as a potential solution to this problem.[2,5] Initially, medicinally active molecules have been attached to antibodies or proteins for site-selective delivery, however the most success has been achieved when small receptor-binding peptides are used as carrier vehicles. Conjugation of the metal complexes to receptor-binding peptides has become a common practice to achieve target specificity in radiopharmaceuticals, imaging, and anticancer or antibacterial applications as well as in cellular uptake and internalization studies.[11]

1.2.1.1 Radiopharmaceuticals and imaging agents

Radiopharmaceuticals and imaging agents are drugs that use radioactive metal complexes as therapeutics or biosensors. In a typical approach, radioactive metal complexes are tethered to a target-selective organic molecule or a peptide for delivery.[3] Such conjugates

have found numerous applications in radiopharmaceuticals or biosensors for imaging thrombi, tumors and infection/inflammation. Several conjugates of this type are currently in clinical trials.[2] Metal complexes used in such applications are sensitive, reactive and usually possess short half-lives, hence the post-conjugation method is often used for their synthesis. Success of the peptide-based radiopharmaceuticals and imaging agents depends on the choice of three components: a radioactive metal, a ligand and a suitable peptide.

Several radiometals such as ^{99m}Tc, ^{111}In, ^{64}Cu, and $^{66/67/68}$Ga have been used as radionuclei in these applications.[3] Among all the radiometals technetium is cheap, convenient in handling, possesses excellent imaging characteristics and does not produce α or β radiation. These qualities make technetium the most used radiometal in these applications. However for delayed imaging studies, technetium is not suitable due to its moderate half-life (6 h). For such applications long-lived ^{111}In (half life = 2.8 days) is more suitable. Some of the drawbacks of ^{111}In complexes include high cost, limited availability and relatively high radiation burden. In addition to technetium and indium, ^{64}Cu(II) and $^{66/67/68}$Ga have also found application in PET imaging radiotherapy.

Stability of radiometal complexes is an important factor in the success of radiopharmaceuticals and imaging agents. The stability of radiometal complexes is governed by the ligand structure and hence a choice of ligand depends on the type of radiometal used. A variety of ligands such as N_3S, N_2S_2, tetraamine, DADT, and HYNIC are conveniently used in technetium labeled radiopharmaceuticals, while for ^{111}In labeling DTPA, EDTA, NOTA and DOTA are more suitable.[3] For ^{64}Cu complexes unconventional ligands such as TETA and CPTA are developed while Ga-peptide conjugates utilize DFO (desferrioxamine), NOTA and DOTA ligands.[3]

The most critical component that is responsible for the selectivity of radiopharmaceuticals and imaging agents is the structure of the peptide. Since the selectivity is achieved through an affinity of the peptide vector to the appropriate receptor, the choice of peptide vector solely depends on the biological target. For instance, radiopharmaceuticals containing RGD sequences have been used for thrombus imaging.[3] The more prevalent peptides carriers are somatostatin analogues, bombesin analogues and analogues of gonadotropin releasing hormone (GnRH) or luteinizing hormone releasing hormone (LHRH).[100] Somatostatin receptors are overexpressed in several tumors of neuroendocrine origin, neuroblastomas, medullary thyroid cancers, pheochromocytomas and small cell lung cancers.[101] Octreotide is an octapeptide analogue of the somatostatin that has been evolved as the most successful delivery vector (Figure 1.7). Ligands are usually attached to the *N*-terminus of an octreotide during its biomedicinal applications. For instance, octreotide derivative **105** containing ^{111}In·DTPA complex at its *N*-terminus is the first peptide radiopharmaceutical approved for clinical use.[5]

Bombesin analogues are also used extensively as delivery vectors (**106**, Figure 1.7). Bombesin receptors are overexpressed in lung, prostate, breast, gastric, colon and pancreatic cancers as well as glioblastoma.[102] SAR studies have established the importance of the *C*-terminal sequence of the natural bombesin and the linker length in receptor binding process.[32,103] Based on the SAR studies, several analogues of bombesin have been developed by maintaining the *C*-terminus sequence of the natural bombesin and appending ligands in the *N*-terminus region. Moreover, N_3S-bombesin conjugates containing 0, 3, 5, 8 and 11 carbon linkers have shown that derivatives with 3, 5 and 8 carbon spacers possess better binding affinity compared to the corresponding 0 or 11 carbon spacers.[32]

^{111}In-DTPA-Octreotide (OctreoScan®)

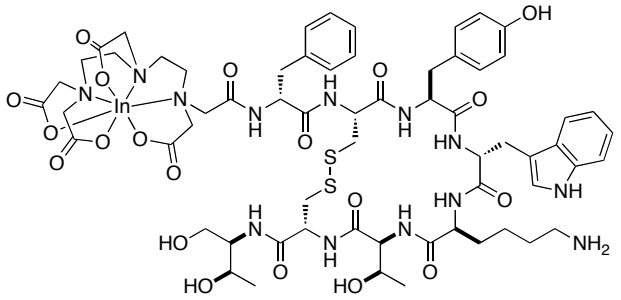

105

^{188}Re-P_2S_2-5-Ava-BBN[7-14]NH_2

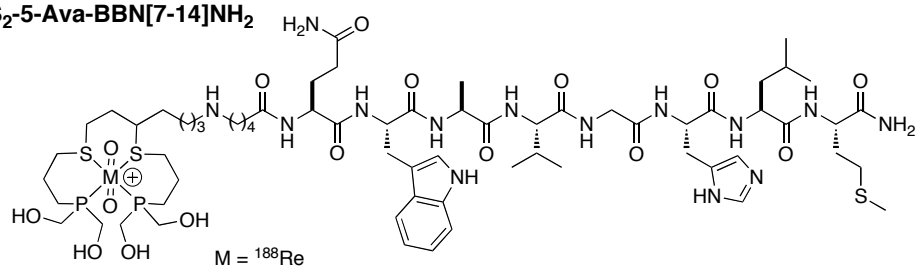

106

^{99m}Tc-P_2S_2-D-Lys^6-LHRH

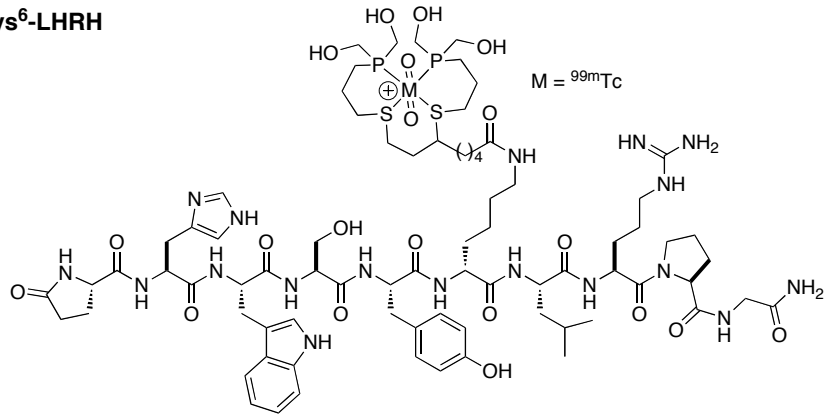

107

Figure 1.7: Representative examples of somatostatin-, bombesin- and LHRH-metal complex conjugates

The most successful peptide delivery vector is derived from LHRH (**107**, Figure 1.7). Receptors for LHRH are overexpressed in ovarian, prostate and breast cancers.[100] Several cytotoxic agents have been incorporated into LHRH analogues leading to successful anticancer agents. However, there are very few examples for LHRH analogues containing

metal complexes. ^{99m}Tc complex of LHRH was synthesized from P_2S_2-LHRH conjugates as described in Scheme 1.2, however its utility was not discussed.[40] In another study, an LHRH analogue containing two thiols at its termini was prepared. Upon complexation with rhenium or technetium the metal-mediated cyclization of LHRH was induced.[104] However, the cyclic analogues were found to be less effective in the binding assay then native LHRH. In another example when ^{68}Ga·DOTA was directly attached to the LHRH through ε-amino moiety of lysine, no receptor binding or internalization was observed.[33]

Apart form somatostatin, bombesin and LHRH, several other peptide vectors such as vasoactive intestinal peptide (VIP), alpha-melanocyte stimulation hormone peptide analogues (α-MSH), neurotensin (NT) peptide analogues, alpha-M2 peptide analogues (α-M2), and cholecystokinin (CCK) peptide analogues are also used as delivery vectors however they are less popular.[3] Besides imaging cancers, the potential of peptide-based radiopharmaceuticals to image infection and inflammation have also been investigated.[3]

1.2.1.2 Inactivation of biomolecules

Inactivation of biomolecules such as DNA, RNA or proteins is an attractive mode of action for therapeutics. A conventional drug inactivates biomolecule by stoichiometric binding. In contrast, a catalytic inhibitor can inactivate multiple copies of target molecules (Figure 1.8).[105] An obvious advantage of catalytic inhibitors is that they have the potential to require low dosage and hence side effects could be significantly reduced. The role of metal complexes has been extensively investigated as potential catalytic inactivating agents for DNA, RNA and proteins. Franz *et al*. has recently reviewed applications of metal complexes as enzyme inhibitors and DNA probes.[106]

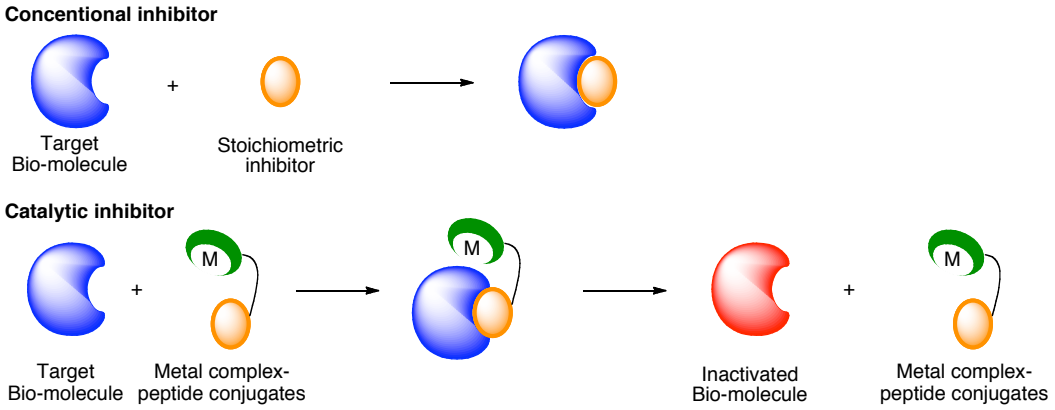

Figure 1.8: Comparison of conventional inhibitors with catalytic inhibitors

To achieve selectivity in a catalytic inhibition mode, metal complexes are usually tethered to peptides, peptidomimetics, peptide nucleic acid conjugates (PNA) or small organic molecules that recognize the target biomolecules. For simplicity, only those examples that include peptide or peptidomimetic conjugates are discussed here. Inhibition of biomolecules usually occurs through three common modes of inactivation such as metal complex induced oxidative damage, hydrolytic cleavage or cross-linking of the biomolecules.

Metal complexes-peptide conjugates are most extensively studied for their potential in targeting and inactivating DNA through hydrolytic cleavage, oxidative damage or cross-linking. A family of rhodium and ruthenium-peptide conjugates was explored for DNA hydrolysis, DNA cross-linking as well as to enhance DNA sequence selectivity. For example $[Rh(bpy3C)(chrysi)(phen)]Cl_3$ complex functionalized with basic cell-penetrating peptides (CPP) induced site-specific cleavage of duplex DNA.[107] In another instance photochemically controlled inactivation of DNA was achieved by series of short peptides containing $[Rh(phi)_2phen]^{3+}$.[108] A selective and efficient cleavage of HIV-1 TAR-RNA has been achieved with metal free cyclen-polyarginine peptide conjugate.[24] However the cleavage was

attributed to the pH-dependent hydrolysis of DNA since the cleavage was inhibited in presence of Eu^{III} or Zn^{II}. In contrast to metal complex-peptide conjugates, metal complex-PNA conjugates have emerged as a unique DNA recognition motif that is stable towards nucleases and proteases. In addition, they have low binding affinity for proteins but still maintain high binding affinity for DNA. In particular, PNA conjugates containing Co^{2+}, Cu^{2+} and Zn^{2+} complexes of dipeptides [H-Cys(uracil)-AA-cyclen] efficiently catalyzed DNA hydrolysis.[10] Likewise, PNA conjugates of mononuclear lanthanide complexes cleaved single-stranded DNA via Zr^{IV} or Ce^{IV} catalyzed reactions.[8,109] Besides this, traditional metal complex-peptide conjugates derived from ATCUN[110-113] and zinc finger motifs or *de novo* designed 32- and 33-residue helix-turn-helix metallopeptides[8] have also demonstrated their capabilities in of DNA and viral RNA cleavage.

Unlike DNA cleavage, protein inactivation mediated by metallopeptides is relatively unexplored. Similar to DNA cleavage, protein inactivation also occurs through hydrolytic cleavage, oxidative damage or cross-linking.[105] A class of metal complexes that inactivates protein via hydrolytic cleavage, known as artificial proteases, has been extensively investigated. For example, artificial proteases derived from Cu^{2+} and Co^{3+} complexes of PNA-cyclen conjugates catalyzed the hydrolysis of myoglobin however only at higher concentrations (> 3 μM) and longer reaction times (> 100 h).[114,115] In order to improve the catalytic efficiency of artificial proteases, several Co^{III}(cyclen)-peptidomimetic conjugates were investigated for their hydrolytic capability on deformylase (PDF) and amyloid β-42 targets.[105]

Oxidative damage of proteins is a complementary approach for protein inactivation when compared to hydrolytic cleavage. Oxidative damage of proteins occurs through either

backbone cleavage or side chain oxidation. When iron(II) or copper(II) complexes were tethered to known inhibitors such as biotin,[116] benzene sulfonamides[117] or trifluoperazine,[118] the conjugates oxidatively cleaved the target protein in the presence of oxygen and reductant. Examples of protein inactivation through side chain oxidation include ATCUN·Cu^{2+} catalyzed inhibition of angiotensin-converting enzyme and endothelin-converting enzyme.[7,119] In a remarkable example, chromophore assisted light inactivation (CALI) of vascular endothelial growth factor (VEGF) was achieved using ruthenium peptoide conjugate.[120] In this example the inhibition potency of ruthenium-peptoide conjugate was increased from nM to pM in presence of light. In line with this example, our group is exploring the use of high valent iron complexes, called ferryl complexes, for amino acid and protein oxidation. We have shown ferryl complexes tethered to guanidine-based inhibitors inactivate chymotrypsin and trypsin selectively.[17] With the aim of developing site-selective iron based protein inactivating agents, such complexes have been recently attached to short peptides.[121] The detailed study for the synthesis and stability of such ferryl-peptide conjugates is described in Chapter 4.

Apart from the traditional oxidative cleavage and side chain oxidation, rather unique oxidative damage has been observed when proteins containing *N*-terminal aspartate were treated with cyclen-peptidomimetic conjugates. In this instance, an oxidative damage of the *N*-terminal aspartate leads to the formation of pyruvate.[122] Although catalytic damage of the protein is a more attractive mode of inactivation, metal complex-peptide conjugates could also be used as stoichiometric inhibitors. When a Co^{III} Schiff base complex was tethered at the *N*-terminus of a thrombin binding peptide, suicide inhibition was achieved, where one of

the labile ligand of the Co^{III} Schiff base complex was exchanged with the histidine side chain of thrombin.[123]

1.2.1.3 Anticancer activity, antibacterial activity, cellular uptake and internalization

Apart from the applications of metal complex-peptide conjugates in radiopharmaceuticals and DNA/protein inactivation, their utility as traditional anticancer/antibacterial agents as well as in cellular uptake and internalization studies has also been investigated.[11] Ferrocene-dipeptide conjugates or cisplatin-tripeptide conjugates have shown antiproliferative activity at low micromolar concentrations.[124-126] Similarly, the conjugation of a cymantrene complex to a cell-penetrating peptide hCT displayed a high cytotoxicity to MCF-7 breast cancer cells.[127] Furthermore, cisplatin and *trans*-bis(salicylaldoximato)copper(II) complexes were appended on a well-known LHRH peptide vector was appended with at its D-Lys^6 side chain.[128] A cisplatin-LHRH conjugate displayed 50 times higher potency than the native hormone, while a conjugate derived from bis(salicylideneimine) complex caused 100% inhibition of ovulation. In addition to the conventional anticancer activity, light mediated activation of metal carbonyl complexes have also been explored, which not only opens a coordination site on a metal complex-peptide conjugate but also releases toxic CO or singlet oxygen.[11,129]

In contrast to anticancer activity, antibacterial activity of metal complex-peptide conjugates has been investigated over the last two decades, however only moderate success has been achieved to date.[11] In this application, antimicrobial peptides are expected to interfere with the bacterial membrane.[130] Some success has been achieved when metallocenes

were incorporated into small peptides, which not only increased the activity but also altered the specificity for Gram-positive or Gram-negative bacteria.[131,132] In this example, alteration in peptide chain or charge on metal complexes was detrimental to the selectivity of conjugates.

The directing ability of peptides was also utilized in studies of cellular signaling peptides. This application requires that conjugates recognize the target biomolecule in a biological process without inhibiting it. For example, metallocene conjugates of nuclear localization signal (NLS) peptides were efficiently translocated into the nuclei of HepG2 cell and were readily taken up by the cells without displaying any cytotoxicity up to 1 mM.[133] With the aim of developing metallochaperones, bis-(2-picolylamine) ligands were also incorporated at the *N*-terminus of the nuclear localization signal (NLS) peptide.[28]

1.2.2 Metal-assisted stabilization of peptide-microstructures

Metal mediated peptide folding plays a critical role in achieving the desired properties and functions of metal complex-peptide conjugates. Zinc-fingers are an interesting example of how metal-binding amino acids can influence protein folding. Inspired by such examples, metal-assisted stabilization of synthetic peptide-ligand conjugates have been explored.[12,13] Such studies are important since stabilization of peptide-microstructures might help developing more active and/or selective secondary structures that eventually could be used in artificial metalloproteins, or to obtain materials with impressive biological activity and novel properties.

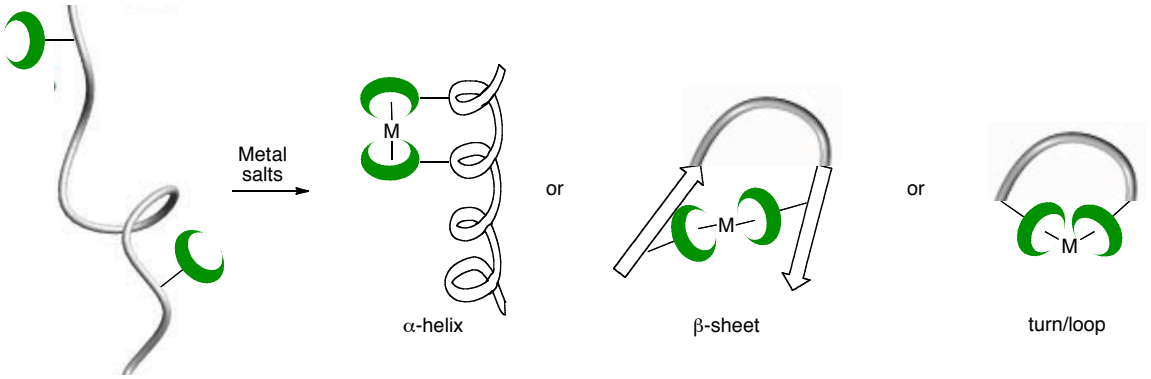

Figure 1.9: Metal-assisted stabilization of peptide-microstructures via formation of α-helix, β-sheet or turn/loop

Peptide-ligand conjugates for this application usually contain multiple ligands in a single peptide, and upon binding to metals they fold into an α-helix, a β-sheet or a metal-assisted turn/loop (Figure 1.9).[12] For such applications, *N*-donor, *P*-donor as well as *O*-donor ligands have been attached within the backbone or at the *N*- and *C*-terminus of peptides. For example, incorporation of multiple copies of 2,2'-bipyridine derivative (**33-37**, Figure 1.3) within the backbone of a peptide have induced the ruthenium-assisted peptide folding[48,49], while incorporation of a 6,6'-substituted 2,2'-bipyridine derivatives into a peptide (**38-41**, Figure 1.3) have induced a β-sheet structures upon binding to Cu(II) salts.[50] Additionally, incorporation of a terpyridine derivative at the *N*- and *C*-terminal is also known to stabilize the corresponding metal complex-peptide conjugates through metal-induced loop/turn formation (Scheme 1.6).[45] Likewise, when phosphine containing SAAC's (**73**, Figure 1.6) were incorporated at *i* and *i*+4 positions of a peptide, the resulting peptide folded into an α-helix structure upon reaction with rhodium salts.[95] Besides *N*- and *P*-donor ligands, *O*-donor catechols are also known to stabilize metal-assisted secondary structures. Amino acid or peptide bridged dicatechol ligands (Scheme 1.7) bind titanium or molybdenum and induce

metal-assisted folding.[46] The orientation of dicatechol-peptide conjugate during complex formation complicated its chemistry in solution phase, however isomeric complexes converted into thermodynamically favored major isomers over several days. Overall, metal-assisted stabilization of peptide-microstructure is a growing application of synthetic peptide-ligand conjugates.

1.2.3 Catalysis in organic transformations

Inspired by the efficiency of metalloenzymes, catalytic potential of small metal complex-peptide conjugates for organic transformations was also explored.[95,134] The ultimate goal was to develop the recycling catalysts or continuous flow reactors, which requires synthetic methods that are suitable for library synthesis via SPPS and produce the material with quantitative yields. To fulfill this requirement, a polyethylene glycol-based resin (PEGA) has been developed, which possesses an open structure, excellent swelling in polar and non-polar solvents and extreme mobility.[135] These properties facilitate the peptide folding on resin that is essential for obtaining a chiral environment around the metal center. Phosphines and carbenes were chosen as ligands for this application due to their ability to form the stable organometallic complexes. Moreover in this application, ligands were placed in close proximity of the peptide backbone in order to transfer the chirality of a secondary structure into the catalytic center.

For the synthesis of chiral metal complex-peptide conjugates, phosphine ligands were initially incorporated within the backbone or through a side chain of peptides. For example, several phosphine based ligands such as diphosphine ligand, P,S-ligand, and phosphine-oxazoline ligand were incorporated into the backbone of peptides (Scheme 1.10).[52,53]

Palladium complexes of these phosphine-peptide conjugates not only served as an excellent catalyst for the Suzuki reaction but the activity of solid supported catalyst was retained even after five recycles. These conjugates were also used in enantioselective *C*-allylation, however in this instance the efficiency was significantly dependent on the type of resin and the stability of the catalyst structure. Interestingly, moving from six-membered (**51a**, Scheme 1.10) to seven-membered (**51b**, Scheme 1.10) palladium complexes, an inversion in the enantioselectivity (from S to R) was observed.[53]

Palladium complexes of phosphine-peptide conjugates, derived from serine, threonine and tyrosine (Scheme 1.15c), served as excellent catalysts in the palladium-catalyzed asymmetric Heck reaction.[94] Alternatively, phosphine-peptide conjugates have also been synthesized by incorporation of phosphine derived SAAC's (**73**, Figure 1.6) into peptides.[78,79] Upon complexation with rhodium and ruthenium, these complexes generated an α-helix or a β-turn sheet structural assembly.[134] Among these, β-turn assembly has relatively better selectivity in alkylation reactions, although the selectivity varied with the substrates. Unfortunately, corresponding rhodium catalysts suffered from poor selectivity in hydrogenation reactions. Moreover, in either case enantioselectivities varied when moving from solid phase to solution phase reactions.

Carbene-peptide conjugates have recently emerged as an alternative to phosphine-peptide conjugates. Carbenes have been incorporated into the peptide backbone[51] (Scheme 1.9) or at the *N*-terminus.[26] The strong interaction of carbenes with transition metals enhances the stability of the resulting catalysts. Although higher reaction temperatures are required due to their stability, their utility in Sonogashira and Suzuki reactions were remarkable as indicated by the short reaction times, low catalyst loading and broad substrate

scope. More interestingly, a reaction can be performed in water and a quantitative conversion could be achieved with solid supported catalyst.[134] The efficiency of the catalyst was demonstrated by carrying out the solution phase reaction with as little as 0.00005 mol% catalyst loading. In contrast, solid supported catalyst required higher loading however they can be recycled up to as many as eight times without affecting the activity.

1.2.4 Miscellaneous

Apart from specialized applications discussed above, metal complex-peptide conjugates have found several other applications. For example, coordination of an amino acid residue of a target protein to the metal center of the metal complex-peptide conjugate can result in a stable coordinative cross-linkage between synthetic conjugate and a biomolecule. This concept has been used in developing protein tags for protein-protein interaction studies as shown by incorporating duplicate copies of **59** (Figure 1.5) into a peptide chain.[67] The zinc complex derived from these conjugates selectively recognized oligo-aspartate sequences and hence served as a D4 tag. Similarly, a zinc complex of a peptide-ligand conjugate containing a single copy of **59** has been used to study the anion-mediated translocation process.[66] A rather unique application in material chemistry is reported where cyclic-tri-*β*-peptide (Scheme 1.15a) was prepared and its ability to form columnar assemblies was explored.[91] A rigid and planar skeleton of this peptide facilitated the rod-shaped molecular assembly while the copper ion provided the electronic conductivity and hence the resulting conjugate is expected to have applications in the electronics field. Another application for self-assembling molecules was demonstrated by the synthesis of light-harvesting nanomaterials.[136] In this example, $[Ru(bpy)_3]^{2+}$ has been attached to the *N*-terminus of a peptide via an amino

hexanoic acid linker. An appropriate mixture of Ru-peptide conjugate and a peptide containing molecular probe has displayed light capturing capacity.

1.3 Ferryl Chemistry

Iron-enzymes have gained significant attention due to their potential as biological oxidants. Heme- and non-heme ferryl species have been proposed as reactive intermediates in such enzymes. Inspired by the selectivity and specificity of these enzymes, several research groups have explored the chemistry of synthetic ferryl complexes over the last two decades.[14,15,137,138] This research has focused mainly on two parent ligand structures, either heme or non-heme ferryl complexes.[14,15] The first well-characterized mononuclear non-heme ferryl complex was reported in 2003. Since then a variety of non-heme ferryls have been synthesized and their utility in oxidation chemistry has been explored. Que and Nam *et al*. have reviewed chemistry of heme and non-heme ferryl complexes.[14,15] In addition, Dr. Abouelatta[139] and Dr. Campanali[140], former Kodanko group members, have recently discussed the progress of ferryl chemistry in their Ph.D. theses. Hence in the following sections synthesis, characterization and applications of the synthetic mononuclear non-heme ferryls will be briefly discussed in the context of the synthetic ferryl-peptide conjugates.

1.3.1 Synthesis and characterization of the synthetic non-heme ferryl complexes

The first mononuclear non-heme ferryl complex was synthesized by reaction of $[Fe^{III}(\text{cyclam-acetato})(CF_3SO_3)]^{2+}$ with oxone at –80 °C and characterized by Mössbauer spectroscopy.[138] Several years later two more ferryl complexes, $[Fe^{IV}(O)(TMC)(MeCN)]^{2+}$

and $[Fe^{IV}(O)(N4Py)]^{2+}$, were synthesized and characterized by X-ray crystallography.[141,142] Typical synthesis procedures include the reaction of non-heme iron(II) complexes with oxidant such as peracids,[141,143-146] PhIO,[147] $KHSO_5$,[145] O_3,[148] NaOCl,[149] NaOBr,[149] hydroperoxide[141,145,150] or molecular oxygen[151] (Figure 1.10). In the case of single oxygen atom donors, two-electron oxidation of Fe(II) to Fe(IV) is responsible for the ferryl generation, while in the presence of hydroperoxide, either homolytic O-O bond cleavage of Fe^{III}-OOR species, or alternatively heterolytic cleavage of Fe^{II}-OOH to form Fe^{IV}(O) are proposed as the reaction mechanism.[152] Analytical techniques such as UV-vis spectroscopy, electrospray ionization mass spectrometry, EPR spectroscopy, Mössbauer, resonance Raman and magnetic circular dichroism have been used to characterize these ferryl complexes.[14] Typically ferryl species contain a low-spin (S = 1) iron center with a short Fe–O bond (~1.64 Å) that resembles a Fe–O double bond.[14]

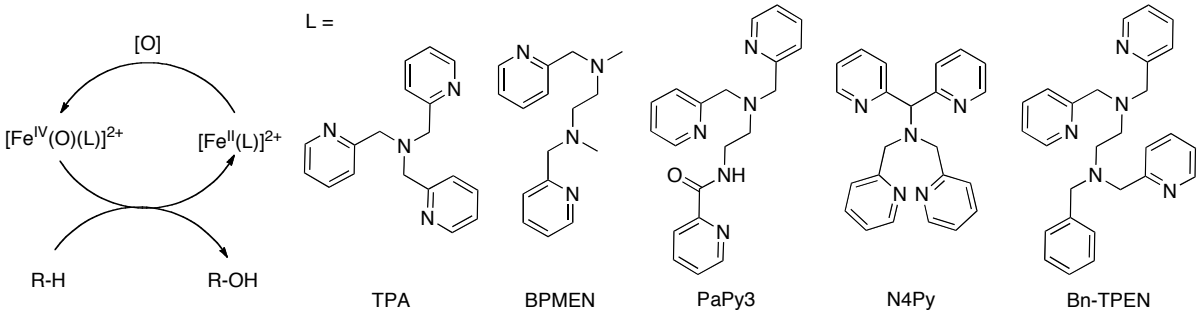

Figure 1.10: Catalytic cycle for formation and reaction of mononuclear non-heme ferryl complexes

1.3.2 Stability and reactivity of non-heme ferryl complexes

The stability and reactivity of the non-heme ferryls depends on ligand structure, pH of the reaction and the type of the axial ligand bound *trans* to the Fe–O bond. For example,

$[Fe^{IV}(O)(TMC)(MeCN)]^{2+}$ and $[Fe^{IV}(O)(N4Py)]^{2+}$ are stable at room temperature while, $[Fe^{IV}(O)(TPA)(MeCN)]^{2+}$ is stable only at –40 °C.[141,143,153] Likewise $[Fe^{IV}(O)(N4Py)]^{2+}$ is stable at lower pH (pH = 5-6) and the stability gradually decreases with the increase in the pH of the solution.[145] Moreover, ligand structure also has a significant influence on the reactivity of the ferryls as indicated by the difference between the reactivity of $[Fe^{IV}(O)(TPA)(MeCN)]^{2+}$ and $[Fe^{IV}(O)(N4Py)]^{2+}$. These complexes oxidize phosphines, sulfides and strong C-H bonds.[141,153,154]

1.3.3 Non-heme ferryl complexes in oxidation reactions

1.3.3.1 Oxidation of organic substrates

One aspect of the reactivity of the non-heme ferryl complexes is their capability to oxidize various organic substrates (Figure 1.11).[14] Primarily the oxidation potential of ferryl complexes has been explored in the oxidation of functional groups such as phosphines,[141] sulfides[151] and alkenes,[143] which are prone to oxidation. However, an impressive reactivity was revealed when ferryls were found to oxidize strong C-H bonds such as those present in cyclohexane or ethyl benzene.[153] Following these results, it has also been established that the ferryls can catalyze aromatic hydroxylation,[155] alcohol oxidation,[156] alkylaromatic oxidation and *N*-dealkylation reactions.[146] In addition to the oxidation of organic substrates, ferryls are also capable of transferring oxygen atoms from $Fe^{IV}(O)$ to $Fe^{II}(L)$ complexes.[157] The oxidation power of ferryl complexes has a strong influence on their capability as oxygen atom transfer reagent. The order of the oxidation power is determined as $[Fe^{IV}(O)(Bn\text{-}TPEN)]^{2+} > [Fe^{IV}(O)(N4Py)]^{2+} > [Fe^{IV}(O)(TMC)(MeCN)]^{2+}$.[158] Our group has explored the reactivity of ferryl complexes towards oxidation of more complex and biologically important

molecules, namely amino acids, peptides and proteins. It has been demonstrated that ferryl complexes oxidize amino acid substrates leading to either backbone cleavage (Gly) or side chain oxidation (Cys, Tyr, Trp, Met).[159,160] Recently ferryl complexes were found to oxidize glutathione, which is a biologically important tripeptide antioxidant.[161]

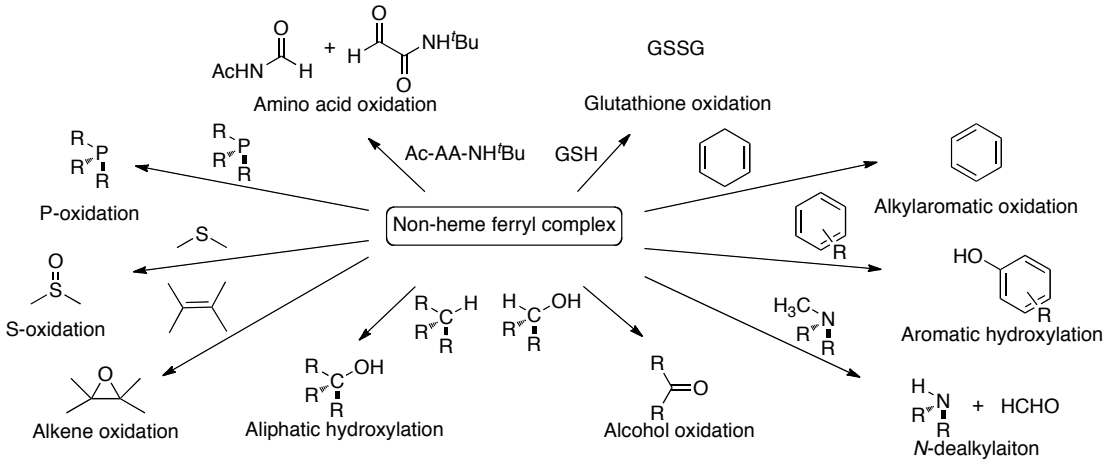

Figure 1.11: Reactivity of mononuclear ferryl complexes with various organic substrates

1.3.3.2 Mechanism of oxidation reactions

Along with the exploration of the reactivity of ferryl complexes, mechanistic investigations have also been carried out. A striking finding born from these studies was the high kinetic isotope effect (KIE > 30) obtained in the ferryl-mediated oxidation of alkanes and alcohols.[153] This suggested that non-heme ferryls oxidize strong C-H bonds via a hydrogen atom abstraction (HAT) mechanism where C-H bond cleavage is the rate-determining step. Unlike the alkane and alcohol oxidation, hydroxylation of aromatic compounds gave KIE's as low as ~0.9 and the rates of hydroxylation were strongly influenced by the electron-donating ability of the substituents as indicated by the larger negative Hammett ρ values (–3.9).[155] Based on these data an electrophilic aromatic

hydroxylation was proposed as a possible mechanism. A rather unique mechanism was established when ferryl complexes were used in *N*-dealkylation reactions. In this instance, KIE (< 5), relatively low but negative Hammett ρ values (~ –2.5) and product analysis with mechanistic probes were consistent with an electron-transfer, proton-transfer (ET-PT) mechanism.[146] In light of these mechanistic investigations, our group has established the mechanism for the reaction of ferryls with various amino acid substrates as well as glutathione. Our findings suggest that Cys, Tyr, Trp and Gly react with ferryls via ET-PT or HAT mechanisms while Met undergoes an oxygen atom transfer reaction.[160] Through detailed kinetic studies and product analysis, the Kodanko group has also demonstrated that ferryls react more selectively with certain amino acids than ·OH, which is only mildly selective in amino acid and protein oxidation.[162,163]

1.3.3.3 Intermolecular vs. intramolecular oxidation

The oxidation reactions of mononuclear non-heme ferryl complexes reported to date can be divided into two reaction modes, an intermolecular and an intramolecular pathway. In most cases ferryl mediated oxidation is performed under pseudo-first order conditions, in which a large excess of substrate is added and the oxidation occurs in an intermolecular fashion. Alternatively, when ligands have been appended with certain functionality such as aromatic rings, an alternate intramolecular oxidation mode was observed. However such examples are relatively rare (Scheme 1.19).[164,165] Reaction of $[Fe^{II}$(6-PhTPA)$(MeCN)_2](ClO_4)_2$ with *tert*-butylhydroperoxide or PhIO yields *ortho*-hydroxylation of α-phenyl moiety (Scheme 1.19a).[164] Under similar reaction conditions the use of PhINTs inserts the NTs group into an aromatic ring. However in either instance the nature of the

oxidant was not identified directly. In another example, reaction of $[Fe^{II}(TPA)(MeCN)_2]^{2+}$ with *m*-CPBA furnished 5-chlorosalicylate, which is derived via *ortho*-hydroxylation of *m*-CPBA (Scheme 1.19b).[165] In this work the formation of a ferryl was well characterized however the mechanistic investigation suggested that the initially generated ferryl was not directly responsible for the aromatic hydroxylation. The *m*-chlorobenzoic acid derived from *m*-CPBA coordinated to the iron center via the carboxylic group, which eventually underwent an intramolecular hydroxylation. It is important to note that in both examples, non-heme ferryls were generated from tetradentate ligands.

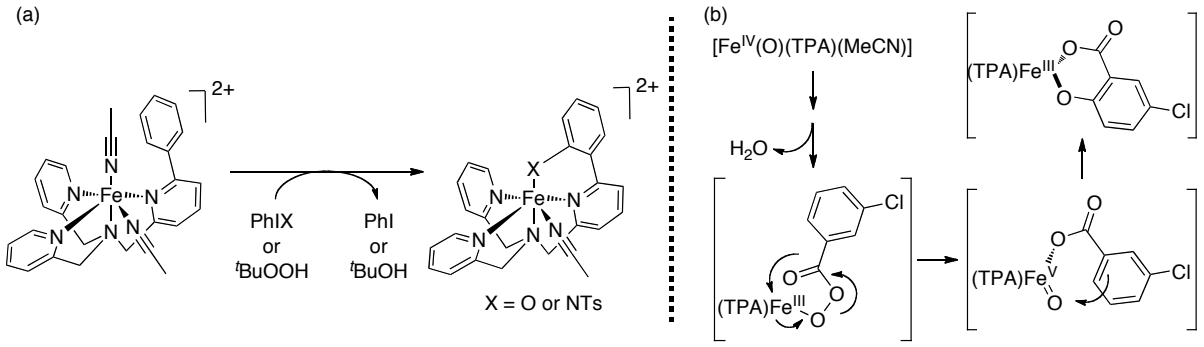

Scheme 1.19: Intramolecular oxidation or amination of aryl functionalized TPA (a) and *ortho* hydroxylation of *m*-CPBA (b)

1.3.4 Applications of synthetic non-heme ferryl complexes

Dr. Abouelatta has recently discussed applications of synthetic non-heme ferryl complexes in his Ph.D. thesis and hence only a summary of this topic has been presented here.[139] Apart from the utility of the ferryl complexes in oxidizing organic substrates as discussed in Section 1.3.3.1, the parent ferrous complexes that can generate reactive oxidants are also useful reagents for oxidation of biomolecules.[166,167] Several bleomycin mimics have been demonstrated to cleave the double stranded DNA in presence of oxygen. Although the

transient ferryl species was proposed as a key oxidant in DNA cleavage, its existence was not proven. Me-TPEN in presence of H_2O_2 and N4Py-acridine conjugate in presence of oxygen were found to participate in DNA scission process.[168,169]

Our group is exploring the utility of ferryl complexes in amino acid, peptide and protein oxidation. To date we have shown that the ferryl complexes can oxidize glutathione (GSH) to its disulfide dimmer (GSSG) as well as oxidize various amino acid substrates leading to either side chain oxidation or backbone cleavage.[161] We have also demonstrated that ferryl complexes are capable of oxidizing chymotrypsin and trypsin, and hence can be utilized as protein inactivating agents.[17]

1.4 Thesis Statement

The chemistry of metal complex-peptide conjugates and synthetic ferryl complexes has arisen simultaneously but independently over the last two decades. Metal complex-peptide conjugates have evolved as target specific therapeutics while ferryls are emerging as selective metal-based oxidants. Merger of these two well-explored research areas is an attractive idea. However it has not been pursued to date, which may in part be due to the lack of the methods for the synthesis of non-heme ligand-peptide conjugates and challenges associated with the synthesis of ferryl-peptide conjugates. The Kodanko group identified this unexplored area in the literature and aspired to integrate these two research areas by exploring the chemistry of ferryl-peptide conjugates and utilizing them for various biological applications. This dissertation is aimed at developing divergent methods for the synthesis of non-heme ligand-peptide conjugates and exploring their utility in library synthesis of biologically important molecules as well as chemistry of ferryl-peptide conjugates. The

overall goals of this dissertation are as follows. (i) Development of a divergent strategy for the synthesis of non-heme ligand-peptide conjugates (Chapter 2); (ii) Applications of the divergent and dual divergent strategies for library synthesis of metal-binding LHRH analogues (Chapter 3) and (iii) Synthesis, characterization and mechanistic studies of the synthetic ferryl-peptide conjugates.

The first goal of this dissertation was to develop a synthetic strategy that allows the rapid and efficient synthesis of non-heme ligand-peptide conjugates (Chapter 2). First, an unnatural amino acid **86** containing a silyloxy ether group was synthesized. Next, the divergent strategy was developed using a model dipeptide substrate derived from amino acid **86**. As a proof of concept three peptide-ligand conjugates were prepared from the model dipeptide substrate via solution phase method. Finally, the extension of this method to solid phase synthesis is discussed.

The second goal of this dissertation was to apply the divergent strategy for library synthesis of peptide-ligand conjugates (Chapter 3). Prior to proceeding with the library synthesis, an extension of the divergent strategy was envisioned. Towards this, a dual divergent strategy was developed where ligands were synthesized in a stepwise fashion. For library synthesis, a decapeptide (LHRH: luteinizing hormone releasing hormone) was chosen as a target peptide. The choice of LHRH peptide was made because of its biological significance as a delivery vector, as well as the diverse array of functional groups that it contains. Despite its success as a drug delivery agent there are very few example of metal-binding LHRH analogues, which motivated us to explore their chemistry. In this goal we aspired to append the diverse array of metal-binding ligands onto LHRH using divergent and dual divergent strategies.

The final goal of this dissertation was to use the peptide-ligand conjugates to explore the chemistry of synthetic ferryl-peptide conjugates (Chapter 4). The project was initiated because our group planned to attach reactive ferryl species to peptide-binding motif for selective protein oxidation. However synthetic ferryl-peptide conjugates were not known in the literature. Hence it was necessary to develop a synthesis of ferryl-peptide conjugate on a model system and establish its stability and reactivity, prior to its incorporation into a complex peptide-binding motif. The knowledge gained about synthetic ferryl-peptide conjugates has potential to be extremely valuable for the synthesis of stable catalysts or artificial oxygenases. In this chapter, synthesis, characterization and reactivity of the first ferryl-peptide conjugate was discussed. During this work we observed that the ferryl-peptide conjugate was decomposing faster then the parent ferryl complex, which led us to investigate the detailed mechanism for its decomposition. The findings of this mechanistic investigation are presented at the end of this chapter.

Experimental procedures and characterization of new compounds as well as tabulated data are presented at the end of Chapters 2, 3 and 4. The dissertation ends with Conclusions and Future Directions (Chapter 5).

Chapter 2: Divergent Strategy for the Synthesis of Peptide-ligand Conjugates

2.1 Introduction

For exploring the chemistry of non-heme ligand-peptide conjugates the most essential requirement is the rapid access to their library synthesis. Hence we sought to develop the divergent strategy for the synthesis of non-heme ligand-peptide conjugates as shown in Figure 2.1. To develop the divergent strategy, a pyridine containing unnatural amino acid Fmoc-HPA(OTBS)-OH (HPA: 2-**H**ydroxymethyl **P**yridyl **A**lanine, **1**) was designed and synthesized that mimics the natural amino acid phenylalanine. Using this unnatural amino acid a model dipeptide **2** was synthesized and the divergent strategy was developed using this model system. The model system contained a *tert*-butyldimethylsilyl (TBS) group on the hydroxymethyl side chain so that it could be cleaved orthogonally in the presence of traditional side chain protecting groups used during Fmoc solid phase peptide synthesis. In the first section of this chapter, a retrosynthetic analysis, synthesis of key intermediates, and asymmetric synthesis of Fmoc-HPA(OTBS)-OH (**1**) is presented. In the second section, the synthesis of a model dipeptide substrate and a three-step divergent strategy is illustrated. Finally, the extension of the divergent strategy to SPPS as well as a study to determine functional group compatibility and scope are discussed.

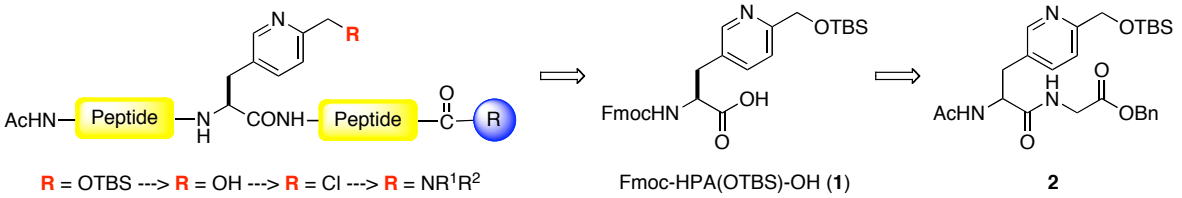

Figure 2.1: Schematic diagram for the divergent strategy

2.2 Results

2.2.1 Synthesis of an unnatural amino acid

2.2.1.1 Retrosynthetic analysis

Two retrosynthetic pathways were considered for the synthesis of the unnatural amino acid **1** (Figure 2.2). The Negishi coupling was an attractive approach because the intermediate **4** can be prepared from serine, which would facilitate enantioselective synthesis of amino acid **1**. This approach was based on the literature precedence for the synthesis of 2-pyridylalanine.[170] Alternatively, an asymmetric alkylation strategy was also possible, which was originally developed by O'Donnell and has been emerged as a well-known method for the synthesis of unnatural amino acids.[83]

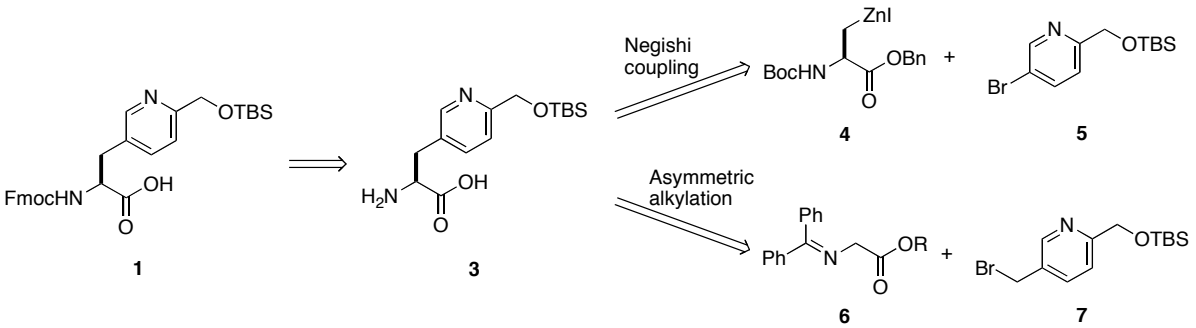

Figure 2.2: Retrosynthetic analysis of Fmoc-HPA(OTBS)-OH

2.2.1.2 Synthesis of intermediates 4-7

Intermediate **4**[170] and **6**[171] were prepared according to the procedures reported in the literature, while the synthesis of **5** and **7** is described in Scheme 2.1. Initially intermediates **5** and **7** were prepared from commercially available 2,5-dibromopyridine (**8**)[172] (Scheme 2.1, Route 1). The sequence began with a selective lithium halogen exchange reaction of **8**, which upon *in situ* formylation followed by reduction furnished **9** in 65% yield. Protection of the hydroxymethyl moiety as a silyloxy ether gave **5**, which upon a second sequence of lithium halogen exchange/formylation/reduction produced alcohol **10**. The transformation of **10** to bromide **7** was straightforward and achieved through Mitsunobu conditions. Although gram quantities of bromide **7** could be prepared via this route in convenient yields, it required rigorous dry reaction conditions and column chromatographic purifications. To make the synthesis more amenable to scale up, we developed an alternate route for **7** (Scheme 1, Route 2). In this route, **13** was synthesized from commercially available **11** via selective reduction of **11** to **12** followed by silyloxy ether protection as described previously.[173,174] Reduction of the C5 ester functionality of **13** by bis-(methoxyethoxy) aluminum hydride produced alcohol **10**. This route did not involve any rigorous dry reaction condition or chromatographic purification. Finally, the alcohol **10** was transformed into corresponding bromide **7**. As a keynote, the bromide **7** is unstable and decomposes within few days upon storage; therefore it should be prepared and used as soon as possible.

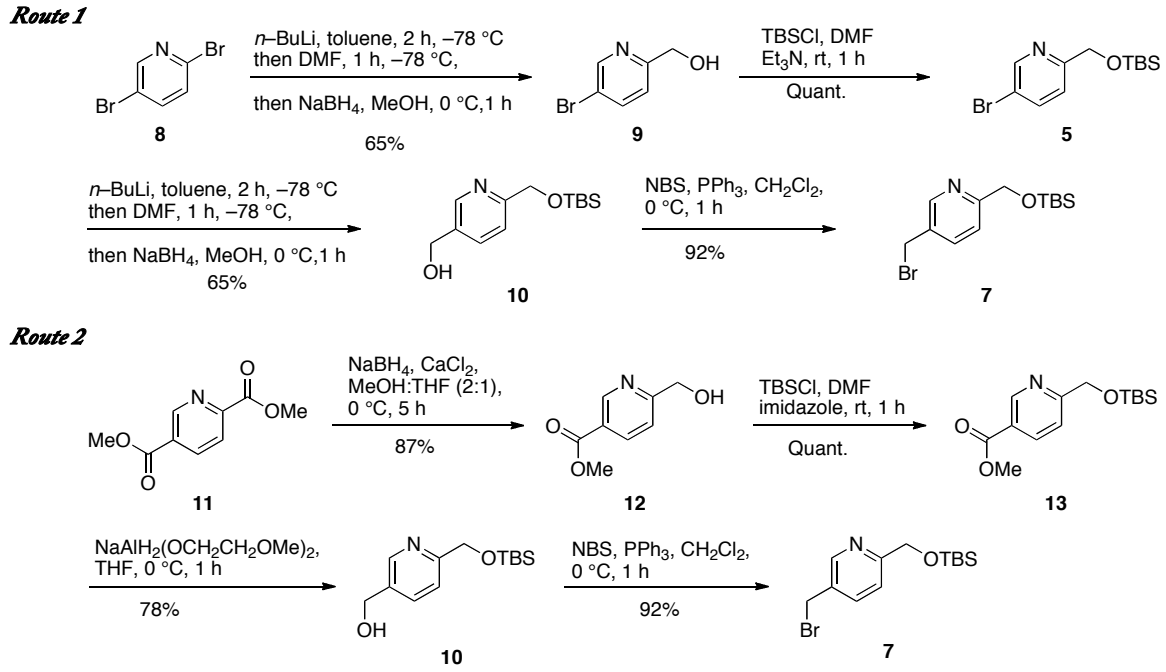

Scheme 2.1: Two routes for the synthesis of bromide intermediates **5** and **7**

2.2.1.3 Forward synthesis of Fmoc-HPA(OTBS)-OH (1)

We began the synthesis of Fmoc-HPA(OTBS)-OH (**1**) via the Negishi coupling between intermediates **4** and **5** using the literature procedure for preparation of 2-pyridylalanine.[170] Unfortunately, the intermediate **4** decomposed under the reaction conditions used for the Negishi coupling, presumably via β-hydride elimination to produce dehydroalanine as a major product. Even after several trials with various palladium catalysts we could not suppress this undesired side reaction. Hence we decided to pursue the asymmetric alkylation strategy.

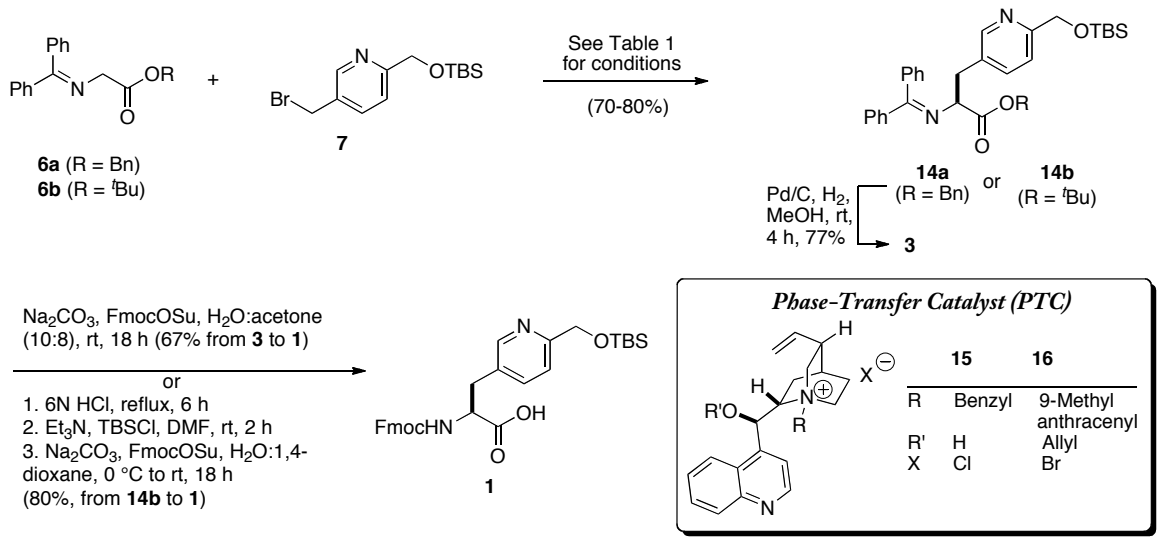

Scheme 2.2: Asymmetric alkylation reaction and synthesis of Fmoc-HPA(OTBS)-OH

The alkylation strategy began with a reaction between **6a** and **7** in the presence of a base and a phase transfer catalyst (PTC, Scheme 2.2). A racemic alkylation of **6a** with bromide **7** using the achiral PTC tetrabutyl ammonium hydrogen sulfate was straightforward and furnished racemic **14a** in 88% yield (Table 1, entry 1).[74,83] Unfortunately alkylation reactions between **6a** and **7** with chiral PTCs (**15**[175] or **16**[176]) gave corresponding alkylation product **14a** in good yield (46-88%) but in low to moderate ee (11-79%) under a variety of conditions (Table 1, entries 3-6).[177] Fortunately, substitution of the benzyl ester substrate **6a** for its *tert*-butyl ester congener **6b** along with *N*-(9-methylanthracenyl)-*O*-allyl-cinchonidine bromide (**17**)[176] as a chiral PTC and $CsOH{\cdot}H_2O$ as a base at –30 °C furnished **14b** in 87% yield and 92% ee (Table 1, entry 7).[83,176] To make the synthesis amenable to scale up, the reaction was optimized further where the base and temperature were changed (Table 1, entry 8-9). Deprotection of the benzyl ester derivative **14a** was straightforward and produced **3** in 77% yield that was transformed into the target **1**. In contrast, the deprotection of *tert*-butyl ester moiety of **14b** in the presence of acid labile silyloxy ether was troublesome. Therefore,

a global deprotection of **14b** with 6N HCl, followed by reprotection with TBSCl and Fmoc-OSu was performed to obtain **1** in 80% yield over the three steps.

Table 2.1: Optimization of asymmetric alkylation reaction for the synthesis of **14**

Entry	PTC (mol%)	R	Base	T (°C)	Yield	ee
1	TBAH[a] (20)	Bn	50% NaOH	0	88%[d]	racemic
2	TBAI[b] (20)	^{t}Bu	50% NaOH	0	70%[d]	racemic
3	**15** (20)	Bn	50% NaOH	0	88%[d]	11%
4	**15** (20)	Bn	CsOH·H_2O	–78	10%[e]	nd[c]
5	**16** (20)	Bn	CsOH·H_2O	–78	46%[e]	79%
6	**16** (20)	Bn	CsOH·H_2O	–30	74%[e]	72%
7	**16** (20)	^{t}Bu	CsOH·H_2O	–30	87%[e]	92%
8	**16** (20)	^{t}Bu	50% NaOH	0	80%[d]	93%
9	**16** (5)	^{t}Bu	50% NaOH	0	70%[d]	93%

[a] TBAH: tetrabutyl-ammonium hydrogensulphate (Bu_4NHSO_4); [b]TBAI: tetrabutyl-ammonium iodide; [c]nd = not determined.

2.2.1.4 Determination of enantiomeric excess

Attempts to determine the enantiomeric excess of **14a** and **14b** using chiral HPLC failed due to lack of separation of two enantiomers on a Chiracel-OD column. Therefore a benzophenone moiety of **14a** and **14b** was selectively removed via a transamination reaction. The resulting amino esters were converted into diastereomeric products via the reaction with α-methylbenzylisocyanate (Figure 2.3). Diastereomeric ratios were determined by ^{1}H NMR analysis using integration of peaks at 8.15 and 8.10 ppm for **14a** and 8.21 and 8.15 ppm for **14b**.

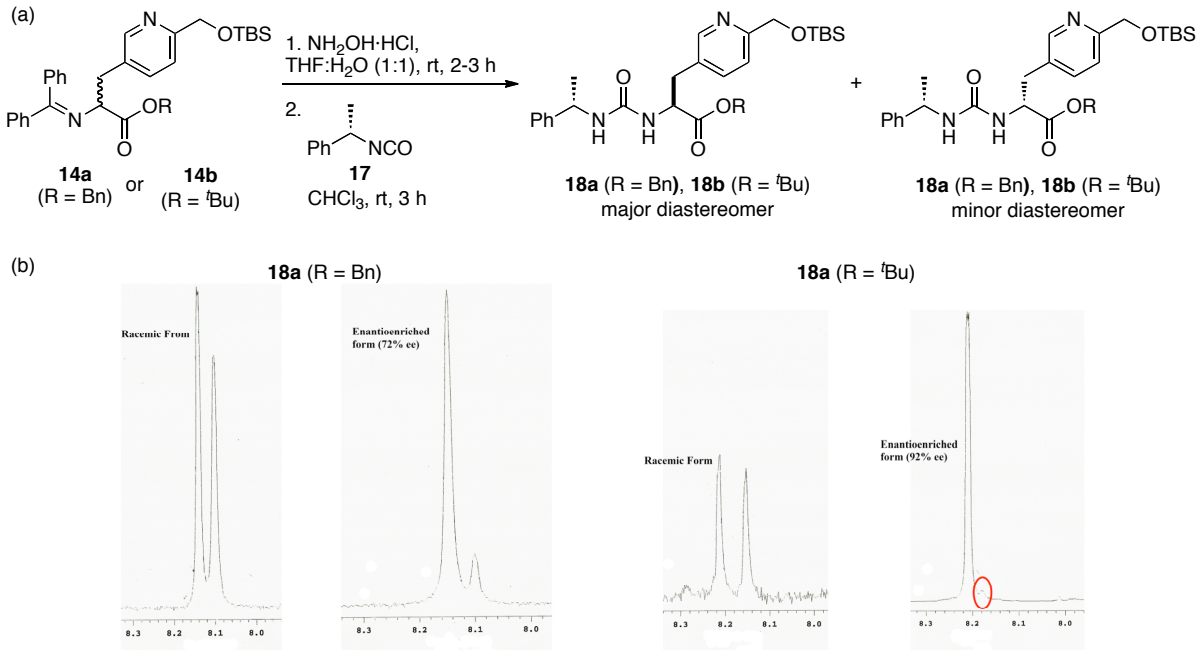

Figure 2.3: Determination of enantiomeric excess. (a) Transformation of **14a** or **14b** into corresponding diastereomers **18a** or **18b** (b) Determination of diastereomeric ratio by ^{1}H NMR

2.2.2 Development of the divergent strategy

2.2.2.1 Development of the divergent strategy via solution phase synthesis

The divergent strategy was initially developed on a model dipeptide substrate **2** via solution phase synthesis. A model dipeptide **2** was synthesized by the *N*-acetylation of racemic H-HPA(OTBS)-OH (**3**), followed by coupling the *C*-terminus with glycine benzyl ester, which furnished the target substrate **2** in 60% overall yield (Scheme 2.3). The next objective was to develop reaction conditions that could elaborate the pyridyl moiety of **2** into various ligands via solution phase syntheses, with the goal that these conditions could be

applied towards solid phase peptide syntheses in the future. Towards this goal, a silyloxy ether side chain of **2** was deprotected using buffered TBAF to unveil the corresponding alcohol, which was transformed into chloride **19** via tosylation followed by its *in situ* displacement with lithium chloride.

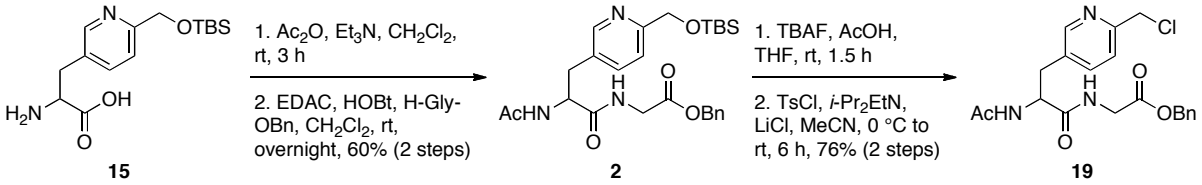

Scheme 2.3: Synthesis of model dipeptide substrate **19** and transformation of the silyloxy ether moiety to the chloride

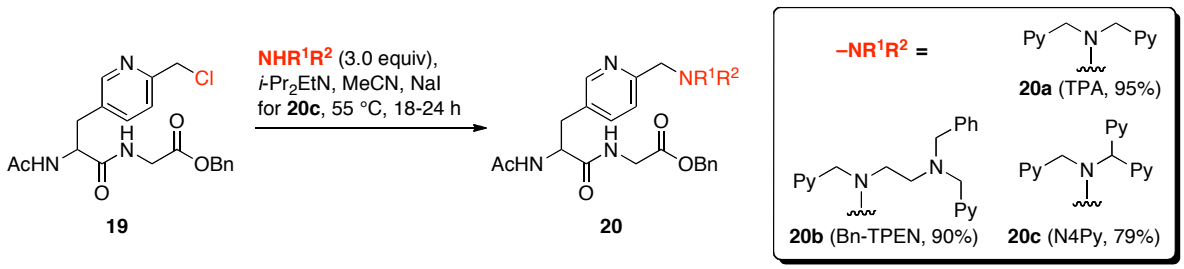

Scheme 2.4: Incorporation of TPA, Bn-TPEN and N4Py into chloride substrate **19**

After developing milder conditions for the silyloxy ether cleavage and chlorination, the next goal was to elaborate the chloromethyl pyridyl functionality of **19** into a variety of non-heme ligands via displacement of the chloride by various secondary amines. The reaction of chloride **19** with excess of bis-(2-picolylamine) in acetonitrile furnished a TPA attached dipeptide substrate **20a** in excellent yield (Scheme 2.4). These conditions were also compatible with relatively more complex secondary amines as demonstrated by incorporation of Bn-TPEN (**20b**) and N4Py (**20c**) into the same dipeptide precursor **19**. A catalytic amount

of sodium iodide was necessary to obtain a better conversion when a hindered secondary amine was used to prepare **20c**.

2.2.2.2 Application of the divergent strategy to solid phase synthesis

The ultimate goal of this project was to demonstrate the applicability of the divergent strategy on SPPS. Towards this goal, a dipeptide substrate (Ac-HPA(OTBS)-Gly-Wang Resin) was constructed in such a way that the *C*-terminus is attached to resin. Conditions developed for the silyloxy ether cleavage and chlorination via solution phase synthesis were conveniently performed on SPPS after some optimization, and using these conditions Ac-HPA(Cl)-Gly-Wang Resin was synthesized. *N*-alkylation of the Wang resin bound chloride followed by acidolytic cleavage from resin gave the corresponding TPA-dipeptide in ~70% purity as judged by NMR analysis. Unfortunately, attempts to incorporate N4Py into the same chloride precursor gave a complex mixture of products. At this point, other colleagues continued the project further and demonstrated that the replacement of the Wang resin with the Rink amide resin not only furnishes the corresponding TPA and N4Py dipeptide conjugates but also facilitates the purification of the resulting non-heme ligand-peptide conjugates (Scheme 2.5). In this study Tomasz Respondek has also demonstrated the functional group compatibility of these conditions by synthesizing TPA-heptapeptide **23**, while Selma Ulku has broadened the scope of the divergent strategy by applying the method to peptides containing two other unnatural amino acids (**22a-c**) as well as by attaching multiple copies of TPA into the same peptide chain (**24**-**25**).[98]

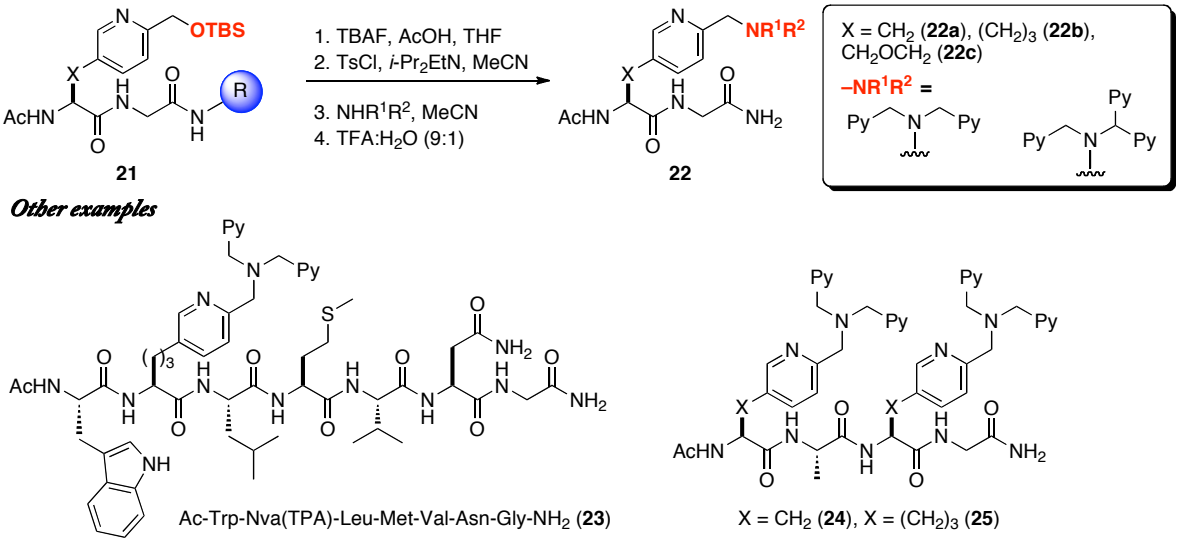

Scheme 2.5: Synthesis of peptide-ligand conjugates via solid phase peptide synthesis

2.3 Discussion

2.3.1 Optimization of key intermediates and Fmoc-HPA(OTBS)-OH

A fundamental requirement for the divergent strategy was an efficient and scalable method for the synthesis of intermediates **6-7** as well as an unnatural amino acid **1**. Towards this, intermediate **6a** and **6b** were easily synthesized by transamination between benzophenone imine and glycine ester derivatives, while two routes were developed for the synthesis of an intermediate **7**. In the first route, a selective lithium halogen exchange of 2,5-dibromopyridine (**8**) was attributed to a non-coordinative nature of toluene, which facilitated the coordination of lithium to the nitrogen of pyridine and eventually resulted in the C2 selectivity (Scheme 2.1, Route 1). For an alternate route, a selective reduction of dimethyl pyridine-2,5-dicarboxylate (**11**) was performed in THF/MeOH instead of THF/EtOH as described in the literature (Scheme 2.1, Route 2). This modification was important during the scale up of **12** since it eliminated issues derived from the transesterification of **11** by EtOH.

This selective reduction of the C2 ester moiety of **11** was attributed to an increased electrophilicity of the C2 ester that was achieved through a chelation of calcium ion to nitrogen and C2 carbonyl group. In contrast, the reduction of C5 ester moiety of **13** required harsher conditions and was accomplished using sodium bis(2-methoxyethoxy)aluminum hydride. In either route, a bromination of **10** was achieved using the Mitsunobu conditions.

When the Negishi coupling was utilized for the synthesis of Fmoc-HPA(OTBS)-OH (**1**), dehydroalanine was obtained instead of the target amino acid. The slow rate for the oxidative addition of palladium to the C-Br bond of **5** compared to the relatively faster β-hydride elimination of **4** was attributed to this undesired side reaction. Towards the asymmetric alkylation route, alkylation of **6** with bromide **7** was straightforward but the asymmetric alkylation required some optimization to obtain the acceptable enantioselectivity. We began the asymmetric alkylation studies on benzyl ester derivative **6a** because it was certainly advantageous over its *tert*-butyl ester congener **6b** since the benzophenone imine as well as the benzyl ester group of the resulting alkylation product **14a** could be cleaved by hydrogenolysis. However, none of the conditions produced the acceptable range of ee when **6a** was employed (Table 1, entry 3-6). Interestingly, employing **6b** in the similar reaction conditions significantly improved the %ee of the alkylation product (Table 1, entry 6 vs. 7), which highlights the importance of the steric bulk of the ester moiety in this reaction. Furthermore, the enantioselectivity of **14b** was unaffected when the reaction was performed with NaOH as the base at 0 °C that made the synthesis of **14b** amenable to scale up (Table 1, entry 8-9).

During the synthesis of **1** from **14b**, the selective deprotection of the *tert*-butyl group in **14b** was challenging due to the presence of an acid labile silyloxy ether moiety. An

attempt to deprotect benzophenone imine of **14b** with $NH_2OH{\cdot}HCl$[178] followed by a selective cleavage of *tert*-butyl ester with TMSOTf/2,6-lutidine[179] furnished the desired amino acid **3**, however in very low yields. Therefore, a three-step global deprotection/reprotection/Fmoc protection sequence was adopted, which produced **1** in 80% overall yield and hence was not optimized further.

2.3.2 Development of the divergent strategy

We began our investigations for the divergent strategy via solution phase synthesis, since the solution phase synthesis allows the isolation and characterization of key intermediates. A model dipeptide **2** used in this study was embraced with benzyl ester at *C*-terminus and acetyl functionality at *N*-terminus to mimic the peptide chain bound to the Wang resin. The first step of the divergent strategy, deprotection of the silyloxy ether moiety to obtain the corresponding alcohol, was straightforward but the transformation of an alcohol to a better leaving group required some optimization (Scheme 2.3, **2** to **19**). After several attempts to tosylate or brominate the hydroxymethyl moiety of **2**, the chlorination was found to be an ideal leaving group and provided an appropriate balance between the reactivity and the stability of **19**.

An elaboration of the chloromethyl pyridyl moiety of **19** into a variety of pyridyl containing non-heme ligands was the key step of the divergent strategy and achieved by heating **19** with excess secondary amines (Scheme 2.4). Excess of secondary amine was used in this reaction considering that these conditions would eventually be applied to SPPS and it would be advantageous to study the effect of excess reagents on this transformation. During optimization we also identified that the *N*-alkylation is sluggish with hindered secondary

amines (e.g. synthesis of **20c**). Incorporation of a catalytic amount of sodium iodide significantly improved the conversion, presumably through *in situ* iodination of **19**. However, we also noticed that the use of excess sodium iodide was detrimental and resulted into a complex mixture of products. Apart from the difficulties associated with synthesis, the purification of peptide-ligand conjugates prepared by solution phase synthesis was also challenging. In a typical procedure, after completion of the reaction, a reaction mixture was concentrated, an excess of secondary amine was removed by alumina column chromatography and a second purification was usually performed on preparative HPLC using 0.1%TFA:MeCN as a mobile phase. Isolation of the purified conjugates by evaporation of the acidic HPLC fractions caused the decomposition of the product, presumably through a hydrolysis of benzyl ester moiety of **20**. Therefore, peptide-ligand conjugates were isolated by neutralization of HPLC fractions followed by extraction with organic solvent.

Efforts to extend the divergent strategy from solution phase synthesis to SPPS were initiated on a model dipeptide bound to Wang resin, since its *C*-terminus was analogues to the model substrate **2**. Two cycles of the buffered TBAF were required to ensure the complete cleavage of silyloxy ether on SPPS. In addition, acetonitrile was found to be a critical solvent for the chlorination reaction, as the reaction performed in DMF furnished a complex mixture of products. Moreover, we were surprised to note that dry reaction conditions were not necessary while performing the chlorination on SPPS. In some instances it was necessary to repeat the chlorination step to obtain the efficient conversion on SPPS. Unfortunately, the *N*-alkylation reaction to incorporate N4Py into Wang resin bound peptide precursor resulted in a mixture of unidentifiable products. This result was indicative of the slow alkylation of the hindered amines observed in solution phase synthesis. Fortunately

replacement of the Wang resin with Rink amide resin, which possesses a stable amide linkage between peptide and resin, allowed the incorporation of N4Py as well as other non-heme ligands into peptides via SPPS (Scheme 2.5).

2.4 Conclusion

A divergent strategy for the incorporation of pyridyl containing non-heme ligands into peptides has been developed. To facilitate the development of the divergent strategy, two routes for the synthesis of an intermediate **7** were established. Straightforward access to this intermediate set up a foundation for the synthesis of an unnatural amino acid **1**. The amino acid **1** was synthesized via asymmetric alkylation to access the enantiomerically enriched building block for the divergent strategy. During optimization of an asymmetric alkylation route it has been established that the *tert*-butyl ester moiety in **6b** is critical to obtain high enantioselectivity of **14b**. Although, the transformation of **14b** to **1** required a sequence of deprotection/reprotection steps, convenient conditions were developed to access multi-gram quantities of the target Fmoc-HPA(OTBS)-OH (**1**) in good yields. Next, the development of the divergent strategy was demonstrated using the model dipeptide substrate **2** in solution phase synthesis. Using this method TPA, Bn-TPEN and N4Py were incorporated into **2**. These conjugates could be used to study the coordination chemistry of non-heme ligand-peptide conjugates as well as in models to study the chemistry of ferryl-peptide conjugates. The divergent strategy was further extended to SPPS where the functional group compatibility and the scope of this method were explored. With these studies, the divergent strategy could provide an easy access to the library synthesis of non-heme ligand-peptide conjugates.

2.5 Experimental Section

2.5.1 General consideration

All reagents were purchased from commercial suppliers and used as received. Rink amide MBHA resin (200-400 mesh, 0.75 mmol/g, 1% DVB) was purchased from Chem-Impex International Inc. NMR spectra were recorded on a Varian FT-NMR Mercury-300 or 400 Spectrometer. Mass spectra were recorded on a Waters ZQ2000 single quadrupole mass spectrometer using an electrospray ionization source. IR spectra were recorded on a Nicolet FT-IR spectrophotometer. HPLC was performed on an Agilent 1200 Preparative Purification System equipped with a multi-wavelength detector. Column purifications were performed using flash chromatography technique and silica gel as a stationary phase unless mentioned otherwise. All reactions were performed under ambient atmosphere unless otherwise noted. Anaerobic reactions were performed in Schlenk tubes. MALDI-TOF analysis was performed on a MALDI-TOF mass spectrometer using the reflectron mode.

2.5.2 Experimental procedures and tabulated characterization data for new compounds

(6-(((*tert*-butyldimethylsilyl)oxy)methyl)pyridin-3-yl)methanol (10).

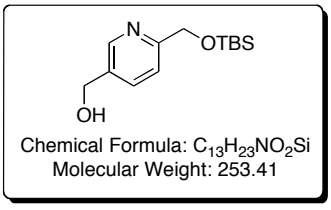

Chemical Formula: $C_{13}H_{23}NO_2Si$
Molecular Weight: 253.41

Route 1:

A solution of compound **5**[172,180] (8.50 g, 2.81 mmol) and distilled toluene (255 mL) was purged with argon for 10 min. The reaction mixture was cooled to –78 °C and *n*-BuLi (1.6M solution in hexanes, 21.0 mL, 3.37 mmol) was added dropwise over 30 min, during which the color of the reaction mixture changed from colorless to reddish orange. The reaction mixture was maintained for 1.5 h at –78 °C and *N*,*N*-dimethyl formamide (2.83 mL, 3.66 mmol) was added over 5 min. The reddish orange solution was maintained at –78 °C for other 1.5 h. The reaction mixture was warmed to 0 °C and methanol (42 mL) was added dropwise over the period of 10 min. $NaBH_4$ (1.06 g, 2.81 mmol) was added to it and the resulting red solution was maintained for 1 h at 0 °C, during which the color of the solution changed from red to yellow. A solution of 0.1M NaOH (100 mL) was added and the reaction mixture was warmed to rt. The reaction mixture was maintained at rt for 15 min and mixed with water (300 mL). After extraction of the aqueous layer with ethyl acetate (4 × 50 mL), the combined organic layer was dried over anhydrous Na_2SO_4 and concentration to obtain crude product. The crude product was recrystallized from cold hexanes to obtain **10** as off-white solid (4.65 g, 65%).

Route 2:

A mixture of **12**[173] (10.0 g, 59.2 mmol), imidazole (6.05 g, 88.8 mmol) and DMF (130 mL) was maintained at rt under a nitrogen atmosphere for 5 min. TBSCl (9.80 g, 65.1 mmol) was added and the reaction mixture was maintained at rt for 2 h. After consumption of the starting material, as judged by TLC analysis, the reaction mixture was mixed with H_2O (250 mL). The aqueous layer was extracted with EtOAc (3 × 75 mL). The combined organic layer was dried over anhydrous Na_2SO_4 and concentrated to obtain the crude product **13** as a yellow viscous oil (16.6 g, quant.)

A solution of **13**[174] (5.00 g, 17.8 mmol) and dry THF (125 mL) was maintained at 0 °C under a nitrogen atmosphere for 10 min. A solution of $NaAlH_2(OCH_2CH_2OMe)$ in toluene (65% w/w, 12.7 mL, 40.8 mmol) was added dropwise over 25 min, resulting in an orange solution. The solution was maintained at 0 °C for 2 h. After consumption of the starting material, as judged by TLC analysis, the reaction mixture was quenched by dropwise addition of MeOH (4.5 mL) and a solution of 0.1M NaOH (10 mL) was added. The reaction mixture was combined with H_2O (200 mL) and the aqueous layer was extracted with EtOAc (3 × 75 mL). The combined organic layer was dried over anhydrous Na_2SO_4 and concentrated to obtain the crude product which upon crystallization from cold hexanes (10 mL) furnished **10** as off-white crystalline solid (3.50 g, 78%). mp = 50-51 °C; ^{1}H NMR (400 MHz, $CDCl_3$) δ 8.34 (brs, 1H), 7.69 (d, *J* = 8.1 Hz, 1H), 7.46 (d, *J* = 8.1 Hz, 1H), 4.76 (s, 2H), 4.64 (s, 2H), 3.57 (b, 1H), 0.91 (s, 9H), 0.07 (s, 6H); ^{13}C NMR (100 MHz, $CDCl_3$) δ 160.4, 147.2, 135.8, 134.7, 119.9, 65.7, 62.2, 25.9, 18.3, –5.4; IR (thin film) 3211 (b), 2953, 2927, 2856, 1604, 1573, 1491, 1458, 1399, 1377, 1358, 1341, 1255, 1102, 1060, 1031, 1006, 860, 839, 776, 670, 647 cm^{-1}; LRMS (ESMS) calcd for $C_{13}H_{24}NO_2Si$ $(M+H)^+$ 254, found: 254.

5-(bromomethyl)-2-(((*tert*-butyldimethylsilyl)oxy)methyl)pyridine (7).

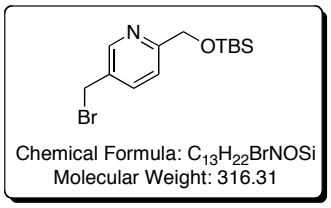

A mixture of (6-((*tert*-butyldimethylsilyloxy)methyl)pyridin-3-yl)methanol **10** (4.65 g, 18.4 mmol) and CH_2Cl_2 (93 mL) was maintained at 0 °C under a nitrogen atmosphere for

10 min. *N*-bromosuccinimide (3.60 g, 20.2 mmol) and triphenylphosphine (5.30 g, 20.2 mmol) were added successively over 15 min. The yellow solution was maintained at 0 °C for 2 h. After consumption of the starting material, as judged by TLC analysis, the reaction mixture was concentrated without warming and the crude product was purified by silica gel chromatography (5% to 15% EtOAc:hexanes) to obtain compound **7** as a pink oil (5.33 g, 92%). *Note: Compound 7 decomposes upon storage, hence should be used immediately.* ^{1}H NMR (400 MHz, $CDCl_3$) δ 8.48 (s, 1H), 7.71 (d, J = 8.1 Hz, 1H), 7.48 (d, J = 8.1 Hz, 1H), 4.80 (s, 2H), 4.44 (s, 2H), 0.93 (s, 9H), 0.09 (s, 6H); ^{13}C NMR (100 MHz, $CDCl_3$) δ 161.6, 148.7, 137.3, 131.7, 120.0, 65.8, 29.8, 25.9, 18.3, –5.4; IR (thin film) 2954, 2929, 2885, 2857, 1600, 1571, 1487, 1471, 1393, 1369, 1252, 1101, 1026, 1006, 938, 838, 778, 725, 670 cm^{-1}; LRMS (ESMS) calcd for $C_{13}H_{23}BrNOSi$ $(M+H)^+$ 316, found: 316.

General Procedures for Preparation of 14a and 14b.

General Procedure A: A mixture of **6a**[171] or **6b**[171] (16.7 mmol), PTC (See Table 2.1) and 7:3 toluene:CH_2Cl_2 (72 mL) was cooled to 0 °C under a nitrogen atmosphere. A 50% aqueous NaOH solution (24.5 mL) was added at 0 °C. 5-(bromomethyl)-2-((*tert*-butyldimethylsilyloxy)methyl)pyridine **7** (5.30 g, 16.7 mmol) was dissolved in 7:3 toluene:CH_2Cl_2 (11 mL) and this solution was added dropwise to the reaction mixture at 0 °C over 10 min. The reaction mixture was stirred vigorously at 0 °C for 3-12 h. After consumption of the starting material as judged by TLC analysis (20% EtOAc:hexanes), the reaction mixture was combined with cold H_2O (40 mL). The organic layer was separated and the aqueous layer was extracted using CH_2Cl_2 (3 × 20 mL). The combined organic layer was dried over anhydrous Na_2SO_4 and concentrated to obtain a brown viscous oil. The crude

product was purified by silica gel chromatography (5% to 15% EtOAc:hexanes) to afford the corresponding product **14a** or **14b**.

General Procedure B: A mixture of **6a**[171] or **6b**[171] (0.79 mmol), **15** or **16** (See Table 2.1), 5-(bromomethyl)-2-((*tert*-butyldimethylsilyloxy)methyl)pyridine **7** (250 mg, 0.79 mmol) and CH_2Cl_2 (2.3 mL) was cooled to the appropriate temperature (See Table 2.1) under a nitrogen atmosphere. Solid $CsOH{\cdot}H_2O$ (1.32 g, 7.89 mmol) was added and the reaction mixture was stirred vigorously for 3-12 h. After consumption of the starting material as judged by TLC analysis (20% EtOAc:hexanes), the reaction mixture was diluted with Et_2O (20 mL) and then combined with cold water (30 mL). The organic layer was separated and the aqueous layer was extracted with CH_2Cl_2 (3 × 15 mL). The combined organic layers were dried over anhydrous Na_2SO_4 and concentrated to get a brown viscous oil. The crude product was purified by silica gel chromatography (5% to 15% EtOAc:hexanes) to afford **14a** or **14b**.

(S)-benzyl 3-(6-(((*tert*-butyldimethylsilyl)oxy)methyl)pyridin-3-yl)-2-((diphenyl methylene)amino)propanoate (14a).

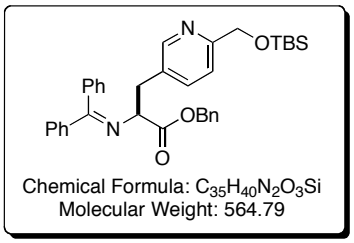

Compound **14a** was synthesized according to general procedure A (Table 2.1, entry 1, 3) or general procedure B (Table 2.1, entry 4-6). ^{1}H NMR (400 MHz, $CDCl_3$) δ 8.20 (s, 1H), 7.55 (d, J = 7.3 Hz, 2H), 7.38-7.22 (m, 13H), 6.63 (d, J = 7.3 Hz, 2H), 5.19 (d, J = 13.0 Hz, 1H), 5.12 (d, J = 13.0 Hz, 1H), 4.76 (s, 2H), 4.26 (dd, J = 8.9, 4.9 Hz, 1H), 3.27-3.16 (m, 2H), 0.91 (s, 9H), 0.72 (s, 6H); ^{13}C NMR (100 MHz, $CDCl_3$) δ 171.5, 171.1, 159.3, 149.7,

139.0, 138.0, 135.9, 135.7, 131.4, 130.5, 128.8, 128.5, 128.5, 128.3, 128.2, 128.1, 128.0, 127.4, 119.5, 66.7, 66.6, 65.9, 36.4, 25.9, 18.3, –5.4; IR (thin film) 3061, 3032, 2954, 2928, 2885, 2856, 1741, 1622, 1599, 1574, 1489, 1471, 1446, 1397, 1372, 1314, 1287, 1252, 1163, 1128, 1104, 1029, 1004, 939, 910, 838, 779, 696, 640 cm^{-1}; LRMS (ESMS) calcd for $C_{35}H_{41}N_2O_3Si$ $(M+H)^+$ 565, found: 565.

(S)-*tert*-butyl 3-(6-(((*tert*-butyldimethylsilyl)oxy)methyl)pyridin-3-yl)-2-((diphenyl methylene)amino)propanoate (14b).

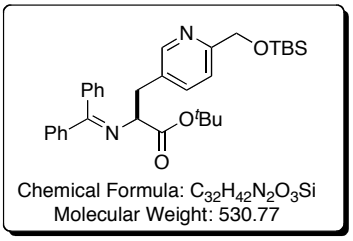

Compound **14b** was synthesized according to general procedure A (Table 2.1, entry 2, 8-9) or general procedure B (Table 2.1, entry 7). ^1H NMR (400 MHz, $CDCl_3$) δ 8.23 (s, 1H), 7.58 (d, J = 7.3 Hz, 2H), 7.43-7.26 (m, 8H), 6.72 (d, J = 6.5 Hz, 2H), 4.79 (s, 2H), 4.13-4.10 (m, 1H), 3.20-3.14 (m, 2H), 1.43 (s, 9H), 0.92 (s, 9H), 0.08 (s, 6H); ^{13}C NMR (100 MHz, $CDCl_3$) δ 170.4, 170.0, 158.8, 149.4, 138.9, 137.7, 135.9, 131.5, 129.9, 128.4, 128.0, 127.9, 127.6, 127.1, 119.1, 88.0, 66.9, 65.6, 36.1, 27.6, 25.5, 18.0, –5.7; IR (thin film) 3059, 2955, 2929, 2885, 2856, 1734, 1624, 1599, 1574, 1488, 1472, 1462, 1446, 1394, 1368, 1314, 1288, 1253, 1151, 1104, 1030, 1006, 977, 938, 910, 840, 815, 779, 731, 696, 670, 641 cm^{-1}; $[\alpha]$ = –132° (c = 1.0, MeOH); HRMS (ESMS) calcd for $C_{32}H_{43}N_2O_3Si$ $(M+H)^+$ 531.3043, found: 531.3037.

General Procedure for the Determination of Enantiomeric Excess.

A mixture of compound **14a** or **14b** (1 eq), 1:1 THF:H_2O and $NH_2OH{\cdot}HCl$ (3 eq) was stirred at rt for 3 h. After consumption of the starting material, as judged by TLC analysis, the reaction mixture was combined with H_2O. The aqueous layer was extracted using hexanes followed by CH_2Cl_2. The combined CH_2Cl_2 layer was dried over anhydrous Na_2SO_4 and concentrated to obtain the crude amino ester.

A solution of (*S*)-α-methylbenzylisocyanate (1.2 eq), amino ester and $CHCl_3$ was maintained at rt for 3 h under a nitrogen atmosphere. The reaction mixture was concentrated under vacuum to obtain a crude oil that was analyzed by ^{1}H NMR spectroscopy. Ratios of diastereomers were determined as discussed in section 2.2.1.4.

(S)-2-amino-3-(6-((*tert*-butyldimethylsilyloxy)methyl)pyridin-3-yl)propanoic acid (3).

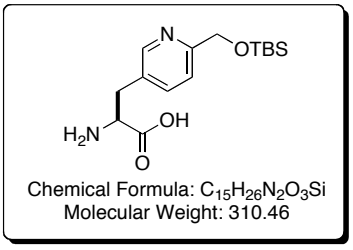

A mixture of **14a** (6.15 g, 10.9 mmol), MeOH (123 mL) and 10% Pd/C (50% w/w moisture, 615 mg) was stirred at rt under H_2 (1 atm) atmosphere for 5 h. After consumption of the starting material, as judged by TLC analysis, the reaction mixture was filtered through celite and the celite bed was washed with methanol. The combined filtrate was concentrated to obtain a sticky white solid, which upon triturating with Et_2O for 10 min furnished **3** as a white amorphous solid. The white solid was isolated by filtration and washed with Et_2O (2.60 g, 77%). ^{1}H NMR (400 MHz, CD_3OD) δ 8.38 (s, 1H), 7.81 (dd, J = 8.1, 2.4 Hz, 1H), 7.54 (d, J = 7.3 Hz, 1H), 4.78 (s, 2H), 3.81 (dd, J = 8.1, 4.9 Hz, 1H), 3.30-3.10 (m, 2H), 0.96 (s, 9H), 0.13 (s, 6H); ^{13}C NMR (100 MHz, CD_3OD) δ 173.2, 161.1, 150.0, 139.8, 132.0,

121.9, 66.5, 57.0, 35.0, 26.3, 19.2, –5.3; IR (KBr) 3405 (b), 2956, 2930, 2887, 2858, 1604, 1524, 1492, 1472, 1463, 1442, 1398, 1361, 1333, 1254, 1108, 838, 778 cm^{-1}; LRMS (ESMS) calcd for $C_{15}H_{27}N_2O_3Si$ $(M+H)^+$ 311, found: 311.

***(S)*-2-(((9H-fluoren-9-yl)methoxy)carbonylamino)-3-(6-((tert-butyldimethylsilyloxy) methyl)pyridin-3-yl)propanoic acid (1).**

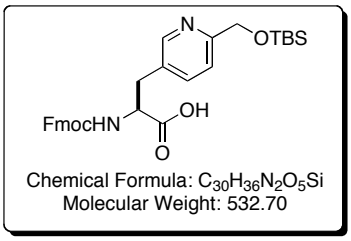

From compound (3): A mixture of compound **3** (1.00 g, 3.22 mmol), Na_2CO_3 (324 mg, 3.06 mmol) and H_2O (10 mL) was maintained at 0 °C for 5 min. The suspension of FmocOSu (1.09 mg, 3.22 mmol) in acetone (8 mL) was added and the reaction mixture was maintained at 0 °C for 1 h. The reaction mixture was allowed to warm up to rt and maintained overnight. Throughout the reaction period the reaction mixture was maintained at pH 7-8. After the consumption of the starting material, as judged by TLC analysis, the reaction mixture was combined with H_2O (130 mL) and the aqueous layer was washed with hexanes (2 × 30 mL). The aqueous layer was acidified to pH 4-5 by slow addition of 10% aqueous citric acid and extracted with EtOAc (5 × 30 mL). The combined EtOAc layers were washed with saturated NaCl (aq). The EtOAc layer was dried over anhydrous Na_2SO_4 and concentrated to obtain the crude product (1.14 g, 67%).

From compound (14b): A solution of compound **14b** (700 mg, 1.32 mmol) and 6N HCl (3.5 mL) was refluxed for 6 h. The reaction mixture was combined with H_2O (5 mL) and extracted with Et_2O (2 × 10 mL). The aqueous layer was concentrated under high vacuum to

obtain a crude product. The crude product was dissolved in H_2O (10 mL) and concentrated under high vacuum (twice) to remove excess HCl. The crude product was dried on high vacuum for 3-4 h to obtain an off-white solid, which was found to be hygroscopic and stored under nitrogen or used immediately for the next reaction.

A mixture of the off-white solid (325 mg, 1.20 mmol), Et_3N (2.8 mL, 19.8 mmol) and DMF (11.5 mL) was maintained at rt under nitrogen atmosphere for 5 min. TBSCl (2.00 g, 13.2 mmol) was added and the reaction mixture was maintained for 2 h under nitrogen atmosphere. The reaction mixture was combined with 0.1% aq Na_2CO_3 (50 mL) and washed with Et_2O (3 × 15 mL). An off-white solid formed that was isolated and combined with the aqueous layer. A mixture of an off-white solid and aqueous layer was cooled to 0 °C and a solution of FmocOSu (489 mg, 1.45 mmol) in 1,4-dioxane (7 mL) was added over 5 min. The reaction mixture was maintained at 0 °C for 1 h and then allowed to warm up to rt. The reaction mixture was maintained at rt overnight, combined with H_2O (50 mL) and extracted with hexanes (2 × 50 mL). The aqueous solution was acidified to pH 4-5 by slow addition of citric acid (10% aq). The aqueous solution was extracted with EtOAc (4 × 25 mL). The combined EtOAc layers were dried over anhydrous Na_2SO_4 and concentrated to obtain the product. The crude product was further purified by silica gel chromatography (0% to 5% MeOH:CH_2Cl_2) (605 mg, 86%). A small sample was recrystallized from MTBE:hexanes (1:2) for analysis. mp = 81-83 °C; ^{1}H NMR (400 MHz, CD_3OD) δ 8.34 (s, 1H), 7.76-7.70 (m, 3H), 7.57-7.43 (m, 3H), 7.38-7.24 (m, 4H), 4.72 (s, 2H), 4.46-4.41 (m, 1H), 4.34-4.28 (m, 1H), 4.19-4.07 (m, 2H), 3.30-3.20 (m, 1H), 3.03-2.93 (m, 1H), 0.91 (s, 9H), 0.06 (s, 6H); ^{13}C NMR (100 MHz, CD_3OD) δ 175.2, 160.2, 158.2, 149.8, 145.2, 142.5 139.8, 133.7, 128.7, 128.1, 126.3, 126.2, 121.5, 120.9, 67.9, 66.3, 56.6, 35.7, 26.3, 19.2, –5.3; IR (KBr) 3419 (b),

3065, 2953, 2928, 2887, 2856, 1713, 1606, 1536, 1450, 1401, 1335, 1253, 1106, 1053, 1007, 839, 779, 759, 740, 671, 621 cm^{-1}; $[\alpha] = -2.5°$ (c = 1.1, MeOH); HRMS (ESMS) calcd for $C_{30}H_{37}N_2O_5Si$ $(M+H)^+$ 533.2472, found: 533.2481.

Benzyl 2-(3-(6-((*tert*-butyldimethylsilyloxy)methyl)pyridin-3-yl)-2-ethanamido propanamido)ethanoate (2).

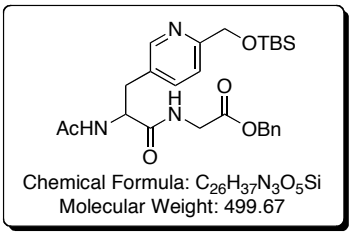

Acetic anhydride (0.4 mL, 3.86 mmol) was added to a mixture of compound **3** (1.00 g, 3.22 mmol), CH_2Cl_2 (25 mL) and Et_3N (2.20 mL, 16.1 mmol). The reaction mixture was maintained at rt under a nitrogen atmosphere for 3 h. After consumption of the starting material, as judged by TLC analysis, the reaction was combined with H_2O (40 mL). The aqueous layer was acidified to pH ~5 by slow addition of citric acid (10% aq). The organic layer was separated and the aqueous layer was extracted with CH_2Cl_2 (3 × 25 mL). *Note: Extracting the organic layer with sat. NaCl at this stage results in precipitation and hence the organic layer should never be washed with sat. NaCl.* The combined organic layers were dried over anhydrous Na_2SO_4 and concentrated to obtain crude Ac-HPA(OTBS)-OH as a yellow viscous semisolid (1.14 g, quantitative).

A mixture of crude Ac-HPA(OTBS)-OH (1.14 g, 3.32 mmol), H-Gly-OBn[181,182] (721 mg, 4.37 mmol), CH_2Cl_2 (35 mL), Et_3N (0.7 mL, 5.03 mmol), and HOBt (610 mg, 3.98 mmol) was maintained at rt under a nitrogen atmosphere for 5 min. EDAC (763 mg, 3.98 mmol) was added and the mixture was stirred vigorously overnight. The reaction mixture

was combined with CH_2Cl_2 (25 mL) and extracted with 5% aq $NaHCO_3$ (3 × 15 mL), sat. aq NH_4Cl (3 × 15 mL) and sat. aq NaCl (3 × 15 mL) respectively. The organic layer was separated, dried over anhydrous Na_2SO_4 and concentrated to obtain the crude **2** as viscous oil. Upon triturating with Et_2O at –20 °C, a white solid formed that was isolated by filtration and washed with cold Et_2O (1.17 g, 72%). mp = 98-100 °C; ^{1}H NMR (400 MHz, $CDCl_3$) δ 8.28 (s, 1H), 7.53 (d, *J* = 8.1 Hz, 1H), 7.39 (d, *J* = 8.1 Hz, 1H), 7.34-7.30 (m, 5H), 7.12 (brs, 1H), 6.57 (d, *J* = 8.1 Hz, 1H), 5.12 (s, 2H), 4.80-4.76 (m, 3H), 4.01-3.98 (m, 2H), 3.09 (dd, *J* = 14.6, 6.5 Hz, 1H), 2.90 (dd, *J* = 13.8, 7.3 Hz, 1H), 1.90 (s, 3H), 0.92 (s, 9H), 0.08 (s, 6H); ^{13}C NMR (100 MHz, $CDCl_3$) δ 171.1, 170.4, 169.2, 160.0, 149.2, 137.5, 135.0, 130.0, 128.6, 128.5, 128.3, 119.8, 67.2, 65.8, 53.6, 41.2, 34.9, 25.9, 23.0, 18.3, –5.4; IR (thin film) 3286 (b), 3067, 2954, 2929, 2886, 2856, 1751, 1649, 1546, 1471, 1456, 1374, 1254, 1188, 1105, 1030, 1005, 839, 778, 734, 697, 670 cm^{-1}; LRMS (ESMS) calcd for $C_{26}H_{38}N_3O_5Si$ $(M+H)^+$ 500, found: 500.

Benzyl 2-(3-(6-(chloromethyl)pyridin-3-yl)-2-ethanamidopropanamido)ethanoate (19).

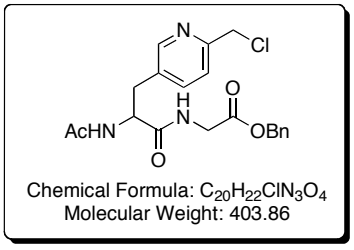

Chemical Formula: $C_{20}H_{22}ClN_3O_4$
Molecular Weight: 403.86

A mixture of compound **2** (300 mg, 600 μmol), acetic acid (34 μL, 600 μmol) and THF (4.2 mL) was maintained under a nitrogen atmosphere for 5 min. A 1M solution of TBAF in THF (1.8 mL, 1.80 mmol) was added and the reaction mixture was maintained for 1-1.5 h. After consumption of the starting material, as judged by TLC analysis, the reaction mixture was combined with H_2O (50 mL) and the solution was adjusted to pH ~ 8 using

Na_2CO_3 (sat. aq). The aqueous layer was extracted with CH_2Cl_2 (7 × 20 mL). The combined organic layers were dried over anhydrous Na_2SO_4 and concentrated to obtain the corresponding alcohol as a white solid. After triturating the solid with Et_2O overnight a white solid was isolated by decantation and used for the next reaction without purification (176 mg, 76%).

A mixture of the crude alcohol (50.0 mg, 0.13 mmol), flame dried LiCl (55 mg, 1.30 mmol), *i*-Pr_2EtN (46 μL, 0.26 mmol) and MeCN (1.9 mL) was maintained under a nitrogen atmosphere at 0 °C for 5 min and TsCl (37 mg, 0.19 mmol) was added under a nitrogen atmosphere. The reaction mixture was stirred at 0 °C for 1.5 h and then warmed to rt. The color of the reaction mixture changed from colorless to red. The red suspension was maintained at rt for 4 h. After consumption of the starting material, as judged by TLC analysis, the reaction mixture was decanted and the residues were rinsed with MeCN (5 mL). The combined MeCN layer was concentrated and the crude product was combined with CH_2Cl_2 (15 mL). The CH_2Cl_2 layer was extracted with an aq $NaHCO_3$ (pH ~ 9) solution (3 × 10 mL). The organic layer was dried over anhydrous Na_2SO_4 and concentrated to furnish the crude product **19** as a red oil. The crude product was purified by silica gel chromatography (0% to 5% MeOH:CH_2Cl_2) to obtain an orange oil (37 mg, 70%). ^{1}H NMR (400 MHz, $CDCl_3$) δ 8.35 (s, 1H), 7.55 (dd, *J* = 8.1, 1.6 Hz, 1H), 7.35-7.25 (m, 7H), 6.74 (d, *J* = 8.1 Hz, 1H), 5.12 (s, 2H), 4.83 (dd, *J* = 14.6, 7.3 Hz, 1H), 4.58 (s, 2H), 4.00 (d, *J* = 4.6 Hz, 2H), 3.11 (dd, *J* = 13.8, 6.5 Hz, 1H), 2.95 (dd, *J* = 13.8, 7.3 Hz, 1H), 1.90 (s, 3H); ^{13}C NMR (100 MHz, $CDCl_3$) δ 170.9, 170.4, 169.2, 155.2, 150.1, 138.0, 135.0, 131.6, 128.7, 128.6, 128.4, 122.6, 67.3, 53.5, 46.4, 41.3, 34.9, 23.0; IR (thin film) 3284 (b), 3065, 1748, 1650, 1544, 1440, 1384, 1190, 753, 697 cm^{-1}; LRMS (ESMS) calcd for $C_{20}H_{23}ClN_3O_4$ $(M+H)^+$ 404, found: 404.

General Procedure for *N*-Alkylation of 19.

A mixture of compound **19**, corresponding secondary amine, MeCN, and *i*-Pr_2EtN was heated at 55 °C for 18-20 h. The reaction mixture was concentrated and the crude product was dissolved in CH_2Cl_2. The organic layer was extracted with 5% aq $NaHCO_3$ (2 × 5 mL). The organic layer was dried over anhydrous Na_2SO_4 and concentrated to obtain the crude product as brown viscous oil.

Benzyl 2-(2-acetamido-3-(6-((bis(pyridin-2-ylmethyl)amino)methyl)pyridin-3-yl)propanamido)acetate (20a).

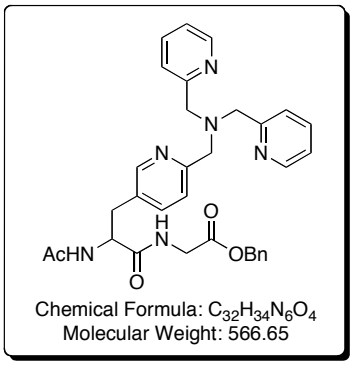

Compound **20a** was prepared by general procedure for *N*-alkylation using **19** (33 mg, 81.6 μmol), MeCN (1.5 mL), *i*-Pr_2EtN (22 μL, 122 μmol) and bis-(2-picolylamine)[175] (21 mg, 106 μmol). A crude product was purified by column chromatography on basic alumina (0% to 5% MeOH:EtOAc) for analysis (29 mg). The yield was calculated by ^1H NMR analysis of a crude product using methyl-*m*-toluate as an internal standard (95%). ^1H NMR (400 MHz, $CDCl_3$) δ 8.48 (d, *J* = 4.0 Hz, 2H), 8.29 (s, 1H), 7.63-7.59 (m, 2H), 7.53-7.46 (m, 4H), 7.33-7.26 (m, 5H), 7.11-7.02 (m, 3H), 6.52 (d, *J* = 8.1 Hz, 1H), 5.07 (s, 2H), 4.73 (dd, *J* = 14.6, 6.5 Hz, 1H), 4.06-3.91 (m, 2H), 3.82-3.80 (m, 6H), 3.07 (dd, *J* = 13.6, 7.3 Hz, 1H), 2.94 (dd, *J* = 13.6, 7.3 Hz, 1H), 1.88 (s, 3H); ^{13}C NMR (100 MHz, $CDCl_3$) δ 171.0, 170.4,

169.2, 159.2, 158.0, 149.6, 149.0, 137.3, 136.4, 135.0, 130.3, 128.6, 128.5, 128.3, 122.9, 122.7, 122.0, 67.2, 60.0, 59.7, 53.6, 41.2, 34.8, 29.6, 23.0; IR (thin film) 3283 (b), 2926, 1749, 1654, 1590, 1569, 1434, 1370, 1188, 994, 756, 698 cm^{-1}; HRMS (ESMS) calcd for $C_{32}H_{35}N_6O_4$ $(M+H)^+$ 567.2720, found: 567.2706.

Benzyl 2-(2-acetamido-3-(6-(((2-(benzyl(pyridin-2-ylmethyl)amino)ethyl) (pyridin-2-ylmethyl)amino)methyl)pyridin-3-yl)propanamido)acetate (20b).

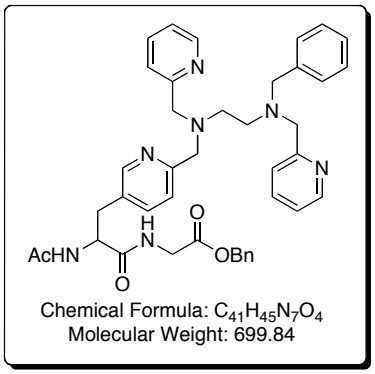

Compound **20b** was prepared by general procedure for *N*-alkylation using compound **19** (20 mg, 49.5 μmol), MeCN (0.9 mL), *i*-Pr_2EtN (35 μL, 198 μmol), and N^1-benzyl-N^1,N^2-bis(pyridin-2-ylmethyl)ethane-1,2-diamine[183] (50 mg, 148 μmol). A sample was purified by preparative HPLC for analysis (14 mg). The yield was calculated by ^{1}H NMR analysis of a crude product using methyl-*m*-toluate as an internal standard (79%). HPLC Conditions: column: Zorbax XDB-C18, 21.2 × 150 mm, 5 micron equipped with guard column; flow rate = 20 mL/min; gradient elution 0-5 min 0-5% MeCN in 0.1% aq TFA, 5-15 min 5-95% MeCN in 0.1% aq TFA; RT = 10.2 min.[184] ^{1}H NMR (400 MHz, $CDCl_3$) δ 8.45 (d, *J* = 4.0 Hz, 2H), 8.26 (s, 1H), 7.58-7.53 (m, 2H), 7.46-7.41 (m, 3H), 7.34-7.08 (m, 14H), 6.44 (b, 1H), 5.10 (s, 2H), 4.70-4.65 (m, 1H), 3.95 (dd, *J* = 13.0, 5.7 Hz, 2H), 3.73-3.69 (m, 4H), 3.58-3.52 (m, 4H), 3.05 (dd, *J* = 13.9, 6.5 Hz, 1H), 2.96 (dd, *J* = 13.9, 6.5 Hz, 1H), 2.69-2.55

(m, 4H), 1.90 (s, 3H); ^{13}C NMR (100 MHz, $CDCl_3$) δ 171.0, 170.3, 169.1, 160.2, 159.6, 158.5, 149.5, 148.9, 148.8, 139.1, 137.2, 136.5, 136.4, 135.1, 130.2, 128.6, 128.5, 128.3, 128.2, 126.9, 122.8, 122.6, 121.9, 67.2, 60.8, 60.5, 60.1, 58.9, 53.9, 51.7, 41.2, 34.9, 23.0; IR (thin film) 3286(b), 2917, 2849, 1749, 1653, 1591, 1539, 1435, 1373, 1260, 1188, 1029, 756, 699, 665 cm^{-1}; HRMS (ESMS) calcd for $C_{41}H_{46}N_7O_4$ $(M+H)^+$ 700.3611, found: 700.3604.

Benzyl 2-(2-acetamido-3-(6-(((dipyridin-2-ylmethyl)(pyridin-2-ylmethyl)amino) methyl)pyridin-3-yl)propanamido)acetate (20c).

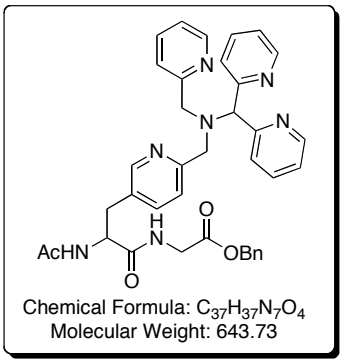

Compound **20c** was prepared by general procedure for *N*-alkylation using compound **19** (52 mg, 130 μmol), MeCN (2.6 mL), *i*-Pr_2EtN (93 μL, 519 μmol), sodium iodide (5 mg, 25.9 μmol) and 1,1-di(pyridin-2-yl)-*N*-(pyridin-2-ylmethyl)methanamine [$NH(PyCH_2)(CHPy_2)$; where Py = 2-pyridyl][168] (107 mg, 389 μmol). The crude product was purified first by column chromatography on basic alumina (0% to 5% MeOH:CH_2Cl_2) and then by preparative HPLC for analysis (21 mg). The yield was calculated by ^{1}H NMR analysis of a crude product using cyclooctadiene as an internal standard (90%). *Note: A catalytic amount of sodium iodide is necessary for the better conversion in this reaction.* HPLC Conditions: column: Zorbax XDB-C18, 21.2 × 150 mm, 5 micron equipped with guard column; flow rate = 20 mL/min; gradient elution 0-5 min 0-20% MeCN in 0.1% aq TFA, 5 -15 min 20-65%

MeCN in 0.1% aq TFA; RT = 8.5 min.[184] ^{1}H NMR (400 MHz, $CDCl_3$) δ 8.51 (d, *J* = 4.9 Hz, 2H), 8.44 (d, *J* = 4.9 Hz, 1H), 8.28 (s, 1H), 7.65-7.56 (m, 6H), 7.50-7.34 (m, 2H), 7.32-7.26 (m, 5H), 7.12-7.04 (m, 3H), 6.94 (brs, 1H), 6.46 (brs, 1H), 5.30 (s, 1H), 5.08 (s, 2H), 4.72-4.65 (m, 1H), 3.99-3.90 (m, 6H), 3.05 (dd, *J* = 14.6, 6.5 Hz, 1H), 2.95 (dd, *J* = 14.6, 6.5 Hz, 1H), 1.88 (s, 3H); ^{13}C NMR (100 MHz, $CDCl_3$) δ 170.9, 170.3, 169.2, 159.9, 159.7, 158.4, 149.6, 149.2, 149.0, 137.3, 136.4, 136.3, 135.0, 130.2, 128.6, 128.5, 128.3, 123.9, 122.9, 122.8, 122.1, 71.9, 67.2, 57.0, 56.7, 53.7, 41.2, 34.7, 23.0; IR (thin film) 3285, 3062, 2928, 1749, 1656, 1588, 1569, 1470, 1433, 1372, 1188, 1030, 996, 911, 732, 698, 645 cm^{-1}; HRMS (ESMS) calcd for $C_{37}H_{38}N_7O_4$ $(M+H)^+$ 644.2985, found: 644.2988.

Chapter 3: Application of the Divergent and Dual Divergent Strategies for a Library Synthesis of Luteinizing Hormone Releasing Hormone (LHRH) Analogues

3.1 Introduction

One goal of the Kodanko group is to investigate the potential of non-heme ligands and their metal complexes as anticancer agents. The most essential requirement for this study is the rapid synthesis of the library of non-heme ligand-peptide conjugates where ligand structures could be rapidly altered to tune the reactivity. The peptide vectors in such conjugates are expected to serve as carriers for the target specific delivery of the metal complexes. The divergent strategy described in Chapter 2 has a potential to elaborate the metal-binding units at the late stage and hence facilitates a straightforward access to the diverse ligand structures.[98] With this strategy, the size of the library would depend only on the number of the available secondary amines. Thus 100 secondary amines would be needed if a library of 100 analogues, each possessing a different ligand, was to be constructed. This could be a major limitation for the rapid synthesis of larger libraries because secondary amines are usually prepared by solution phase synthesis, which is associated with purification and isolation issues. Therefore a modification of the existing divergent strategy was sought prior to utilizing the strategy for library synthesis. A stepwise elaboration of the ligand structure, named dual divergent strategy, was envisioned as a viable alternative to the divergent strategy (Scheme 1.18, Eq 2). This modification would reduce the number of starting material from 100 secondary amines to 10 primary amines and 10 chlorides for the

library of 100 analogues. Moreover, the method could not only avoid a tedious solution phase synthesis but could also be suitable for the split-pool synthesis technique[185] commonly employed in the construction of larger libraries.

The second requirement to explore the utility of non-heme ligands as anticancer agents is the choice of suitable peptide vector that could selectively deliver non-heme ligand to the target site. For this study we chose a decapeptide, luteinizing hormone releasing hormone (LHRH), which is a well-known delivery vector and selectively delivers cytotoxic agents to tumors in vivo. The selectivity is ascribed to the presence of LHRH receptors on various cancer cell lines such as breast, ovarian and prostate cancer cells.[186,187] The research over last two decades have established that the replacement of Gly at position 6 of the natural LHRH with D-lysine provides a point of attachment for cytotoxic agents and improves the serum half-life[188] of the resulting conjugates without affecting the binding affinity (Figure 3.1).[128] For example, analogue such as AN-152, which contains a cytotoxic agent doxorubicin (DOX) at the D-Lys side chain of LHRH, is in phase II clinical trials for the treatment of ovarian cancer.[189]

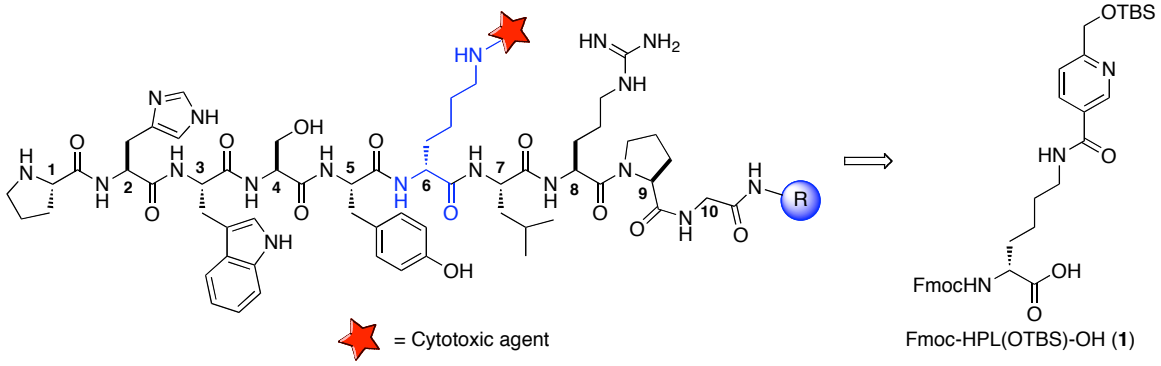

Figure 3.1: Schematic diagram for conjugation of cytotoxic agents to the D-Lys[6][LHRH]

In this chapter the development of the dual divergent strategy on a model substrate is presented. In addition, the scope, limitation and functional group compatibility of the dual divergent strategy are also demonstrated by constructing a small library of metal-binding LHRH analogues. Towards this, an unnatural amino acid Fmoc-HPL(OTBS)-OH (**1**, Figure 3.1) was synthesized in such a way that it possesses a hydroxymethyl pyridyl moiety at the N_{ε}-amine of the D-lysine. Amino acid **1** was incorporated into the LHRH analogue, which provided a suitable functionality through which diverse array of ligand structures were constructed via divergent as well as dual divergent strategy.

3.2 Results

3.2.1 Development of the dual divergent strategy

3.2.1.1 Synthesis of a model substrate on resin

To develop the dual divergent strategy, a model dipeptide substrate **2** was synthesized from commercially available Fmoc-Gly-Rink amide resin using standard SPPS conditions (Scheme 3.1). Transformation of the silyloxy ether side chain of **2** into the corresponding chloride **3** was achieved using a two-step sequence developed during the divergent strategy.[98] The sequence involved the treatment of **2** with buffered TBAF to obtain the corresponding alcohol, which was eventually chlorinated using a combination of tosyl chloride and lithium chloride. A small portion of the peptide **3** was cleaved from resin and the completion of the chlorination reaction was verified using ^{1}H NMR spectroscopic analysis, prior to proceeding with the alkylation reactions. If partial chlorination was observed, the chlorination conditions were repeated.

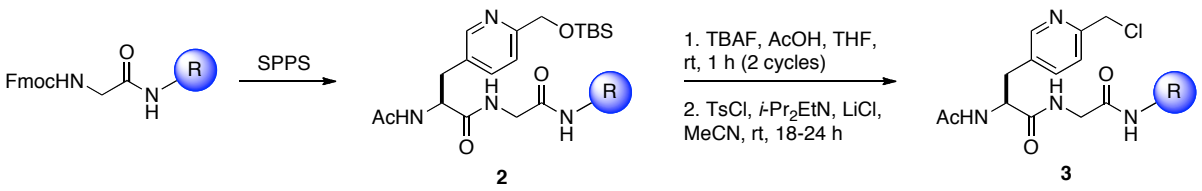

Scheme 3.1: Synthesis of a model substrate and transformation of the silyloxy ether side chain into chloride

3.2.1.2 Development of dual divergent strategy on the model substrate

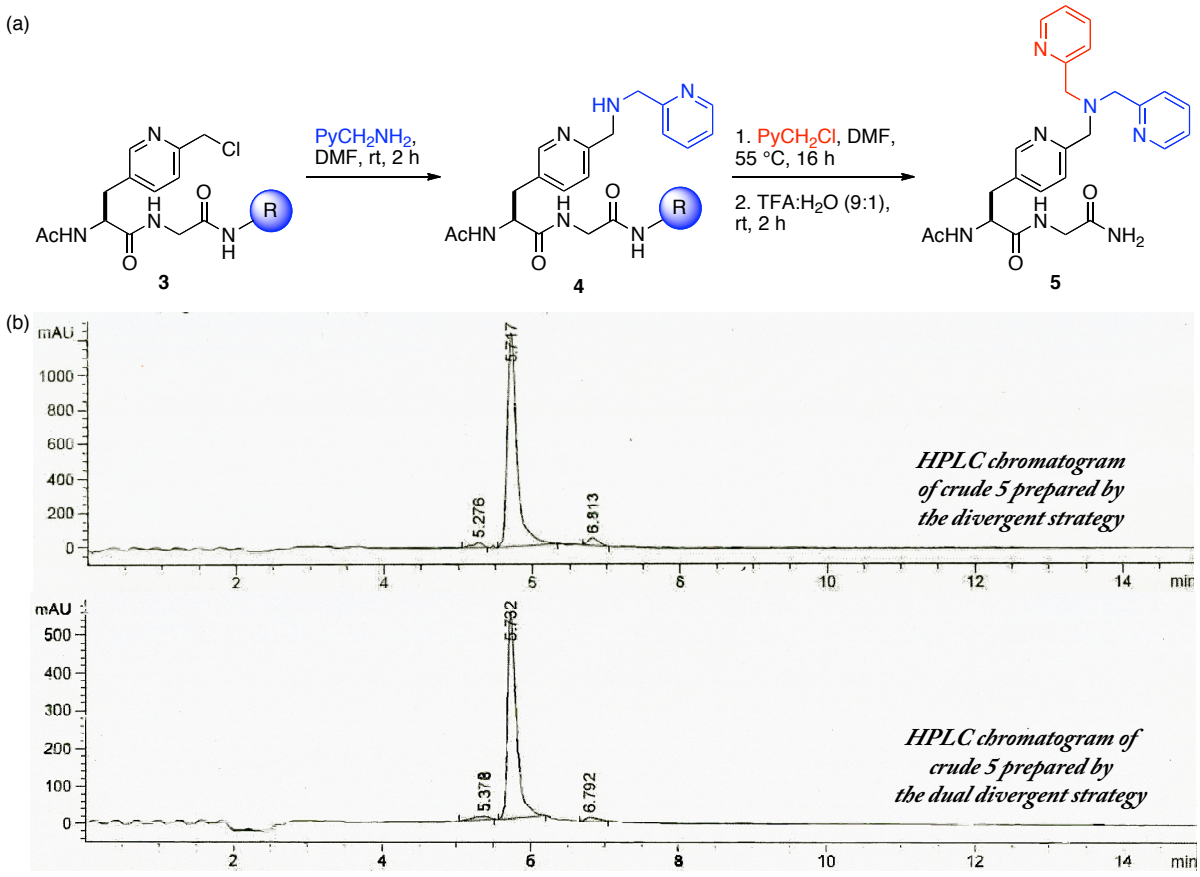

Figure 3.2: (a) Development of the dual divergent strategy on the model substrate (b) HPLC chromatogram of crude **5** prepared by the divergent and the dual divergent strategy

The dual divergent strategy was investigated (Scheme 3.2) by the *N*-alkylation of the chloride **3** with excess primary amine using the conditions developed for the divergent strategy (MeCN, 55 °C, 18 h). The *N*-alkylation gave the desired secondary amine **4**, albeit in low purity. Delightfully, performing the reaction in DMF at rt instead of heating in MeCN significantly minimized the side reactions and furnished the desired secondary amine **4** as the major product (Figure 3.2a). The second alkylation of **4** was straightforward and achieved by heating **4** with 10 equiv of 2-picolylchloride. Interestingly, the HPLC chromatogram of the crude TPA-dipeptide **5** obtained via this route was indistinguishable to the conjugate obtained via the divergent strategy (Figure 3.2b).

3.2.2 Application of the divergent and dual divergent strategies to a library synthesis of LHRH analogues

3.2.2.1 Synthesis of Fmoc-HPL(OTBS)-OH

To investigate the scope and the functional group compatibility of the dual divergent strategy, an unnatural amino acid Fmoc-HPL(OTBS)-OH (**1**, HPL: **H**ydroxymethyl **P**yridyl **L**ysine) was designed in such a way that the hydroxymethyl pyridyl moiety containing the silyloxy ether side chain was connected on the side chain of D-lysine. The synthesis of **1** began with a hydrolysis of intermediate **6** to obtain **7**, which was transformed into an activated ester **8** upon coupling with *N*-hydroxysuccinimide. Selective substitution at the N_ε-position of D-lysine was achieved using the literature procedure for the N_ε-protection of lysine (Scheme 3.2). The synthesis involved the protection of an α-amino acid group of D-lysine as a Cu^{II} chelate, followed by amidation of the N_ε-amine with **8**. Isolation of the

resulting copper complex by centrifugation followed by decomplexation using EDTA and subsequent Fmoc protection furnished the target amino acid **1** in 62% overall yield.

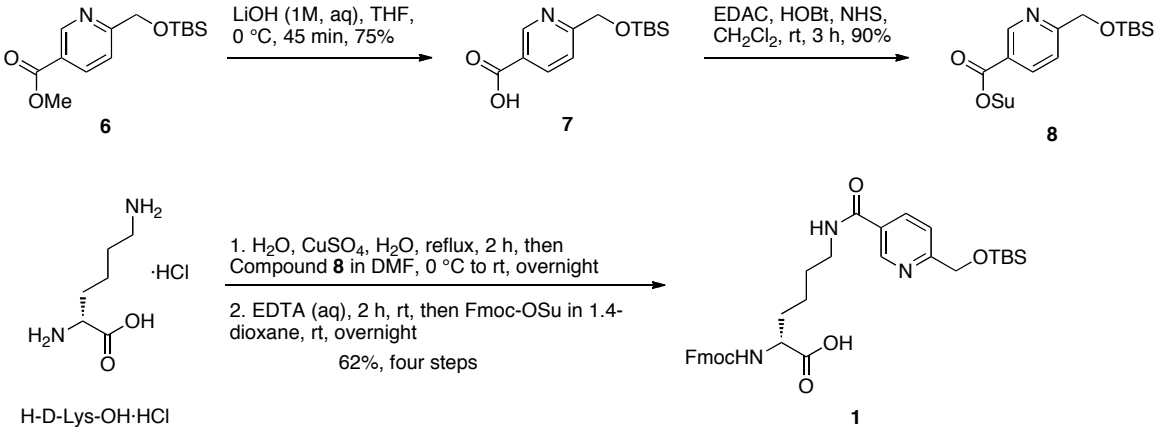

Scheme 3.2: Synthesis of the unnatural amino acid Fmoc-HPL(OTBS)-OH (**1**)

3.2.2.2 Library synthesis via divergent and dual divergent strategies

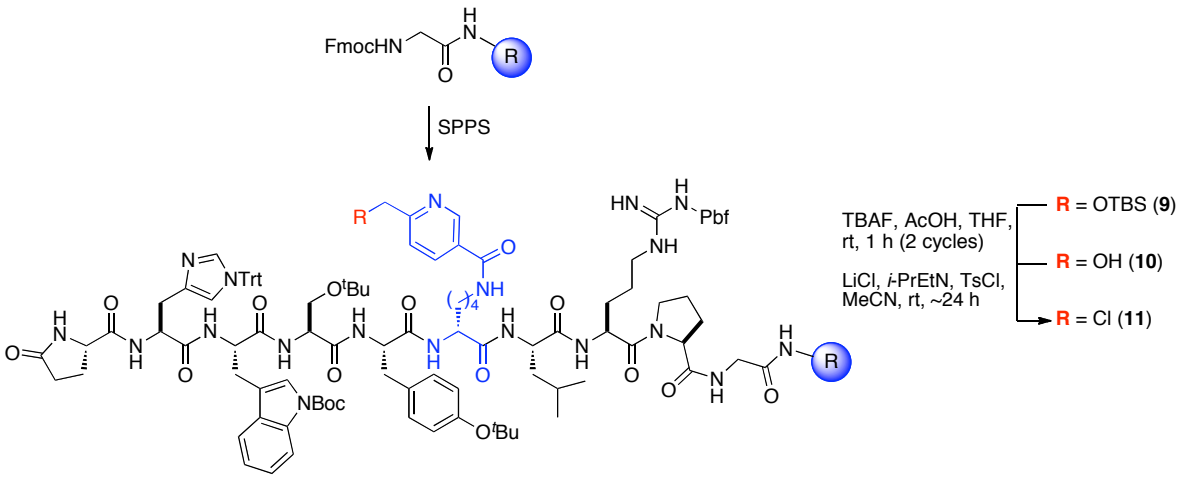

Scheme 3.3: Incorporation of **1** into LHRH and transformation of the silyloxy ether side chain into chloride

With an amino acid **1** in hand, we embarked on constructing the metal-binding analogues of LHRH. A decapeptide **9** was synthesized by incorporating **1** at position 6 of

LHRH via standard SPPS synthesis (Scheme 3.3). Transformation of the silyloxy ether side chain of **9** to chloride **11** was straightforward and achieved using conditions employed in the model substrate. MALDI analysis of the crude chloride, obtained from the cleavage of a small amount of the peptide from resin **11**, suggested that the alcohol **10** was completely consumed under the chlorination conditions.

To explore the scope of the dual divergent strategy, a mini-library of LHRH analogues was synthesized from **11** using two primary amines and three chlorides that provided a diverse array of *O*-donor and *N*-donor metal-binding units (Scheme 3.4). The synthesis began with two parallel first alkylations of the chloride **11**, one with 2-picolylamine (**12a-c**) and the other with *N*-(2-aminoethyl)picolinamide (**12d-f**). The first alkylation products were split into three portions and reacted with 2-(chloromethyl)pyridine, 2-(chloromethyl)pyrazine or *tert*-butyl 2-chloroacetate, thus producing six (2 primary amines × 3 chloride) metal-binding LHRH analogues (Scheme 3.4, Dual divergent strategy). This clearly demonstrates that the conditions used for the dual divergent strategy are compatible with *O*-donor carboxylates as well as several *N*-donors such as pyridine, pyrazine and basic amine groups. A limitation to this strategy was also revealed when the first alkylation was attempted with *N*-benzyl ethylenediamine. The first alkylation using this amine, which would provide Bn-TPEN derivatives, gave a mixture of products under these conditions presumably due to a lack of selectivity between alkylation of primary and secondary amines. Since the pentadentate ligands such as Bn-TPEN and N4Py have shown promising results during the HeLa cell studies,[16] we incorporated these two ligands (**13a-b**) into the LHRH peptide via the divergent strategy (Scheme 3.4, Divergent Strategy). These eight analogues were cleaved

from resin and purified by reverse phase HPLC to obtain a small library of metal-binding LHRH analogues.

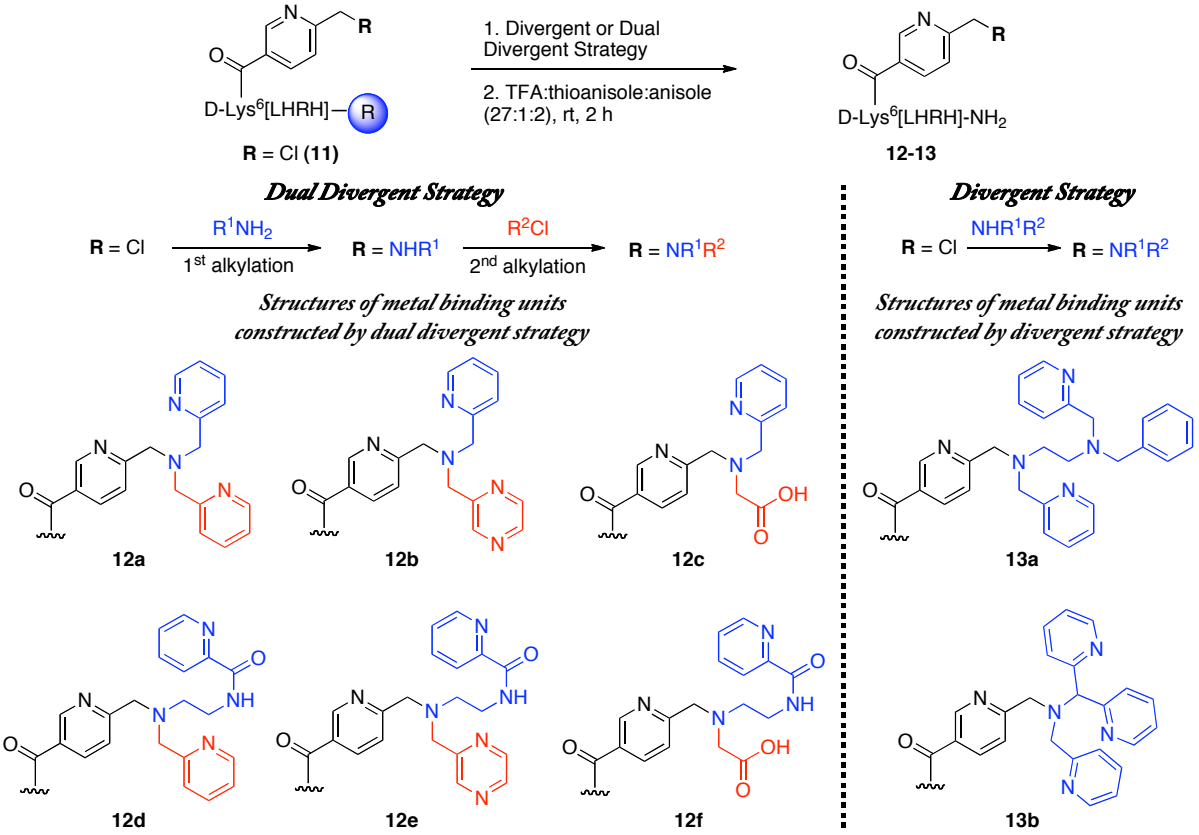

Scheme 3.4: Synthesis of mini-library of metal-binding LHRH analogues via divergent and dual-divergent strategy

3.2.2.3 Metal-binding studies of LHRH analogues

The next goal was to demonstrate that LHRH analogues have similar metal-binding properties to their parent ligands. For this study we choose TPA·LHRH analogue **12a** and PaPy3·LHRH analogue **12d** since the metal-binding properties of parent TPA and PaPy3 ligands were well established. Initial attempts to characterize Fe^{II} or Fe^{III} complexes of TPA and **12a** were unsuccessful, however by the virtue of diamagnetic zinc complexes, the

reaction of **12a** with $ZnCl_2$ could be monitored by ^1H NMR spectroscopic analysis (Figure 3.3). Addition of 0, 0.5 and 1 equiv of $ZnCl_2$ to the solution of TPA in D_2O have shown a gradual shift towards the downfield region (e.g. a to a' in Figure 3.3a). Similar shifts were also observed when the experiment was performed with a solution of **12a** (a/b to a'/b' in Figure 3.3b). Interestingly, the part of the ligand not participating in the complex formation either retains the chemical shift (e.g. c to c') or experiences minor chemical shifts (e.g. d/e to d'/e') as shown in Figure 3.3b.

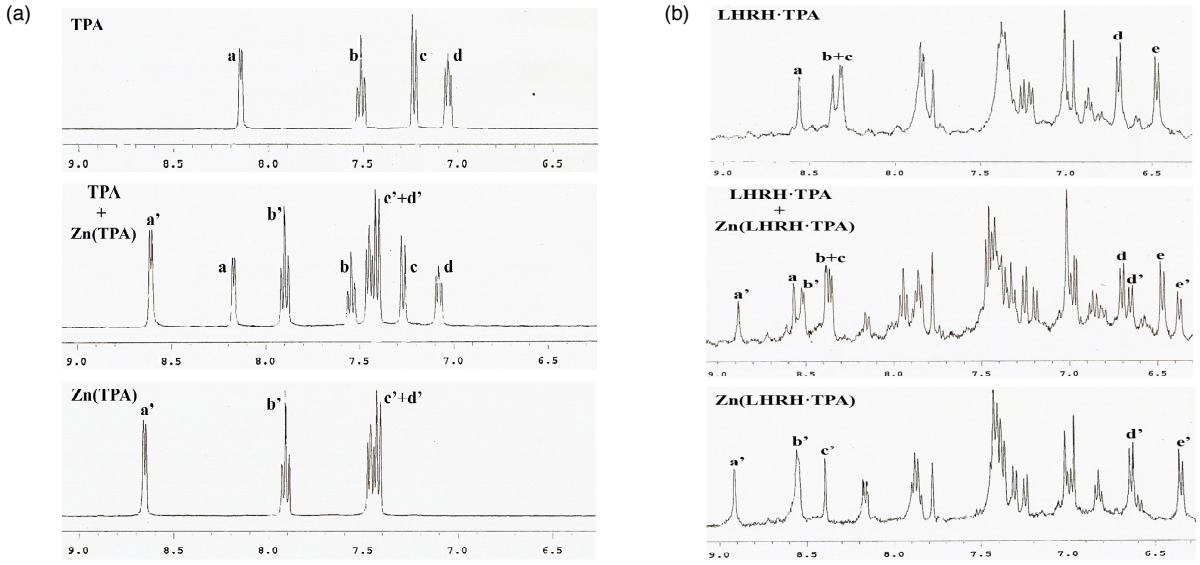

Figure 3.3: ^1H NMR spectra of TPA (a) and **12a** (b) after addition of 0, 0.5 and 1 equiv (top to bottom) of $ZnCl_2$ in D_2O

Ferric complexes of PaPy3 exhibit characteristic UV-vis absorption bands in water as well as in methanol media. Affinities of PaPy3 and **12d** for Fe^{III} were confirmed by titrating the aqueous solutions of PaPy3 and **12d** with a solution of $Fe^{III}(ClO_4)_3$. Although, the titration curve for **12d** was found to plateau at higher amounts of Fe^{III} than corresponding PaPy3 (Figure 3.4, left), UV-vis spectra (λ_{max} = 500 nm, ε = 1830 $M^{-1}cm^{-1}$ for PaPy3 and

λ_{max} = 505 nm, ε = 1520 $M^{-1}cm^{-1}$ for **12d**) of the newly formed red species were in well agreement with the literature data (Figure 3.4, right).[190] The difference of 5 nm in their absorption maxima was attributed to the electron-withdrawing amide group present on the pyridyl ring of **12d**.

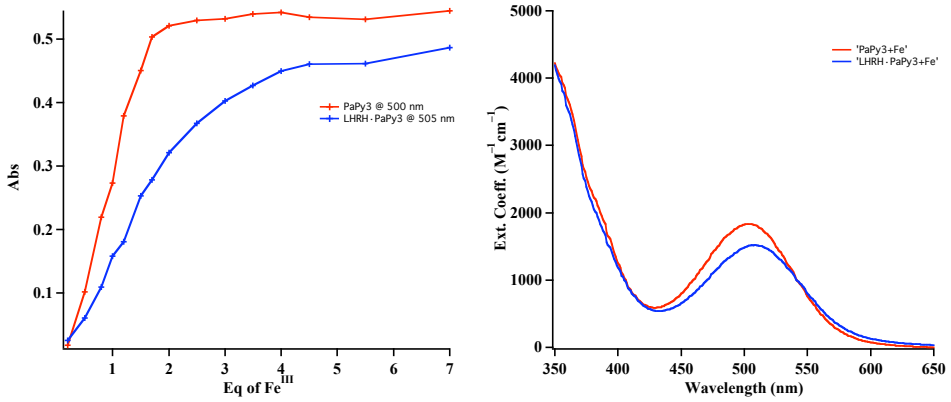

Figure 3.4: Titration of PaPy3 (red) and **12d** (blue) with $Fe(ClO_4)_3 \cdot xH_2O$ (left) and; UV-vis spectra of PaPy3 (red) and **12d** (blue) upon addition of $Fe(ClO_4)_3 \cdot xH_2O$ (right)

3.3 Discussion

3.3.1 Optimization of the dual divergent strategy

The fundamental goals of this project were to expand the divergent strategy by investigating the dual divergent strategy and apply both strategies for the library synthesis of biologically important molecules. Towards this goal, a model dipeptide substrate **2** was chosen to investigate the dual divergent strategy. Since the divergent strategy was established on the same substrate[98], the comparison between the divergent and the dual divergent strategy would be straightforward. During initial attempts to alkylate the chloride **3** (**3** to **4**, Scheme 3.2) with 2-picolylamine in MeCN, a complex mixture of products was obtained

including an apparent product derived from the undesired reaction between **4** with **3** as judged by MALDI and ^{1}H NMR spectroscopic analysis. The undesired product was most likely derived from the reaction between **3** and **4** of the same resin bead, what is essentially an intramolecular reaction. In contrast, an intermolecular reaction between two resin beads containing **3** and **4** is less likely since it would require a reaction to occur between two solid particles. If this assumption is true, reducing the effective concentration of **3** and **4** on the resin beads is expected to lower the rate of intramolecular type of reactivity. The use of lower initial loading or improving the swelling of the resin should reduce the concentration of **3** and **4** on resin. Indeed, performing the reaction in DMF, a superior solvent for SPPS and facilitates excellent bead swelling, minimized the side reaction and furnished the desired secondary amine **4** at room temperature. Initial attempts to reduce the equivalents of primary amine (100 eq.) in the first alkylation were unsuccessful and no further studies were conducted. As expected the alkylation of the secondary amine **4** required relatively higher temperature but could be achieved with only 10 equiv of 2-picolylchloride.

3.3.2 Library synthesis and metal-binding studies of LHRH analogues

For the library synthesis of metal-binding LHRH analogues, an unnatural amino acid Fmoc-HPL(OTBS)-OH (**1**) was designed and synthesized (Scheme 3.2). The synthesis began with the hydrolysis of a known intermediate **6**, in which lower temperatures for the reaction as well as work up were critical to obtain a higher yield. When the hydrolysis reaction was allowed to warm up to room temperature, cleavage of the silyloxy ether was observed, probably due to the high pH of the reaction media. While designing **1**, a stable amide bond

was chosen to connect the hydroxymethyl pyridyl moiety to D-lysine, since the amide linkage is stable in both the divergent and the dual divergent strategies as well as acidolytic cleavage conditions. Incorporation of **1** into LHRH analogue and deprotection of the silyloxy ether side chain was uneventful (**9** to **10**). The alcohol was transformed into the corresponding chloride **11**, which was reacted with 2-picolylamine and then with 2-picolylchloride to construct TPA onto the LHRH analogue (**12a**, Scheme 3.4, Dual divergent strategy). The chlorination as well as the first and second alkylation reactions were monitored by MALDI and ^{1}H NMR analysis. Based on the MALDI data, an additional peak was observed during chlorination that was transformed into a new peak upon reaction with 2-picolylamine. The new peak suggested the addition of two units of 2-picolylamine into **11**. This newly formed peak remained unchanged during the reaction with 2-picolylchloride. This undesired side reaction could be explained if the pyroglutamic acid (Glp) moiety of the chloride **11** undergoes *N*-tosylation under chlorination conditions. Subsequently, a nucleophilic addition of 2-picolylamine to the *N*-tosylated Glp would result in the undesired product that should be inert towards the second alkylation. Incorporating Glp containing an electron rich protecting group could minimize this side reaction. However, since this side reaction was only a minor pathway, as judged by HPLC analysis, we decided to employ the present conditions for the library synthesis (Scheme 3.4). Selective alkylation of the chloride **11** using *N*-benzyl ethylendiamine was unsuccessful due to the poor selectivity between primary and secondary amines of *N*-benzyl ethylendiamine under the reaction conditions, which required us to use the divergent strategy for the incorporation of Bn-TPEN and N4Py into LHRH analogue.

To establish the metal-binding capabilities of the LHRH analogues, **12a** and **12d** were chosen since the metal-binding properties of the parent ligands were well established. The characterization of Fe^{II}·**12a** was limited due to the sensitivity/stability of the complex while Fe^{III}·**12a** was spectroscopically silent when analyzed by UV-vis spectrophotometer. Fortunately, ^{1}H NMR analysis of the Zn^{II}·**12a** complexes has displayed a clear change in the chemical shifts when the ligand was bound to zinc. Moreover, the change in the chemical shifts is identical between **12a** and the parent TPA ligand suggested that TPA and **12a** bind to zinc in a similar fashion. For the characterization of Fe^{III}·PaPy3 and Fe^{III}·**12d** complexes, their characteristic absorption maxima were compared. Although the complex formation could not be monitored in buffered solution due to the absence of characteristic UV-vis absorption in MOPS buffer (pH =6.9), the use of distilled water in identical reaction conditions furnished characteristic red species for each complex that could be monitored by UV-vis spectroscopy.

3.4 Conclusion

The dual divergent strategy has been developed by extension of the divergent strategy. The reaction conditions were optimized using a model substrate and the scope as well as functional group compatibility of the method were established by synthesizing a small library of metal-binding LHRH analogues. By virtue of the dual divergent strategy, the library synthesis of peptide-ligand conjugates could be rapidly accessed, since the tedious solution phase synthesis and purification of secondary amines could be avoided. Moreover, various *N*-donor and *O*-donor ligand structures could be rapidly synthesized in a stepwise fashion. This is particularly beneficial to study the effect of electronics and overall charge of

the complex on the biological properties of the resulting conjugates. In addition, the dual divergent strategy would allow the use of split-pool method for the library synthesis that exponentially increases the size of the library. During this study a limitation of the dual divergent strategy was also revealed when primary amines could not be selectively alkylated in the presence of secondary amine. Due to this limitation, Bn-TPEN could not be incorporated into LHRH using the dual divergent strategy. Hence, relatively more complex Bn-TPEN and N4Py ligands were incorporated into LHRH via the traditional divergent strategy. This indicates that, although the dual divergent strategy is more ideal, the divergent strategy is also important in the synthesis of certain higher dentate ligands.

3.5 Experimental Section

3.5.1 General consideration

See section 2.5.1 for the general considerations. Compounds bis(pyridin-2-ylmethyl)amine,[191] 2-(chloromethyl)pyrazine,[192] *N*-(2-aminoethyl)picolinamide,[190] **2**[98]and **5**[98] used in this report were synthesized according to previously reported literature procedures.

3.5.2 Experimental procedures and tabulated characterization data for new compounds

6-(((*tert*-butyldimethylsilyl)oxy)methyl)nicotinic acid (7).

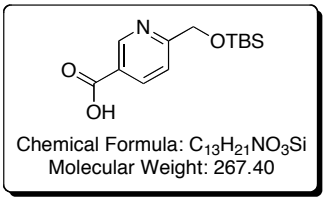

Chemical Formula: $C_{13}H_{21}NO_3Si$
Molecular Weight: 267.40

A solution of ester **6** (3.00 g, 10.7 mmol) in THF (60 mL) was cooled to 0 °C. A 1M aqueous solution of LiOH (64.0 mL, 64.0 mmol) was added dropwise over the period of 50 min while maintaining the temperature below 5 °C. The reaction mixture was maintained at 0-5 °C for 45 min. After consumption of the starting material, as judged by TLC analysis, the reaction mixture was acidified to pH ~6.5 by dropwise addition of 5% citric acid (aq) over a period of 25 min during which the temperature of the reaction mixture was maintained below 5 °C. The aqueous layer was extracted using EtOAc (3 × 50 mL). The combined organic layer was dried over anhydrous Na_2SO_4 and evaporated under vacuum to obtain **7** as a white solid (2.15 g, 75%). A portion of **7** was purified by silica gel chromatography (50% to 100% EtOAc:hexanes) for analysis. ^{1}H NMR (400 MHz, $CDCl_3$) δ 11.8 (brs, 1H), 9.25 (d, J = 1.6 Hz, 1H), 8.44 (dd, J = 8.1, 2.4 Hz, 1H), 7.69 (d, J = 8.1 Hz, 1H), 4.96 (s, 2H), 0.95 (s, 9H), 0.13 (s, 6H); ^{13}C NMR (100 MHz, $CDCl_3$) δ 168.9, 165.8, 149.8, 139.1, 124.9, 120.0, 65.3, 25.8, 18.3, –5.4; IR (thin film) 2955, 2928, 2891, 2857, 1720, 1608, 1389, 1295, 1260, 1127, 1104, 1035, 850, 838, 776, 758, 641 cm^{-1}; HRMS (ESMS) calcd for $C_{13}H_{22}NO_3Si$ ($M+H^+$) 268.1369, found: 268.1376.

2,5-dioxopyrrolidin-1-yl 6-(((*tert*-butyldimethylsilyl)oxy)methyl)nicotinate (8).

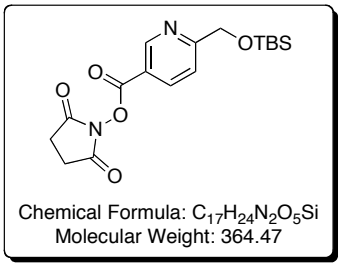

A mixture of crude **7** (2.00 g, 7.48 mmol), *N*-Hydroxysuccinimide (1.03 g, 8.97 mmol), HOBt (1.37 g, 8.97 mmol) and Et_3N (1.56 mL, 11.2 mmol) in CH_2Cl_2 (60 mL) was maintained at rt for 5 min under nitrogen atmosphere. EDAC (1.72 g, 8.97 mmol) was added

and the mixture was maintained under nitrogen atmosphere for 3 h. After consumption of the starting material, as judged by TLC analysis, the reaction mixture was mixed with CH_2Cl_2 (40 mL) and extracted with sat. NH_4Cl solution (3 × 20 mL), 5% $NaHCO_3$ solution (3 × 20 mL) and brine solution (1 × 20 mL). The combined organic layer was dried over anhydrous Na_2SO_4 and evaporated under vacuum to obtain **8** as a white solid (2.45 g, 90%). A portion of **8** was purified by silica gel chromatography (20% to 40% EtOAc:hexanes) for characterization. ^{1}H NMR (400 MHz, $CDCl_3$) δ 9.17 (d, *J* = 1.6 Hz, 1H), 8.37 (dd, *J* = 8.1, 2.4 Hz, 1H), 7.67 (d, *J* = 8.1 Hz, 1H), 4.88 (s, 2H), 2.89 (s, 4H), 0.93 (s, 9H), 0.10 (s, 6H); ^{13}C NMR (100 MHz, $CDCl_3$) δ 169.0, 168.4, 160.9, 150.5, 138.6, 119.8, 119.7, 65.9, 25.8, 25.6, 18.3, –5.4; IR (thin film) 3518, 2952, 2930, 2894, 2857, 1773, 1744, 1647, 1598, 1568, 1484, 1471, 1463, 1445, 1426, 1394, 1386, 1362, 1309, 1285, 1259, 1210, 1137, 1105, 1072, 1048, 1040, 1001, 945, 938, 909, 844, 814, 778, 744, 670, 650, 635, 601 cm^{-1}; HRMS (ESMS) calcd for $C_{17}H_{25}N_2O_5Si$ ($M+H^+$) 365.1533, found: 365.1533.

(R)-2-((((9H-fluoren-9-yl)methoxy)carbonyl)amino)-6-(6-(((*tert*-butyldimethylsilyl) oxy)methyl)nicotinamido)hexanoic acid (1).

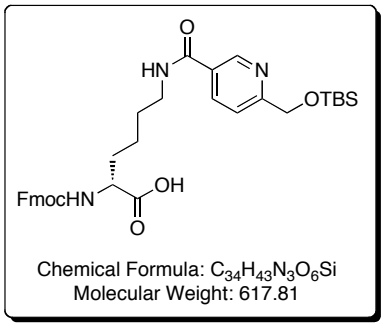

Chemical Formula: $C_{34}H_{43}N_3O_6Si$
Molecular Weight: 617.81

A mixture of H-D-Lys-OH·HCl (100 mg, 0.55 mmol), $CuSO_4·5H_2O$ (68.0 mg, 0.27 mmol), $NaHCO_3$ (92.0 mg, 1.10 mmol) and H_2O (1.5 mL) was refluxed for 2 h. The mixture was cooled to 0 °C and a solution of **8** in DMF (1 mL) was added dropwise over the period of 1 h.

After addition, the reaction mixture was allowed to warm to rt and stirred vigorously overnight during which a blue solid was formed. The reaction mixture was combined with H_2O (10 mL) and the resulting blue solid was isolated by centrifugation. The solid was washed with H_2O (2 × 10 mL), acetone (1 × 5 mL) and dried under high vacuum for 3-4 h (230 mg).

This solid was stirred with an aqueous solution (10 mL H_2O) of EDTA (1.20 g, 2.74 mmol) containing $NaHCO_3$ (92.0 mg, 1.10 mmol) for 2 h during which the colorless solution turned blue and the blue solid changed to white. The pH of this reaction mixture was adjusted to ~7.7 by dropwise addition of 5% $NaHCO_3$. The reaction mixture was cooled to 0-5 °C and a solution of FmocOSu (183 mg, 0.55 mmol) in 1,4-dioxane (2 mL) was added dropwise over the period of 1 h. The reaction mixture was allowed to warm to rt and maintained overnight. The reaction mixture was combined with H_2O (30 mL) and acidified to pH ~6 by dropwise addition of 15% citric acid. The aqueous layer was extracted with Et_2O (7 × 10 mL). The combined organic layer was dried over anhydrous Na_2SO_4 and evaporated under vacuum to obtain the crude product as a white solid. The crude product was purified by silica gel chromatography (0% to 15% MeOH:CH_2Cl_2) to afford **1** (210 mg, 62%). ^{1}H NMR (400 MHz, CD_3OD) δ 8.86 (s, 1H), 8.19 (dd, *J* = 8.1, 1.6 Hz, 1H), 7.72 (d, *J* = 7.3 Hz, 2H), 7.59-7.54 (m, 3H), 7.32 (t, *J* = 7.3 Hz, 2H), 7.23 (t, *J* = 7.3 Hz, 2H), 4.76 (s, 2H), 4.30-4.21 (m, 2H), 4.13-4.10 (m, 2H), 3.40-3.30 (m, 2H), 1.88-1.46 (m, 6H), 0.93 (s, 9H), 0.09 (s, 6H); ^{13}C NMR (100 MHz, CD_3OD) 167.7, 165.1, 158.6, 148.5, 145.3, 145.1, 142.5, 137.5, 130.3, 128.7, 128.1, 126.2, 121.2, 120.9, 67.8, 66.5, 56.0, 48.4, 40.8, 32.8, 29.9, 26.3, 24.3, 19.2, –5.3; IR (thin film) 3328 (br), 3067, 2953, 2929, 2857, 1704, 1644, 1600, 1547, 1462, 1450,

1379, 1320, 1258, 1105, 1051 1007, 938, 839, 778, 758, 739 cm^{-1}; [α] = –2.7° (c = 1.0, $CHCl_3$); HRMS (ESMS) calcd for $C_{34}H_{44}N_3O_6Si$ ($M+H^+$) 618.2999, found: 618.2998.

General Procedure for Peptide Syntheses.

All coupling reactions were performed on a 0.15-0.4 mmol scale by standard SPPS method using Fmoc amino acid with HBTU-activated ester chemistry in a Peptide Synthesis Vessel (manual synthesis). Typical protocols for coupling steps involved 1-4 h coupling cycles with 2-4 eq of Fmoc amino acid. However, for the unnatural amino acids **1**, only 2 eq of **1** were used. During coupling reactions Fmoc amino acids were pre-activated by stirring their solution in DMF with HBTU and *i*-Pr_2EtN for 1-2 min. The Fmoc deprotection was performed using 20% piperidine in DMF with two cycles 20-30 min each. After each reaction step, the resin was washed with DMF (2 × 2 mL), *i*-PrOH (2 × 2 mL) and CH_2Cl_2 (2 × 2 mL). Kaiser test was used to monitor the coupling reactions and deprotection of the Fmoc group. Standard SPPS steps and equivalence of the reagents are summarized in Table 3.1. *Note: No capping was performed after any coupling step.*

Table 3.1: Conditions for SPPS and divergent/dual divergent strategy

Operation	**Reagent**	**Vol**	**Time/temp**	**Scale**
Fmoc deprotection	20% Piperidine in DMF	5 mL	2 × 20 min (each)/rt	0.3 mmol
Drain and wash	DMF, *i*-PrOH, CH_2Cl_2	2-4 mL (each)	2 × 2 min (each)/rt	
Coupling of Fmoc-AA-OH	Fmoc-AA-OH (0.6 mmol), HBTU (0.6 mmol), *i*-Pr_2EtN (0.6 mmol)	5 mL, DMF	1 × 2-3 h/rt	0.3 mmol
Coupling of Fmoc-D-HPL(OTBS)-OH	Fmoc-AA-OH (0.6 mmol), HBTU (0.6 mmol), *i*-Pr_2EtN (0.6 mmol)	5 mL, DMF	1 × 4-5 h/rt	0.3 mmol

TBS cleavage	TBAF (1M, 1.2 mmol), AcOH (0.3 mmol)	5 mL, THF	2 × 1 h/rt	0.3 mmol
Chlorination	LiCl (3.75 mmol), *i*-Pr_2EtN (1.13 mmol), TsCl (0.75 mmol)	2.7 mL, MeCN	1 × ~24 h/rt	75 µmol
1st Alkylation	R^1NH_2 (6.0 mmol)	1.6 mL, DMF	1 × 2 h/rt	60 µmol
2nd Alkylation	R^2Cl (0.2 mmol), *i*-Pr_2EtN (0.45 mmol)	1.1 mL, DMF	1 × 18 h/55 °C	20 µmol

Cleavage of the TBS group: A mixture of the peptide (0.3 mmol scale), TBAF (1M in THF, 1.2 mmol), acetic acid (0.3 mmol) and THF was shaken in a peptide synthesis vessel for 1 h at rt. Two cycles were performed to confirm the complete cleavage of TBS group. The resin was successively washed with DMF (2 × 2 mL), *i*-PrOH (2 × 2 mL) and CH_2Cl_2 (2 × 2 mL) dried under vacuum and stored at –30 °C.

Chlorination: The mixture of peptide (75 µmol), lithium chloride (3.75 mmol), *i*-Pr_2EtN (1.13 mmol), tosyl chloride (0.75 mmol) and MeCN (1.7 mL) was shaken in peptide syntheses vessel for 20-24 h at rt. The resin was washed successively with DMF (2 × 1 mL), *i*-PrOH (2 × 1 mL) and CH_2Cl_2 (2 × 1 mL) dried under vacuum and used for alkylation reactions.

Alkylation: In a typical procedure for alkylation, a mixture of chloride (60 µmol), primary amine (6 mmol) and DMF (1.6 mL) was shaken in peptide syntheses vessel for 2 h at rt. The resin was washed successively with DMF (2 × 1 mL), *i*-PrOH (2 × 1 mL) and CH_2Cl_2 (2 × 1 mL) dried under vacuum, split into three portions (20 µmol each) and transferred into vials. This resin was mixed with *i*-Pr_2EtN (0.45 mmol), the corresponding chloride (0.2 mmol) and DMF (1.1 mL) and stirred slowly (< 200 rpm) at 55 °C for 18-20 h. The resin was

successively washed with DMF (2 × 1 mL), *i*-PrOH (2 × 1 mL) and CH_2Cl_2 (2 × 1 mL) and dried under vacuum.

Cleavage of the peptides from resin: The peptide-ligand conjugate were cleaved from the resin by stirring the resin (25-30 mg) with a 27:1:2 mixture of TFA:anisole:thioanisole (2mL) for 2 h at rt. The resin was removed by filtration and the filtrate was mixed with cold Et_2O (10 mL). The resulting precipitate was isolated by centrifugation. The residue was washed with cold ether (2 × 4 mL) dried under vacuum and used for purification/analysis.

MALDI analysis: MALDI-TOF data were acquired on a MALDI-TOF mass spectrometer using the reflectron mode. Samples for MALDI analysis of peptide-ligand conjugates were prepared according to the following procedure. 5-10 mg of peptide-ligand conjugate was dissolved in 2 mL of MeOH:H_2O (1:1). 2 μL of this sample solution was diluted in 40 μL MeOH. 2 μL of this diluted sample was mixed with 4 μL matrix solution (α-Cyano-4-hydroxy cinnamic acid in 7:3 MeCN:0.1% aq TFA) and spotted on MALDI plate for analysis. The nitrogen containing ligands used herein have strong affinities for Zn^{2+} and hence showed M+Zn species in addition to M+Na adducts due to trace amounts of Zn^{2+} present in the buffer solution. Addition of 4 μL of sat EDTA (aq) to the sample solutions before spotting on MALDI plate reduced the abundance of M+Zn peak.

Peptide-ligand conjugate 12a.

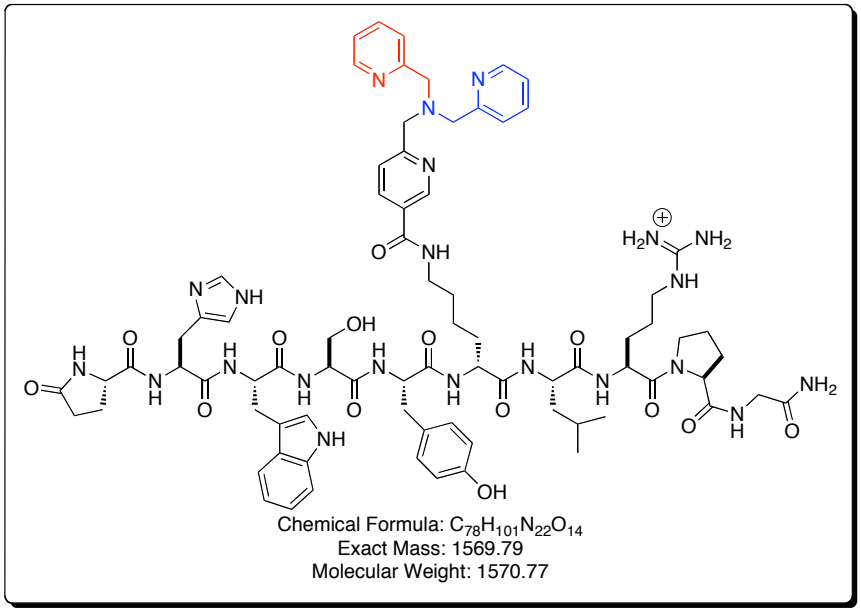

The crude product was purified by preparative HPLC. HPLC Conditions: column: XDB-C18 (ZORBAX) 21.2 × 150 mm, 5 micron; Mobile phase: 0.1% aq TFA and MeOH; Flow rate = 20 mL/min; Gradient elution: 0-5 min 5-40% MeOH in aq TFA, 5-14 min 40-65% MeOH in aq TFA, 14-15 min 65-100% MeOH in aq TFA, 15-20 min 100% MeOH in aq TFA, 20-21 min 5% MeOH in aq TFA; RT = 8.5 min. Desired fractions were evaporated under high vacuum (at rt) and analyzed by HPLC to confirm the purity (Mobile phase: 0.1% aq TFA and MeOH; Flow rate = 20 mL/min; Gradient elution: 0-5 min 10-40% MeOH in aq TFA, 5-16 min 40-60% MeOH in aq TFA, 16-17 min 60-100% MeOH in aq TFA; RT = 8.9 min; purity = 96%). MALDI-TOF MS (ESMS) calc'd for $C_{78}H_{101}N_{22}O_{14}$ (M^+) 1569.79, found: 1569.40.

Peptide-ligand conjugate 12b.

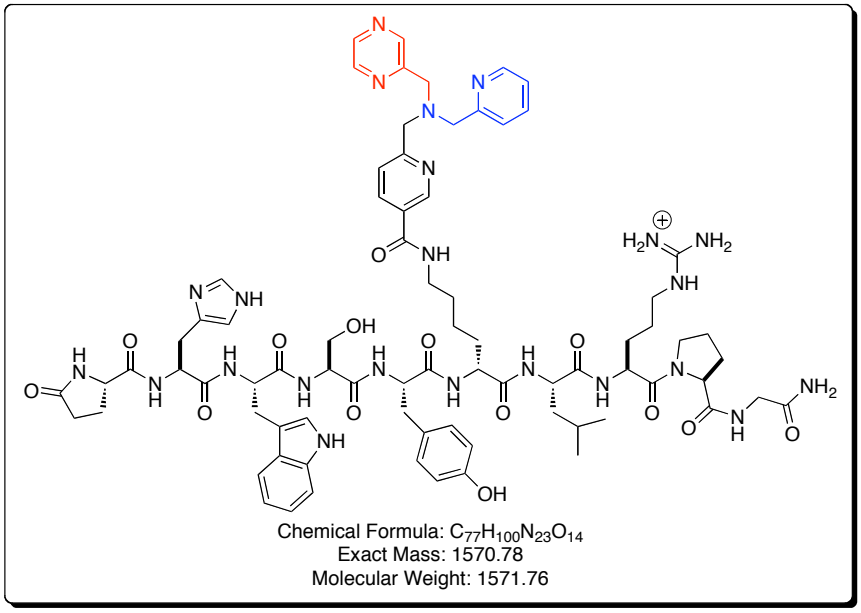

The crude product was purified by preparative HPLC. HPLC Conditions: column: XDB-C18 (ZORBAX) 21.2 × 150 mm, 5 micron; Mobile phase: 0.1% aq TFA and MeOH; Flow rate = 20 mL/min; Gradient elution: 0-5 min 5-40% MeOH in aq TFA, 5-14 min 40-65% MeOH in aq TFA, 14-15 min 65-100% MeOH in aq TFA, 15-20 min 100% MeOH in aq TFA, 20-21 min 5% MeOH in aq TFA; RT = 8.9 min. Desired fractions were evaporated under high vacuum (at rt) and analyzed by HPLC to confirm the purity (Mobile phase: 0.1% aq TFA and MeOH; Flow rate = 20 mL/min; Gradient elution: 0-5 min 10-40% MeOH in aq TFA, 5-16 min 40-60% MeOH in aq TFA, 16-17 min 60-100% MeOH in aq TFA; RT = 9.5 min; purity = 95%). MALDI-TOF MS (ESMS) calc'd for $C_{77}H_{100}N_{23}O_{14}$ (M^+) 1570.78, found: 1570.44.

Peptide-ligand conjugate 12c.

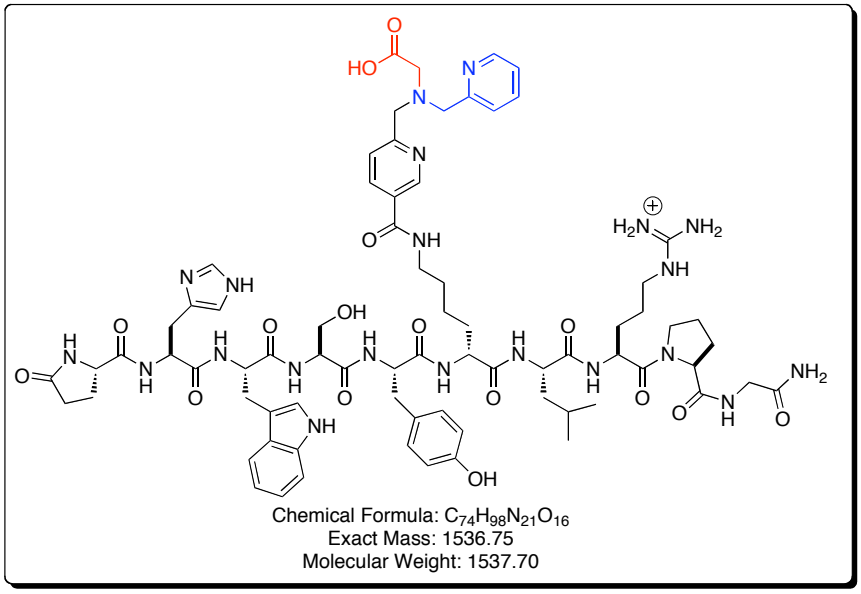

The crude product was purified by preparative HPLC. HPLC Conditions: column: XDB-C18 (ZORBAX) 21.2 × 150 mm, 5 micron; Mobile phase: 0.1% aq TFA and MeOH; Flow rate = 20 mL/min; Gradient elution: 0-5 min 5-40% MeOH in aq TFA, 5-14 min 40-65% MeOH in aq TFA, 14-15 min 65-100% MeOH in aq TFA, 15-20 min 100% MeOH in aq TFA, 20-21 min 5% MeOH in aq TFA; RT = 8.5 min. Desired fractions were evaporated under high vacuum (at rt) and analyzed by HPLC to confirm the purity (Mobile phase: 0.1% aq TFA and MeOH; Flow rate = 20 mL/min; Gradient elution: 0-5 min 10-40% MeOH in aq TFA, 5-16 min 40-60% MeOH in aq TFA, 16-17 min 60-100% MeOH in aq TFA; RT = 8.8 min; purity = 99%). MALDI-TOF MS (ESMS) calc'd for $C_{74}H_{98}N_{21}O_{16}$ (M^+) 1536.75, found: 1536.63.

Peptide-ligand conjugate 12d.

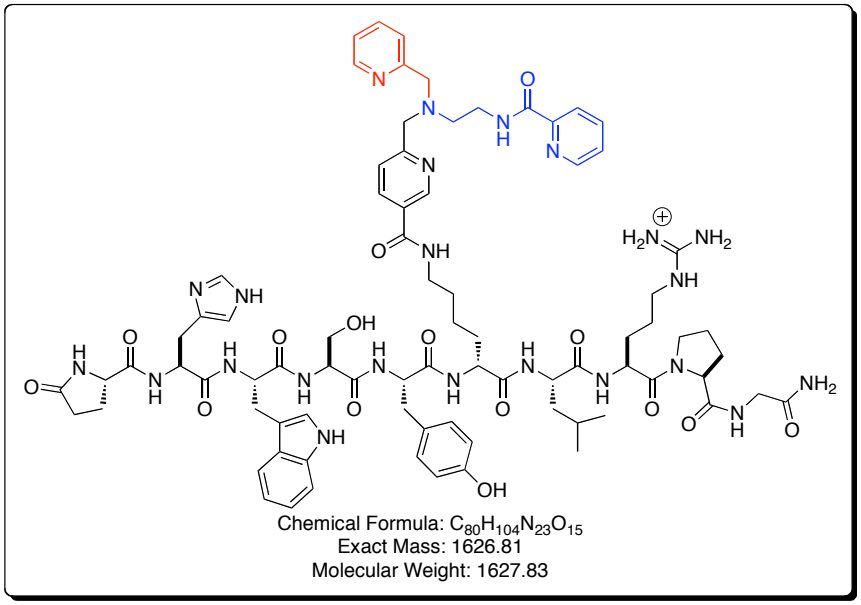

The crude product was purified by preparative HPLC. HPLC Conditions: column: XDB-C18 (ZORBAX) 21.2 × 150 mm, 5 micron; Mobile phase: 0.1% aq TFA and MeOH; Flow rate = 20 mL/min; Gradient elution: 0-5 min 5-40% MeOH in aq TFA, 5-16 min 40-60% MeOH in aq TFA, 16-17 min 60-100% MeOH in aq TFA, 17-22 min 100% MeOH in aq TFA, 22-23 min 5% MeOH in aq TFA; RT = 9.9 min. Desired fractions were evaporated under high vacuum (at rt) and analyzed by HPLC to confirm the purity (Mobile phase: 0.1% aq TFA and MeOH; Flow rate = 20 mL/min; Gradient elution: 0-5 min 10-40% MeOH in aq TFA, 5-16 min 40-60% MeOH in aq TFA, 16-17 min 60-100% MeOH in aq TFA; RT = 10.5 min; purity = 95%). MALDI-TOF MS (ESMS) calc'd for $C_{80}H_{104}N_{23}O_{15}$ (M^+) 1626.81, found: 1626.72.

Peptide-ligand conjugate 12e.

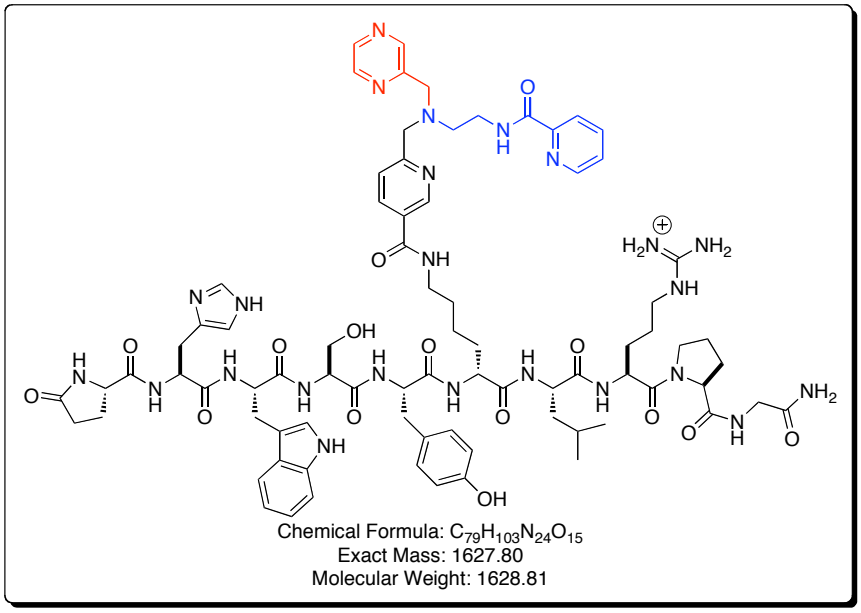

The crude product was purified by preparative HPLC. HPLC Conditions: column: XDB-C18 (ZORBAX) 21.2 × 150 mm, 5 micron; Mobile phase: 0.1% aq TFA and MeOH; Flow rate = 20 mL/min; Gradient elution: 0-5 min 5-40% MeOH in aq TFA, 5-16 min 40-60% MeOH in aq TFA, 16-17 min 60-100% MeOH in aq TFA, 17-22 min 100% MeOH in aq TFA, 22-23 min 5% MeOH in aq TFA; RT = 10.1 min. Desired fractions were evaporated under high vacuum (at rt) and analyzed by HPLC to confirm the purity (Mobile phase: 0.1% aq TFA and MeOH; Flow rate = 20 mL/min; Gradient elution: 0-5 min 10-40% MeOH in aq TFA, 5-16 min 40-60% MeOH in aq TFA, 16-17 min 60-100% MeOH in aq TFA; RT = 10.4 min; purity = 98%). MALDI-TOF MS (ESMS) calc'd for $C_{79}H_{103}N_{24}O_{15}$ (M^+) 1627.80, found: 1627.56.

Peptide-ligand conjugate 12f.

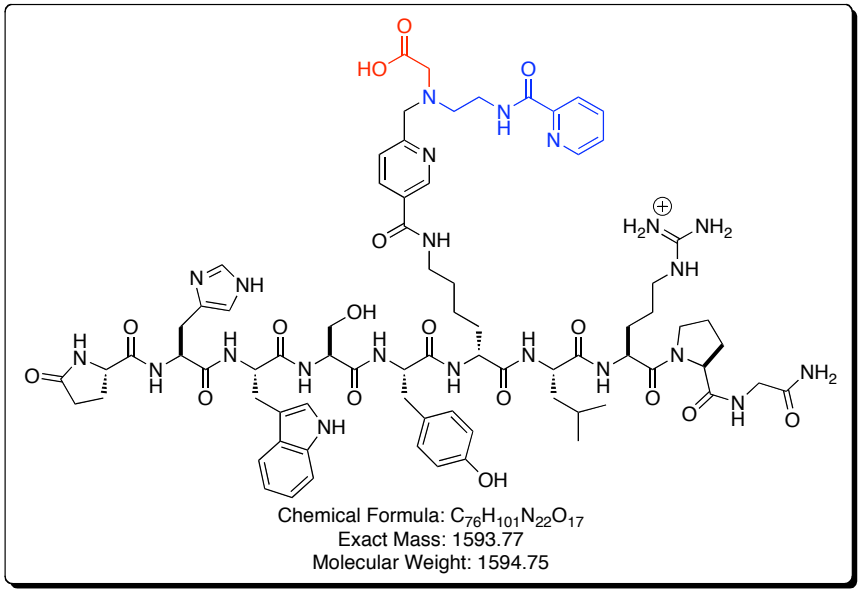

The crude product was purified by preparative HPLC. HPLC Conditions: column: XDB-C18 (ZORBAX) 21.2 × 150 mm, 5 micron; Mobile phase: 0.1% aq TFA and MeOH; Flow rate = 20 mL/min; Gradient elution: 0-5 min 5-40% MeOH in aq TFA, 5-16 min 40-60% MeOH in aq TFA, 16-17 min 60-100% MeOH in aq TFA, 17-22 min 100% MeOH in aq TFA, 22-23 min 5% MeOH in aq TFA; RT = 9.7 min. Desired fractions were evaporated under high vacuum (at rt) and analyzed by HPLC to confirm the purity (Mobile phase: 0.1% aq TFA and MeOH; Flow rate = 20 mL/min; Gradient elution: 0-5 min 10-40% MeOH in aq TFA, 5-16 min 40-60% MeOH in aq TFA, 16-17 min 60-100% MeOH in aq TFA; RT = 10.0 min; purity = 95%). MALDI-TOF MS (ESMS) calc'd for $C_{76}H_{101}N_{22}O_{17}$ (M^+) 1593.77, found: 1593.55.

Peptide-ligand conjugate 13a.

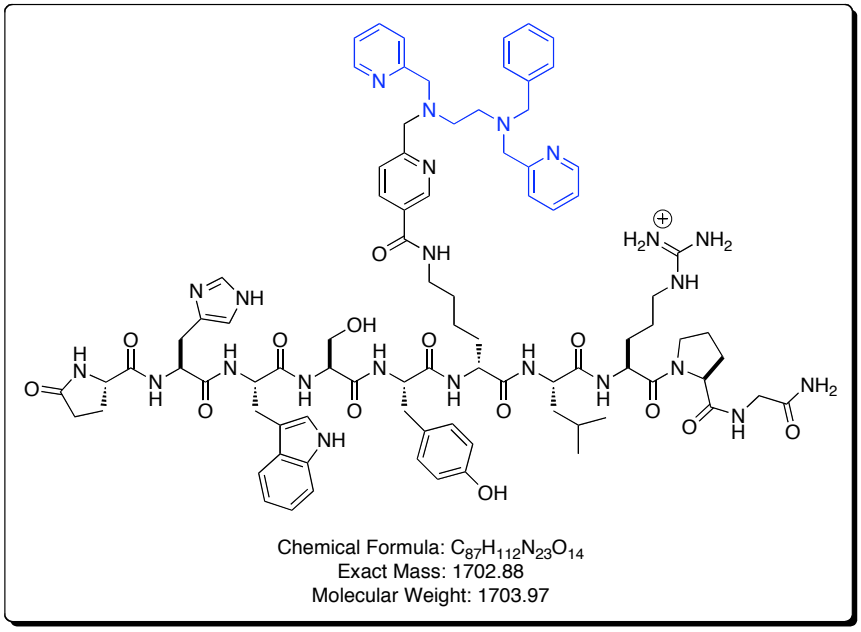

The crude product was purified by preparative HPLC. HPLC Conditions: column: XDB-C18 (ZORBAX) 21.2 × 150 mm, 5 micron; Mobile phase: 0.1% aq TFA and MeOH; Flow rate = 20 mL/min; Gradient elution: 0-5 min 10-40% MeOH in aq TFA, 5-16 min 40-60% MeOH in aq TFA, 16-17 min 60-100% MeOH in aq TFA, 17-22 min 100% MeOH in aq TFA, 22-23 min 10% MeOH in aq TFA; RT = 11.4 min. Desired fractions were evaporated under high vacuum (at rt) and analyzed by HPLC to confirm the purity (Mobile phase: 0.1% aq TFA and MeOH; Flow rate = 20 mL/min; Gradient elution: 0-5 min 10-40% MeOH in aq TFA, 5-16 min 40-60% MeOH in aq TFA, 16-17 min 60-100% MeOH in aq TFA; RT = 11.6 min; purity = 95%). MALDI-TOF MS (ESMS) calc'd for $C_{87}H_{112}N_{23}O_{14}$ (M^+) 1702.88, found: 1702.54.

Peptide-ligand conjugate 13b.

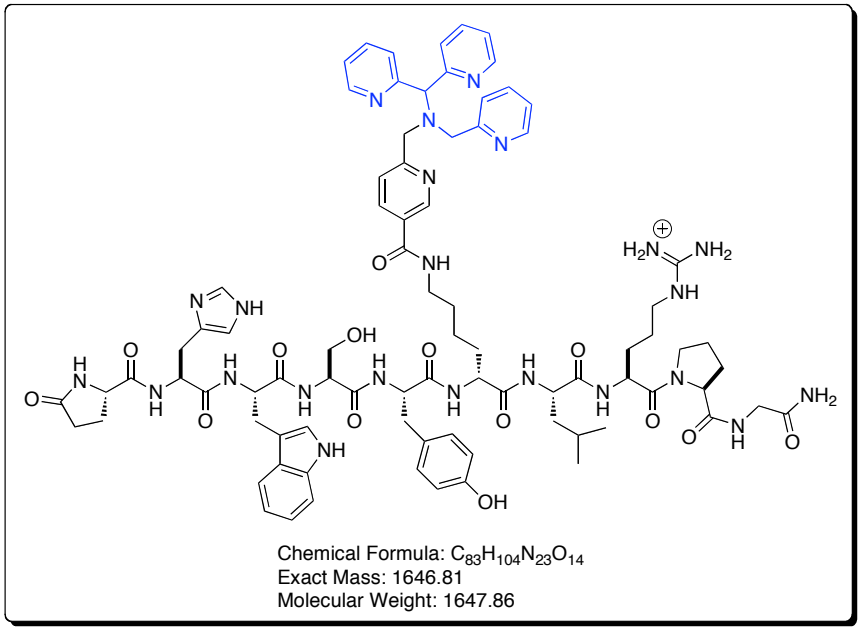

The crude product was purified by preparative HPLC. HPLC Conditions: column: XDB-C18 (ZORBAX) 21.2 × 150 mm, 5 micron; Mobile phase: 0.1% aq TFA and MeOH; Flow rate = 20 mL/min; Gradient elution: 0-5 min 10-40% MeOH in aq TFA, 5-16 min 40-60% MeOH in aq TFA, 16-17 min 60-100% MeOH in aq TFA, 17-22 min 100% MeOH in aq TFA, 22-23 min 10% MeOH in aq TFA, RT = 9.6 min. Desired fractions were evaporated under high vacuum (at rt) and analyzed by HPLC to confirm the purity (Mobile phase: 0.1% aq TFA and MeOH; Flow rate = 20 mL/min; Gradient elution: 0-5 min 10-40% MeOH in aq TFA, 5-16 min 40-60% MeOH in aq TFA, 16-17 min 60-100% MeOH in aq TFA; RT = 9.9 min; purity = 96%). MALDI-TOF MS (ESMS) calc'd for $C_{83}H_{104}N_{23}O_{14}$ (M^+) 1646.81, found: 1646.68.

Chapter 4: Synthesis, Characterization and Mechanistic Studies of Ferryl-peptide Conjugates

4.1 Introduction

Mononuclear non-heme ferryl complexes have been proposed as key intermediates in several enzymes that carry out oxidation reactions in nature.[193] Inspired by the efficiency of these enzymes, biomimetic ferryl complexes have been extensively explored over the last decade as models for such enzymes.[14,15] These synthetic ferryl complexes oxidize organic substrates such as phosphines, sulfides, alkenes, aromatics as well as alkanes and alcohols.[14] Our group has investigated the reactivity of ferryl complexes towards the oxidation of amino acid substrates,[160] peptides[161] and proteins.[17] By virtue of their oxidation power, mechanistic studies of the synthetic ferryl complexes that oxidize organic substrate in an intermolecular fashion are also extensively investigated.[14] In contrast, intramolecular oxidation of organic molecules tethered to ferryl complexes are rare.[164] This information is particularly important because studies pertaining to the ferryl enzymes suggest that the protein radicals, generated during the reactivity of the ferryls, transfer radicals from tryptophan to a remote tyrosine residue via intramolecular long-range electron-transfer (LRET) process.[194-197] In addition, LRET process was also depended on the distance between the radical and the electron-donating group.[197] Moreover, although ferryls are proposed as nature's oxidants, information about which functionalities could be tolerated around them is absent. The fundamental knowledge about how ferryls reacts with target substrates without destroying the parent protein and how the distance between ferryls and reactive groups affects the stability of

ferryls is very important to understand the chemistry of ferryl containing enzymes. This knowledge can also be utilized to construct stable catalysts as well as artificial oxygenases. Since our group aspires to explore the applications of non-heme ligand-peptide conjugates, which could generate ferryl species in bioorganic chemistry, we decided to explore the chemistry of ferryl-peptide conjugates.

In this chapter, synthesis, characterization and reactivity of the first ferryl-peptide conjugate are presented. In the first section, synthesis and characterization of ferrous- and ferryl-peptide conjugates derived from model N4Py-dipeptide conjugate **1** are described. In the second section, the reactivity of ferryl-peptide conjugates and a mechanistic investigation are presented.

4.2 Results

4.2.1 Ferryl-peptide conjugate

4.2.1.1 Synthesis and characterization of Fe^{II} and Fe^{IV} complexes

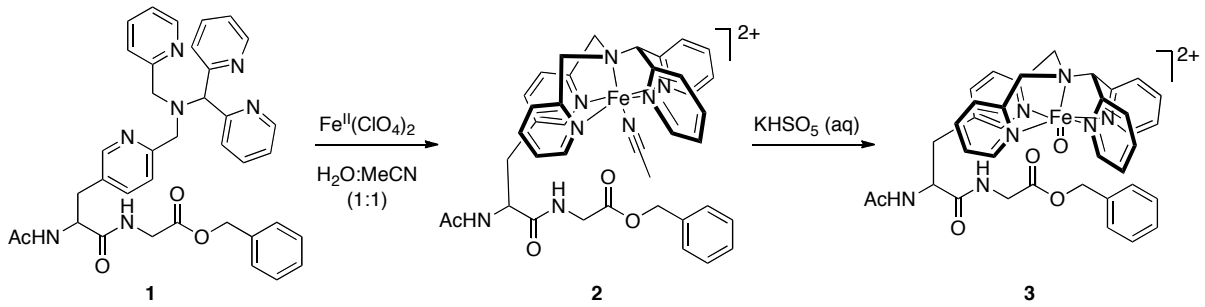

Scheme 4.1: Synthesis of ferrous- and ferryl-peptide conjugates of **1**

Strategies described in the previous chapters produced various non-heme ligand-peptide conjugates that are capable of generating ferryl complexes. Among the pool of these

peptide-ligand conjugates, a N4Py-dipeptide analogue **1** was chosen for this study due to the capability of the N4Py ligand to generate stable ferryl complexes in aqueous/aerobic conditions. First, the ferrous-peptide conjugate **2** was synthesized *in situ* by treating the solution of **1** in 1:1 H_2O:MeCN with an aqueous solution of $Fe^{II}(ClO_4)_2$ to obtain an orange solution (Scheme 4.1). The reaction of this orange species with an aqueous solution of $KHSO_5$ generated the corresponding ferryl-peptide conjugate **3** as a pale-green species.

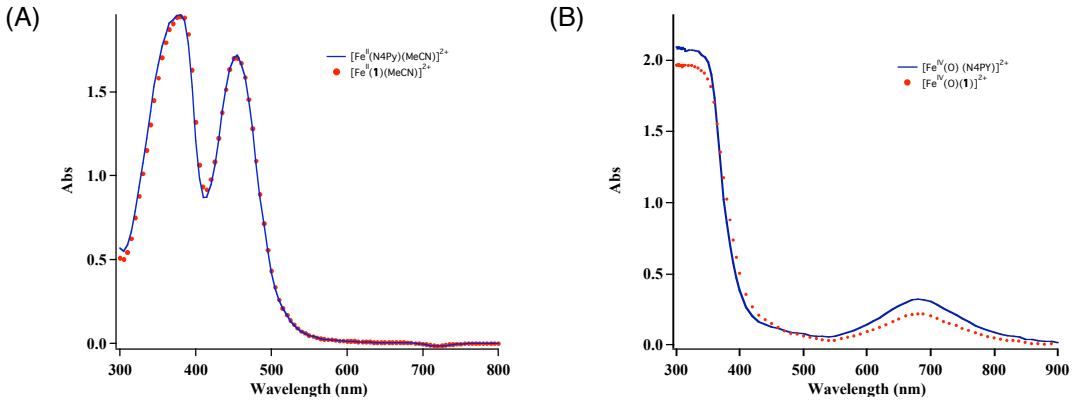

Figure 4.1: (A) Comparison between the UV-vis spectra of ferrous-peptide conjugate **2** (red) with the parent complex $[Fe^{II}(N4Py)(MeCN)]^{2+}$ (blue); (B) Comparison between the UV-vis spectra of ferryl-peptide conjugate **3** (red) with the parent complex $[Fe^{IV}(O)(N4Py)]^{2+}$ (blue)

Ferrous- and ferryl-peptide conjugates were characterized by comparing their UV-vis spectra with the UV-vis spectra of the corresponding parent N4Py complexes. For example, the spectral data for the ferrous-peptide conjugate **2** (ε_{380} = 4200 $M^{-1}cm^{-1}$ and ε_{455} = 3600 $M^{-1}cm^{-1}$) was in agreement with the data of the parent complex $[Fe^{II}(N4Py)(MeCN)]^{2+}$ (ε_{380} = 4200 $M^{-1}cm^{-1}$ and ε_{455} = 3700 $M^{-1}cm^{-1}$) when prepared under identical reaction conditions (Figure 4.1A). Similarly, the absorption maximum (λ_{max} = 680 nm) for the ferryl-peptide conjugate **3** was identical to the corresponding $[Fe^{IV}(O)(N4Py)]^{2+}$ complex (Figure 4.1B).

The absorption at 680 nm decreased prior to complete generation of ferryl-peptide conjugate **3**, which did not allow us to calculate the extinction coefficient from the absorption maximum. Instead, a plot of ln(Abs) vs. time (Figure 4.4B) was extrapolated at $t = 0$ to obtain the extinction coefficient ($\varepsilon_{680} = 200\ M^{-1}cm^{-1}$).

To confirm the formation of ferrous- and ferryl-peptide conjugates, electrospray data were acquired. As shown in Figure 4.2A, N4Py-dipeptide conjugate **1** upon reaction with $Fe(ClO_4)_2 \cdot xH_2O$ furnished a clear molecular ion peak in low resolution ESMS that corresponds to a doubly charged $[Fe^{II}(N4Py)(MeCN)]^{2+}$ species. Moreover, when the reaction of ferrous-peptide conjugate **2** with $KHSO_5$ was monitored by high-resolution ESMS, a dominant molecular ion peak at m/z = 357.6093 was observed (Figure 4.2B). The experimentally obtained isotope pattern was in well agreement with the calculated isotope pattern and corresponds to the formula $[Fe^{IV}(O)(N4Py)]^{2+}$. Interestingly, this molecular ion was not observed in the samples injected after 10 min of the reaction.

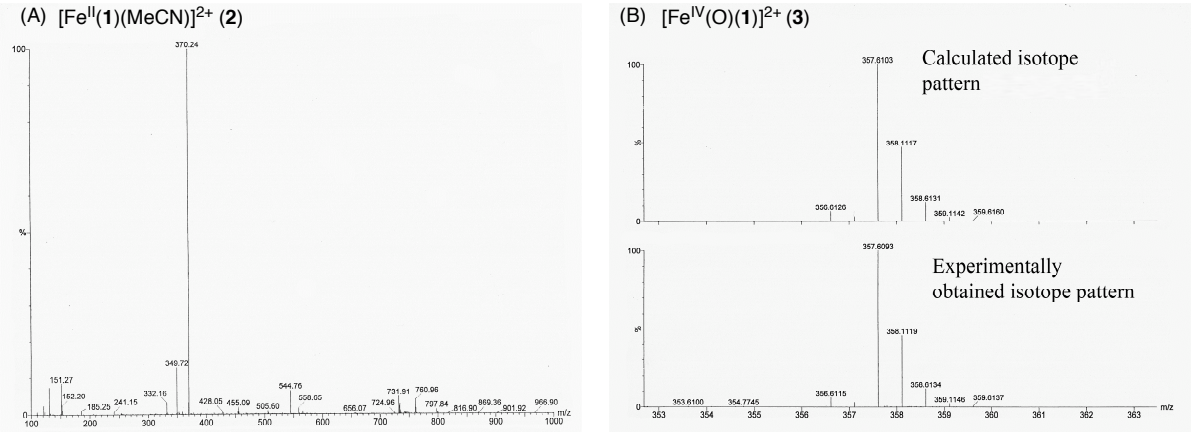

Figure 4.2: (A) LRMS for $[Fe^{II}(\mathbf{1})(MeCN)]^{2+}$; (B) HRMS of $[Fe^{IV}(O)(\mathbf{1})]^{2+}$ showing the calculated (top) and experimental isotope pattern

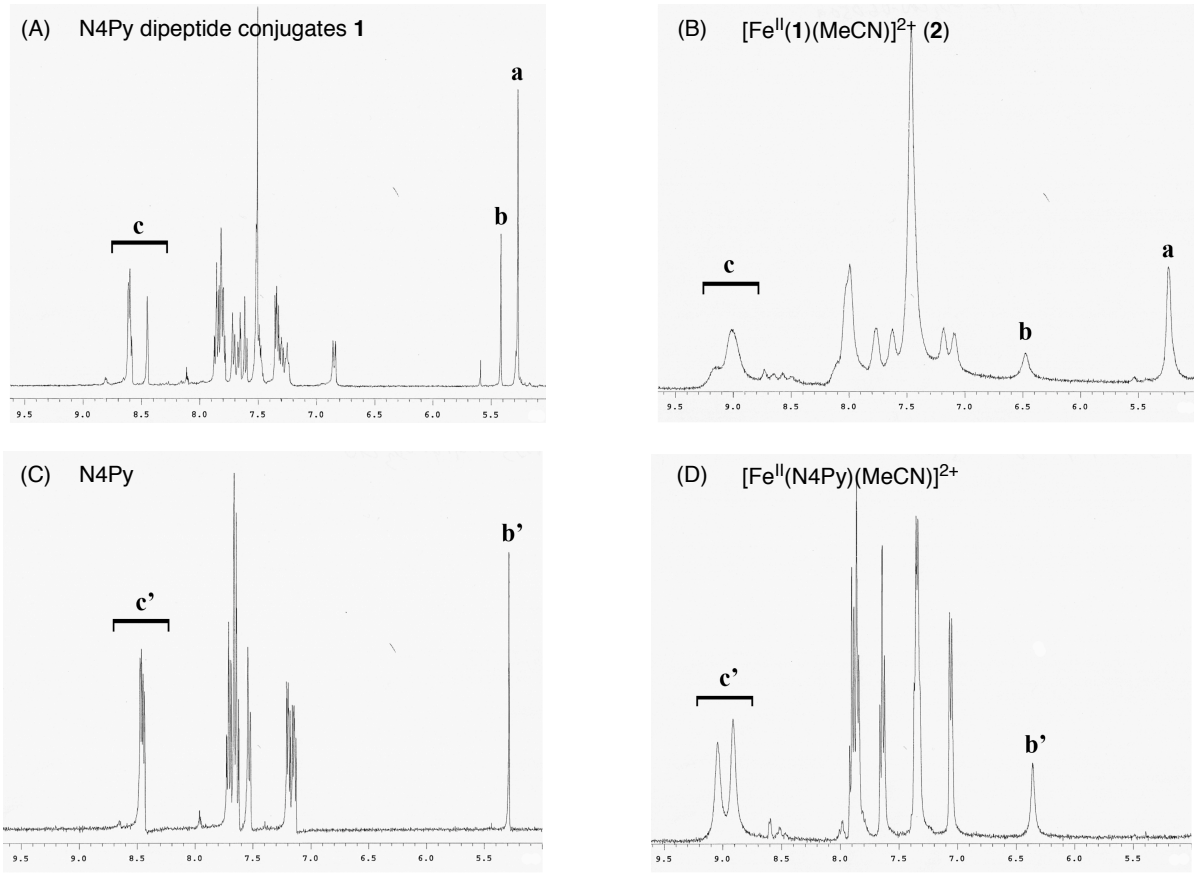

Figure 4.3: (A) ^{1}H NMR of **1** in 1:1 CD_3CN:D_2O; (B) ^{1}H NMR of **1** + $Fe(ClO_4)_2 \cdot xH_2O$ in 1:1 CD_3CN:D_2O; (C) ^{1}H NMR of N4Py in 1:1 CD_3CN:D_2O; (D) ^{1}H NMR of N4Py + $Fe(ClO_4)_2 \cdot xH_2O$ in 1:1 CD_3CN:D_2O

In addition, the reaction of **1** with $Fe(ClO_4)_2 \cdot xH_2O$ was also monitored by ^{1}H NMR spectroscopy, which showed a clear change in the chemical shifts of **1** upon binding with iron (Figure 4.3, A vs. B). It is important to note that the methine proton of N4Py in **1** experienced a shift of ~1 ppm upon coordination to iron (proton b), which is similar to that observed in $[Fe^{II}(N4Py)(MeCN)]^{2+}$ complex when prepared under identical reaction conditions (Figure 4.3, C vs. D). In contrast, benzylic protons that do not participate in the coordination process remained unchanged (proton a). Furthermore, all the NMR resonances are within 0 to 10 ppm

suggesting that the ferrous-peptide conjugate is a low-spin complex. Attempts to characterize the ferryl-peptide conjugate **3** by ^{1}H NMR analysis were unsuccessful due to the rapid decomposition of **3** at the higher concentration that was needed for NMR studies.

Overall, the findings suggested that the ferryl-peptide conjugate **3** is more reactive than the parent N4Py ferryl complex, which eventually caused its rapid decomposition as observed by UV-vis, ESMS and ^{1}H NMR analysis. In fact the ferryl-peptide conjugate **3** was stable for ~1 h compared to the parent $[Fe^{IV}(O)(N4Py)]^{2+}$ that is stable for ~3 days. Since the Kodanko group is planning to attach ferryls to protein-binding motifs for selective protein targeting in the future, the knowledge of its self-decomposition would be valuable for the synthesis of stable catalysts. Hence, we directed our studies towards understanding the rapid decomposition of the ferryl-peptide conjugate **3**. In the following section of this chapter, the reactivity of the ferryl-peptide conjugate **3** and a detailed mechanistic investigation to understand its decomposition are presented.

4.2.1.2 Reactivity and mechanistic studies of the ferryl-peptide conjugate

The reactivity of ferryl complexes towards the benzyl group and the glycine residue was proposed as the cause of the inherent decomposition of the ferryl-peptide conjugate **3**. To probe the reactivity of **3**, five structurally and electronically different derivatives of **1** were synthesized. Derivatives **4a**-**d** were prepared via transesterification by heating **1** with excess alcohol and a catalytic amount of K_2CO_3 (Scheme 4.2a), while derivative **4e** was synthesized from the model dipeptide substrate **5** in five steps (Scheme 4.2b).

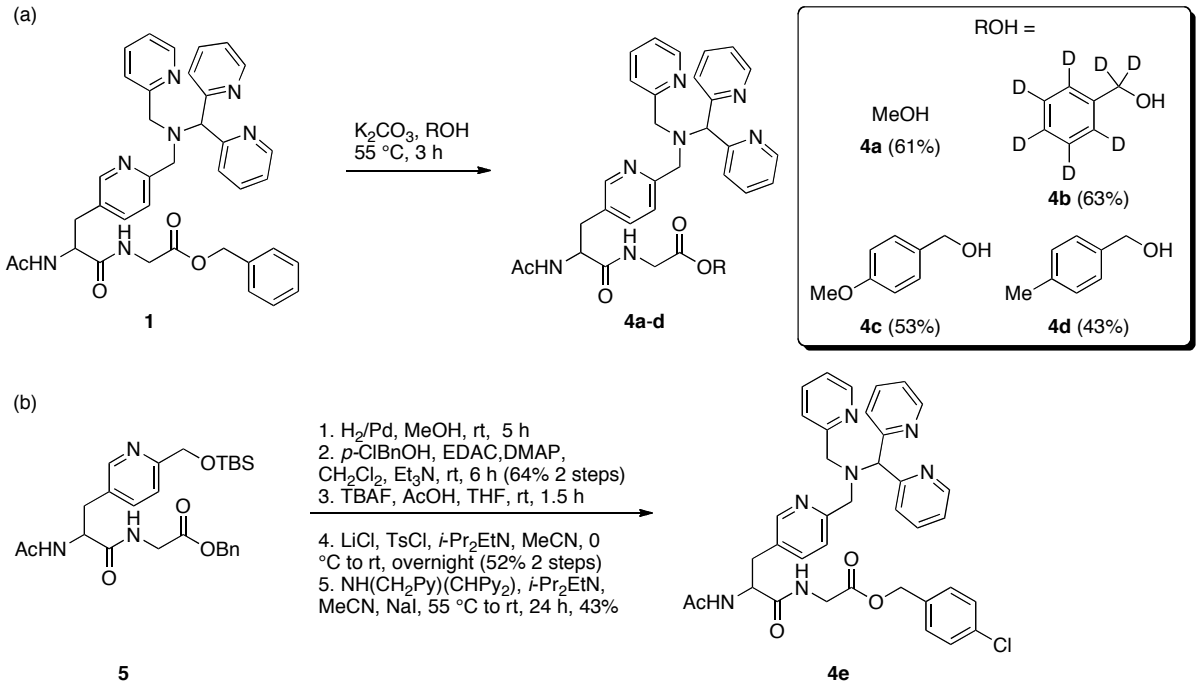

Scheme 4.2: Synthesis of structurally and electronically diverse ester derivatives of **1**

The derivatives of **3** were prepared from each of the ester derivative **4a-e** using the procedures for the formation of **3**. The reactivity of each ferryl-peptide conjugates was determined as shown in Figure 4.4. In a typical procedure, a solution of $[Fe^{II}(L)(MeCN)]^{2+}$ (1.67 mM) was treated with 1 equiv of $KHSO_5$ and the change in the absorbance was monitored at various time intervals. After initial 10 min the absorbance at 680 nm decreased and the absorbance at 450 nm increased indicating the decomposition of ferryl-peptide conjugate and the regeneration of ferrous-peptide conjugate, respectively (Figure 4.4A). A graph of ln(Abs) vs. time at 680 nm furnished a linear plot after an initial induction period of ~10 min (Figure 4.4B). Extinction coefficients of the ferryl-peptide conjugates were calculated by extrapolation of the linear plot to $t = 0$ (ε_{680} = 200 $M^{-1}cm^{-1}$) and were in good agreement with that of the $[Fe^{IV}(O)(N4Py)]^{2+}$ (ε_{680} = 160 $M^{-1}cm^{-1}$) when prepared under identical conditions. In addition, the slope of the plot also furnished rates of the

decomposition for ferryl-peptide conjugates that were used to compare their reactivity (Table 4.1).

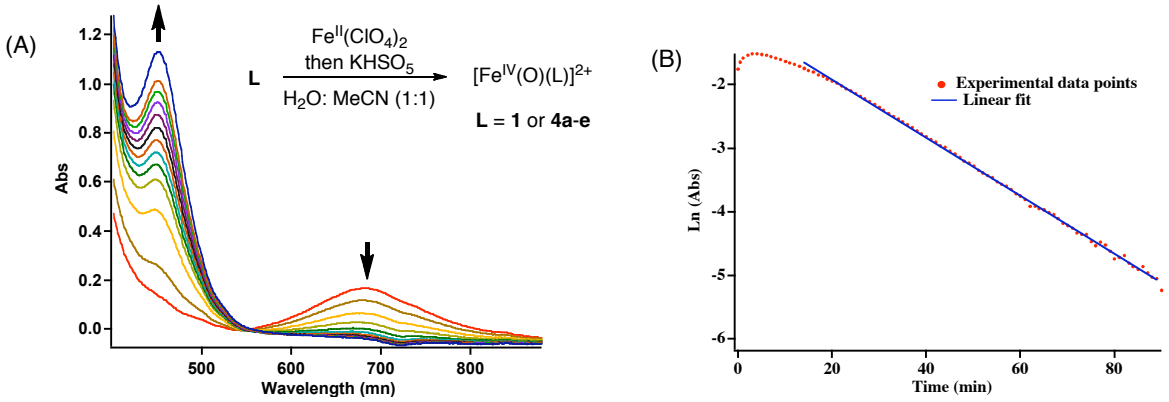

Figure 4.4: (A) Example of the UV-vis spectra for the decomposition of ferryl-peptide conjugates **3**. The decrease in λ_{max} = 680 nm and an increase in λ_{max} = 450 nm indicates the decomposition of the ferryl and regeneration of the ferrous complex, respectively; (B) Example of ln(Abs) vs. time plot (red) and the linear fit (blue) for the ferryl-peptide conjugate **3** at λ_{max} = 680 nm

Table 4.1: Rates of decomposition obtained from the slopes of the ln(Abs) vs. time plots for various ferryl-peptide conjugates

Entry	Ferryl-peptide conjugate	rate (s^{-1})[a,b]	k_{rel}
1	$[Fe^{IV}(O)(\mathbf{1})]^{2+}$ (**3**)	$7.3(6) \times 10^{-4}$	1.0
2	$[Fe^{IV}(O)(\mathbf{4a})]^{2+}$ (Me-ester)	$6.3(3) \times 10^{-5}$	0.086
3	$[Fe^{IV}(O)(\mathbf{4b})]^{2+}$ (Bn-d_7-ester)	$1.6(2) \times 10^{-4}$	0.22
4	$[Fe^{IV}(O)(\mathbf{4c})]^{2+}$ (*p*OMe-Bn-ester)	$1.6(3) \times 10^{-3}$	2.2
5	$[Fe^{IV}(O)(\mathbf{4d})]^{2+}$ (*p*Me-Bn-ester)	$1.2(2) \times 10^{-3}$	1.6
6	$[Fe^{IV}(O)(\mathbf{4e})]^{2+}$ (*p*Cl-Bn-ester)	$3.6(2) \times 10^{-4}$	0.49

[a]Rates were determined from the slope of ln(Abs) vs. time plots. [b]Number reported is the average of at least three runs; error as standard deviation is given in parentheses.

To understand which functional groups within the ferryl-peptide conjugate **3** were responsible for its decomposition, the rate of decomposition of $[Fe^{IV}(O)(\mathbf{4a})]^{2+}$ (Me-ester) was compared with that of the corresponding $[Fe^{IV}(O)(\mathbf{1})]^{2+}$ (**3**). The ferryl generated from the methyl ester derivative was 12 times more stable than the corresponding benzyl ester

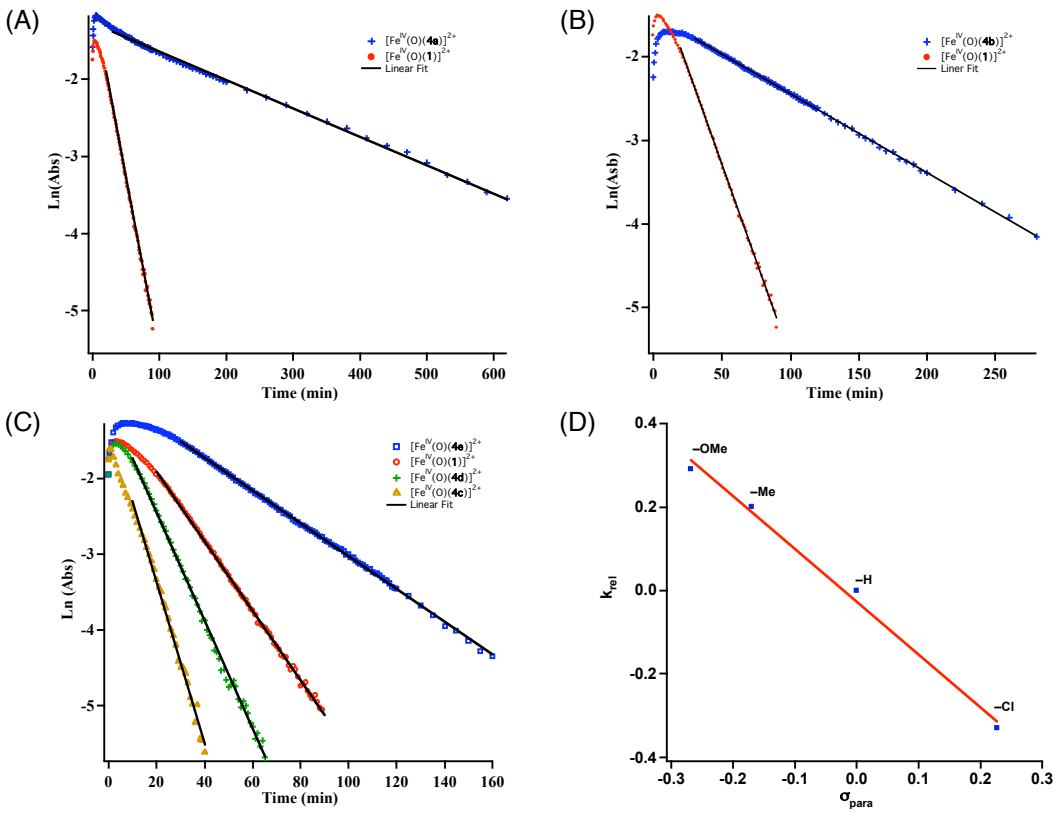

Figure 4.5: (A): Comparison between the rate of decomposition of Me-ester (blue) and Bn-ester (red); (B): Comparison between the rate of decomposition of Bn- d_7-ester (blue) and Bn-ester (red); (C): Comparison between the rate of decomposition of various ferryl-peptide conjugates derived from the *para*-substituted Bn-esters; (D): Hammett plot derived from the rate of decomposition of various ferryls derived from the benzyl ester derivatives

derivative (Figure 4.5A). This clearly implied the role of the benzyl ester moiety in the decomposition of the ferryl species. Furthermore, $[Fe^{IV}(O)(\mathbf{4b})]^{2+}$ (d_7-Bn-ester) also decomposed more slowly than $[Fe^{IV}(O)(\mathbf{1})]^{2+}$ and furnished the kinetic isotope effect (KIE) of 4.5 (Figure 4.5B). To understand the effect of electronics on the decomposition process, ferryls were generated from *para*-substituted benzyl ester derivatives **4c-e** and their rates of decomposition were obtained (Figure 4.5C). Using these rates, a Hammett plot was constructed that displayed a strong linear correlation (r = 0.99) between σ_p and log k_{rel} and gave a ρ value of –1.3 (Figure 4.5D). The small negative value suggested that the ferryl

reacted with the benzylic hydrogen via a hydrogen atom transfer (HAT) mechanism and not via an electron-transfer proton-transfer (ETPT) mechanism, which have given a more negative ρ value.

To probe the reaction further, an effect of the concentration on the decomposition process was also investigated. Towards this, absorbance vs. time data were collected for variable concentrations of $[Fe^{II}(\mathbf{1})(MeCN)]^{2+}$ (0.8-1.7 mM). Using the DynaFit software, the data was fit with various theoretical models by varying the estimated rate constant values (Figure 4.6). The best fits were obtained using model 4, which considers the formation of the ferryl as a bimolecular process and the decay as a unimolecular process. These fits also furnished the second order (k_1 = 5.2(4) $M^{-1}s^{-1}$) and the first order (k_2 = 5.9(1) × 10^{-4} s^{-1}) rate constants for the formation and the decay process respectively. Moreover, the addition of 1 equiv of benzyl alcohol or benzyl acetate did not affect the rate of decomposition of the ferryl-peptide conjugate, however the rates did change when the equivalents of these substrates were increased (Table 4.2).

Table 4.2: Comparison of k_{obs} upon addition of benzyl alcohol and benzyl acetate

Additives	Conc.	k_{obs} s^{-1}	k_{rel}
None	--	7.3(6) × 10^{-4}	--
Benzyl alcohol	1 eq.	7.6 x 10^{-4}	1.0
	5 eq	1.3 x 10^{-3}	1.8
	10 eq.	2.2 x 10^{-3}	3.0
Benzyl acetate	1 eq.	7.4 x 10^{-4}	1.0
	5 eq	9.8 x 10^{-4}	1.3
	10 eq.	1.1 x 10^{-3}	1.5

Model 1

A + B ⟶ C : k_1 ; formation step

C + C ⟶ D + E : k_2 ; bimolecular decay

Where A = $[Fe^{II}(\mathbf{1})(MeCN)]^{2+}$; B = $KHSO_5$, C = $[Fe^{IV}(O)(\mathbf{1})]^{2+}$; D and E = products

Model 2

A + B ⟶ C : k_1 ; formation step

C ⟶ D : k_2 ; electron transfer

D + E ⟶ F + G : k_3 ; proton transfer

Where A = $[Fe^{II}(\mathbf{1})(MeCN)]^{2+}$; B = $KHSO_5$, C = $[Fe^{IV}(O)(\mathbf{1})]^{2+}$; D = radical cation; E = base or solvent; F and G = products

Model 3

A ⟶ B : k_1 ; electron transfer

B + C ⟶ D + E : k_2 ; proton transfer

Where A = $[Fe^{IV}(O)(\mathbf{1})]^{2+}$; B = radical cation; C = base or solvent; D and E = products (Formation step excluded in this model)

Model 4

A + B ⟶ C : k_1 ; formation step

C ⟶ D : k_2 ; unimolecular decay

Where A = $[Fe^{II}(\mathbf{1})(MeCN)]^{2+}$; B = $KHSO_5$; C = $[Fe^{IV}(O)(\mathbf{1})]^{2+}$; D = decomposition

Fit from the DynaFit program using model 4

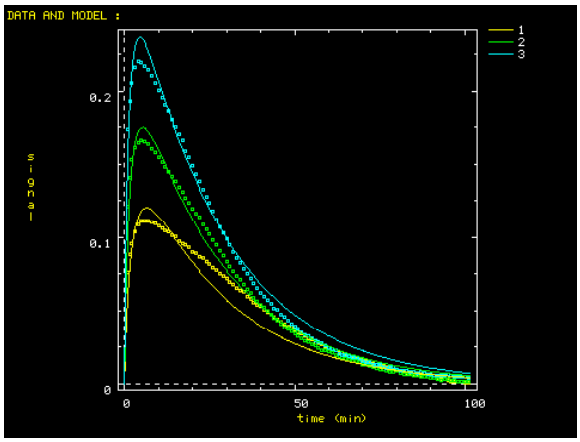

Figure 4.6: Mechanistic models considered in DynaFit; Best fit obtained from DynaFit using model 4 for experimental data (dots) vs. estimated fit (lines) for 0.83 mM (yellow), 1.25 mM (green), and 1.67 mM (blue) of $[Fe^{IV}(O)(\mathbf{1})]^{2+}$

Finally, the products derived from the decomposition of ferryl-peptide conjugates were also characterized using ^{1}H NMR and ESMS analysis to support the mechanism (Scheme 4.3). Formation of benzaldehyde and the acid derivative **7** in this process were indicative of the oxidation of the benzylic position. Moreover, dipyridyl ketone and ~34% of the parent ligand were present in the reaction mixture suggesting a side reaction derived from the decomposition of the ligand moiety.

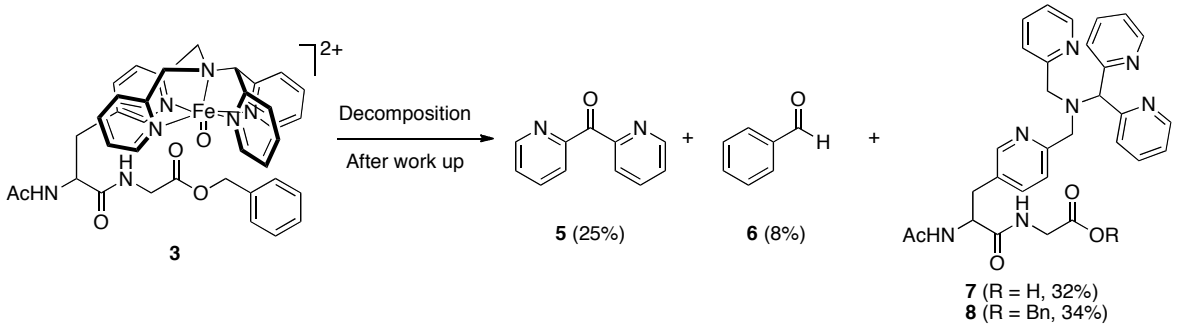

Scheme 4.3: Characterization of the decomposition products

4.3 Discussion

4.3.1 Synthesis and characterization of ferryl-peptide conjugates

Synthesis and characterization of the ferrous- and ferryl-peptide conjugates were straightforward and achieved using the procedures reported for the synthesis of the corresponding N4Py complexes. Interestingly, the ferryl-peptide conjugate $[Fe^{IV}(O)(\mathbf{1})]^{2+}$ (**3**) displayed the faster self-decomposition ($t_{1/2}$ = ~15 min) compared to the corresponding $[Fe^{IV}(O)(N4Py)]^{2+}$ complex ($t_{1/2}$ = ~12 h). Due to this self-decomposition process, a simultaneous formation and decay of the ferryl-peptide conjugate **3** were observed at the initial time period (Figure 4.4B), which led to several challenges during its characterization as well as in the mechanistic studies. For example, the absorption maximum of **3** was lower than the one for $[Fe^{IV}(O)(N4Py)]^{2+}$ (Figure 4.1B), which required its extinction coefficient to be derived indirectly by extrapolating ln(Abs) vs. time plot at $t = 0$ (Figure 4.4B). Moreover, high-resolution ESMS analysis of **3** has shown the molecular ion only at the initial time period (Figure 4.2B), while the ^{1}H NMR analysis of **3** was unsuccessful. Despite these challenges, the characterization data obtained for **2** and **3** were in good agreement with

$[Fe^{IV}(N4Py)(MeCN)]^{2+}$ and $[Fe^{IV}(O)(N4Py)]^{2+}$ complexes respectively, when prepared under identical reaction conditions. The self-decomposition of **3** was attributed to the reactive functionalities of the ferryl-peptide conjugates. Since the knowledge about the stability of the ferryl-peptide conjugate is critical, we decided to investigate the detailed mechanism for the self-decomposition of the ferryl-peptide conjugates.

4.3.2 Mechanistic studies

Considering the literature precedence for the reactivity of ferryl complexes, mechanistic studies were directed towards understanding whether the decomposition is caused by hydroxylation of the phenyl ring or by oxidation of the benzylic or the glycyl moieties of **3**. Towards this, various ester derivatives (**4a-e**) were conveniently prepared. Transesterification of **1** furnished **4a-d**, however attempts to produce the electron withdrawing *p*-nitro benzyl ester or *p*-chloro benzyl ester derivatives by this method were unsuccessful. The poor nucleophilicity of the corresponding alcohol resulted in no reaction at the desired position and gave a complex mixture of products. Alternatively the benzyl ester moiety of **5** was transformed into *p*-chloro benzyl ester prior to incorporation of the N4Py ligand (Scheme 4.2b, **5** to **4e**).

Reaction of 1 equiv of $KHSO_5$ with a solution of $[Fe^{II}(\mathbf{L})(MeCN)]^{2+}$ (where L = **1**, **4a-e**), furnished a pale-green species whose absorption at 680 nm maximized within 10-20 min and then decayed (Figure 4.4A). The linear plot of ln(Abs) vs. time at 680 nm furnished the rate of the decomposition process as well as suggested that the decay process is first-order with respect to the ferryl species (Figure 4.4B). Moreover, an induction period of ~10 min also indicated that the decay process began before the ferryl was fully generated. Therefore,

the ferryl is never fully generated. Rates of decomposition and the relative rates for the ferryls generated from **1** and **4a**-**e** were used to compare their reactivity.

Twelve times slower decomposition of $[Fe^{IV}(O)(\mathbf{4a})]^{2+}$ (Me-ester) compared to $[Fe^{IV}(O)(\mathbf{1})]^{2+}$ (Bn-ester) was clear evidence that the benzyl ester was the primary cause for the decomposition (Figure 4.5A). The KIE of 4.5 (Figure 4.5B) and a Hammett value of ρ = –1.3 (Figure 4.5D) obtained in this process were analogues to that observed in oxidation of ethyl ethers (KIE = 4.4)[198] and *para*-substituted toluene derivatives (ρ = –1.6)[199] by cytochrome P450. The KIE value of 4.5 suggested that the reaction was occurring at the benzylic position and not via aromatic hydroxylation since it would have furnished KIE values close to unity. The negative ρ value indicated that the substantial positive charge is building at the benzylic position. A smaller magnitude of the negative ρ value proves that the hydrogen atom of the benzylic group was abstracted via a hydrogen atom transfer (HAT) mechanism. If a reaction were occurring through an electron-transfer, proton-transfer (ETPT) mechanism a higher magnitude for the negative ρ value (–2.2 to –3.3) would have been observed.[146]

The final goal of the mechanistic studies was to identify whether the decomposition occurs through an inter- or intramolecular pathway. A linear plot of ln(Abs) vs. time at the later time points clearly suggested that the decay process is first-order and hence unimolecular with respect to the ferryl species. This was further supported by the fact that the absorbance vs. time data obtained at various concentrations of $[Fe^{II}(\mathbf{1})(MeCN)]^{2+}$ fitted best into the DynaFit program, when the formation of the ferryl was considered as a bimolecular process and the decay being a unimolecular process (Figure 4.6). Interestingly, the first order rate constant (k_2) obtained from these fits was within the error of the rate constant obtained

from the slop of ln(Abs) vs. time plot (Figure 4.4B). In addition, the inability of 1 equiv of benzyl acetate or benzyl alcohol to alter the rate of decomposition suggested that the process is unimolecular. The slow change in the rate of decomposition upon increasing the amount of additional substrates can be explained if a unimolecular reaction was competing with the bimolecular reaction at the higher concentration (Table 4.2).

From the results obtained in these studies, the mechanistic model was proposed for the decomposition of the ferryl-peptide conjugate (Scheme 4.4A). Ferrous-peptide conjugate **2** reacts with $KHSO_5$ in a bimolecular fashion to furnish the ferryl-peptide conjugate **3**, which upon intramolecular hydrogen atom transfer generates a benzyl radical **9** that eventually decomposes. The proposed mechanistic model also explains the formation of oxidation products (Figure 4.4B). The reactive benzyl radical **9** undergoes a radical rebound process to furnish the corresponding hydroxylated product **10** that eventually collapsed to give benzaldehyde (**6**) and acid **7**. The lower percentage of benzaldehyde compared to **7** was attributed to the issues associated with its isolation. In addition, reaction of the benzyl radical **9** with the methine C-H of the N4Py moiety, presumably through an intermolecular pathway, led to the hydroxylated product **11** and regenerated **1** (34%). The further decomposition of **11** explains the formation of 2-dipyridylketone (**5**) as well as other oxidation products **12**-**14** that were detected in trace amounts by ESMS analysis.

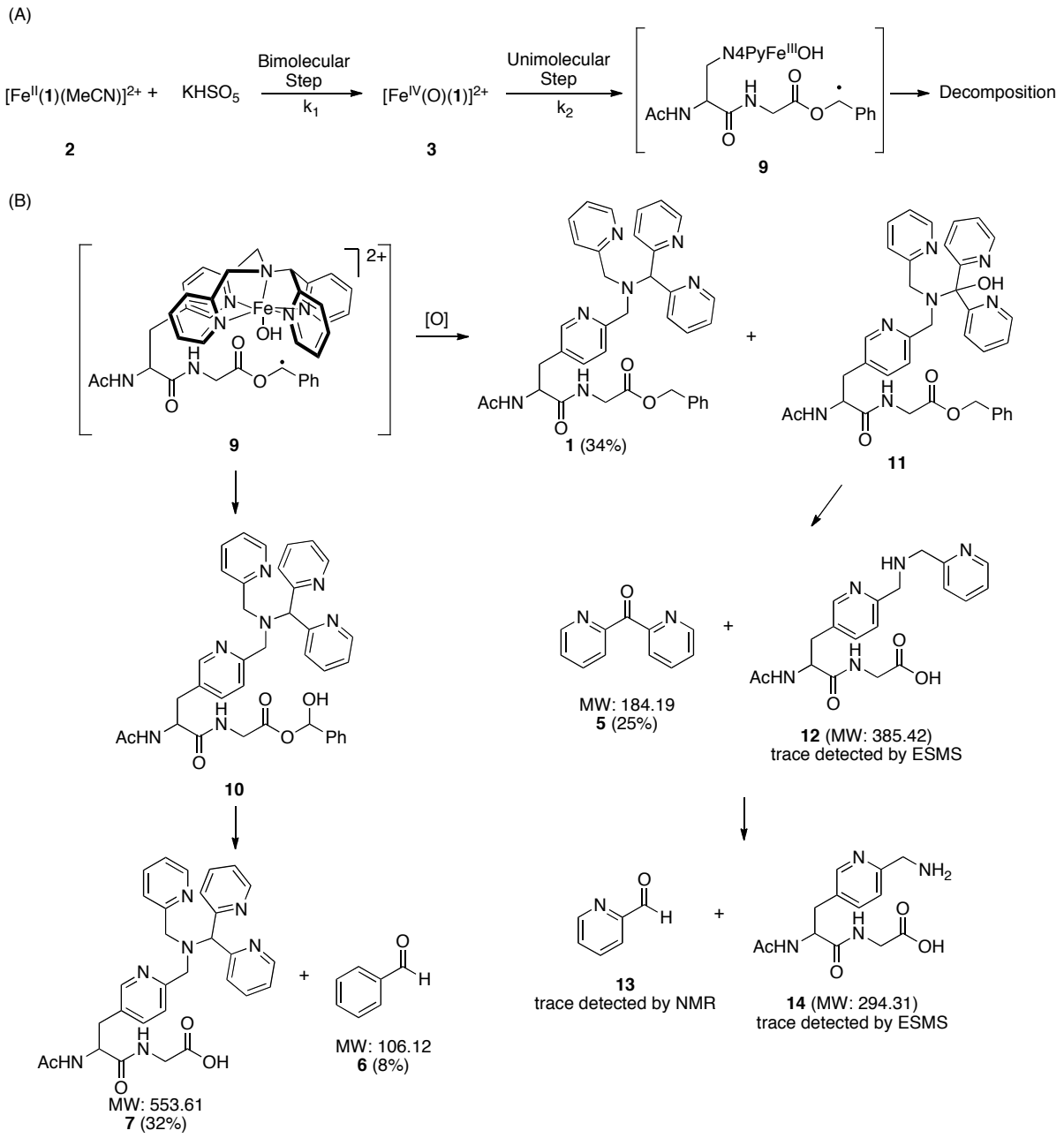

Scheme 4.4: (A) Proposed mechanistic model for the decomposition of the ferryl-peptide conjugate; (B) Formation of various oxidation products in decomposition process (***Note***: products presented herein are after the work up, therefore iron is omitted)

4.4 Conclusion

The first ferryl-peptide conjugate was synthesized and characterized using ^{1}H NMR spectroscopy, UV-vis spectroscopy and HRMS analysis. The ferryl-peptide conjugate was more reactive than the corresponding ferryl complex when it was not tethered to a peptide, which led to its rapid decomposition. This observation has raised the question about the functional group compatibility of the ferryl-peptide conjugates. To understand which functionality on the ferryl-peptide conjugate was responsible for its decomposition, a detailed mechanistic investigation was carried out. Using various mechanistic tools such as KIE, Hammett plot and oxidation product analysis, it has been established that the decomposition was caused by an intramolecular oxidation of the benzylic position by the ferryl. Moreover, the data also suggested that the reaction occurred via a hydrogen atom transfer mechanism. Overall, the knowledge about the functional groups that can be tolerated around ferryls is critical and the study presented herein has set up a foundation to investigate the functional group compatibility of the ferryl complexes. The information gained from this study will be very important to build stable catalysts, and may be applied in the future towards the synthesis of artificial oxygenases.

4.5 Experimental Section

4.5.1 General consideration

See section 2.5.1 for the general considerations. UV-vis spectra were recorded on a Cary 50 spectrophotometer. Fitting of kinetic data was carried out using the program Igor Pro.

4.5.2 Experimental procedures and tabulated characterization data for new compounds

General procedure for transesterification of 1.

A mixture of compound **1**, the corresponding alcohol and potassium carbonate was heated at 75 °C for 3-4 h. The crude reaction mixture was dissolved in ethyl acetate (0.5 mL) and passed through alumina. The excess of alcohol was removed using ethyl acetate as an eluent. The product was then eluted using 2-5% MeOH:CH_2Cl_2 and was purified again either by alumina chromatography or preparative HPLC.

Methyl 2-(2-acetamido-3-(6-(((dipyridin-2-ylmethyl)(pyridin-2-ylmethyl)amino)methyl) pyridin-3-yl)propanamido)acetate (4a).

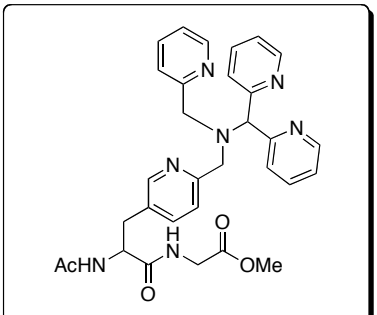

Compound **4a** was prepared by the general procedure for transesterification using **1** (-30 mg, 46.6 μmol), methanol (0.6 mL), and potassium carbonate (3.2 mg, 23.3 μmol). The reaction mixture was concentrated and the crude product was first purified by column chromatography (basic alumina, 0% to 5% MeOH:CH_2Cl_2) and then by preparative HPLC (16 mg, 61%). HPLC Conditions: column: Zorbax XDB-C18, 21.2 × 150 mm, 5 micron equipped with a guard column; flow rate = 20 mL/min; gradient elution 0-5 min 0-20% MeCN in 0.1% aq TFA, 5-15 min 20-65% MeCN in 0.1% aq TFA; RT = 10.2 min.[184] ^{1}H

NMR (400 MHz, $CDCl_3$) δ 8.52 (d, *J* = 4.0 Hz, 2H), 8.46 (d, *J* = 4.9 Hz, 1H), 8.30 (s, 1H), 7.64-7.58 (m, 6H), 7.54-7.47 (m, 2H), 7.13-7.06 (m, 3H), 6.79 (brs, 1H), 6.37 (d, *J* = 7.3 Hz, 1H), 5.30 (s, 1H), 4.69 (dd, *J* = 14.6, *J* = 7.3 Hz, 1H), 3.94-3.87 (m, 6H), 3.66 (s, 3H), 3.06 (dd, *J* = 13.8, 6.5 Hz, 1H), 2.97 (dd, *J* = 13.8, 6.5 Hz, 1H), 1.92 (s, 3H); ^{13}C NMR (100 MHz, $CDCl_3$) δ 171.8, 170.3, 169.7, 159.9, 159.8, 158.6, 149.6, 149.2, 149.0, 137.3, 136.4, 136.3, 130.1, 123.9, 122.9, 122.7, 122.1, 121.8, 71.7, 57.1, 56.7, 53.7, 52.3, 41.1, 34.8, 23.1; IR (thin film) 3288, 3054, 3009, 2951, 2918, 2849, 1752, 1654, 1588, 1569, 1548, 1487, 1471, 1433, 1400, 1371, 1288, 1261, 1210, 1181, 1149, 1126, 1089, 1049, 1032, 996, 984, 911, 785, 755, 731, 646 cm^{-1}; LRMS (ESMS) calcd for $C_{31}H_{34}N_7O_4$ $(M+H)^+$ 568, found: 568.

d_7-Benzyl 2-(2-acetamido-3-(6-(((dipyridin-2-ylmethyl)(pyridin-2-ylmethyl)amino) methyl)pyridin-3-yl)propanamido)acetate (4b).

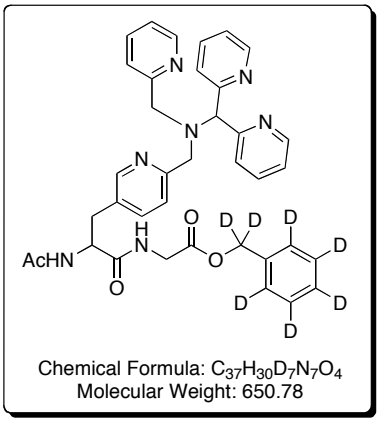

Compound **4b** was prepared by the general procedure for transesterification using **1** (-30 mg, 46.6 μmol), d_7-benzyl alcohol (269 μL, 2.3 mmol), and potassium carbonate (3.2 mg, 23.3 μmol). The crude product was purified by column chromatography (basic alumina, 100% EtOAc to elute excess alcohol and then 0% to 5% MeOH:CH_2Cl_2 to elute product) (19 mg, 63%). ^1H NMR (400 MHz, $CDCl_3$) δ 8.51 (d, *J* = 4.0 Hz, 2H), 8.44 (d, *J* = 4.0 Hz, 1H),

8.30 (s, 1H), 7.63-7.47 (m, 8H), 7.10-7.03 (m, 4H), 6.54 (brs, 1H), 5.30 (s, 1H), 4.73-4.68 (m, 1H), 4.03-3.81 (m, 6H), 3.06 (dd, *J* = 13.8, 6.5 Hz, 1H), 2.96 (dd, *J* = 13.8, 6.5 Hz, 1H), 1.88 (s, 3H); ^{13}C NMR (100 MHz, $CDCl_3$) δ 171.0, 170.4, 169.2, 159.9, 159.6, 158.3, 149.6, 149.2, 149.0, 137.4, 136.4, 136.3, 130.3, 123.9, 122.9, 122.8, 122.1, 121.8, 71.9, 57.0, 56.7, 53.7, 41.2, 34.7, 23.0; IR (thin film) 3286, 1748, 1656, 1588, 1569, 1433, 1372, 1187, 1031, 995, 730 cm^{-1}; HRMS (ESMS) calcd for $C_{37}H_{31}D_7N_7O_4$ $(M+H)^+$ 651.3425, found: 651.3405.

4-methoxybenzyl 2-(2-acetamido-3-(6-(((dipyridin-2-ylmethyl)(pyridin-2-ylmethyl) amino)methyl)pyridin-3-yl)propanamido)acetate (4c).

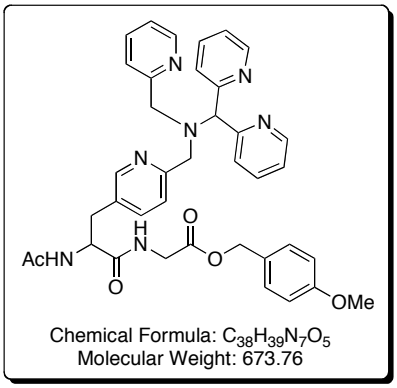

Compound **4c** was prepared by the general procedure for transesterification using **1** (-40 mg, 62.2 μmol), *p*-methoxy benzyl alcohol (429 mg, 3.1 mmol), and potassium carbonate (4.3 mg, 31.1 μmol). The crude product was purified by column chromatography (basic alumina, 100% EtOAc to elute excess alcohol and then 0% to 5% MeOH:CH_2Cl_2 to elute product). The resulting product was stirred with 4:6 Et_2O:hexanes (3 × 2 mL) and a solid was isolated by decantation. The product was further by preparative HPLC (22 mg, 53%). HPLC Conditions: column: Zorbax XDB-C18, 21.2 × 150 mm, 5 micron equipped with guard column; flow rate = 20 mL/min; gradient elution 0-5 min 0-20% MeCN in 0.1% aq TFA, 5-15 min 20-65% MeCN in 0.1% aq TFA; RT = 9.0 min.[184] ^{1}H NMR (400 MHz, CD_3CN) δ

8.45-8.42 (m, 3H), 8.28 (d, *J* = 1.6 Hz, 1H), 7.72-7.62 (m, 5H), 7.56 (d, *J* = 8.1 Hz, 1H), 7.51-7.44 (m, 2H), 7.28 (d, 2H), 7.20-7.10 (m, 4H), 6.89 (d, *J* = 8.9 Hz, 2H), 6.73 (d, *J* = 8.1 Hz, 1H), 5.23 (s, 1H), 5.04 (s, 2H), 4.59-4.53 (m, 1H), 3.87-3.85 (m, 6H), 3.75 (s, 3H), 3.06 (dd, *J* = 14.6, 5.7 Hz, 1H), 2.78 (dd, *J* = 14.6, 8.9 Hz, 1H), 1.77 (s, 3H); ^{13}C NMR (100 MHz, CD_3CN) δ 172.4, 170.9, 170.5, 161.4, 160.9, 159.0, 150.6, 149.9, 149.8, 138.0, 137.3, 137.2, 132.2, 131.1, 129.0, 124.8, 123.8, 123.4, 123.1, 122.9, 118.3, 114.8, 72.8, 67.3, 57.9, 57.6, 55.9, 54.7, 41.8, 35.3, 22.9; IR (thin film) 3286, 3051, 2933, 2837, 1747, 1658, 1613, 1588, 1569, 1515, 1469, 1433, 1373, 1249, 1173, 1032, 995, 824, 756, 734, 700 cm^{-1}; HRMS (ESMS) calcd for $C_{38}H_{40}N_7O_5$ $(M+H)^+$ 674.3091, found: 674.3084.

4-methylbenzyl 2-(2-acetamido-3-(6-(((dipyridin-2-ylmethyl)(pyridin-2-ylmethyl) amino)methyl)pyridin-3-yl)propanamido)acetate (4d).

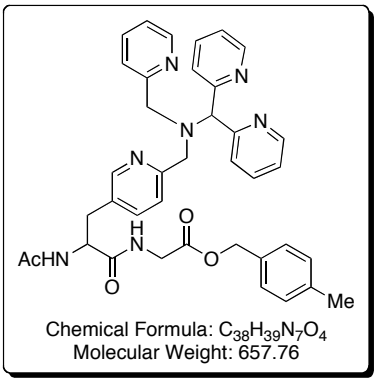

Compound **4d** was prepared by the general procedure for transesterification using **1** (-30 mg, 46.6 μmol), *p*-methyl benzyl alcohol (357 mg, 2.3 mmol), and potassium carbonate (3.2 mg, 23.3 μmol). The crude product was heated at 75 °C under high vacuum (~ 0.3 mm/Hg) to remove excess *p*-methyl benzyl alcohol. The resulting product was further purified by preparative HPLC (13 mg, 43%). HPLC Conditions: column: Zorbax XDB-C18, 21.2 × 150 mm, 5 micron equipped with guard column; flow rate = 20 mL/min; gradient

elution 0-5 min 5-20% MeCN in 0.1% aq TFA, 5-15 min 20-50% MeCN in 0.1% aq TFA, 15-16 min 50-95% MeCN in 0.1% aq TFA; RT = 10.8 min.[184] ^{1}H NMR (400 MHz, $CDCl_3$) δ 8.52 (d, *J* = 4.9 Hz, 2H), 8.45 (d, *J* = 4.9 Hz, 1H), 8.29 (s, 1H), 7.64-7.57 (m, 6H), 7.53-7.46 (m, 2H), 7.18-7.05 (m, 7H), 6.81 (t, *J* = 4.9 Hz, 1H), 6.36 (d, *J* = 7.3 Hz, 1H), 5.30 (s, 1H), 5.05 (s, 2H), 4.71-4.66 (m, 1H), 4.02-3.88 (m, 6H), 3.05 (dd, *J* = 13.8, 6.5 Hz, 1H), 2.95 (dd, *J* = 13.8, 6.5 Hz, 1H), 2.30 (s, 3H), 1.89 (s, 3H); ^{13}C NMR (100 MHz, $CDCl_3$) δ 170.8, 170.3, 169.2, 159.9, 159.7, 158.5, 149.6, 149.2, 149.0, 137.3, 136.4, 136.3, 130.1, 129.3, 128.6, 123.9, 122.9, 122.8, 122.1, 121.8, 71.9, 67.2, 57.0, 56.7, 53.7, 41.3, 34.8, 23.1, 21.2; IR (thin film) 3285, 3052, 2925, 1749, 1654, 1588, 1569, 1471, 1433, 1377, 1180, 1031, 995, 755 cm^{-1}; LRMS (ESMS) calcd for $C_{38}H_{40}N_7O_4$ $(M+H)^+$ 658, found: 658.

4-chlorobenzyl 2-(2-acetamido-3-(6-((tert-butyldimethylsilyloxy)methyl)pyridin-3-yl) propanamido)acetate (15).

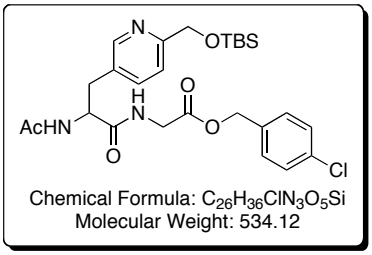

A mixture of compound **5** (1.3 g, 2.6 mmol), MeOH (39 mL) and 5% Pd/C (130 mg) was stirred at rt under H_2 (1 atm) for 5 h. After consumption of the starting material, as judged by TLC analysis, the reaction mixture was filtered through celite. The filtrate was concentrated to obtain a sticky white solid, which upon triturating with Et_2O for 30 min furnished Ac-HPA(OTBS)-Gly-OH as a white solid. The white solid was isolated by filtration and washed with Et_2O (1.06 g, quantitative).

A mixture of Ac-HPA(OTBS)-Gly-OH (50 mg, 122 μmol), 4-chlorobenzyl alcohol (17.4 mg, 122 μmol), CH_2Cl_2 (1 mL), Et_3N (25 μL, 183 μmol), and DMAP (3 mg, 30.5 μmol) was maintained at rt under a nitrogen atmosphere for 5 min. EDAC (28 mg, 146 μmol) was added and the mixture was maintained for 5-6 h. The reaction mixture was combined with CH_2Cl_2 (25 mL) and the organic layer was extracted with $NaHCO_3$ (5% aq, 3 × 15 mL), NH_4Cl (sat. aq, 3 × 15 mL) and NaCl (sat. aq, 3 × 15 mL) respectively. The organic layer was separated, dried over anhydrous Na_2SO_4 and concentrated to obtain the crude product as a viscous oil (42 mg, 64%). A small portion of the crude product was purified by column chromatography (silica gel, 0% to 3% MeOH:CH_2Cl_2) for analysis. ^{1}H NMR (400 MHz, $CDCl_3$) δ 8.31 (s, 1H), 7.56 (d, *J* = 8.1 Hz, 1H), 7.42 (d, *J* = 8.1 Hz, 1H), 7.32-7.23 (m, 4H), 6.85 (brs, 1H), 6.32 (brs, 1H), 5.09 (s, 2H), 4.77-4.71 (m, 3H), 4.06-3.93 (m, 2H), 3.11 (dd, *J* = 13.8, 7.3 Hz, 1H), 2.98 (dd, *J* = 13.8, 7.3 Hz, 1H), 1.93 (s, 3H), 0.92 (s, 9H), 0.08 (s, 6H); ^{13}C NMR (100 MHz, $CDCl_3$) δ 170.9, 170.4, 169.1, 160.0, 149.0, 137.8, 134.5, 133.5, 130.1, 129.8, 128.8, 120.0, 66.4, 65.7, 53.7, 41.2, 34.8, 25.9, 23.1, 18.3, –5.4; IR (thin film) 3284 (b), 3066, 2954, 2929, 2857, 1752, 1651, 1602, 1548, 1493, 1471, 1374, 1254, 1187, 1096, 1032, 1017, 839, 809, 779, 732 cm^{-1}; LRMS (ESMS) calcd for $C_{26}H_{37}ClN_3O_5Si$ $(M+H)^+$ 534, found: 534.

4-chlorobenzyl 2-(2-acetamido-3-(6-(chloromethyl)pyridin-3-yl)propanamido)acetate (16).

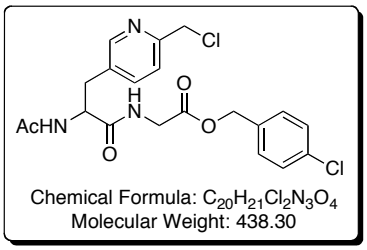

A mixture of crude compound **15** (42 mg, 78.6 μmol), acetic acid (4.5 μL, 78.6 μmol) and THF (0.6 mL) was maintained under a nitrogen atmosphere for 5 min. A 1M solution of TBAF in THF (157 μL, 157 μmol) was added and the reaction mixture was maintained for 1.5 h. After consumption of the starting material, as judged by TLC analysis, the reaction mixture was combined with H_2O (20 mL) and the solution was adjusted to pH ~8 using Na_2CO_3 (sat. aq). The aqueous layer was extracted with CH_2Cl_2 (15 × 5 mL). The combined organic layers were dried over anhydrous Na_2SO_4 and concentrated to obtain the corresponding alcohol as a white solid. After triturating the solid with Et_2O overnight a white solid was isolated by decantation (26 mg, 79%).

A mixture of alcohol (26 mg, 62 μmol), flame dried LiCl (26 mg, 620 μmol), MeCN (1 mL), and *i*-Pr_2EtN (22 μL, 124 μmol) was cooled to 0 °C and TsCl (18 mg, 93 μmol) was added under a nitrogen atmosphere. The reaction mixture was stirred at 0 °C for 1.5 h and then warmed to rt. The color of the reaction mixture changed from colorless to orange. The orange suspension was maintained at rt for overnight. After consumption of the starting material, as judged by TLC analysis, the reaction mixture was decanted and the residues were rinsed with MeCN (5 mL). The combined MeCN layer was concentrated and the crude product was combined with CH_2Cl_2 (15 mL). The CH_2Cl_2 layer was extracted with an aqueous $NaHCO_3$ (pH ~9) solution (3 × 10 mL). The organic layer was dried over anhydrous Na_2SO_4 and concentrated to obtain crude product as a red oil. The crude product was purified by column chromatography (basic alumina, 0% to 5% MeOH:CH_2Cl_2) to provide an orange oil (14 mg, 52%). ^{1}H NMR (400 MHz, $CDCl_3$) δ 8.38 (s, 1H), 7.60 (dd, J = 8.1 Hz, 1H), 7.37 (dd, J = 7.3 Hz, 1H), 7.32-7.26 (m, 4H), 7.06 (brs, 1H), 6.44 (d, J = 7.3 Hz, 1H), 5.09 (s, 2H), 4.82-4.76 (m, 1H), 4.62 (s, 2H), 4.00 (d, J = 5.7 Hz, 2H), 3.14 (dd, J = 13.8, 6.5 Hz,

1H), 2.99 (dd, J = 13.8, 6.5 Hz, 1H), 1.93 (s, 3H); ^{13}C NMR (100 MHz, $CDCl_3$) δ 170.9, 170.4, 169.1, 155.1, 149.9, 138.2, 134.5, 133.5, 131.7, 129.8, 128.8, 122.7, 66.4, 53.5, 46.2, 41.2, 34.9, 23.0; IR (thin film) 3290 (b), 3065, 1749, 1651, 1546, 1493, 1380, 1188, 1093, 1016, 806 cm^{-1}; LRMS (ESMS) calcd for $C_{20}H_{22}Cl_2N_3O_4$ $(M+H)^+$ 438, found: 438.

4-chlorobenzyl 2-(2-acetamido-3-(6-(((dipyridin-2-ylmethyl)(pyridin-2-ylmethyl)amino) methyl)pyridin-3-yl)propanamido)acetate (4e).

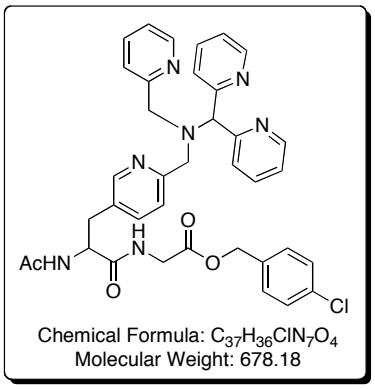

A mixture of compound **16** (39 mg, 89 μmol), MeCN (2 mL), *i*-Pr_2EtN (64 μL, 0.36 mmol), sodium iodide (3.3 mg, 18 μmol) and 1,1-di(pyridin-2-yl)-*N*-(pyridin-2-ylmethyl)methanamine [NH($PyCH_2$) ($CHPy_2$); where Py = 2-pyridyl] (74 mg, 0.27 mmol) was heated at 55 °C for 24 h. The reaction mixture was condensed under vacuum and the resulting oil was dissolved in CH_2Cl_2 (10 mL). The organic layer was extracted with $NaHCO_3$ (5% aq, 3 × 5 mL). The organic layer was dried over anhydrous Na_2SO_4 and concentrated to obtain the crude product. The product was purified first by column chromatography (basic alumina, 0% to 5% MeOH:CH_2Cl_2) and then by preparative HPLC (26 mg, 43%). HPLC Conditions: column: Zorbax XDB-C18, 21.2 × 150 mm, 5 micron equipped with guard column; flow rate = 20 mL/min; gradient elution 0-5 min 0-20% MeCN in 0.1% aq TFA, 5-15 min 20-65% MeCN in 0.1% aq TFA; RT = 9.7 min.[184] ^{1}H NMR (400

MHz, $CDCl_3$) δ 8.52-8.47 (m, 3H), 8.40 (s, 1H), 7.64-7.44 (m, 9H), 7.28-7.19 (m, 4H), 7.12-7.06 (m, 3H), 6.76 (brs, 1H), 5.31 (s, 1H), 5.07 (s, 2H), 4.71 (dd, *J* = 14.6, 7.3 Hz, 1H), 4.02-3.90 (m, 6H), 3.08 (dd, *J* = 13.8, 6.5 Hz, 1H), 2.98 (dd, *J* = 13.8, 6.5 Hz, 1H), 1.89 (s, 3H); ^{13}C NMR (100 MHz, $CDCl_3$) δ 171.0, 170.4, 169.1, 159.8, 159.6, 158.3, 149.4, 149.2, 149.0, 137.5, 136.4, 136.3, 134.4, 133.6, 130.4, 129.7, 128.8, 123.9, 122.9, 122.8, 122.2, 121.9, 71.8, 66.2, 57.1, 56.6, 53.8, 41.2, 34.7, 23.0; IR (thin film) 3288 (b), 3054, 2931, 1751, 1655, 1588, 1569, 1492, 1471, 1433, 1375, 1186, 1093, 996, 910, 731, 645 cm^{-1}; LRMS (ESMS) calcd for $C_{37}H_{37}ClN_7O_4$ $(M+H)^+$ 678, found: 678.

Synthesis and Characterization of $[Fe^{II}(1)(MeCN)]^{2+}$ and $[Fe^{IV}(O)(1)]^{2+}$.

^1H NMR Data (Figure 4.3)

The methine (b) and pyridyl (c) protons of **1** were clearly shifted downfield (Figure 4.3, A and B) upon addition of 1 eq of $Fe(ClO_4)_2 \cdot xH_2O$ (aq) to the solution of **1** (5-7 mg) in 1:1 MeCN:H_2O. These shifts were inline with the shifts obtained from the corresponding methine (b') and pyridyl protons (c') of the reference N4Py ligand (Figure 4.3, C and D) under identical experimental conditions.

Mass Spectrometry Data (Figure 4.2)

Mass spectra were recorded in positive ion mode using Waters ZQ2000 single quadrupole mass spectrometer using an electrospray ionization source or Waters-Micromass LCT Premier XE time of flight mass spectrometer equipped with an electrospray ionization source (ESI). The key parameters used for the experiment are as follows: Capillary voltage 3.3 kV, Sample cone voltage 5 V, Desolvation temperature 300 °C, Source temperature 120 °C, Cone gas Flow 200, Desolvation gas flow 700. The instrument was equilibrated with MeCN before injecting the sample.

360 μL, 2 mM solution of **1** (1:1 MeCN:H_2O) was mixed with 36 μL, 20 mM solution of $Fe^{II}(ClO_4)_2 \cdot xH_2O$ (in H_2O) to obtain a yellow solution. 5 μL of this solution was mixed with 150 μL MeCN and 10 μL of the resulting solution was injected in the Waters ZQ2000 single quadrupole mass spectrometer. Mass spectra were processed using MassLynx software. The dominant molecular ion was observed at m/z 370, which is consistent with its molecular formula $[Fe^{II}(\mathbf{1})(MeCN)]^{2+}$ (Figure 4.2A).

The species **3** (1.67 mM) was freshly prepared and 5 μL of this solution was mixed with 50 μL MeCN at various time periods up to 13 min. 10 μL of these solutions were injected each time in the Waters-Micromass LCT Premier XE time of flight mass spectrometer. Mass spectra were processed using MassLynx software. In the sample injected at the 8th min, the dominant molecular ion was observed at m/z 357.6093, along with a suitable isotopic pattern, which is consistent with its formula $[Fe^{IV}(O)(\mathbf{1})]^{2+}$ (**3**) (calc. m/z 357.6103, Figure 4.3B).

UV-vis Data (Figure 4.1)

Table 4.3: Extinction coefficients for the ferrous- and ferryl-peptide conjugate and corresponding N4Py complexes in identical reaction conditions

Species	**ε ($M^{-1}cm^{-1}$)**	**λ_{max}(nm)**
$[Fe^{II}(N4Py)(MeCN)]^{2+}$	4.2×10^3	380
	3.7×10^3	455
$[Fe^{II}(\mathbf{1})(MeCN)]^{2+}$ (**2**)	4.2×10^3	380
	3.6×10^3	455
$[Fe^{IV}(O)(N4Py)]^{2+}$	1.6×10^2	680
$[Fe^{IV}(O)(\mathbf{1})]^{2+}$ (**3**)	2.0×10^2	680

Product analysis for decomposition of ferryl-peptide conjugate 3.

A solution of **1** (13 mg, 20 μmol) in 1:1 H_2O:MeCN (12 mL) was treated with 1 equiv. of $Fe^{II}(ClO_4)_2 \cdot xH_2O$ in H_2O (20 μmol) followed by 1 equiv. of $KHSO_5$ in H_2O (20 μmol). After 1.5 h, the reaction mixture was concentrated to dryness and combined with a dilute aqueous $NaHCO_3$ (10 mL) and CH_2Cl_2 (10 mL). The organic layer was separated and the aqueous layer was extracted with CH_2Cl_2 (2 × 10 mL). The organics were combined, dried, filtered and concentrated. The aqueous layer was concentrated. The organic and aqueous fractions were analyzed by ESMS and ^1H NMR spectroscopy using 4-methylpyrimidine as an internal standard in $CDCl_3$ and D_2O, respectively. Products and yields are shown in Scheme 4.4B. The low isolated yield of benzaldehyde (8%) is likely due to the volatility of this product.

General procedure for kinetic studies.

The formation and decomposition studies of $[Fe^{IV}(O)(\mathbf{L})]^{2+}$ species (where **L** = **1**, **4a-e**) were conducted at 25 °C under aerobic conditions. Observed rate constants represent the average of three runs. The reactions were monitored using a UV-vis spectrophotometer at 680 nm and were performed using the following standard procedure.

<u>For determination of KIE and Hammett plot:</u>

A 2 mM solution of **L** (Where **L** = **1**, **4a-e**) in 1:1 H_2O:MeCN (360 μL, 0.72 μmol) was treated with a 20 mM solution of $Fe^{II}(ClO_4)_2 \cdot xH_2O$ in H_2O (36 μL, 0.72 μmol) followed by a 20 mM solution of $KHSO_5$ in H_2O (36 μL, 0.72 μmol).

In each of the above experiments, upon addition of $Fe^{II}(ClO_4)_2 \cdot xH_2O$ to the solution of **L**, the resulting solution turned yellowish orange. After addition of $KHSO_5$ this solution turned from yellowish orange to green (while mixing the solution). The reactions were

monitored by UV-vis spectroscopy (Figure 4.4A). The absorption at 680 nm was found to increase approximately for about 10 min, suggesting the formation of the species $[Fe^{IV}(O)(\mathbf{L})]^{2+}$, and then started decreasing, indicating the decomposition of $[Fe^{IV}(O)(\mathbf{L})]^{2+}$. The natural log of absorbance at λ_{max} = 680 nm was plotted against time and the linear portion of the plot was fit with line equation Y = a + bX (Figure 4.4B). The slope (b) of the line furnished the observed rate constants.

DynaFit modeling for concentration dependence studies.

The absorbance vs. time traces for three concentrations (0.83 mM, 1.25 mM, and 1.67 mM) of species **3** was used for the calculations. The data was fit with four possible mechanistic models (see Models 1 to 4 in Figure 4.6), by varying the estimated rate constant values. The fitting parameters were further optimized by varying the initial concentrations of $[Fe^{II}(\mathbf{1})(MeCN)]^{+2}$ and $KHSO_5$ within the error range. The best fit was obtained when the model 4 was used.

Table 4.4: Parameters and standard errors obtained from DynaFit

Parameter	Initial ($M^{-1}s^{-1}$)	Unit	Fit ($M^{-1}s^{-1}$)	Unit	Error	%Error
k_1	5.365666667	$M^{-1}s^{-1}$	5.365	$M^{-1}s^{-1}$	0.012	3.6
k_2	0.00059175	s^{-1}	0.000618833	s^{-1}	0.00045	1.2
r_C	200	$M^{-1}cm^{-1}$	190	$M^{-1}cm^{-1}$	0.0017	0.9

* r_C : Extinction coefficient for C, i.e. $[Fe^{IV}(O)(\mathbf{1})]^{2+}$

Chapter 5: Conclusion

This conclusion chapter is divided into two sections. The first section includes the accomplishments of the research goals and suggestions to improve the present outcome of this research. The second section includes conclusion and future directions that demonstrate the significance and scope of the research presented in this dissertation.

5.1 Accomplishments and suggestions

5.1.1 Development of the divergent and dual divergent strategies for the synthesis of non-heme ligand-peptide conjugates

Applications of metal complex-peptide conjugates have been extensively explored over the last two decades. Considering their applications, several synthesis strategies have been developed to construct a variety of peptide-ligand conjugates. Despite the wide scope of non-heme ligands in bioorganic chemistry, very few methods are known for tethering nitrogen-rich non-heme ligands into peptides. Surprisingly, none of these methods allow the incorporation of such ligands into peptides in a divergent fashion. This is important because lack of such methods has limited the applications of non-heme ligand-peptide conjugates. In effort to contribute to this research, we have developed divergent and dual divergent strategies via solution and/or solid phase synthesis (Chapter 2 and 3). In addition, functional group compatibilities and the scope of these strategies were also explored. The two requirements for the strategies were to synthesize unnatural amino acids and to develop conditions for these strategies that can be easily performed in solution as well as solid phase synthesis. Towards this, I developed scalable routes for the synthesis of key intermediates

and synthesized two unnatural amino acids Fmoc-HPA(OTBS)-OH and Fmoc-HPL(OTBS)-OH. The unnatural amino acid HPA resembles phenylalanine, so that it can be placed into peptidomimetic enzyme inhibitors without significantly altering their structures. I also developed conditions for the divergent and dual divergent strategy to incorporated non-heme ligands into the peptide. Using these methods, various tetra- and pentadentate ligands such as TPA, Bn-TPEN, N4Py and PaPy3 were incorporated into peptides. It is important to note that several of these ligands generate ferryl complexes, which display a remarkable oxidizing power.[14,15] Particularly, the ferryl derived from N4Py ligand is stable in aqueous conditions and can oxidize various organic substrates,[14] amino acid substrates,[160] proteins[17] and glutathione.[161] In addition, metal complexes derived from tetradentate ligand TPA have shown numerous applications in photo-responsive materials,[200] zinc sensing agents[201] as well as in inhibition studies.[202] The pentadentate ligand PaPy3 and derivatives have been used to construct CO/NO delivering agents.[203,204] Our group has demonstrated the potential of these ligands in cancer cell cytotoxicity studies.[16] Considering numerous applications of non-heme ligands, the synthesis strategies presented herein will be very important in exploring their utility in bioorganic chemistry.

Although the strategies presented herein facilitate easy excess to the synthesis of peptide-ligand conjugates via solution as well as solid phase synthesis, the following modifications could make these strategies more convenient. For example, the synthesis of Fmoc-HPA(OTBS)-OH can produce multigram quantities of the target amino acid. However if the Negishi coupling is performed using iodopyridine instead of the bromopyridine derivative to produce Fmoc-HPA(OTBS)-OH, a multi-step synthesis presently used for the synthesis of Fmoc-HPA(OTBS)-OH could be avoided. A convenient route for the synthesis

of iodopyridine derivative has to be developed prior to attempting the Negishi coupling. Incorporation of N4Py onto Wang resin bound peptide was unsuccessful, however N4Py containing a SAAC derivative could be used to synthesize corresponding conjugates on Wang resin. This is important because certain peptide vectors might require *C*-terminal acids for their biological activity and the ability to incorporate these ligands into peptide-acids would expand the scope of these conjugates.

5.1.2 Applications of the non-heme ligand-peptide conjugates

Among numerous applications, the utility of the divergent and dual divergent strategies to synthesize the library of biologically important peptide-ligand conjugates and to explore the chemistry of ferryl-peptide conjugates were explored in this dissertation. A small library of LHRH analogues was synthesized by incorporating Bn-TPEN, N4Py, TPA and PaPy3 at the side chain of Fmoc-HPL(OTBS)-OH. Biological applications of metal complexes are significantly influenced by the nature of donor atom, chelate rings and the charge.[106] For example, replacement of a pyridyl moiety with quinoline has a significant effect on the NO releasing ability of PaPy3.[203] Therefore, the ease of varying the ligand framework is very important while exploring the biological applications of such conjugates. The dual divergent strategy facilitated the manipulation in ligand structures as demonstrated by synthesizing pyrazine and carboxylate chelators containing TPA and PaPy3 derivatives.

During the library synthesis, chlorination conditions were shown to tosylate pyroglutamic acid (Glp) of LHRH as a minor reaction. Although the method was not optimized further at this point, I suggest protecting Glp by an electron-rich protecting group such as trityl for the future libraries. For simplicity, the metal-binding units were directly

attached to the N_ε-amine of the D-lysine in the library synthesized in this dissertation. However linkers between metal-binding ligands and peptide vectors could play a critical role in their biological activity. For instance, when DOTA was directly appended on LHRH, the conjugate lost the binding affinity to the target cell.[33] In another example, the spacer length between N_3S ligands and bombesin impacts the binding process of the resulting conjugates.[32] Considering the importance of linkers between metal-binding ligand and peptide vectors, in the future the role of spacer has to be established. For conveniently varying the linkers, LHRH analogues should be synthesized by incorporating Fmoc-D-Lys(PG)-OH where N_ε-amine of the D-lysine is protected by orthogonal protecting groups such as Dde, ivDde or allyl. This modification will ease the incorporation of various linkers between pyridyl moiety and D-lysine.

Another significantly recognized application of non-heme ligands is their utility in ferryl chemistry. Given the fact that ferryl complexes play critical role in several enzymes, synthetic ferryl complexes and their utility in enzyme models as well as in catalysis has been well established. However none of the examples has shown the formation of ferryl using peptide bound non-heme ligands until we synthesized and characterized the ferryl-peptide conjugate from N4Py-dipeptide conjugate (Chapter 4). This work is significant because it supports the hypothesis that ferryls can be generated on a peptide-like (i.e. protein) scaffold. A detailed mechanistic study that was performed to understand the higher reactivity of these conjugates suggested that ferryl reacts with a remote benzyl group via intramolecular hydrogen atom transfer reaction. This clearly suggests the importance of the strategic arrangement of the reactive functional groups around the ferryl species; however, the knowledge about which groups can be tolerated around the ferryl species in enzymes was not

known. The studies presented herein have set up a strong foundation to explore the functional group compatibility of ferryl-peptide conjugates. The role of protein radicals has been studied in view of aging, lipid peroxidation, catalytic mechanisms and various deceases.[194] For example, ferryl myoglobin generates ferryl species upon reaction with H_2O_2 that eventually reacts with distal tyrosine residues to form the corresponding tyrosine radicals.[195-197] A distance dependent intramolecular long-range electron-transfer (LRET) was found to be responsible for this process.[197] The intramolecular reactivity of ferryl-peptide conjugates established in this dissertation is analogues to the LRET process of protein radicals and could be used to study the LRET process on small model system.

While the synthesis and characterization of ferryl-peptide conjugates were straightforward, the mechanistic investigations were challenging. Simultaneous formation and decomposition of the ferryl species during the initial time period did not allow the kinetic analysis of the decay process as an individual step. Moreover, along with the oxidation of the benzyl group, a parallel destruction of the metal-binding unit was observed. These issues made the kinetic studies challenging and I suggest following modifications for further investigation. A stable ligand such as MeN4Py has shown greater stability towards oxidation conditions. Therefore, the ferryl-peptide conjugates should be generated from the MeN4Py-peptide conjugate and their reactivity should be studied in a similar fashion. This modified system should be used to address the question: which functional groups can be tolerated on ferryl-peptide conjugates? The knowledge gained from this study will be important for the utility of these conjugates in the future. In addition, isolation of the ferrous-peptide conjugates and establishment of their solid-state structure could give insight into the 3D-orientation.

5.2 Conclusion and future directions

In conclusion, we have established divergent and dual divergent strategies that allow the rapid synthesis of non-heme ligand-peptide conjugates. We have also explored the functional group compatibility and scope that suggests a wide applicability of these strategies. Easy access to the synthesis of non-heme ligand-peptide conjugates will play a critical role in exploring wide variety of applications. In this dissertation we have demonstrated the utility of these strategies in the library synthesis of metal-binding LHRH analogue and in exploring the chemistry of ferryl-peptide conjugate.

Considering the applications of metal complexes containing non-heme ligands as oxidants,[14,15] CO/NO delivering agents[129,205] and biomolecule inactivating agents,[106,206] the methodology described herein has a great potential in bioorganic research. In the future, the dual divergent strategy could be used to expand the library of metal-binding LHRH analogues by constructing more diverse ligands onto LHRH analogues. By changing the ligand framework the reactivity and the specificity of the resulting conjugates could be tuned to obtain the conjugates with desired properties. Moreover, similar libraries could be constructed on other delivery vectors such as bombesin and somatostatin for different biological targets. The dual divergent strategy could also be used to synthesize larger libraries via the split-pool method. These studies would facilitate the development of site-selective catalytic agents for therapeutics.

The chemistry of ferryl-peptide conjugates also has great scope and must be explored further. During our initial studies, we have found that replacement of glycine with alanine did not have any influence on the reactivity of ferryl-peptide conjugates.[207] In the future, it will be very interesting to study the effect of tryptophan or histidine in the vicinity of ferryl

species. Such studies will provide further insight into the environment of the natural ferryls found in several enzymes. Moreover, multiple glycine spacers could be incorporated between benzyl ester moiety and the ferryl species to study the distance dependence on the reactivity of ferryl complexes. This will provide a simpler model to study the intramolecular long-range electron-transfer processes that are investigated only on protein radicals to date. We have already shown the capability of the divergent strategy to incorporate multiple ligands into a single peptide chain.[98] Such conjugates will have great potential to construct iron μ-oxo complexes that could mimic binuclear iron enzymes.[208,209] This is particularly important because such binuclear complexes can activate dioxygen and serve as oxidants. This idea can open a new research area in enzyme model studies as well as in catalytic inhibitions that utilize dioxygen for their activity. The knowledge gathered in these studies could eventually be used to construct stable catalysts as well as in the research of artificial oxygenases.

Overall, two synthesis strategies developed in this dissertation will have significant influence on how non-heme ligand-peptide conjugates have been synthesized to date. A library synthesis of biologically important molecules and chemistry of ferryl-peptide conjugates demonstrates the utility of these strategies. Thus, the study presented herein has as set up a strong foundation for exploration of the applications of non-heme ligand-peptide conjugates as enzyme models, artificial oxygenases, and potentially in the long term, new therapeutic strategies.

APPENDIX

(6-(((*tert*-butyldimethylsilyl)oxy)methyl)pyridin-3-yl)methanol

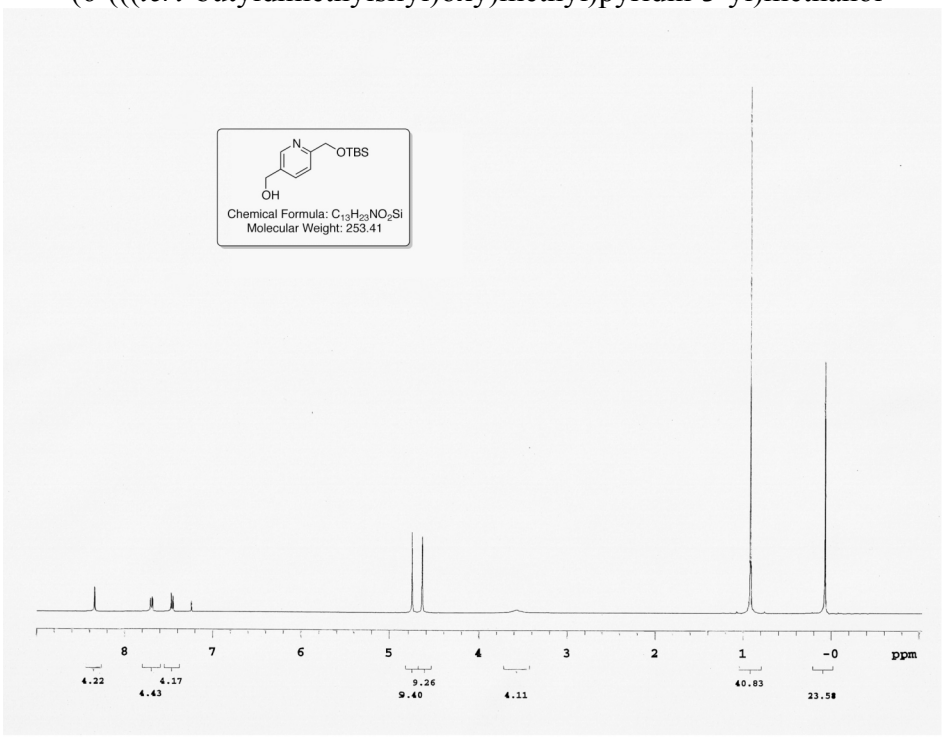

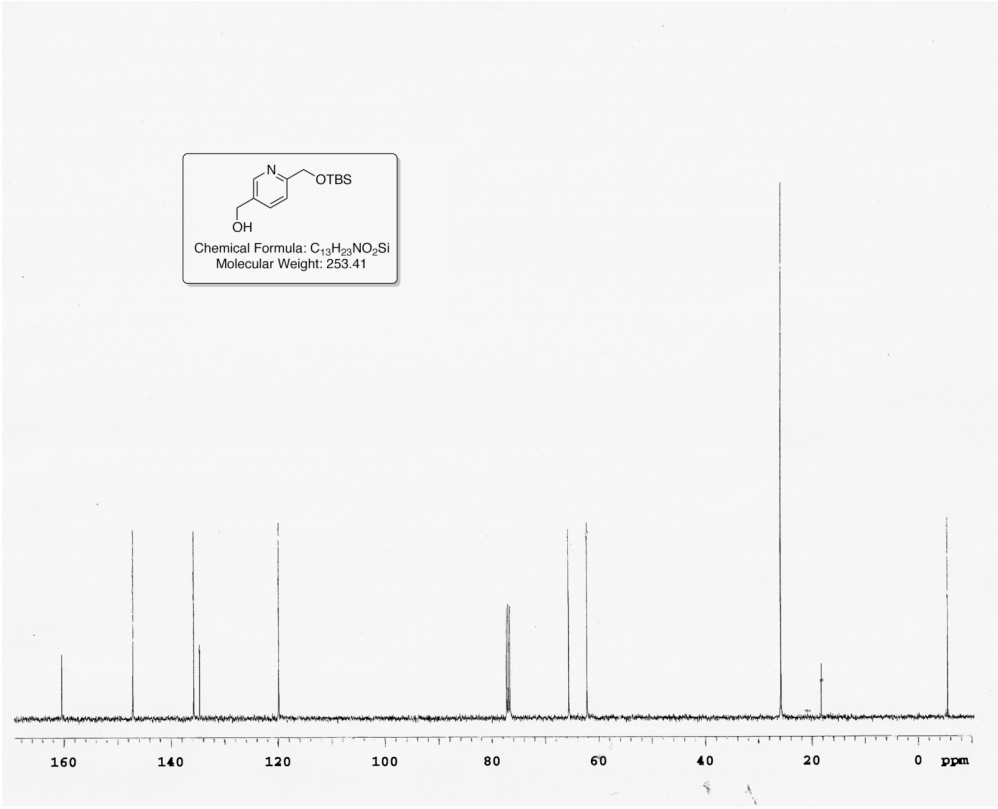

5-(bromomethyl)-2-(((*tert*-butyldimethylsilyl)oxy)methyl)pyridine

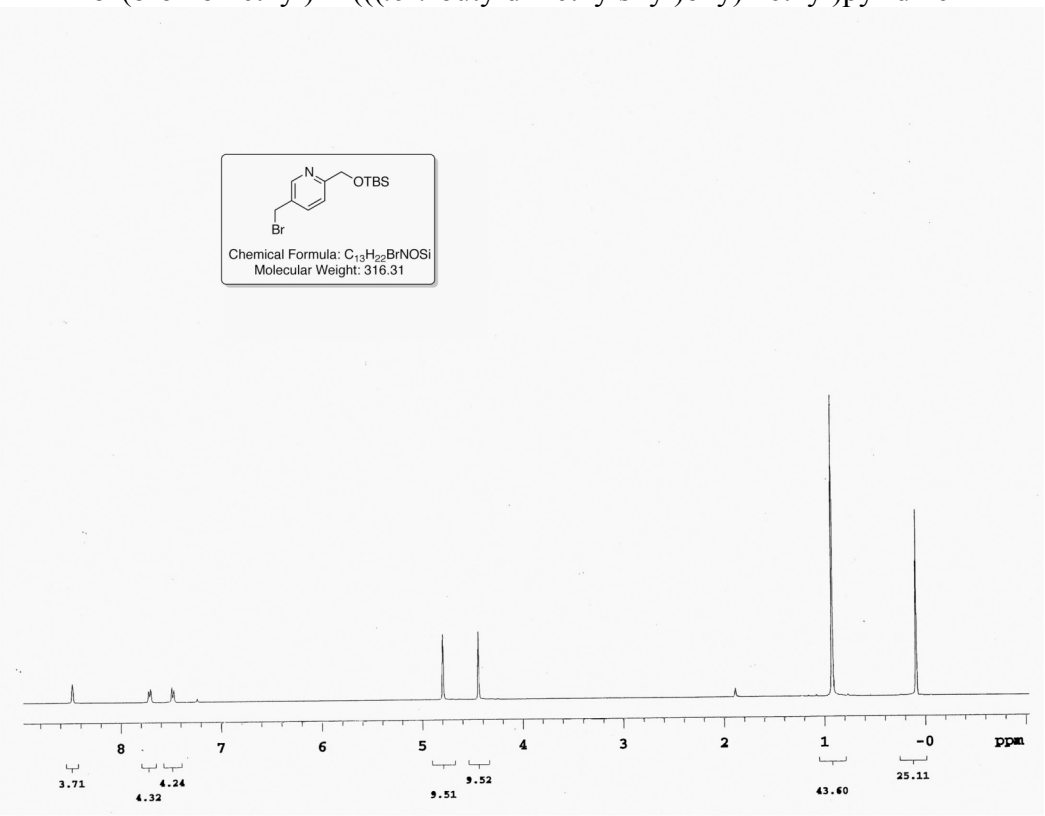

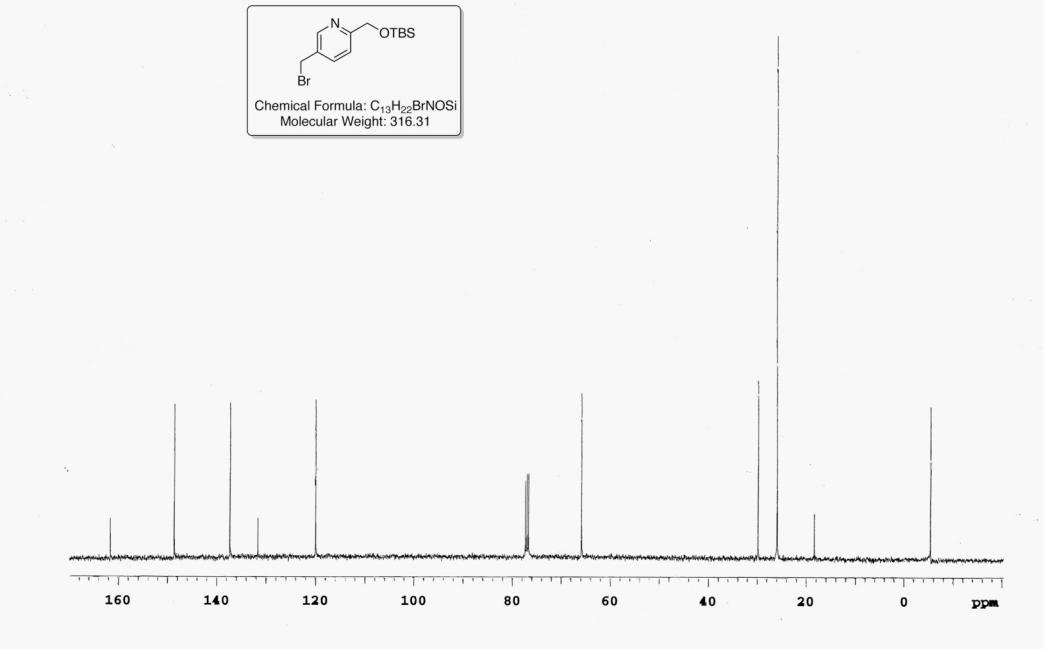

(S)-benzyl 3-(6-(((*tert*-butyldimethylsilyl)oxy)methyl)pyridin-3-yl)-2-((diphenyl methylene)amino)propanoate

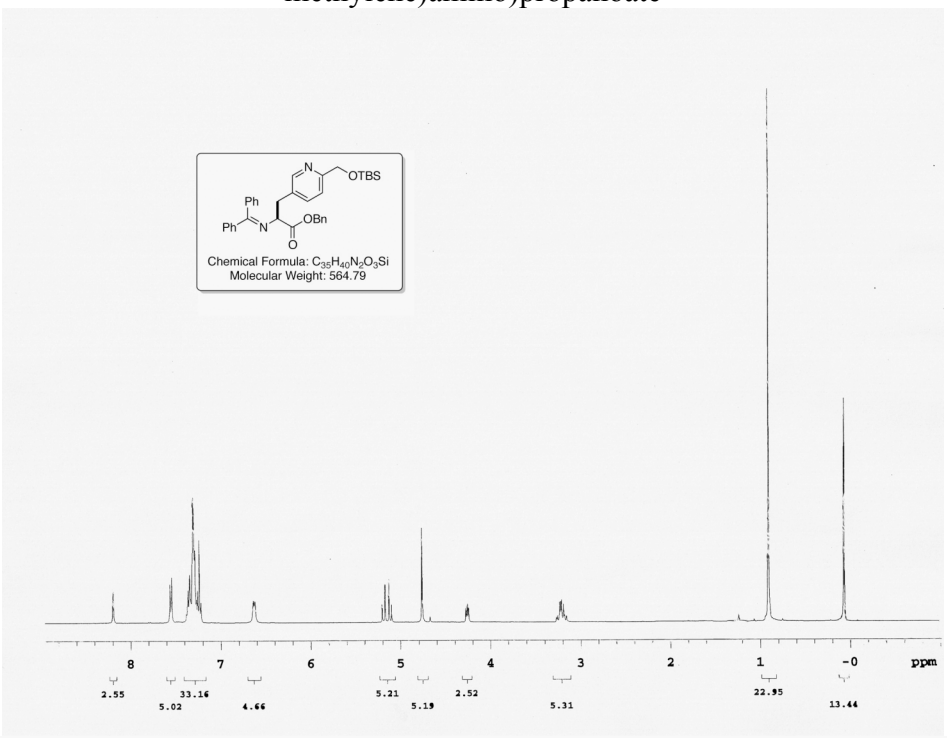

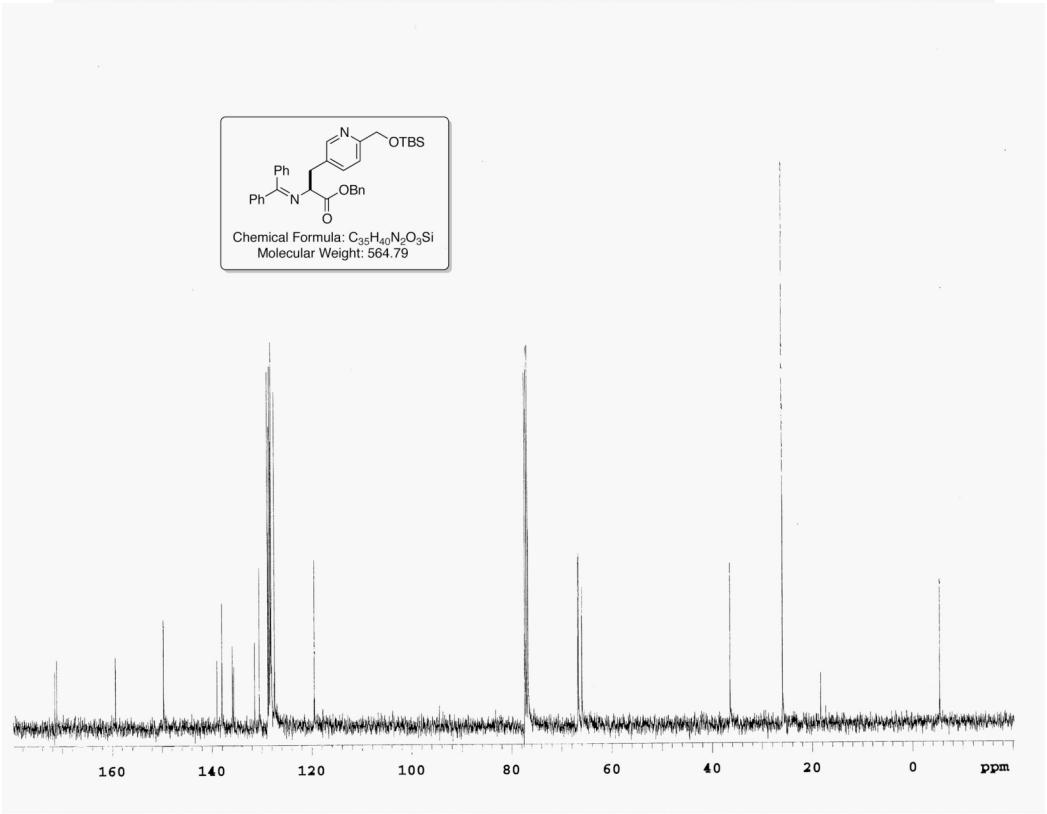

(S)-*tert*-butyl 3-(6-(((*tert*-butyldimethylsilyl)oxy)methyl)pyridin-3-yl)-2-((diphenyl methylene)amino)propanoate

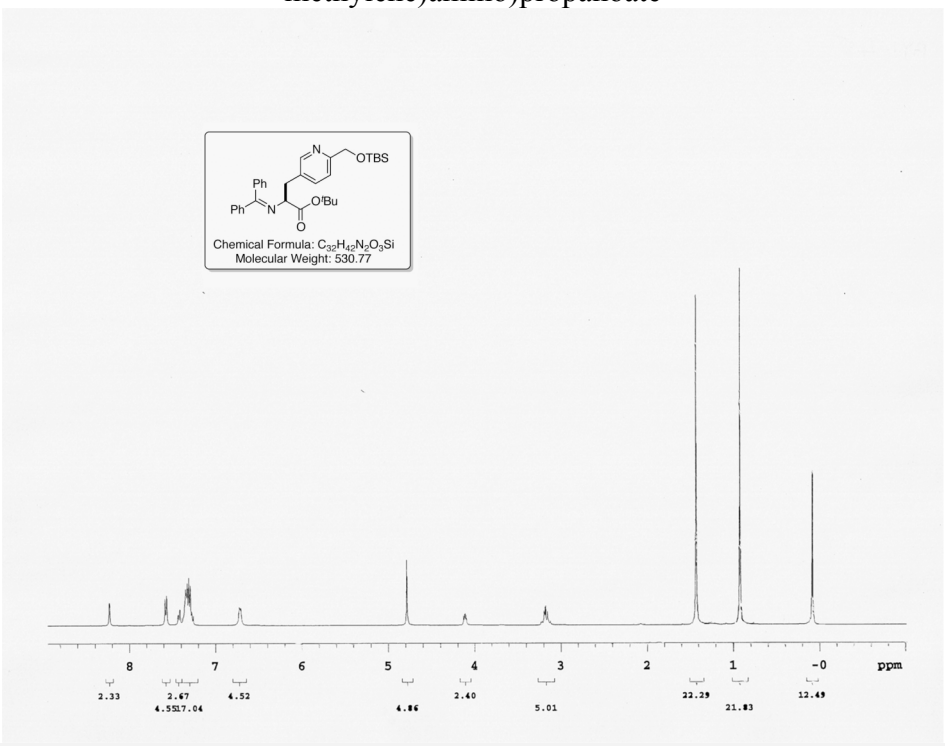

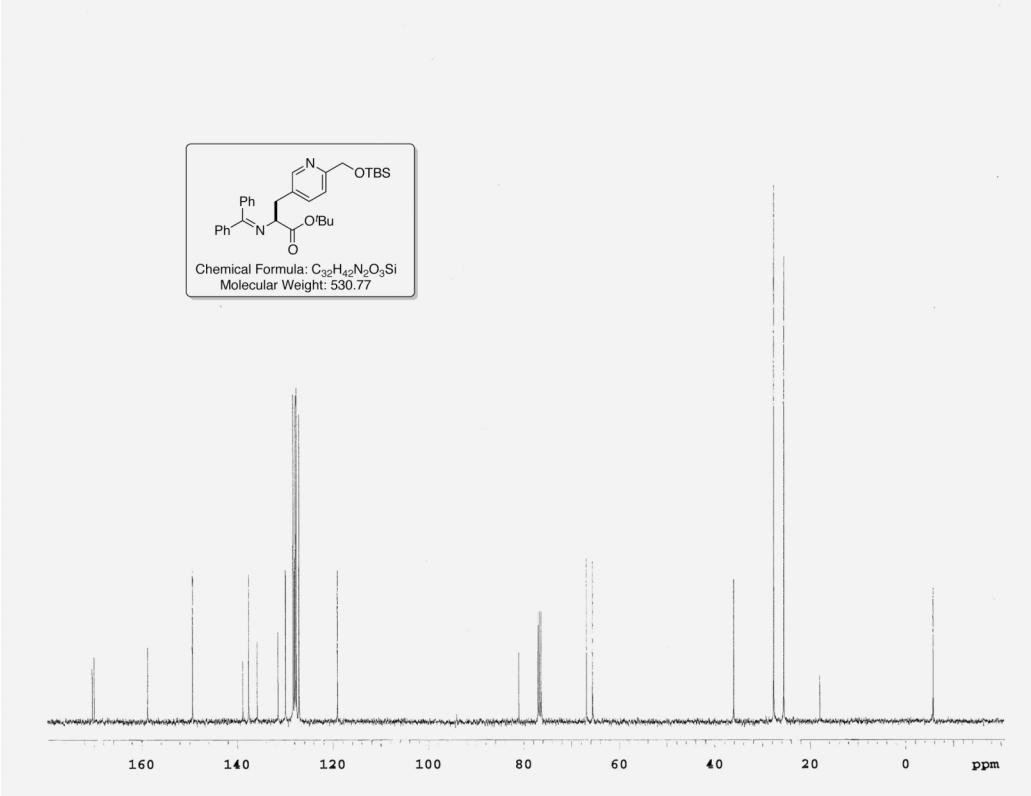

(S)-2-amino-3-(6-((*tert*-butyldimethylsilyloxy)methyl)pyridin-3-yl)propanoic acid

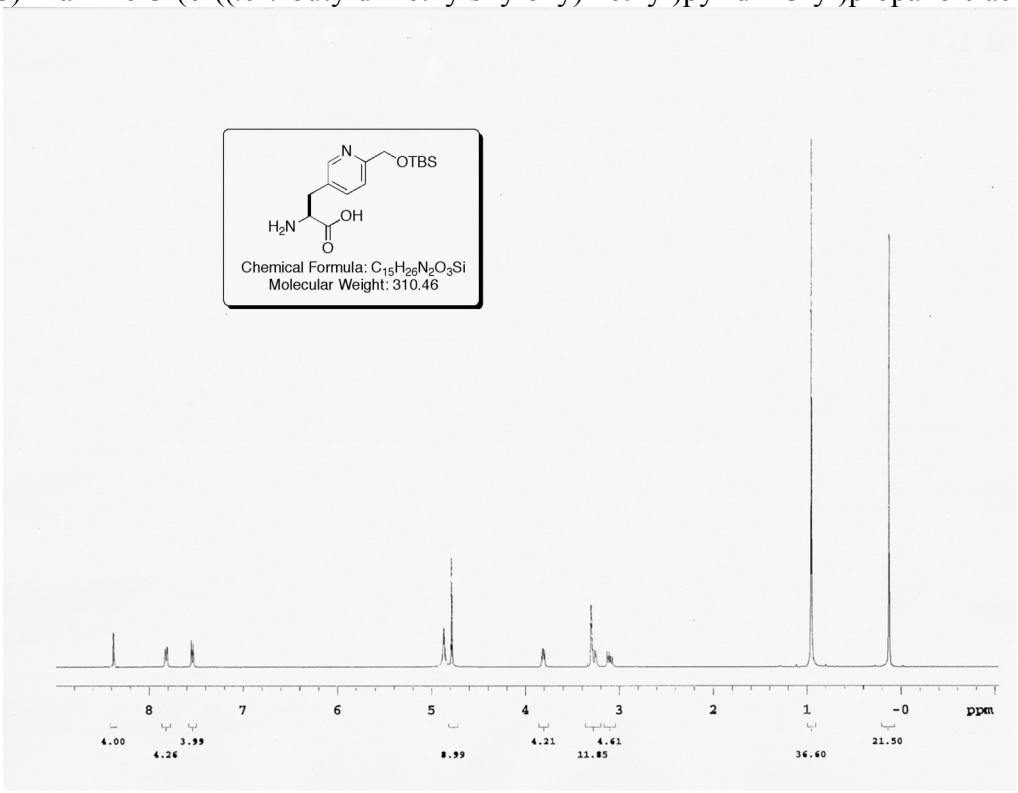

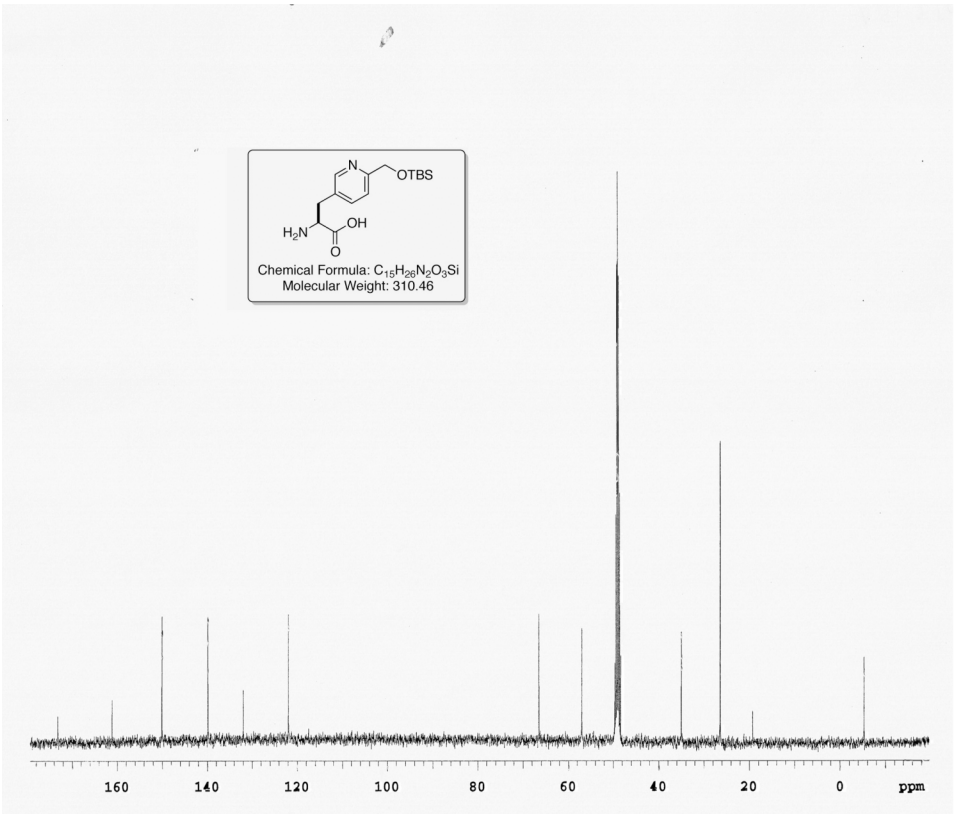

(S)-2-(((9H-fluoren-9-yl)methoxy)carbonylamino)-3-(6-((tert-butyldimethylsilyloxy) methyl)pyridin-3-yl)propanoic acid

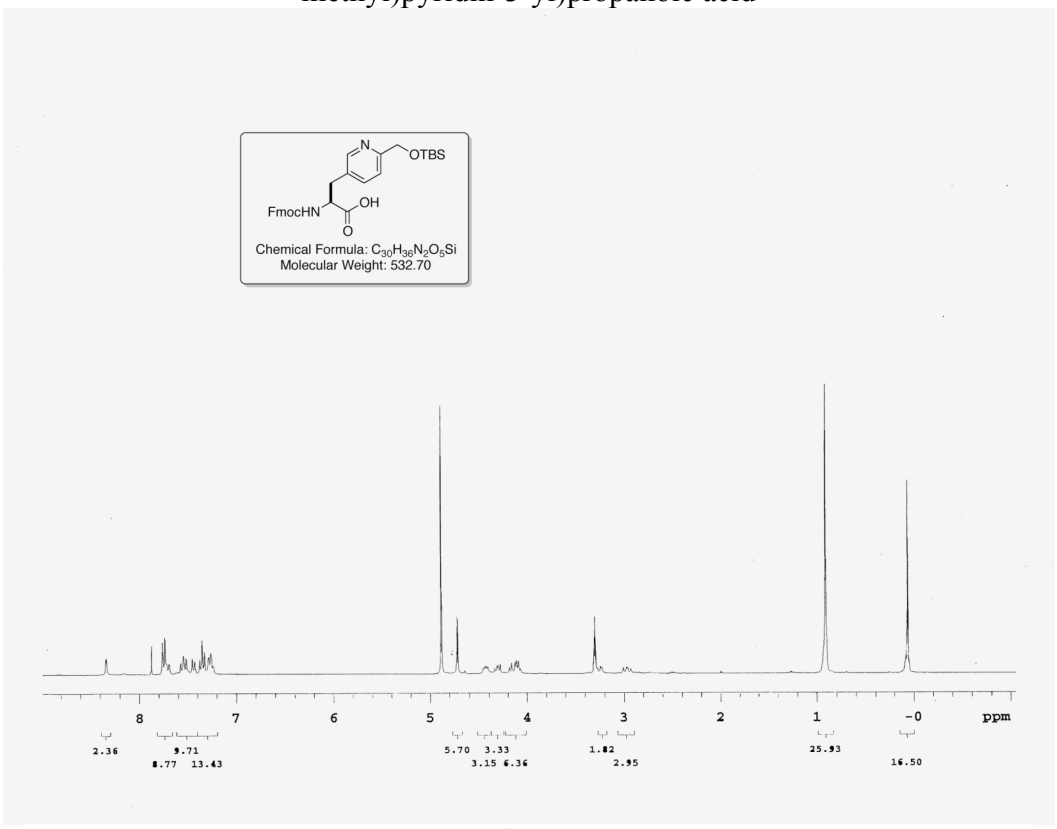

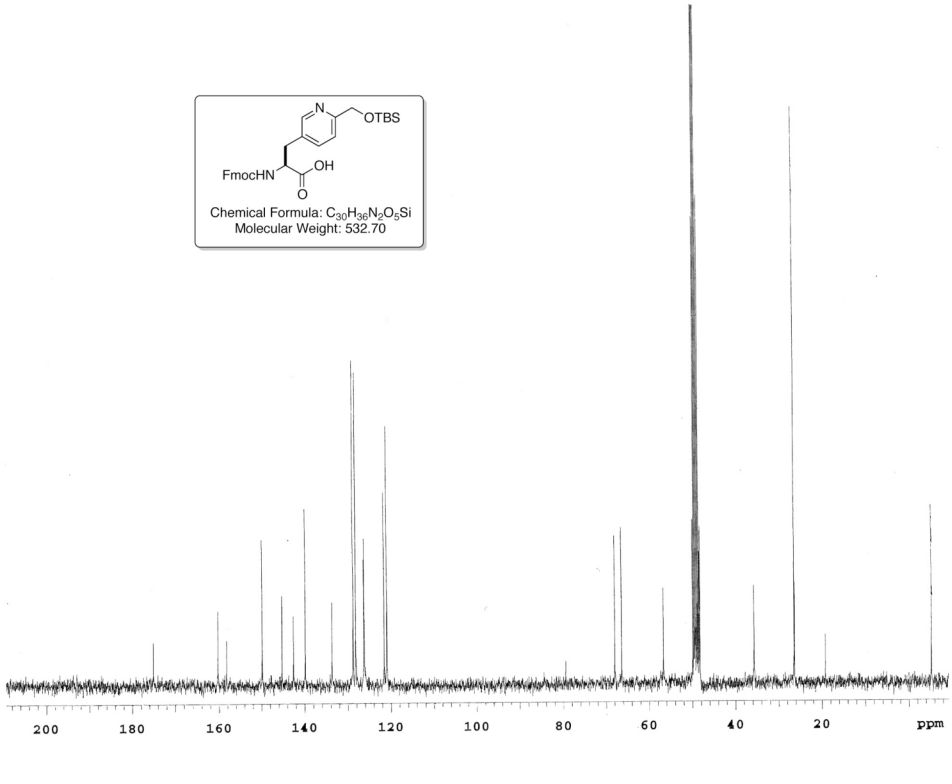

Benzyl 2-(3-(6-((*tert*-butyldimethylsilyloxy)methyl)pyridin-3-yl)-2-ethanamido propanamido)ethanoate

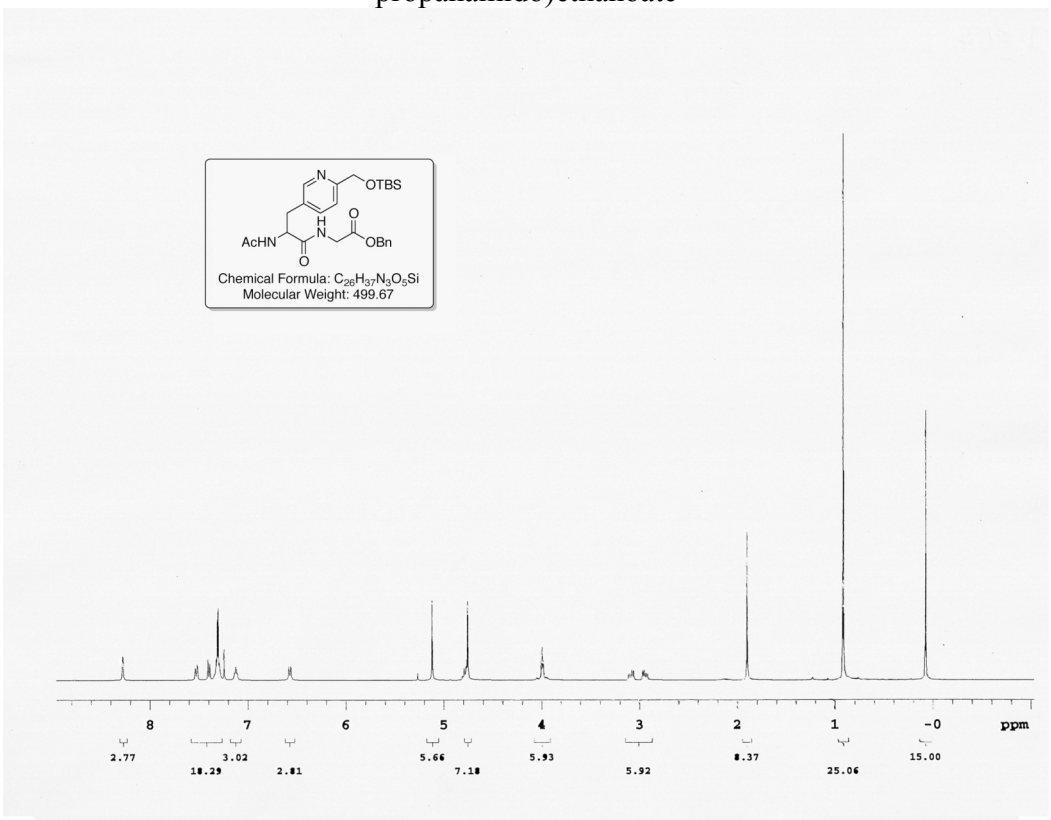

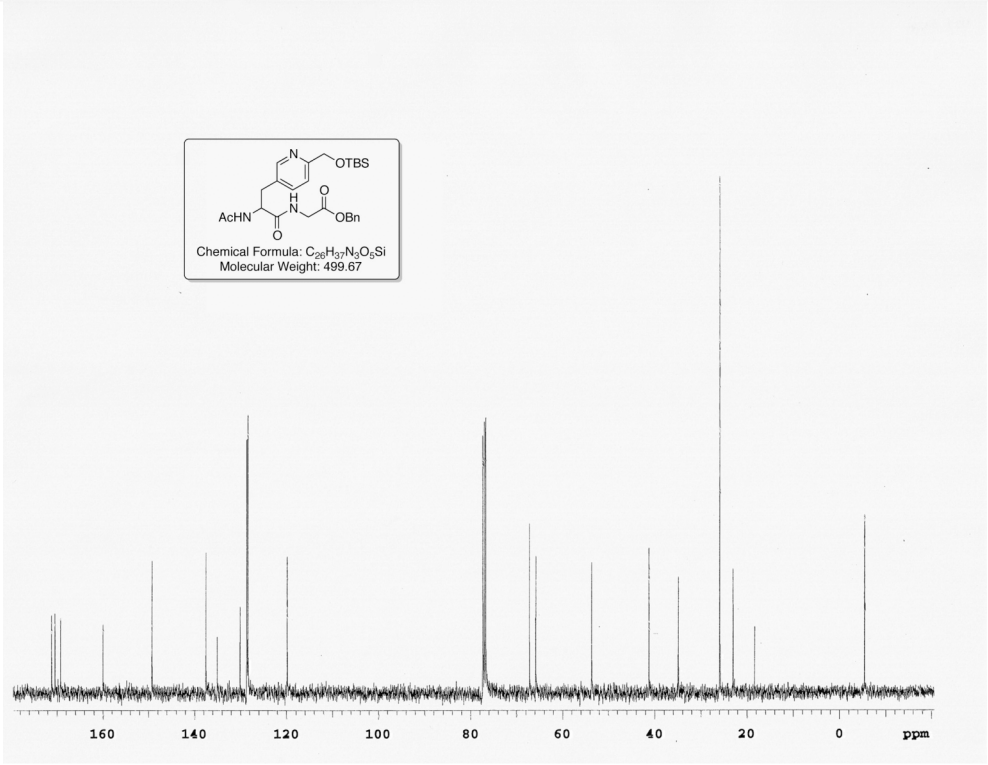

Benzyl 2-(3-(6-(chloromethyl)pyridin-3-yl)-2-ethanamidopropanamido)ethanoate

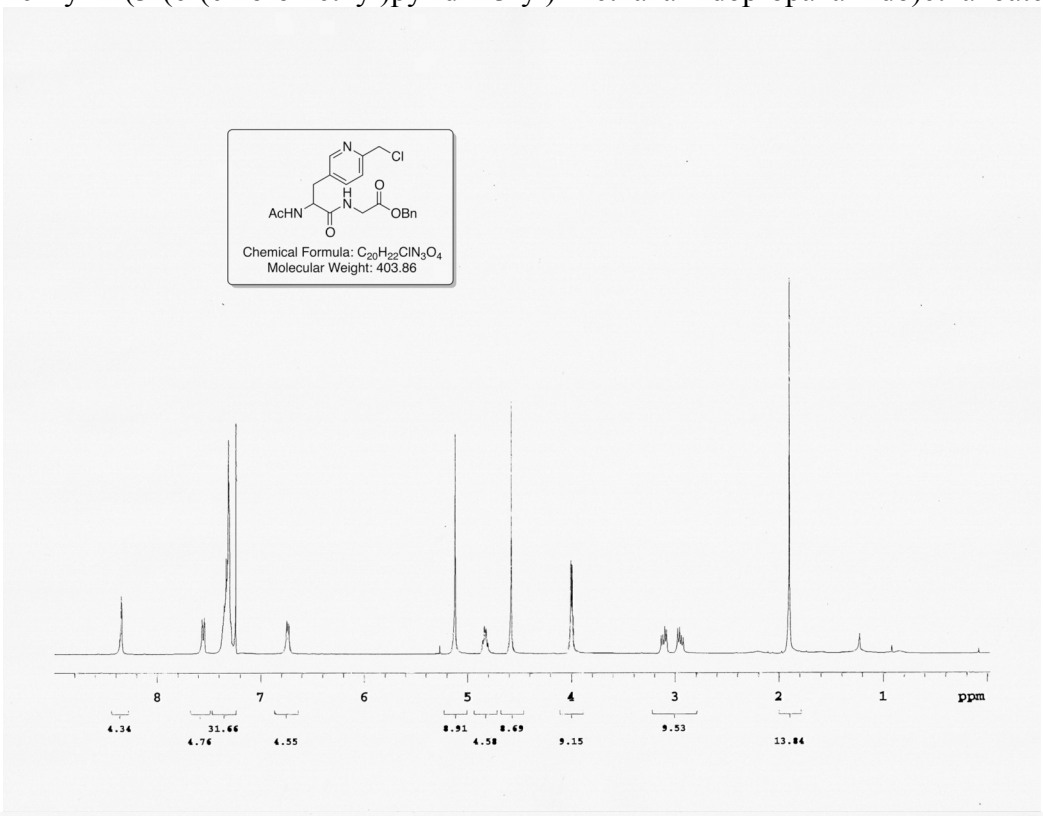

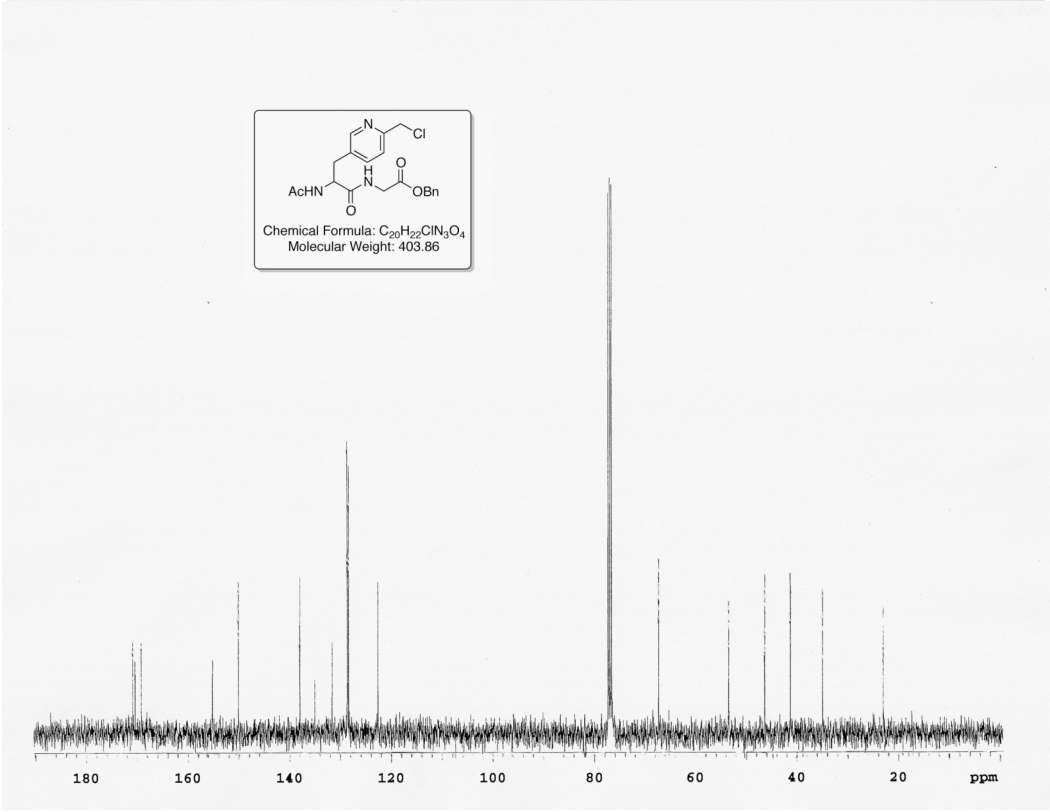

Benzyl 2-(2-acetamido-3-(6-((bis(pyridin-2-ylmethyl)amino)methyl)pyridin-3-yl)propanamido)acetate

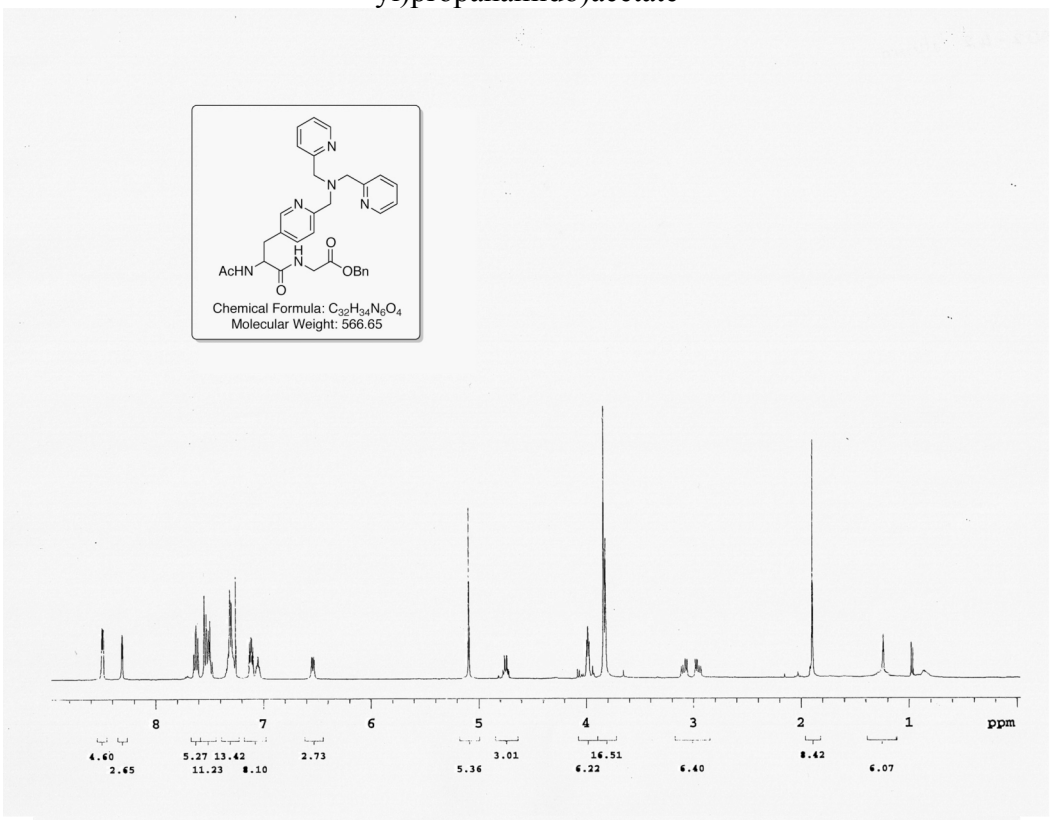

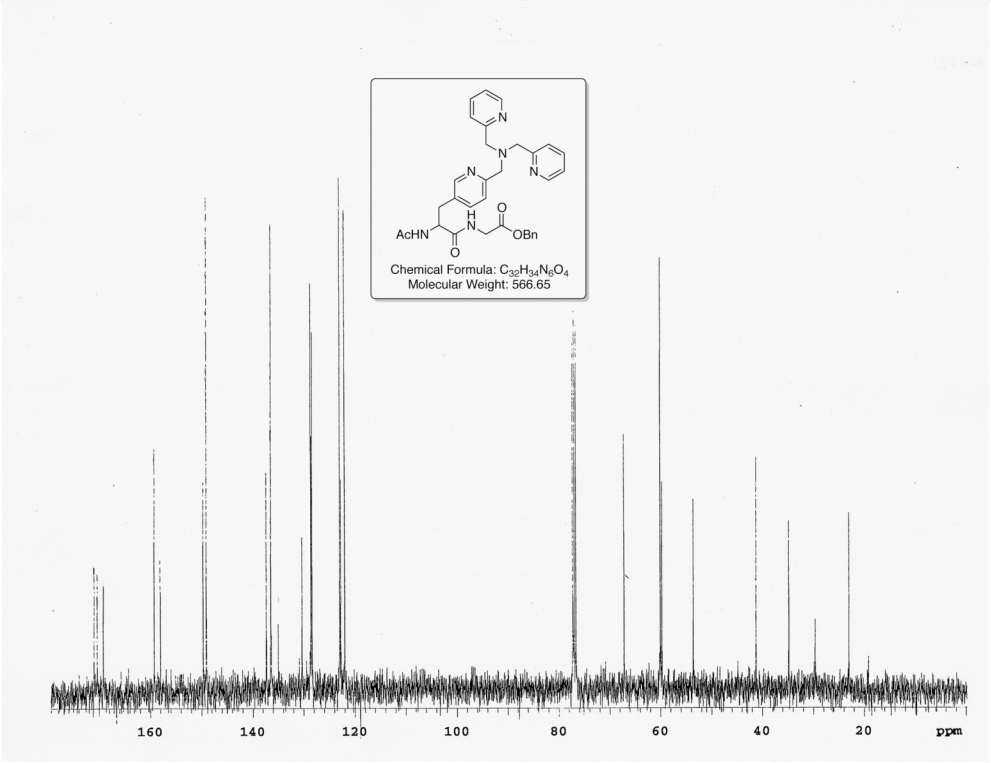

Benzyl 2-(2-acetamido-3-(6-(((2-(benzyl(pyridin-2-ylmethyl)amino)ethyl) (pyridin-2-ylmethyl)amino)methyl)pyridin-3-yl)propanamido)acetate

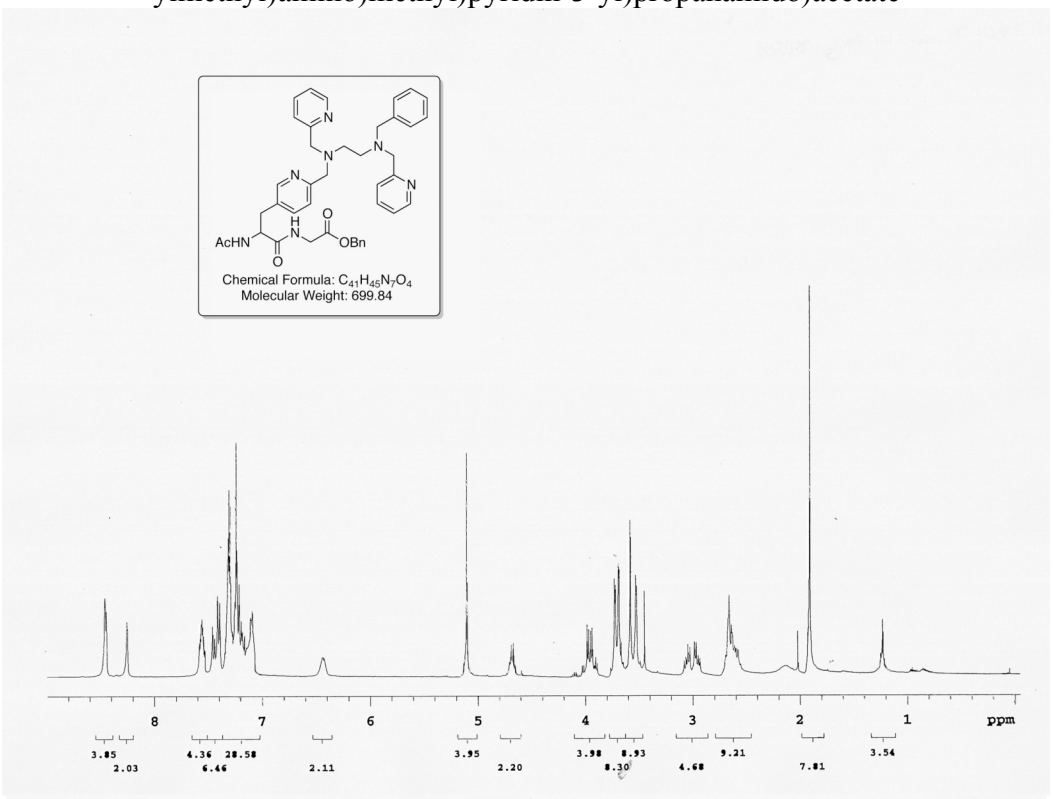

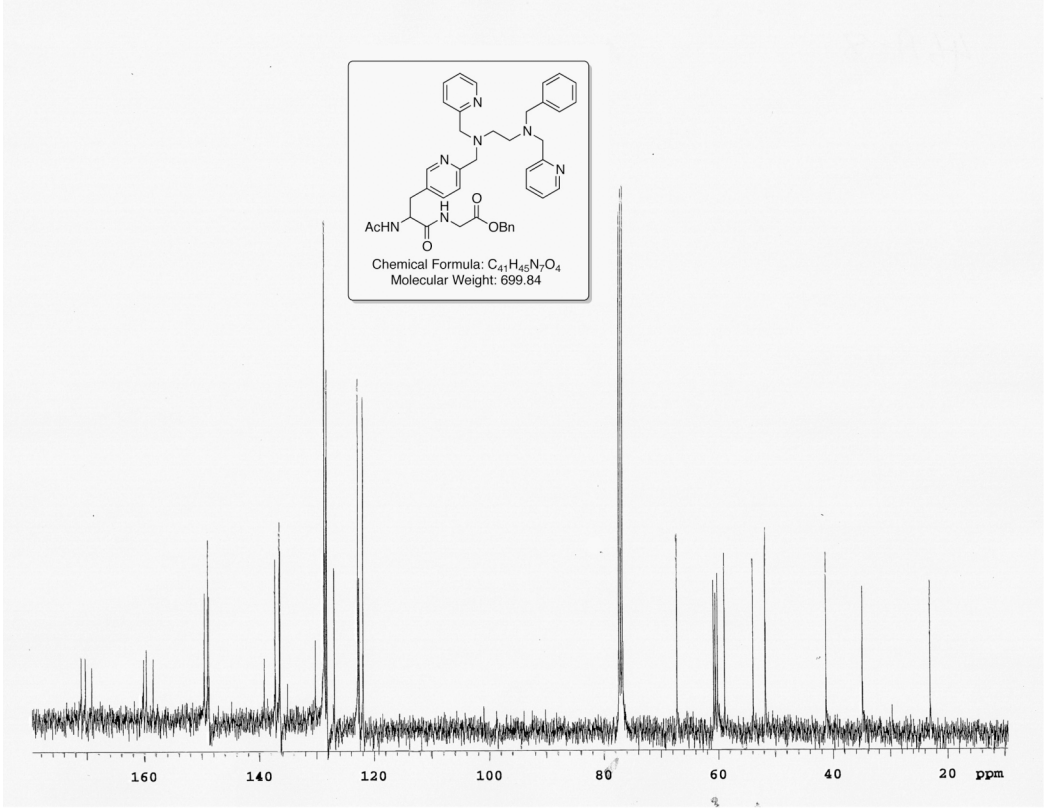

Benzyl 2-(2-acetamido-3-(6-(((dipyridin-2-ylmethyl)(pyridin-2-ylmethyl)amino)methyl)pyridin-3-yl)propanamido)acetate

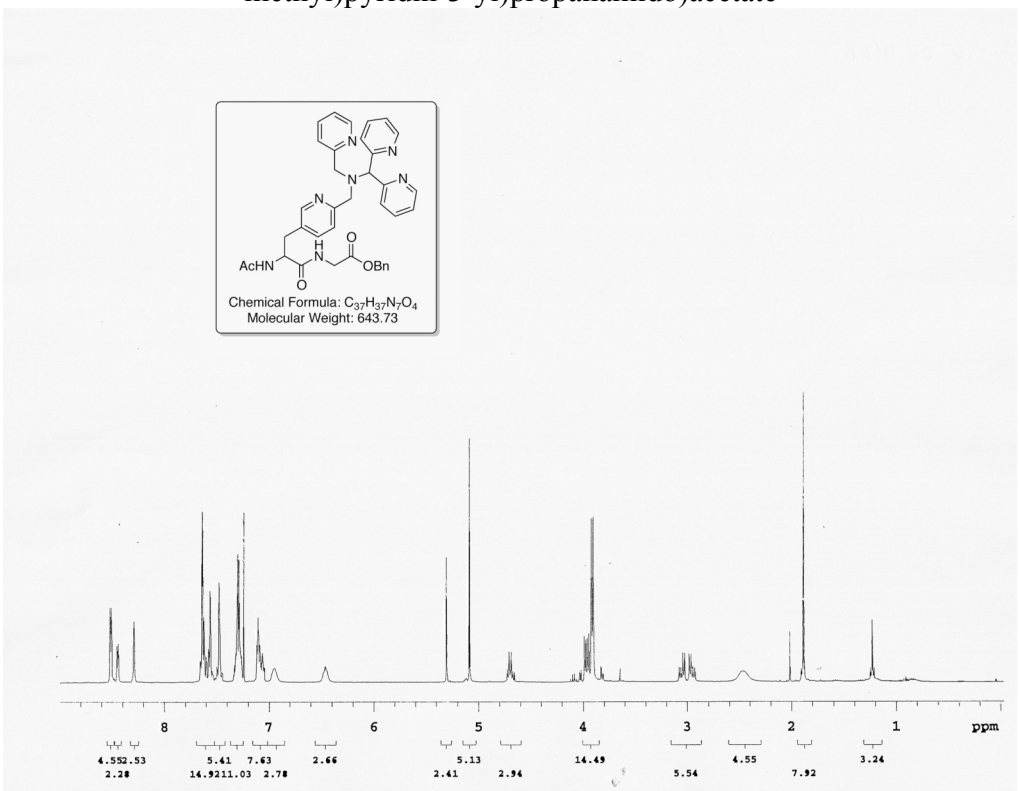

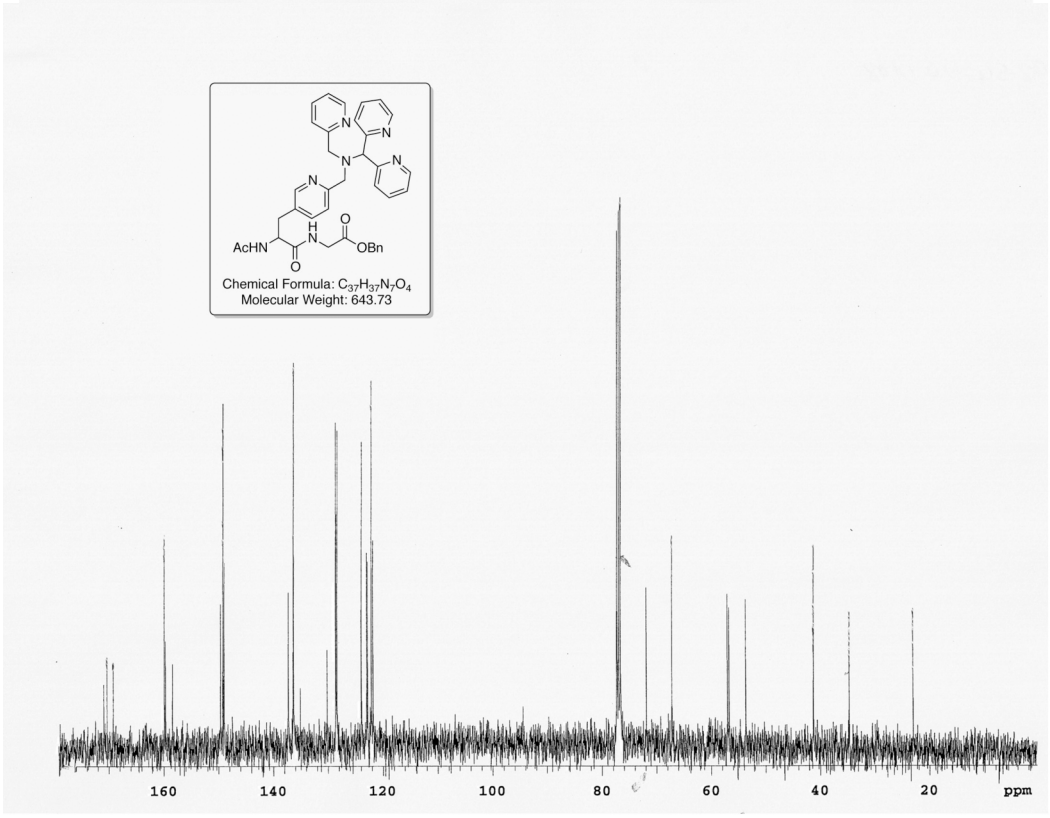

6-(((*tert*-butyldimethylsilyl)oxy)methyl)nicotinic acid

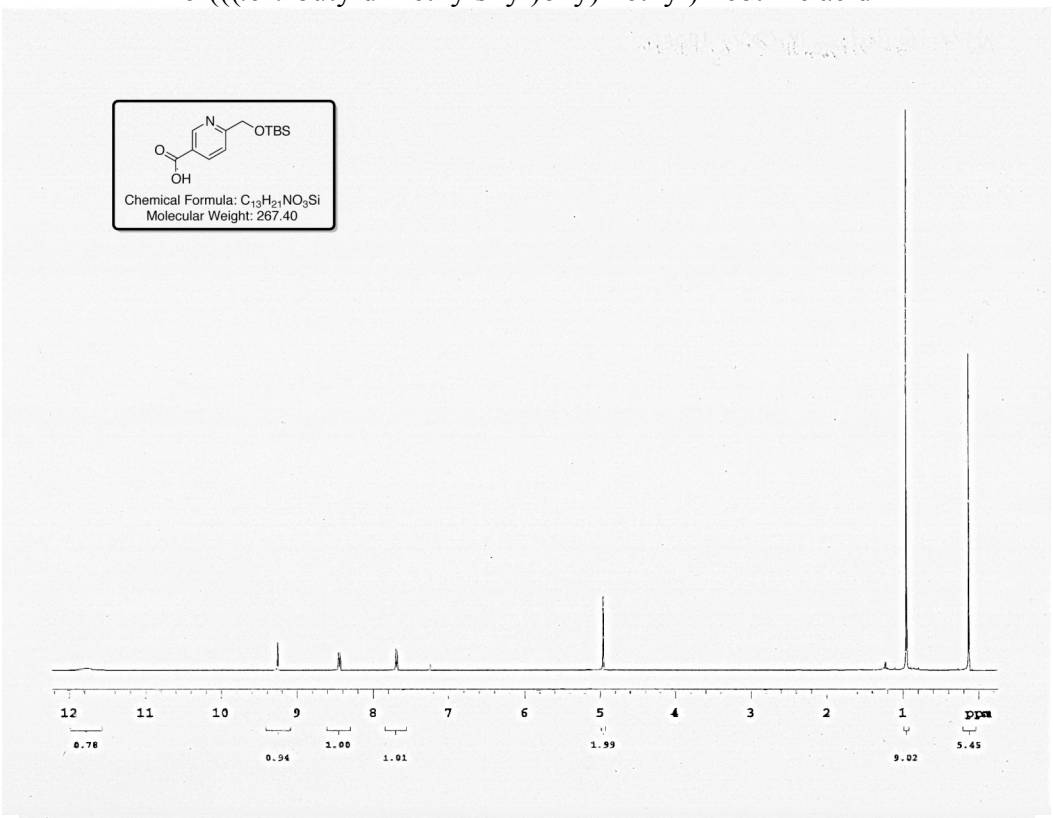

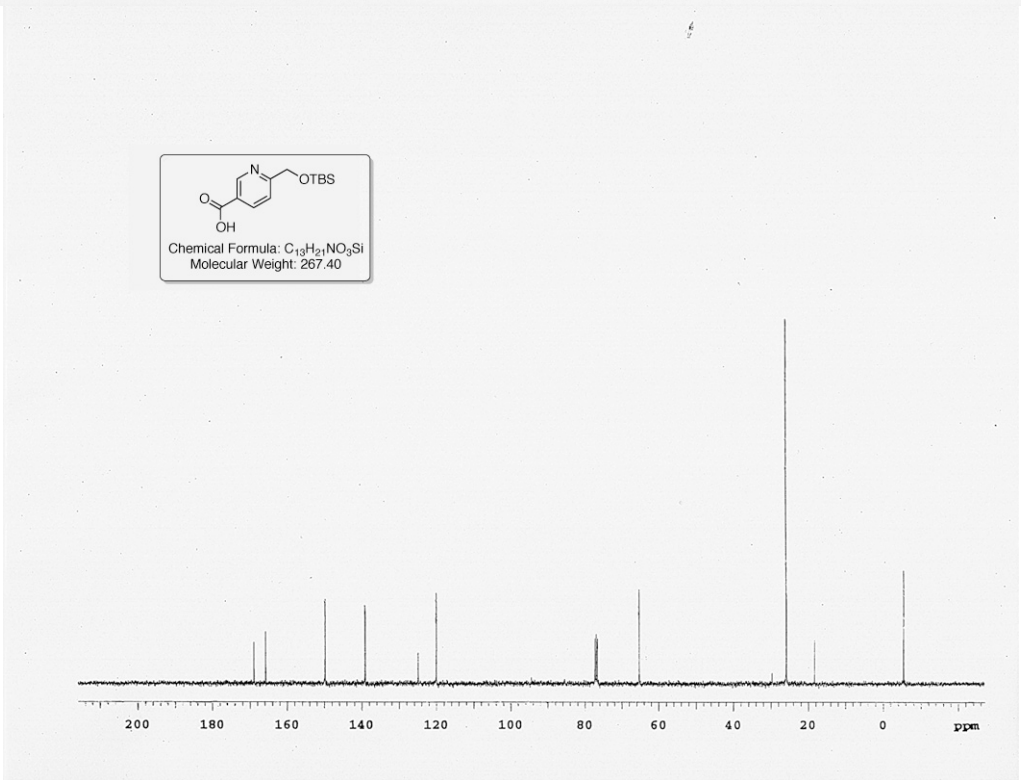

2,5-dioxopyrrolidin-1-yl 6-(((*tert*-butyldimethylsilyl)oxy)methyl)nicotinate

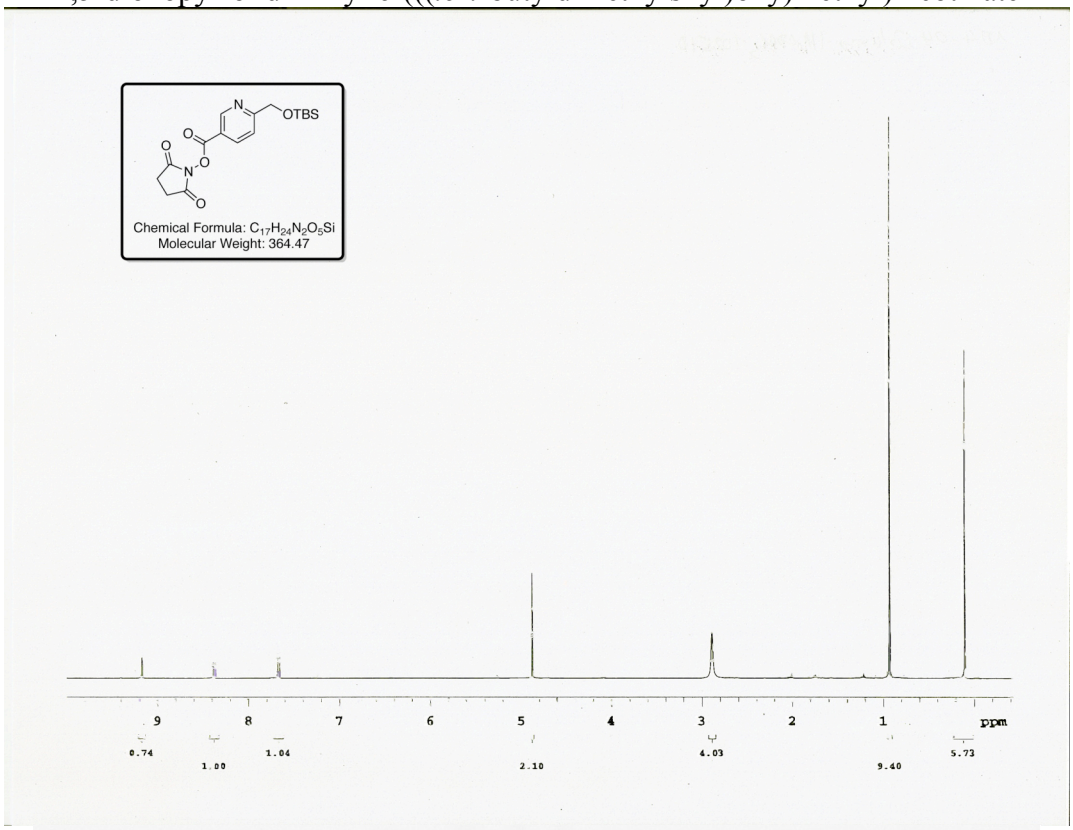

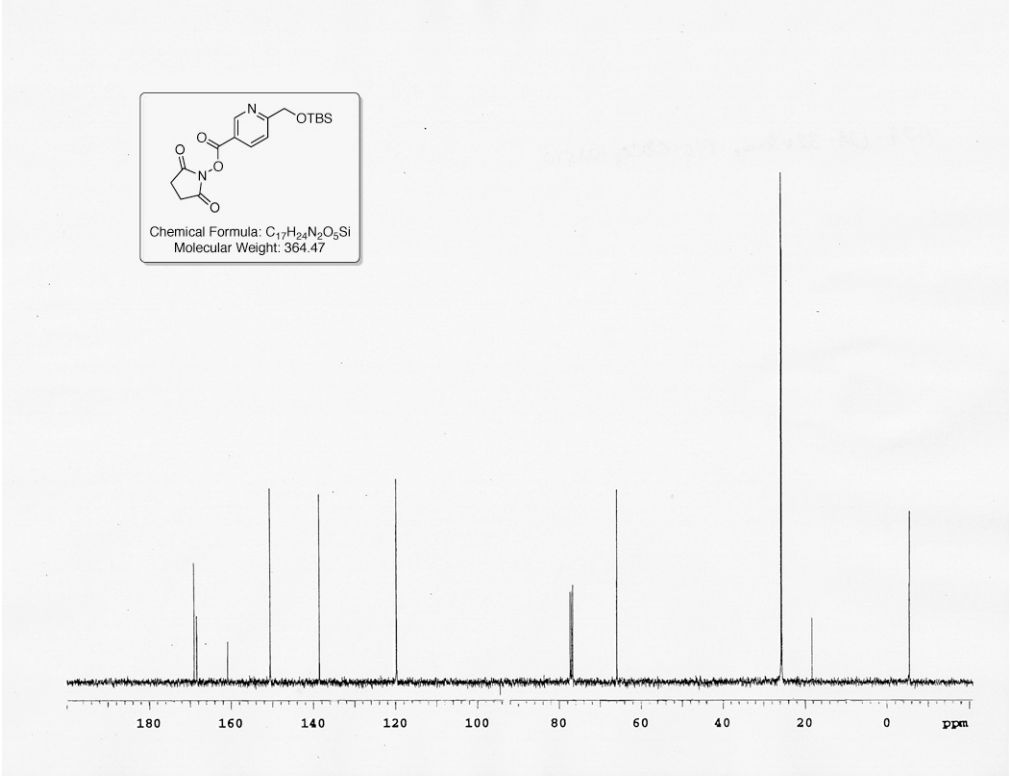

(R)-2-((((9H-fluoren-9-yl)methoxy)carbonyl)amino)-6-(6-(((*tert*-butyldimethylsilyl)oxy)methyl)nicotinamido)hexanoic acid

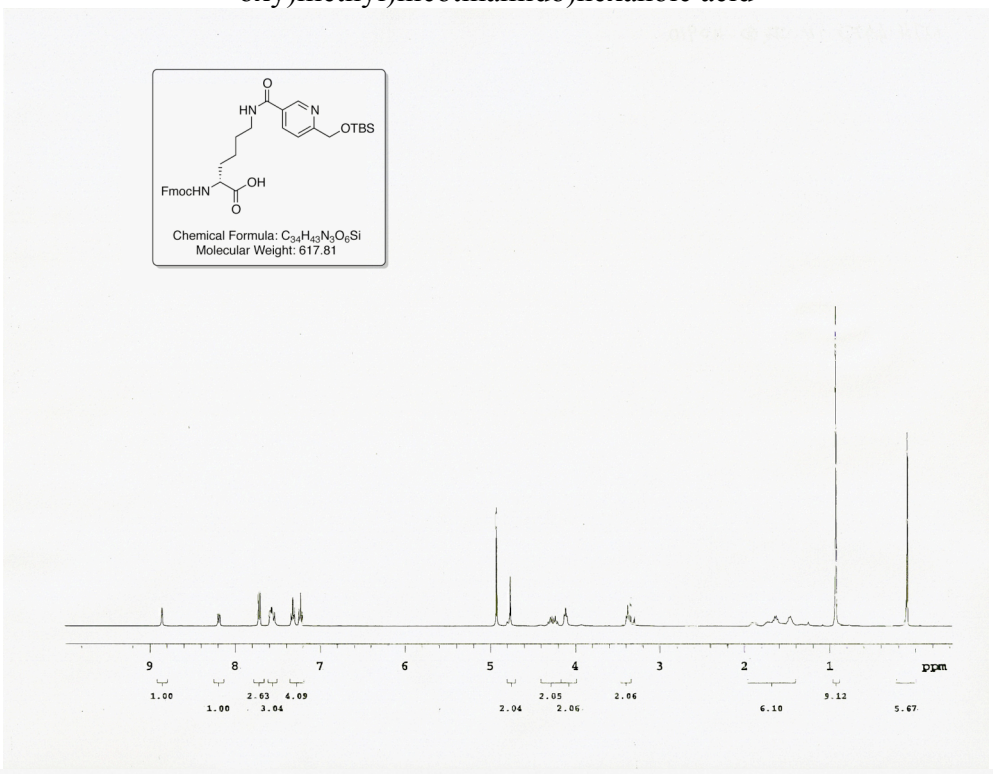

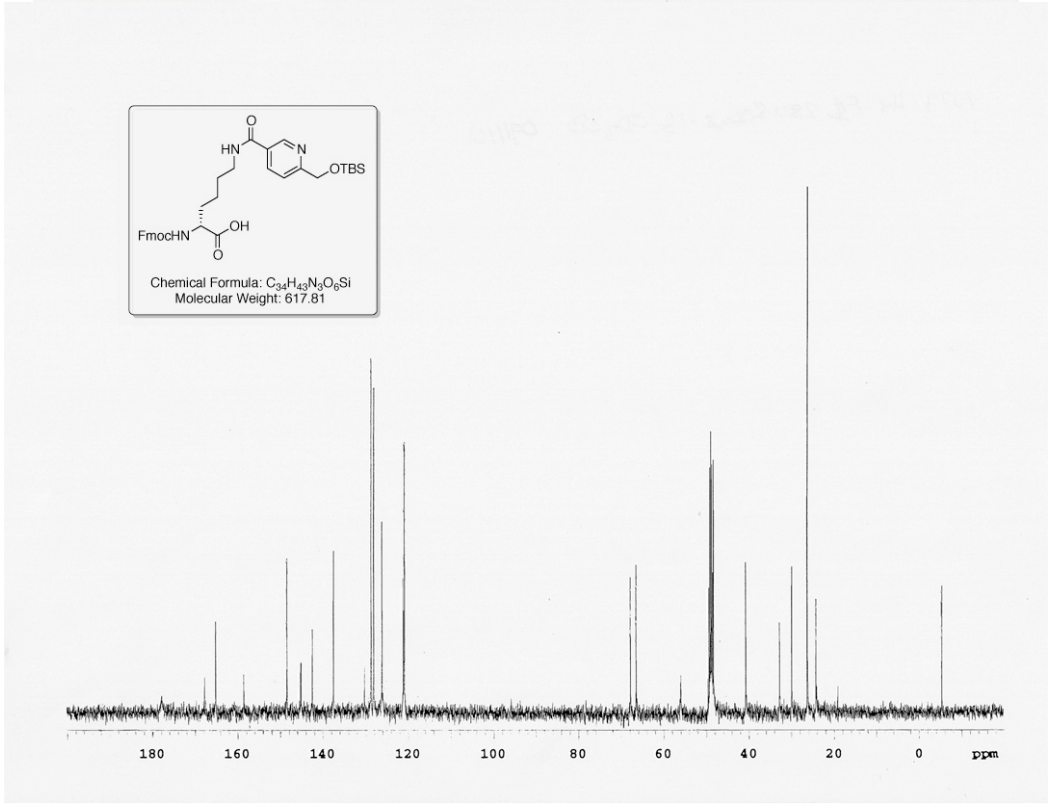

TPA·LHRH conjugate

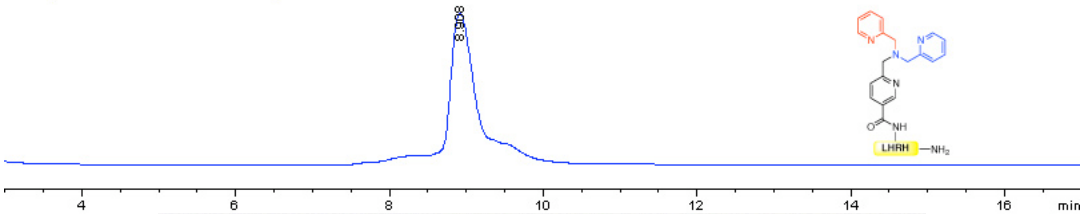

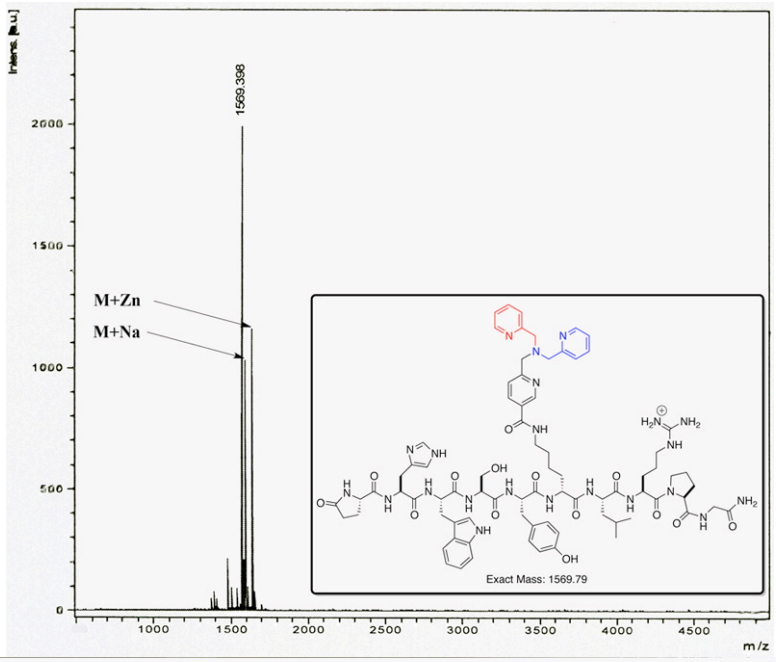

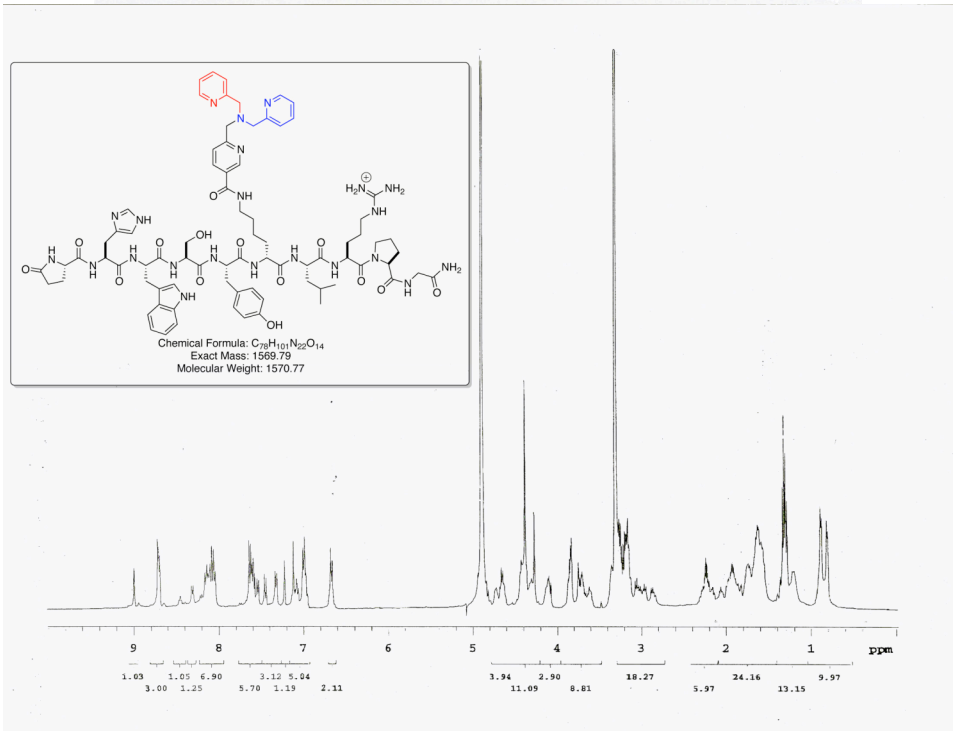

Pyrazine derivative of TPA·LHRH conjugate

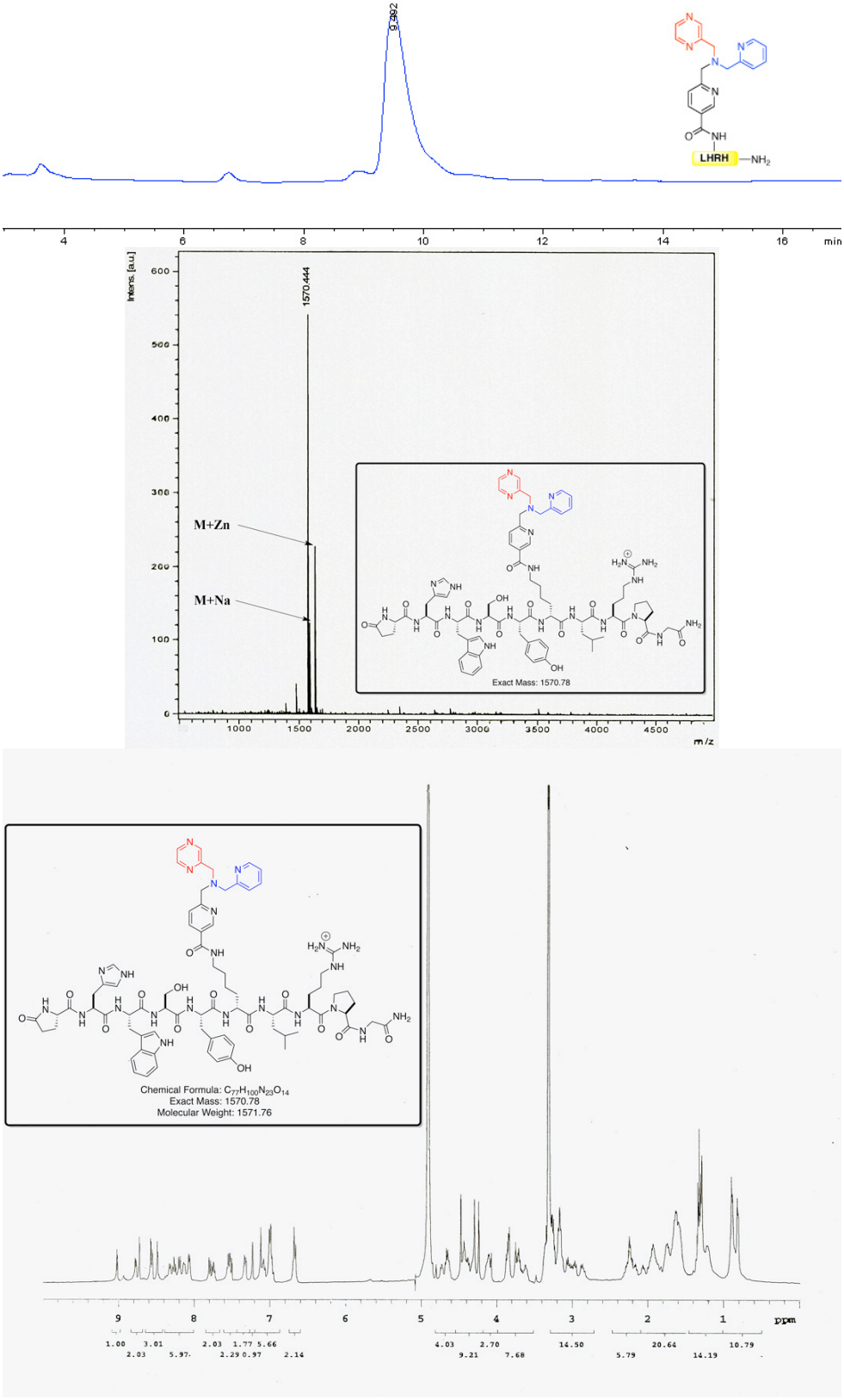

Carboxylate derivative of TPA·LHRH conjugate

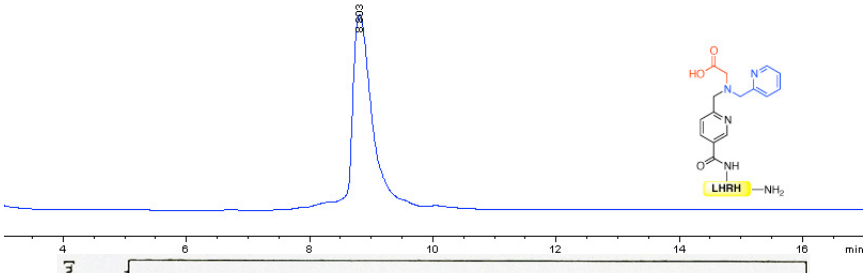

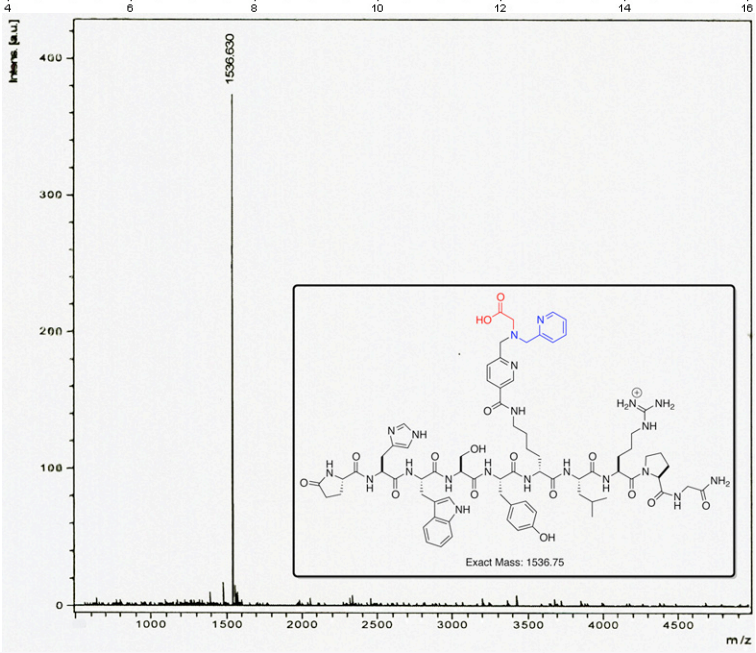

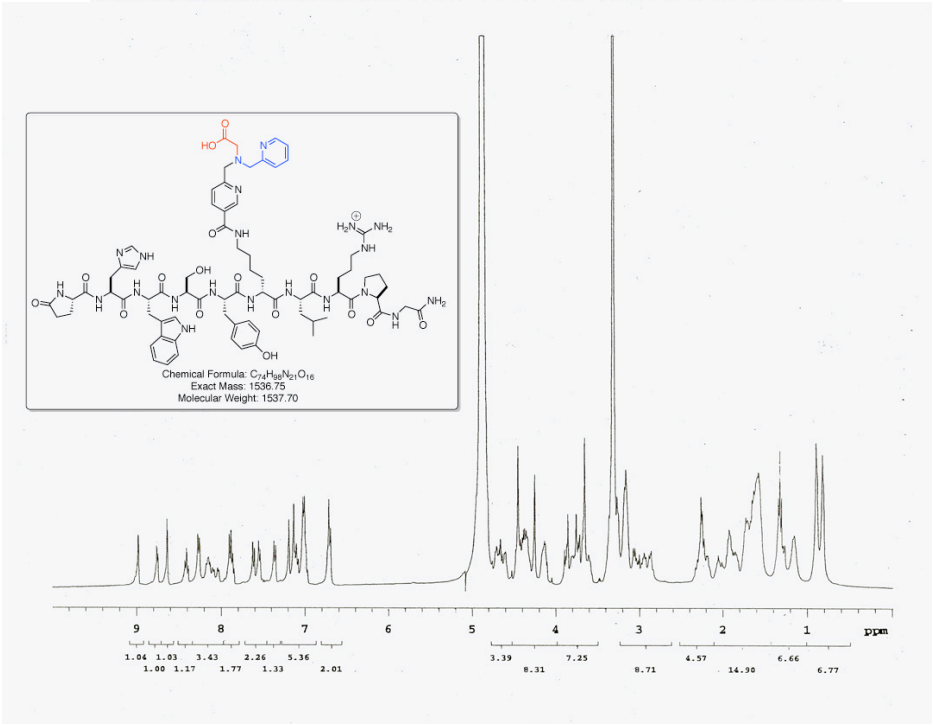

PaPy3·LHRH conjugate

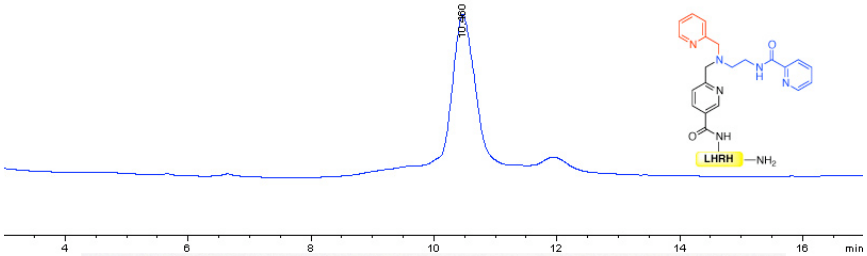

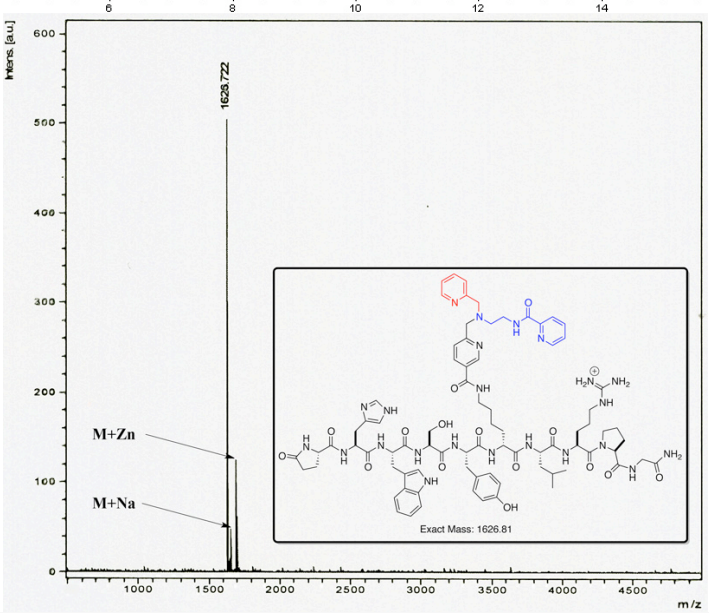

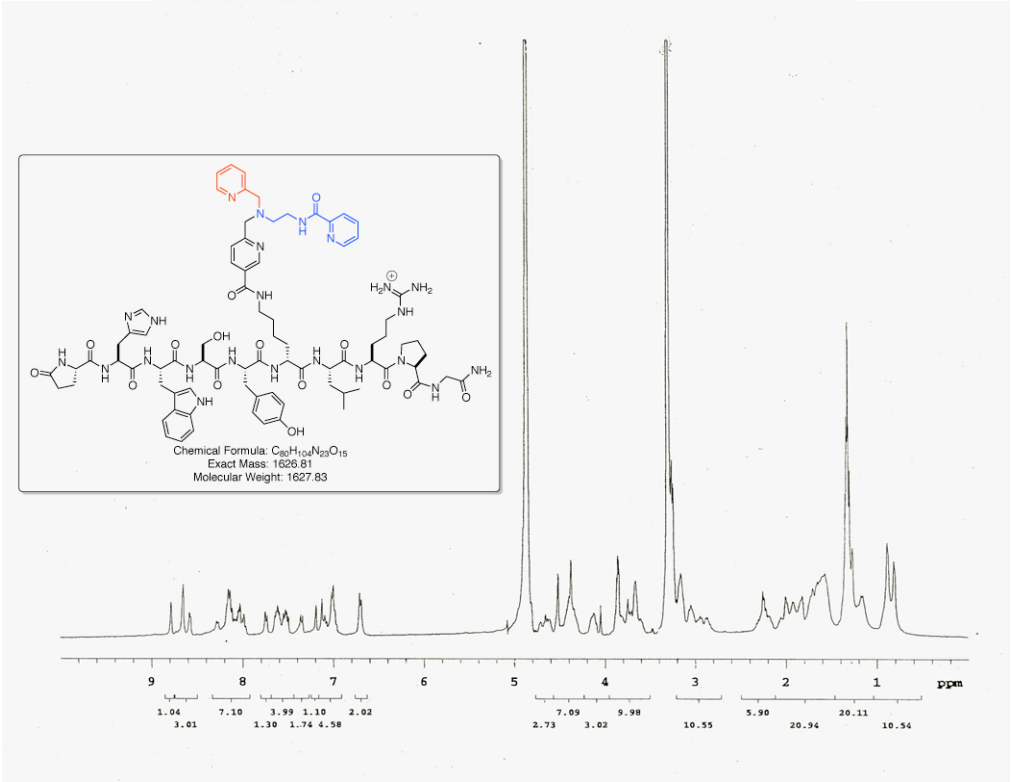

Pyrazine derivative of PaPy3·LHRH conjugate

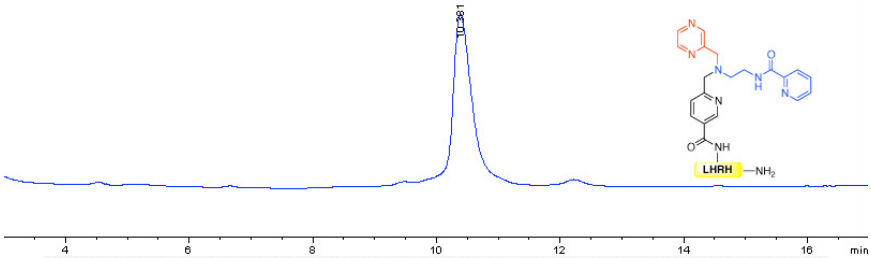

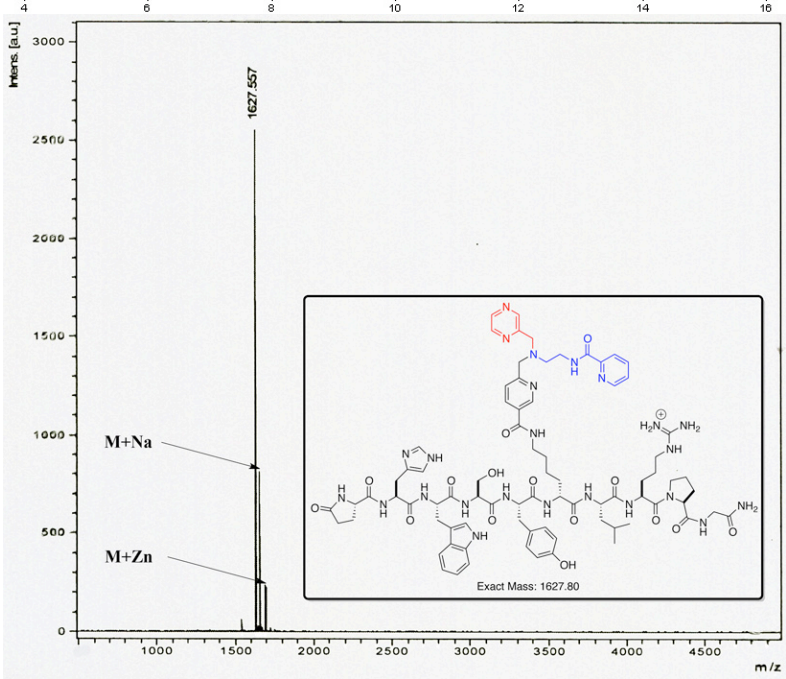

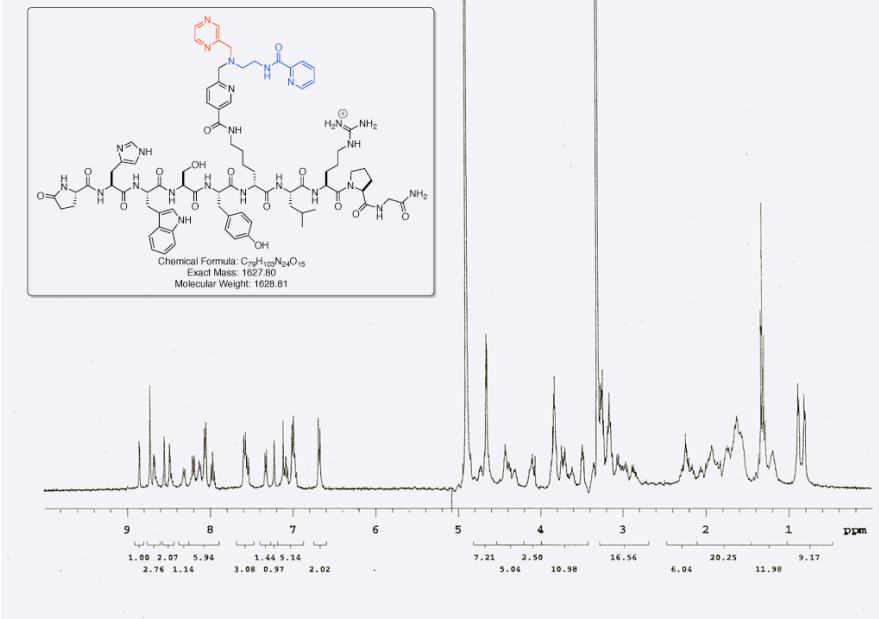

Carboxylate derivative of PaPy3·LHRH conjugate

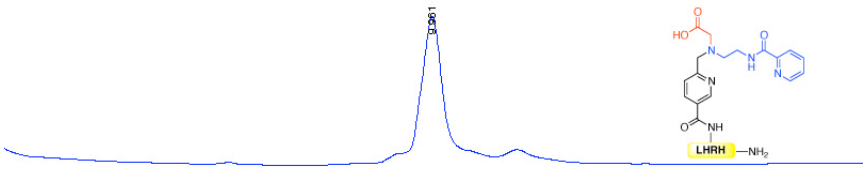

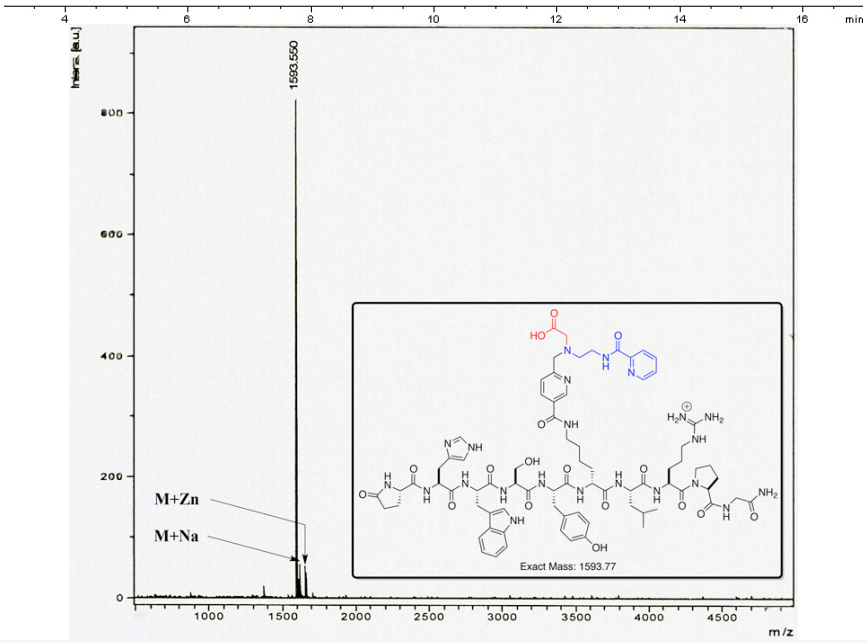

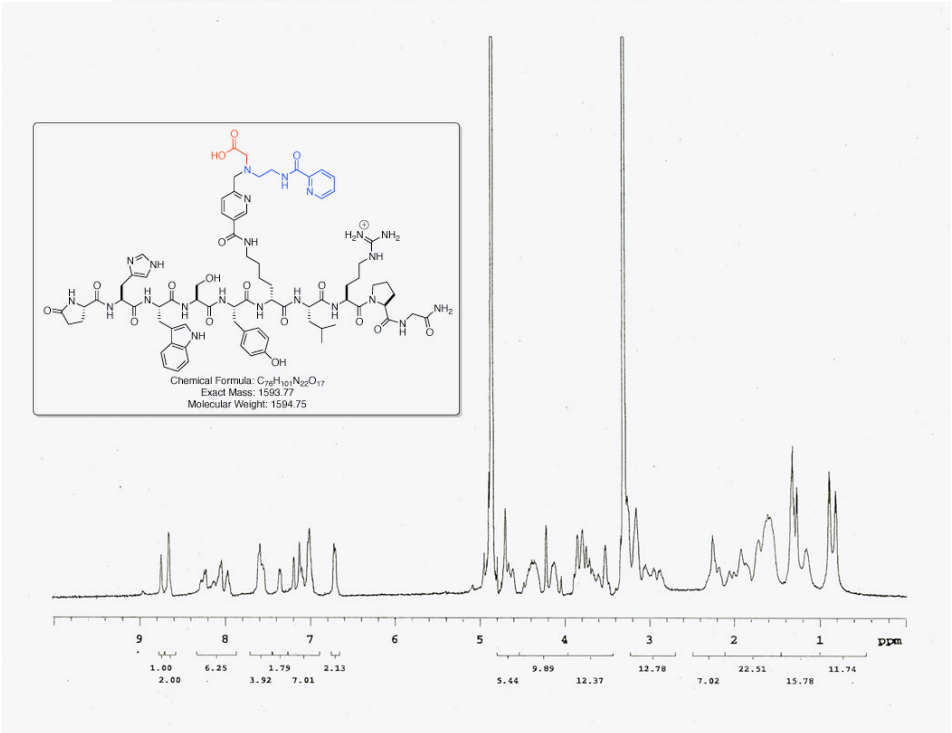

Bn-TPEN·LHRH conjugate

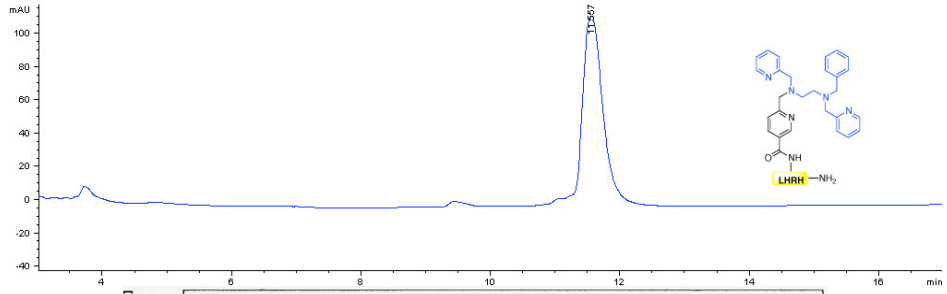

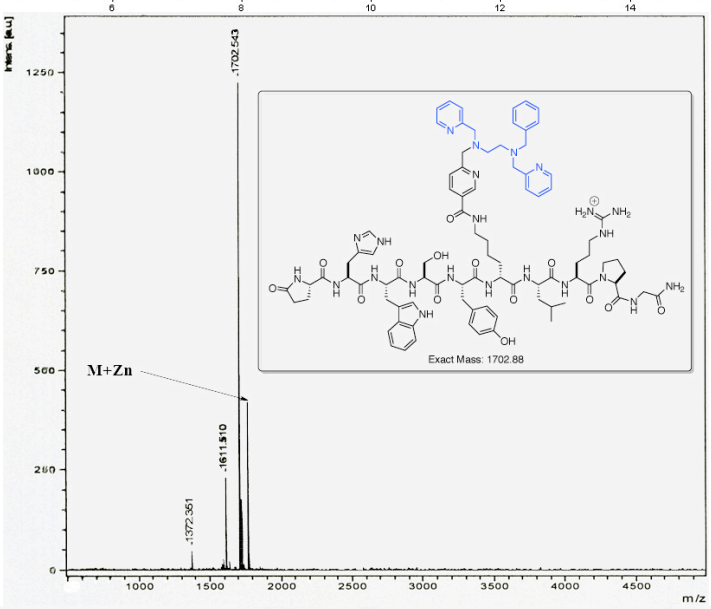

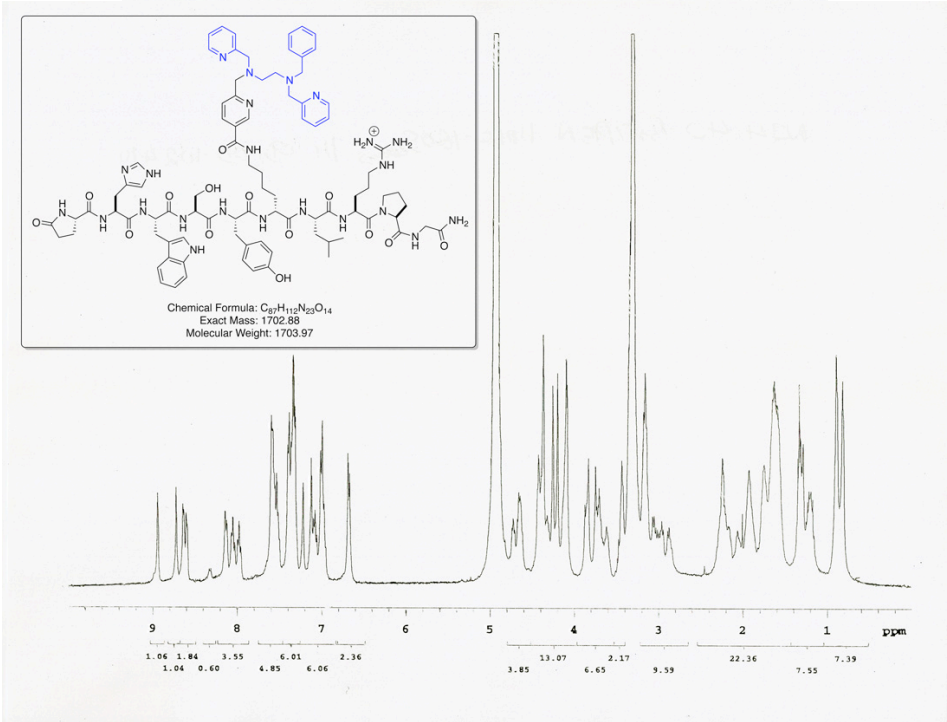

N4Py·LHRH conjugate

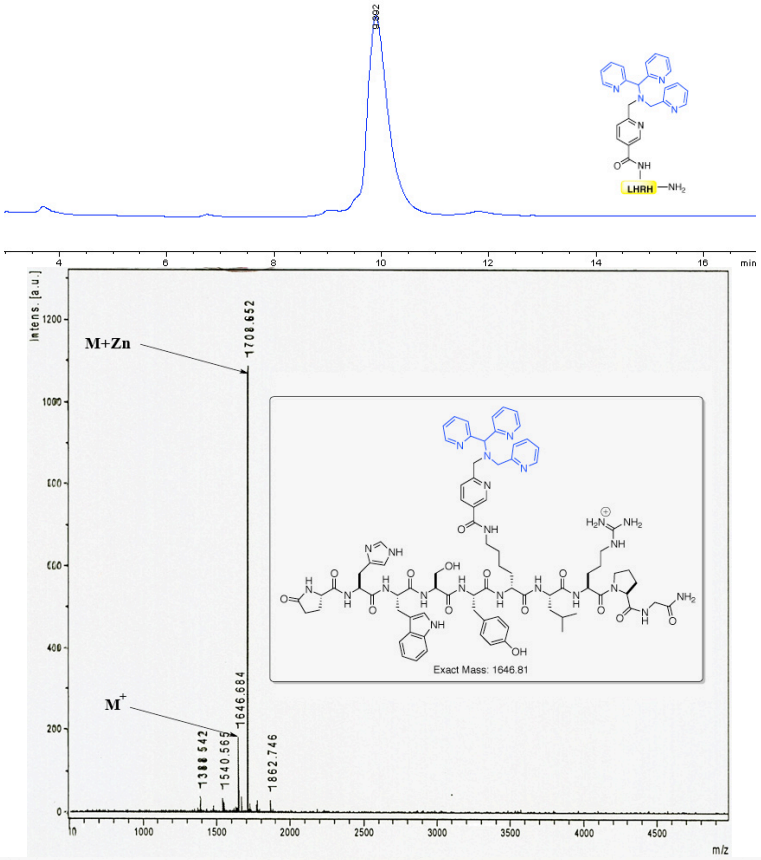

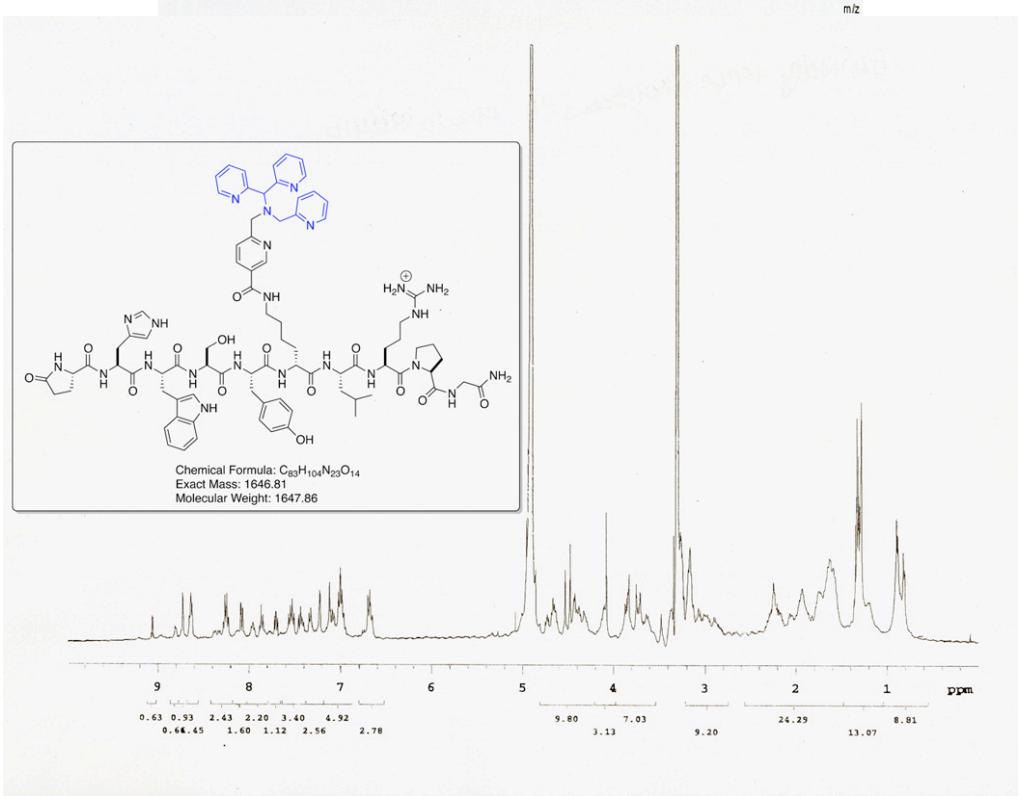

Methyl 2-(2-acetamido-3-(6-(((dipyridin-2-ylmethyl)(pyridin-2-ylmethyl)amino)methyl) pyridin-3-yl)propanamido)acetate

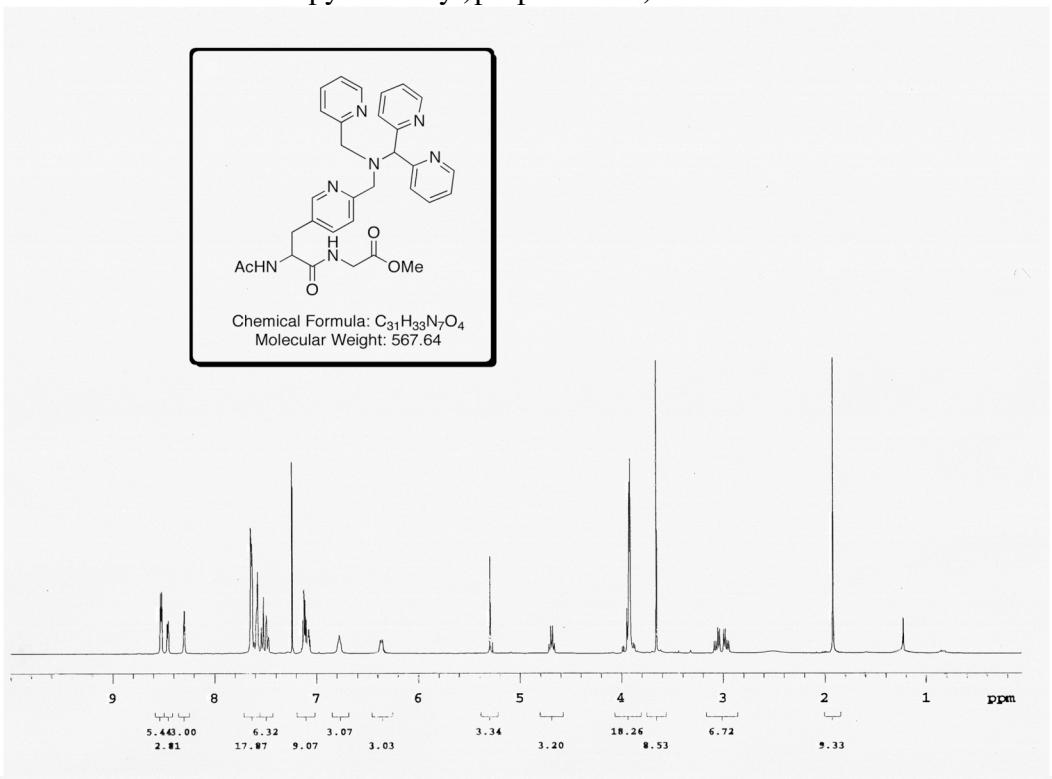

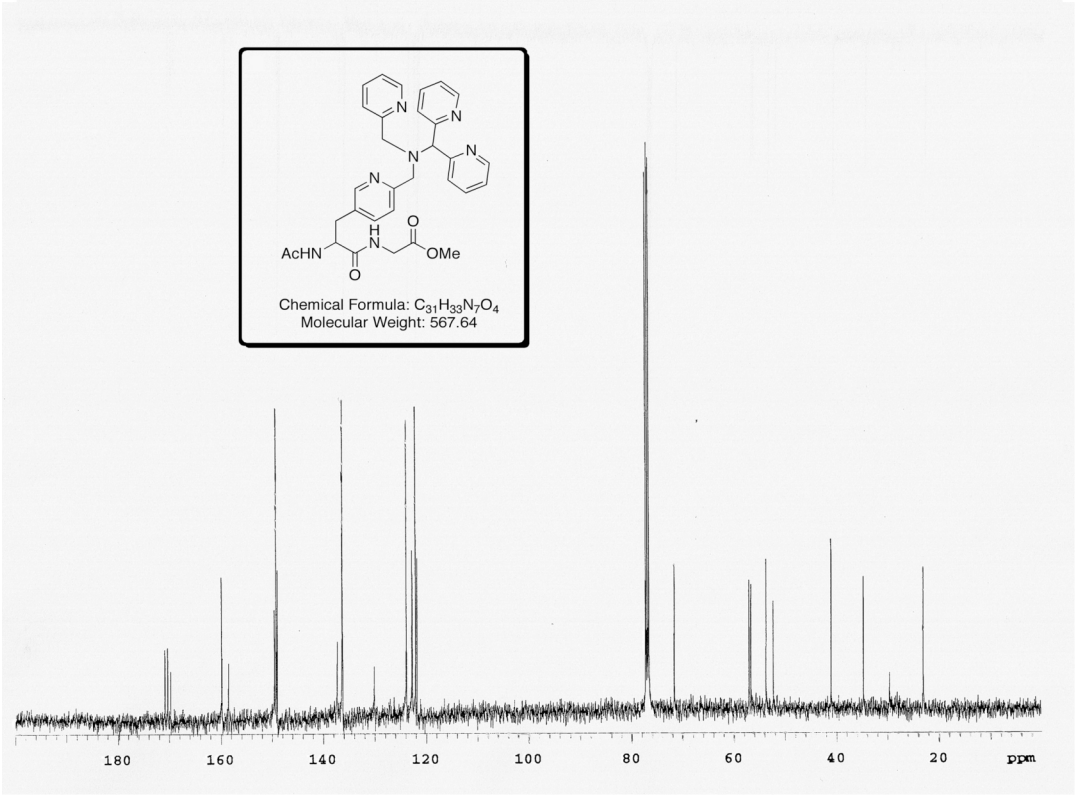

d_7-Benzyl 2-(2-acetamido-3-(6-(((dipyridin-2-ylmethyl)(pyridin-2-ylmethyl)amino)methyl)pyridin-3-yl)propanamido)acetate

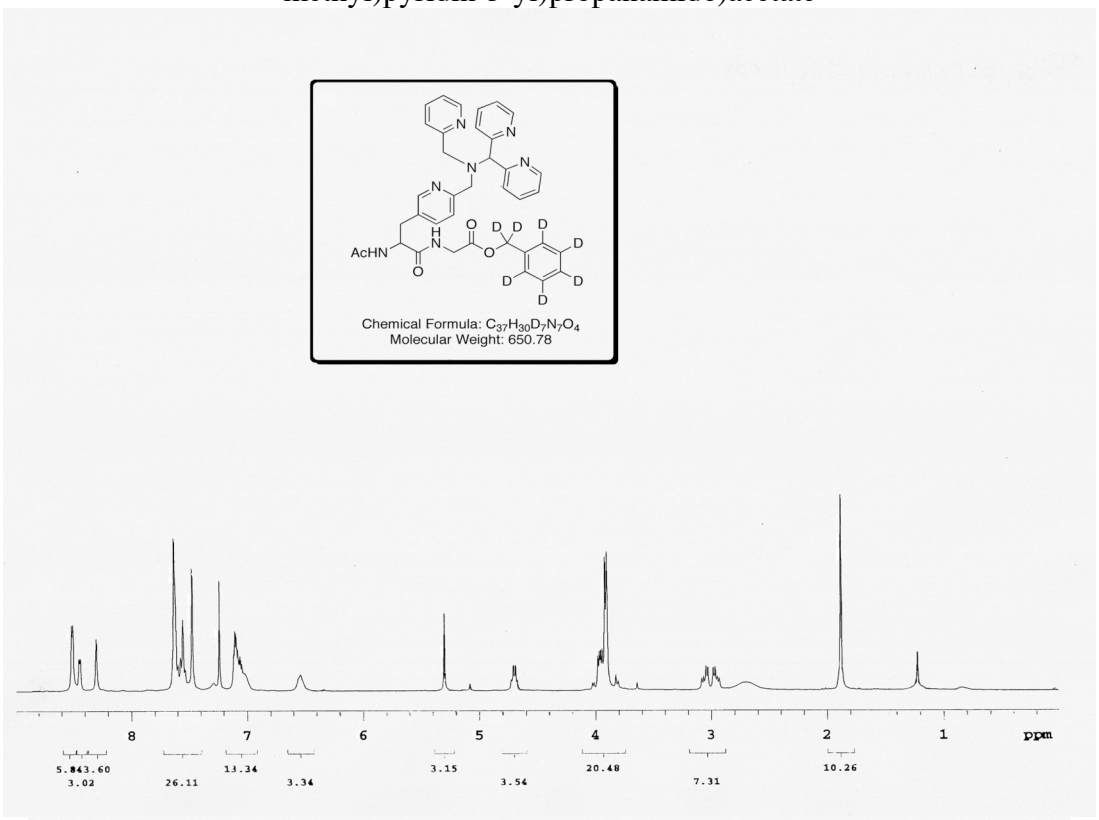

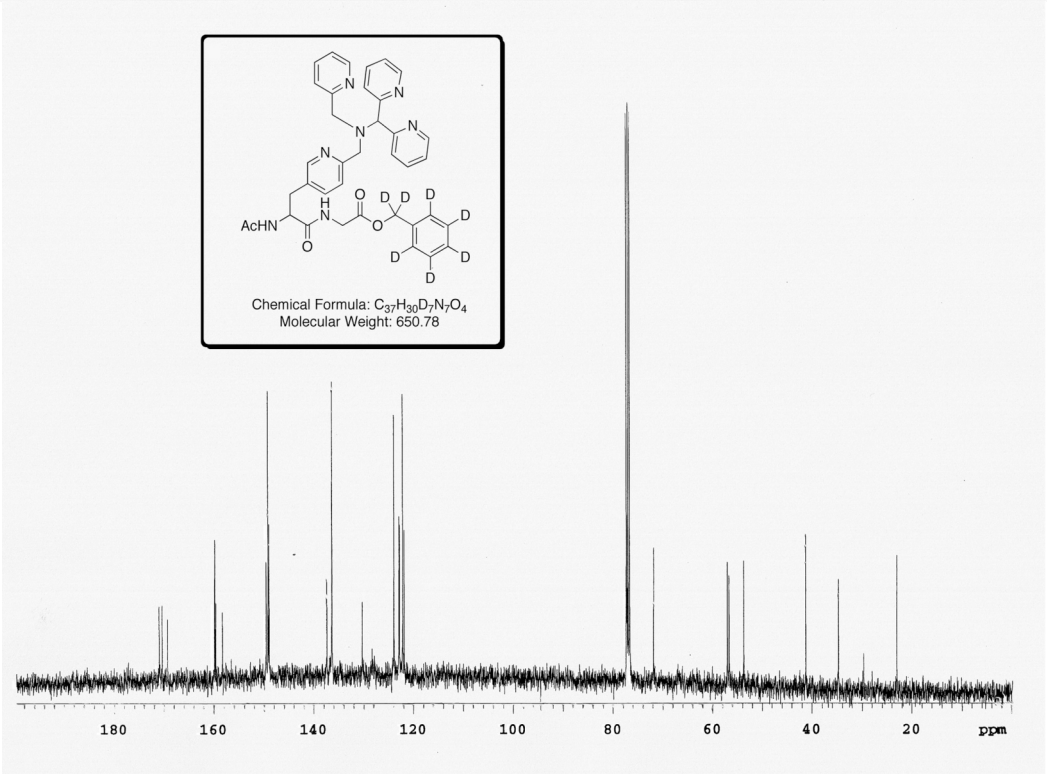

4-methoxybenzyl 2-(2-acetamido-3-(6-((((dipyridin-2-ylmethyl)(pyridin-2-ylmethyl) amino)methyl)pyridin-3-yl)propanamido)acetate

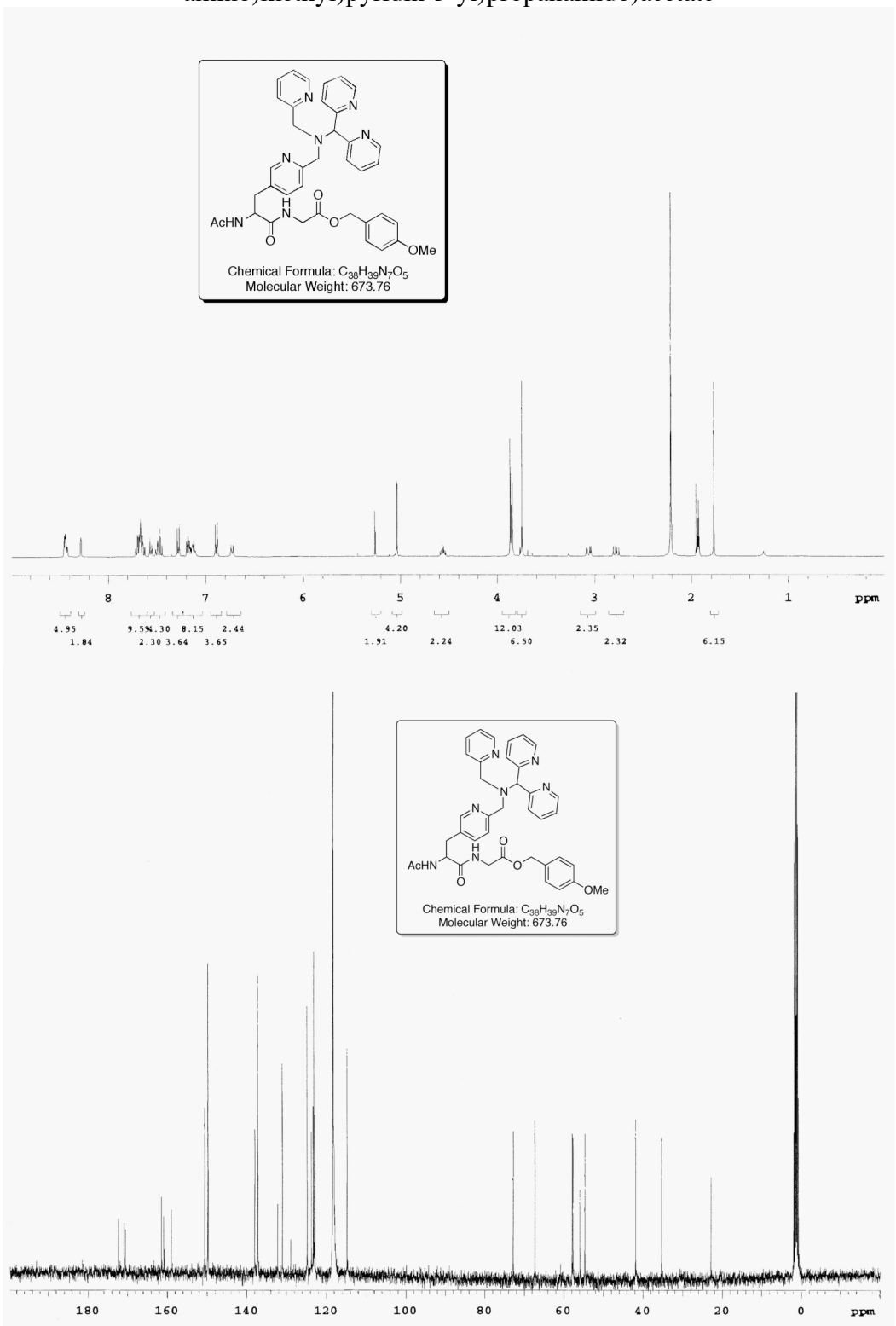

4-methylbenzyl 2-(2-acetamido-3-(6-((((dipyridin-2-ylmethyl)(pyridin-2-ylmethyl) amino)methyl)pyridin-3-yl)propanamido)acetate

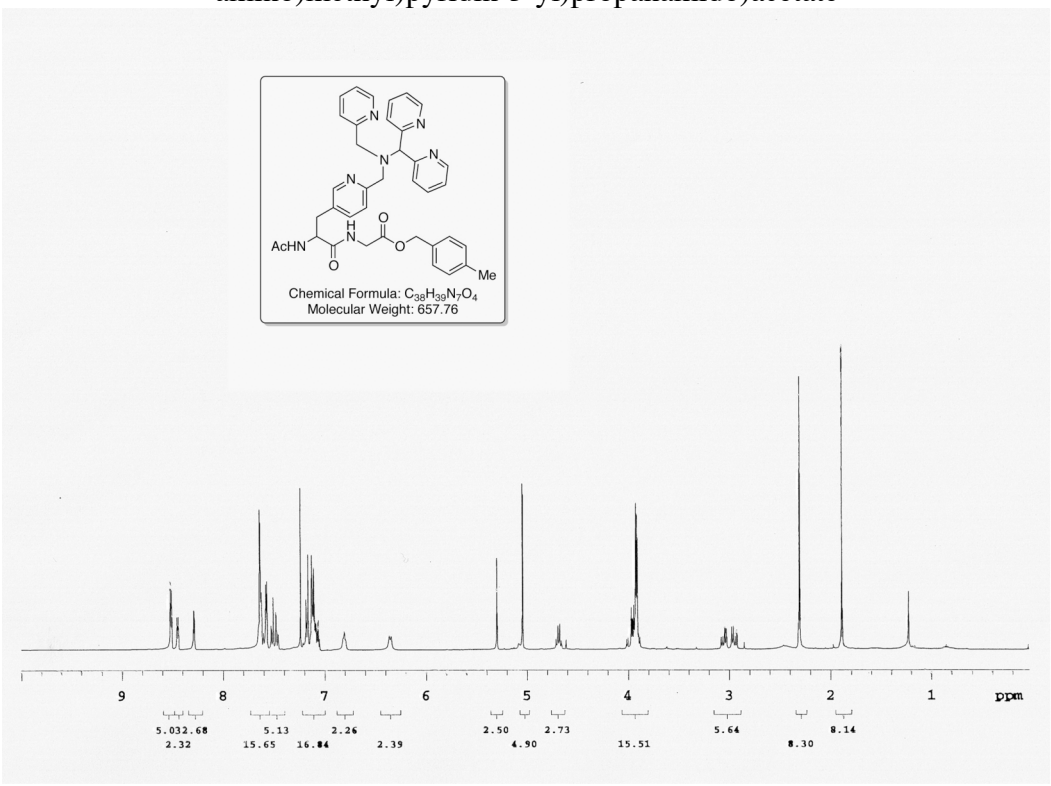

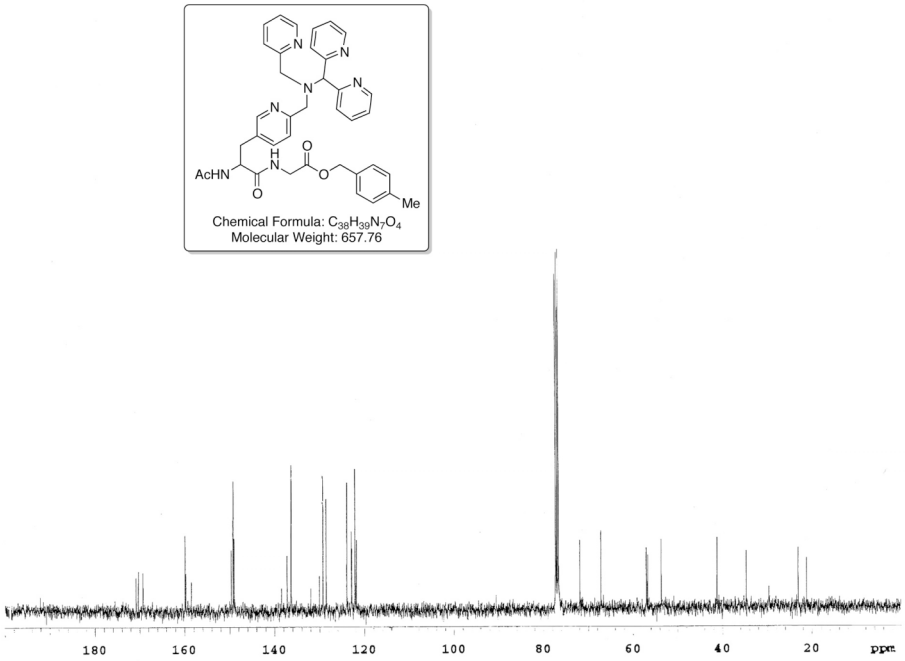

4-chlorobenzyl 2-(2-acetamido-3-(6-((tert-butyldimethylsilyloxy)methyl)pyridin-3-yl) propanamido)acetate

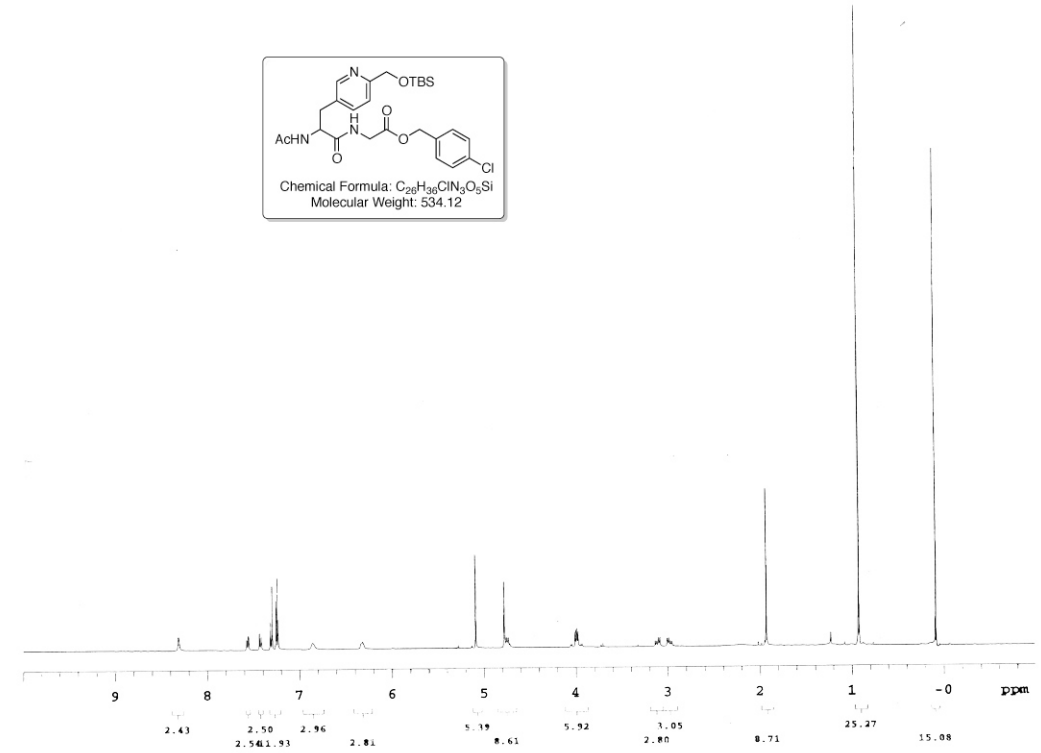

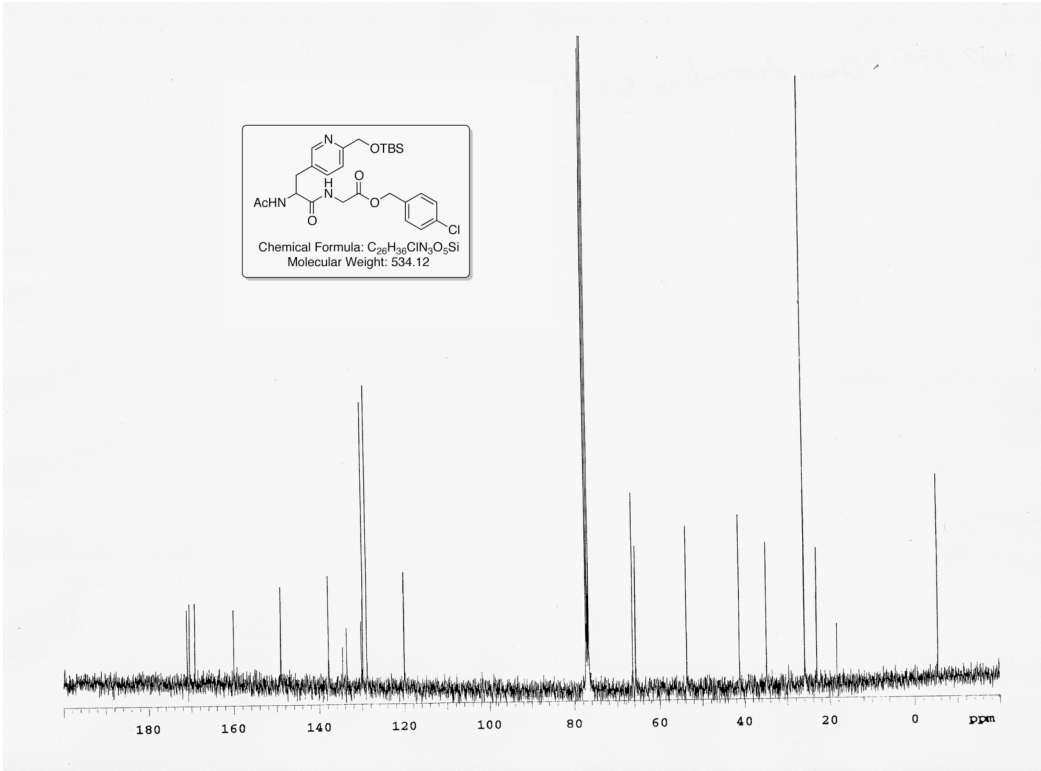

4-chlorobenzyl 2-(2-acetamido-3-(6-(chloromethyl)pyridin-3-yl)propanamido)acetate

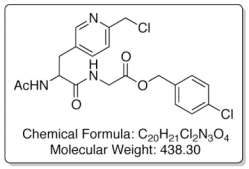

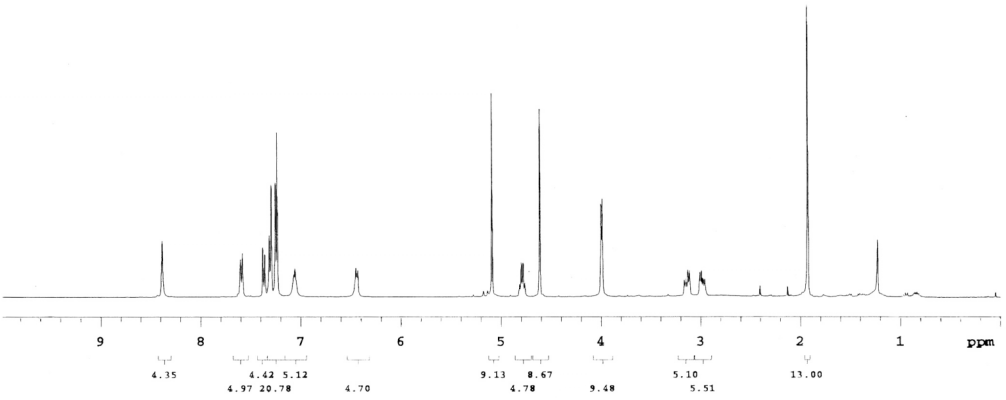

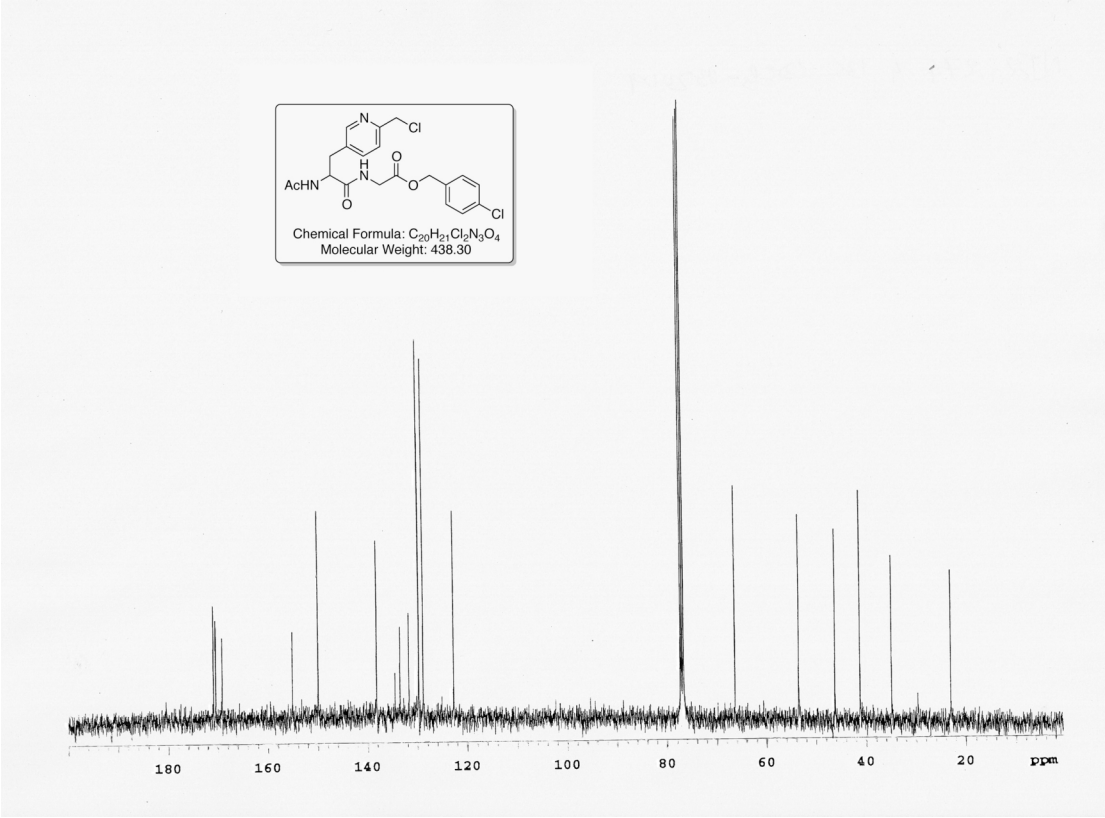

4-chlorobenzyl 2-(2-acetamido-3-(6-(((dipyridin-2-ylmethyl)(pyridin-2-ylmethyl)amino)methyl)pyridin-3-yl)propanamido)acetate

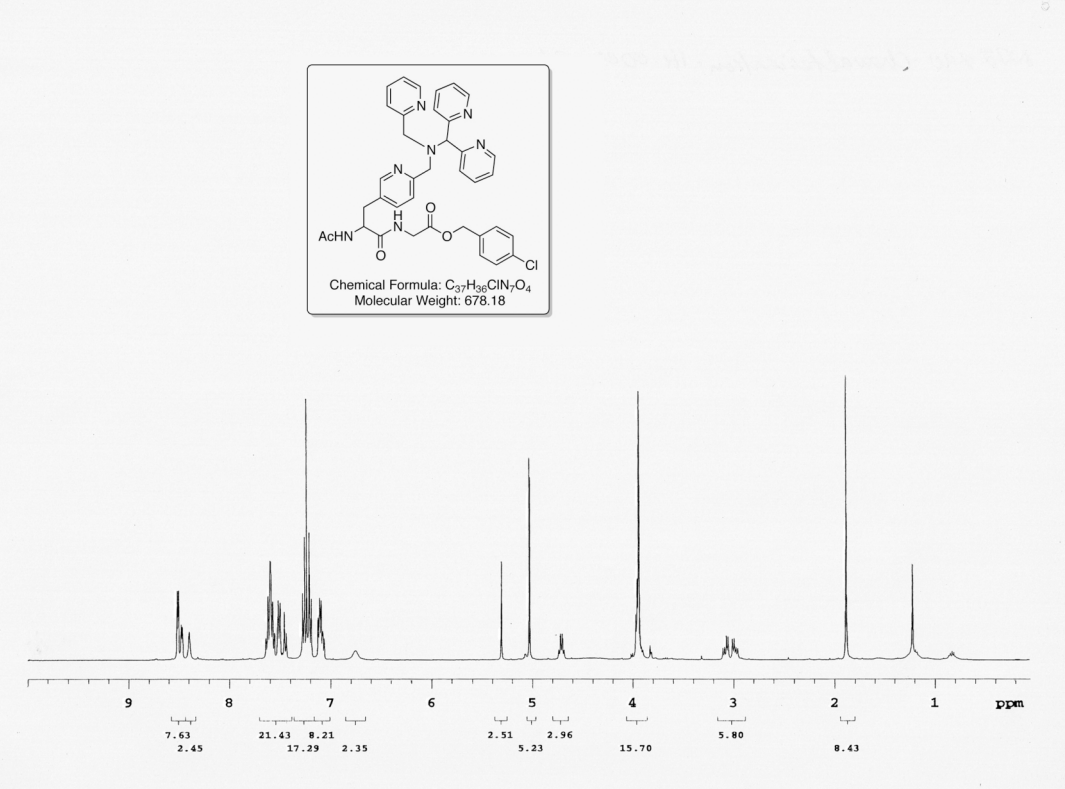

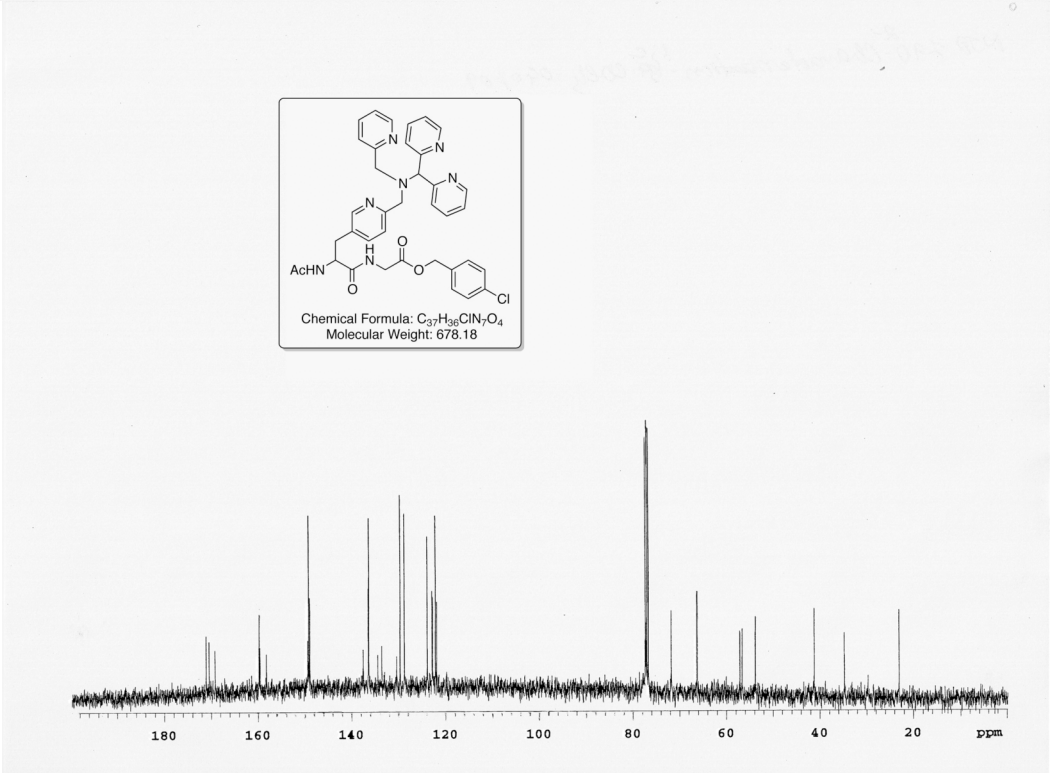

REFERENCES

1. Liu, S.; Edwards, D. S. *Bioconjugate Chem.* **2001,** *12*, 7-34.

2. Volkert, W. A.; Hoffman, T. J. *Chem. Rev.* **1999,** *99*, 2269-2292.

3. Okarvi, S. M. *Med. Res. Rev.* **2004,** *24*, 357-397.

4. Fichna, J.; Janecka, A. *Bioconjugate Chem.* **2003,** *14*, 3-17.

5. Liu, S.; Edwards, D. S. *Chem. Rev.* **1999,** *99*, 2235-2268.

6. Wheate, N. J.; Brodie, C. R.; Collins, J. G.; Kemp, S.; Aldrich-Wright, J. R. *Mini-Rev. Med. Chem.* **2007,** *7*, 627-648.

7. Gokhale, N. H.; Cowan, J. A. *Chem. Commun.* **2005**, 5916-5918.

8. Kovacic, R. T.; Welch, J. T.; Franklin, S. J. *J. Am. Chem. Soc.* **2003,** *125*, 6656-6662.

9. Liu, C.; Wang, L. *Dalton Trans.* **2009**, 227-239.

10. Wang, X.-Y.; Zhang, J.; Li, K.; Jiang, N.; Chen, S.-Y.; Lin, H.-H.; Huang, Y.; Ma, L.-J.; Yu, X.-Q. *Bioorg. Med. Chem.* **2006,** *14*, 6745-6751.

11. Metzler-Nolte, N. *Top. Organomet. Chem.* **2010,** *32*, 195-217.

12. Albrecht, M.; Stortz, P.; Nolting, R. *Synthesis* **2003**, 1307-1320.

13. Albrecht, M.; Stortz, P. *Chem. Soc. Rev.* **2005,** *34*, 496-506.

14. Nam, W. *Acc. Chem. Res.* **2007,** *40*, 522-531.

15. Que, L. *Acc. Chem. Res.* **2007,** *40*, 493-500.

16. Jackson, C. S.; Kodanko, J. J., Unpublished results.

17. Prakash, J.; Kodanko, J. J. *Inorg. Chem.* **2011**, In press.

18. Paterson, B. M.; Karas, J. A.; Scanlon, D. B.; White, J. M.; Donnelly, P. S. *Inorg. Chem.* *49*, 1884-1893.

19. Cowley, A. R.; Dilworth, J. R.; Donnelly, P. S.; Heslop, J. M.; Ratcliffe, S. J. *Dalton Trans.* **2007**, 209-217.

20. Hueting, R.; Christlieb, M.; Dilworth, J. R.; Garayoa, E. G.; Gouverneur, V.; Jones, M. W.; Maes, V.; Schibli, R.; Sun, X.; Tourwe, D. A. *Dalton Trans. 39*, 3620-3632.

21. Robillard, M. S.; Valentijn, A. R. P. M.; Meeuwenoord, N. J.; Van der Marel, G. A.; Van Boom, J. H.; Reedijk, J. *Angew. Chem., Int. Ed.* **2000,** *39*, 3096-3099.

22. Robillard, M. S.; Bacac, M.; van den Elst, H.; Flamigni, A.; van der Marel, G. A.; van Boom, J. H.; Reedijk, J. *J. Comb. Chem.* **2003,** *5*, 821-825.

23. Robillard, M. S.; van Alphen, S.; Meeuwenoord, N. J.; Jansen, B. A. J.; van der Marel, G. A.; van Boom, J. H.; Reedijk, J. *New J. Chem.* **2005,** *29*, 220-225.

24. Michaelis, K.; Kalesse, M. *Angew. Chem., Int. Ed.* **1999,** *38*, 2243-2245.

25. van Staveren, D. R.; Metzler-Nolte, N. *Chem. Commun.* **2002**, 1406-1407.

26. Lemke, J.; Metzler-Nolte, N. *Eur. J. Inorg. Chem.* **2008**, 3359-3366.

27. Dervan, P. B. *Methods Enzymol.* **1991,** *208*, 497-515.

28. Kirin, S. I.; Duebon, P.; Weyhermueller, T.; Bill, E.; Metzler-Nolte, N. *Inorg. Chem.* **2005,** *44*, 5405-5415.

29. De Leon-Rodriguez, L. M.; Ortiz, A.; Weiner, A. L.; Zhang, S.; Kovacs, Z.; Kodadek, T.; Sherry, A. D. *J. Am. Chem. Soc.* **2002,** *124*, 3514-3515.

30. Gariepy, J.; Remy, S.; Zhang, X.; Ballinger, J. R.; Bolewska-Pedyczak, E.; Rauth, M.; Bisland, S. K. *Bioconjugate Chem.* **2002,** *13*, 679-684.

31. Blok, D.; Feitsma, H. I. J.; Kooy, Y. M. C.; Welling, M. M.; Ossendorp, F.; Vermeij, P.; Drijfhout, J. W. *Nucl. Med. Biol.* **2004,** *31*, 815-820.

32. Smith, C. J.; Gali, H.; Sieckman, G. L.; Higginbotham, C.; Volkert, W. A.; Hoffman, T. J. *Bioconjugate Chem.* **2003,** *14*, 93-102.

33. Schottelius, M.; Berger, S.; Poethko, T.; Schwaiger, M.; Wester, H.-J. *Bioconjugate Chem.* **2008,** *19*, 1256-1268.

34. Yim, C.-B.; Boerman, O. C.; de Visser, M.; de Jong, M.; Dechesne, A. C.; Rijkers, D. T. S.; Liskamp, R. M. J. *Bioconjugate Chem.* **2009,** *20*, 1323-1331.

35. Kovacs, Z.; De Leon-Rodriguez, L. M. *Mini-Rev. Org. Chem.* **2007,** *4*, 281-291.

36. De Leon-Rodriguez, L. M.; Kovacs, Z. *Bioconjugate Chem.* **2008,** *19*, 391-402.

37. Yim, C.-B.; Dijkgraaf, I.; Merkx, R.; Versluis, C.; Eek, A.; Mulder, G. E.; Rijkers, D. T. S.; Boerman, O. C.; Liskamp, R. M. J. *J. Med. Chem.* **2010,** *53*, 3944-3953.

38. Kolakowski, R. V.; Shangguan, N.; Sauers, R. R.; Williams, L. J. *J. Am. Chem. Soc.* **2006,** *128*, 5695-5702.

39. Shangguan, N.; Katukojvala, S.; Greenberg, R.; Williams, L. J. *J. Am. Chem. Soc.* **2003,** *125*, 7754-7755.

40. Gali, H.; Hoffman, T. J.; Sieckman, G. L.; Owen, N. K.; Katti, K. V.; Volkert, W. A. *Bioconjugate Chem.* **2001,** *12*, 354-363.

41. Guerin, B.; Ait-Mohand, S.; Tremblay, M.-C.; Dumulon-Perreault, V.; Fournier, P.; Benard, F. *Org. Lett.* **2010,** *12*, 280-283.

42. Riddoch, R. W.; Schaffer, P.; Valliant, J. F. *Bioconjugate Chem.* **2006,** *17*, 226-235.

43. Yoo, B.; Pagel, M. D. *Bioconjugate Chem.* **2007,** *18*, 903-911.

44. Gasser, G.; Neukamm, M. A.; Ewers, A.; Brosch, O.; Weyhermuller, T.; Metzler-Nolte, N. *Inorg. Chem.* **2009,** *48*, 3157-3166.

45. Constable, E. C.; Housecroft, C. E.; Mundwiler, S. *Dalton Trans.* **2003**, 2112-2114.

46. Albrecht, M.; Stortz, P.; Runsink, J.; Weis, P. *Chem.--Eur. J.* **2004,** *10*, 3657-3666.

47. Graham, K. A. N.; Wang, Q.; Eisenhut, M.; Haberkorn, U.; Mier, W. *Tetrahedron Lett.* **2002,** *43*, 5021-5024.

48. Ishida, H.; Kyakuno, M.; Oishi, S. *Biopolymers* **2004,** *76*, 69-82.

49. Bishop, B. M.; McCafferty, D. G.; Erickson, B. W. *Tetrahedron* **2000,** *56*, 4629-4638.

50. Schneider, J. P.; Kelly, J. W. *J. Am. Chem. Soc.* **1995,** *117*, 2533-2546.

51. Jensen, J. F.; Worm-Leonhard, K.; Meldal, M. *Eur. J. Org. Chem.* **2008**, 3785-3797, S3785/3781-S3785/3729.

52. Christensen, C. A.; Meldal, M. *Chem.--Eur. J.* **2005,** *11*, 4121-4131.

53. Christensen, C. A.; Meldal, M. *J. Comb. Chem.* **2007,** *9*, 79-85.

54. Dirscherl, G.; Knape, R.; Hanson, P.; Koenig, B. *Tetrahedron* **2007,** *63*, 4918-4928.

55. Greenland, W. E. P.; Howland, K.; Hardy, J.; Fogelman, I.; Blower, P. J. *J. Med. Chem.* **2003,** *46*, 1751-1757.

56. De Leon-Rodriguez, L. M.; Kovacs, Z.; Dieckmann, G. R.; Sherry, A. D. *Chem.--Eur. J.* **2004,** *10*, 1149-1155.

57. Hutschenreiter, S.; Neumann, L.; Raedler, U.; Schmitt, L.; Tampe, R. *ChemBioChem* **2003,** *4*, 1340-1344.

58. Cisnetti, F.; Gateau, C.; Lebrun, C.; Delangle, P. *Chem.--Eur. J.* **2009,** *15*, 7456-7469, S7456/7451-S7456/7418.

59. Ruan, F.; Chen, Y.; Itoh, K.; Sasaki, T.; Hopkins, P. B. *J. Org. Chem.* **1991,** *56*, 4347-4354.

60. Clavaud, C.; Heckenroth, M.; Stricane, C.; Menez, A.; Dugave, C. *Bioconjugate Chem.* **2006,** *17*, 807-814.

61. Stephenson, K. A.; Banerjee, S. R.; Besanger, T.; Sogbein, O. O.; Levadala, M. K.; McFarlane, N.; Lemon, J. A.; Boreham, D. R.; Maresca, K. P.; Brennan, J. D.; Babich, J. W.; Zubieta, J.; Valliant, J. F. *J. Am. Chem. Soc.* **2004,** *126*, 8598-8599.

62. Stephenson, K. A.; Banerjee, S. R.; Sogbein, O. O.; Levadala, M. K.; McFarlane, N.; Boreham, D. R.; Maresca, K. P.; Babich, J. W.; Zubieta, J.; Valliant, J. F. *Bioconjugate Chem.* **2005,** *16*, 1189-1195.

63. Stephenson, K. A.; Reid, L. C.; Zubieta, J.; Babich, J. W.; Kung, M.-P.; Kung, H. F.; Valliant, J. F. *Bioconjugate Chem.* **2008,** *19*, 1087-1094.

64. Stephenson, K. A.; Zubieta, J.; Banerjee, S. R.; Levadala, M. K.; Taggart, L.; Ryan, L.; McFarlane, N.; Boreham, D. R.; Maresca, K. P.; Babich, J. W.; Valliant, J. F. *Bioconjugate Chem.* **2004,** *15*, 128-136.

65. De Leon-Rodriguez, L. M.; Kovacs, Z.; Sherry, A. D. *Lett. Org. Chem.* **2005,** *2*, 160-164.

66. Jiang, H.; O'Neil, E. J.; DiVittorio, K. M.; Smith, B. D. *Org. Lett.* **2005,** *7*, 3013-3016.

67. Ojida, A.; Honda, K.; Shinmi, D.; Kiyonaka, S.; Mori, Y.; Hamachi, I. *J. Am. Chem. Soc.* **2006,** *128*, 10452-10459.

68. Nakonieczna, L.; Przychodzen, W.; Chimiak, A. *Liebigs Ann. Chem.* **1994**, 1055-1058.

69. Peuralahti, J.; Hakala, H.; Mukkala, V.-M.; Loman, K.; Hurskainen, P.; Mulari, O.; Hovinen, J. *Bioconjugate Chem.* **2002,** *13*, 870-875.

70. Song, A. I.; Rana, T. M. *Bioconjugate Chem.* **1997,** *8*, 249-252.

71. Imperiali, B.; Fisher, S. L. *J. Am. Chem. Soc.* **1991,** *113*, 8527-8528.

72. Imperiali, B.; Fisher, S. L. *J. Org. Chem.* **1992,** *57*, 757-759.

73. Imperiali, B.; Prins, T. J.; Fisher, S. L. *J. Org. Chem.* **1993,** *58*, 1613-1616.

74. Imperiali, B.; Roy, R. S. *J. Org. Chem.* **1995,** *60*, 1891-1894.

75. Cheng, R. P.; Fisher, S. L.; Imperiali, B. *J. Am. Chem. Soc.* **1996,** *118*, 11349-11356.

76. Wilson, S. R.; Yasmin, A.; Wu, Y. *J. Org. Chem.* **1992,** *57*, 6941-6945.

77. Huang, X.; Long, E. C. *Bioorg. Med. Chem. Lett.* **1995,** *5*, 1937-1940.

78. Gilbertson, S. R.; Chen, G.; McLoughlin, M. *J. Am. Chem. Soc.* **1994,** *116*, 4481-4482.

79. Gilbertson, S. R.; Wang, X. *J. Org. Chem.* **1996,** *61*, 434-435.

80. Nadler, A.; Hain, C.; Diederichsen, U. *Eur. J. Org. Chem.* **2009**, 4593-4599.

81. Rossi, P.; Felluga, F.; Scrimin, P. *Tetrahedron Lett.* **1998,** *39*, 7159-7162.

82. Rossi, P.; Tecilla, P.; Baltzer, L.; Scrimin, P. *Chem.--Eur. J.* **2004,** *10*, 4163-4170.

83. O'Donnell, M. J.; Bennett, W. D.; Wu, S. *J. Am. Chem. Soc.* **1989,** *111*, 2353-2355.

84. O'Donnell, M. J. *Acc. Chem. Res.* **2004,** *37*, 506-517.

85. Stephenson, K. A.; Banerjee, S. R.; McFarlane, N.; Boreham, D. R.; Maresca, K. P.; Babich, J. W.; Zubieta, J.; Valliant, J. F. *Can. J. Chem.* **2005,** *83*, 2060-2066.

86. Lattuada, L.; Cappelletti, E.; De Miranda, M.; Umbelli, C. *Lett. Org. Chem.* **2009,** *6*, 624-629.

87. Dijkgraaf, I.; Rijnders, A. Y.; Soede, A.; Dechesne, A. C.; Van Esse, G. W.; Brouwer, A. J.; Corstens, F. H. M.; Boerman, O. C.; Rijkers, D. T. S.; Liskamp, R. M. J. *Org. Biomol. Chem.* **2007,** *5*, 935-944.

88. Martin, M. E.; Parameswarappa, S. G.; O'Dorisio, M. S.; Pigge, F. C.; Schultz, M. K. *Bioorg. Med. Chem. Lett. 20*, 4805-4807.

89. Tanaka, K.; Masuyama, T.; Hasegawa, K.; Tahara, T.; Mizuma, H.; Wada, Y.; Watanabe, Y.; Fukase, K. *Angew. Chem., Int. Ed.* **2008,** *47*, 102-105.

90. van den Heuvel, M.; van den Berg, T. A.; Kellogg, R. M.; Choma, C. T.; Feringa, B. L. *J. Org. Chem.* **2004,** *69*, 250-262.

91. Fujimura, F.; Kimura, S. *Org. Lett.* **2007,** *9*, 793-796.

92. Kersebohm, T.; Kirin, S. I.; Metzler-Nolte, N. *Bioorg. Med. Chem. Lett.* **2006,** *16*, 2964-2968.

93. Bernini, R.; Barontini, M.; Crisante, F.; Ginnasi, M. C.; Saladino, R. *Tetrahedron Lett.* **2009,** *50*, 6519-6521.

94. Jayasinghe, D.; Kraatz, H.-B. *Inorg. Chim. Acta* **2006,** *359*, 3054-3065.

95. Agarkov, A.; Greenfield, S.; Xie, D.; Pawlick, R.; Starkey, G.; Gilbertson Scott, R. *Biopolymers* **2006,** *84*, 48-73.

96. Mattila, K.; Siltainsuu, J.; Balaspiri, L.; Ora, M.; Loennberg, H. *Org. Biomol. Chem.* **2005,** *3*, 3039-3044.

97. Mindt, T. L.; Schweinsberg, C.; Brans, L.; Hagenbach, A.; Abram, U.; Tourwe, D.; Garcia-Garayoa, E.; Schibli, R. *ChemMedChem* **2009,** *4*, 529-539.

98. Jabre, N. D.; Respondek, T.; Ulku, S. A.; Korostelova, N.; Kodanko, J. J. *J. Org. Chem.* **2010,** *75*, 650-659.

99. Jabre, N. D.; Korostelova, N.; Kodanko, J. J. *J. Org. Chem.* **2011,** *76*, 2273-2276.

100. Schally, A. V.; Nagy, A. *Eur. J. Endocrinol.* **1999,** *141*, 1-14.

101. Kwekkeboom Dik, J.; Krenning Eric, P. *Semin Nucl Med* **2002,** *32*, 84-91.

102. Gugger, M.; Reubi, J. C. *Am. J. Pathol.* **1999,** *155*, 2067-2076.

103. Hoffman, T. J.; Quinn, T. P.; Volkert, W. A. *Nucl. Med. Biol.* **2001,** *28*, 527-539.

104. Barda, Y.; Cohen, N.; Lev, V.; Ben-Aroya, N.; Koch, Y.; Mishani, E.; Fridkin, M.; Gilon, C. *Nucl. Med. Biol.* **2004,** *31*, 921-933.

105. Suh, J.; Chei, W. S. *Curr. Opin. Chem. Biol.* **2008,** *12*, 207-213.

106. Haas, K. L.; Franz, K. J. *Chem. Rev.* **2009,** *109*, 4921-4960.

107. Brunner, J.; Barton, J. K. *Biochemistry* **2006,** *45*, 12295-12302.

108. Jackson, B. A.; Alekseyev, V. Y.; Barton, J. K. *Biochemistry* **1999,** *38*, 4655-4662.

109. Zelder, F. H.; Mokhir, A. A.; Kraemer, R. *Inorg. Chem.* **2003,** *42*, 8618-8620.

110. Long, E. C. *Acc. Chem. Res.* **1999,** *32*, 827-836.

111. Mack, D. P.; Dervan, P. B. *J. Am. Chem. Soc.* **1990,** *112*, 4604-4606.

112. Harford, C.; Sarkar, B. *Acc. Chem. Res.* **1997,** *30*, 123-130.

113. Jin, Y.; Cowan, J. A. *J. Am. Chem. Soc.* **2005,** *127*, 8408-8415.

114. Jeon, J. W.; Son, S. J.; Yoo, C. E.; Hong, I. S.; Song, J. B.; Suh, J. *Org. Lett.* **2002,** *4*, 4155-4158.

115. Jeon, J. W.; Son, S. J.; Yoo, C. E.; Hong, I. S.; Suh, J. *Bioorg. Med. Chem.* **2003,** *11*, 2901-2910.

116. Hoyer, D.; Cho, H.; Schultz, P. G. *J. Am. Chem. Soc.* **1990,** *112*, 3249-3250.

117. Gallagher, J.; Zelenko, O.; Walts, A. D.; Sigman, D. S. *Biochemistry* **1998,** *37*, 2096-2104.

118. Schepartz, A.; Cuenoud, B. *J. Am. Chem. Soc.* **1990,** *112*, 3247-3249.

119. Gokhale, N. H.; Cowan, J. A. *JBIC, J. Biol. Inorg. Chem.* **2006,** *11*, 937-947.

120. Lee, J.; Udugamasooriya, D. G.; Lim, H.-S.; Kodadek, T. *Nat. Chem. Biol.* **2010,** *6*, 258-260.

121. Jabre, N. D.; Hryhorczuk, L.; Kodanko, J. J. *Inorg. Chem.* **2009,** *48*, 8078-8080.

122. Kim, M.-s.; Jeon, J. W.; Suh, J. *JBIC, J. Biol. Inorg. Chem.* **2005,** *10*, 364-372.

123. Takeuchi, T.; Boettcher, A.; Quezada, C. M.; Simon, M. I.; Meade, T. J.; Gray, H. B. *J. Am. Chem. Soc.* **1998,** *120*, 8555-8556.

124. Corry, A. J.; Mooney, A.; O'Sullivan, D.; Kenny, P. T. M. *Inorg. Chim. Acta* **2009,** *362*, 2957-2961.

125. Corry, A. J.; O'Donovan, N.; Mooney, A.; O'Sullivan, D.; Rai, D. K.; Kenny, P. T. M. *J. Organomet. Chem.* **2009,** *694*, 880-885.

126. Mooney, A.; Corry, A. J.; O'Sullivan, D.; Rai, D. K.; Kenny, P. T. M. *J. Organomet. Chem.* **2009,** *694*, 886-894.

127. Neundorf, I.; Hoyer, J.; Splith, K.; Rennert, R.; Peindy N'Dongo, H. W.; Schatzschneider, U. *Chem. Commun.* **2008**, 5604-5606.

128. Bajusz, S.; Janaky, T.; Csernus, V. J.; Bokser, L.; Fekete, M.; Srkalovic, G.; Redding, T. W.; Schally, A. V. *Proc. Natl. Acad. Sci. U. S. A.* **1989,** *86*, 6313-6317.

129. Niesel, J.; Pinto, A.; Peindy N'Dongo, H. W.; Merz, K.; Ott, I.; Gust, R.; Schatzschneider, U. *Chem. Commun.* **2008**, 1798-1800.

130. Palffy, R.; Gardlik, R.; Behuliak, M.; Kadasi, L.; Turna, J.; Celec, P. *Mol. Med.* **2009,** *15*, 51-59.

131. Chantson, J. T.; Falzacappa, M. V. V.; Crovella, S.; Metzler-Nolte, N. *J. Organomet. Chem.* **2005,** *690*, 4564-4572.

132. Chantson, J. T.; Falzacappa, M. V. V.; Crovella, S.; Metzler-Nolte, N. *ChemMedChem* **2006,** *1*, 1268-1274.

133. Noor, F.; Wuestholz, A.; Kinscherf, R.; Metzler-Nolte, N. *Angew. Chem., Int. Ed.* **2005,** *44*, 2429-2432.

134. Meldal, M.; Tornoe Christian, W.; Nielsen Thomas, E.; Diness, F.; Le Quement Sebastian, T.; Christensen Christian, A.; Jensen Jakob, F.; Worm-Leonhard, K.; Groth, T.; Bouakaz, L.; Wu, B.; Hagel, G.; Keinicke, L. *Biopolymers* **2010,** *94*, 161-182.

135. Meldal, M. *Tetrahedron Lett.* **1992,** *33*, 3077-3080.

136. Channon, K. J.; Devlin, G. L.; MacPhee, C. E. *J. Am. Chem. Soc.* **2009,** *131*, 12520-12521.

137. Groves, J. T. *J. Inorg. Biochem.* **2006,** *100*, 434-447.

138. Grapperhaus, C. A.; Mienert, B.; Bill, E.; Weyhermueller, T.; Wieghardt, K. *Inorg. Chem.* **2000,** *39*, 5306-5317.

139. Abouelatta, A. I. *Ph.D. Thesis* **2011**.

140. Campanali, A. A. *Ph.D. Thesis* **2011**.

141. Rohde, J.-U.; In, J.-H.; Lim, M. H.; Brennessel, W. W.; Bukowski, M. R.; Stubna, A.; Muenck, E.; Nam, W.; Que, L., Jr. *Science* **2003,** *299*, 1037-1039.

142. Klinker, E. J.; Kaizer, J.; Brennessel, W. W.; Woodrum, N. L.; Cramer, C. J.; Que, L., Jr. *Angew. Chem., Int. Ed.* **2005,** *44*, 3690-3694.

143. Lim, M. H.; Rohde, J.-U.; Stubna, A.; Bukowski, M. R.; Costas, M.; Ho, R. Y. N.; Munck, E.; Nam, W.; Que, L., Jr. *Proc. Natl. Acad. Sci. U. S. A.* **2003,** *100*, 3665-3670.

144. Bukowski, M. R.; Koehntop, K. D.; Stubna, A.; Bominaar, E. L.; Halfen, J. A.; Muenck, E.; Nam, W.; Que, L., Jr. *Science* **2005,** *310*, 1000-1002.

145. Sastri, C. V.; Seo, M. S.; Park, M. J.; Kim, K. M.; Nam, W. *Chem. Commun.* **2005**, 1405-1407.

146. Nehru, K.; Seo, M. S.; Kim, J.; Nam, W. *Inorg. Chem.* **2007,** *46*, 293-298.

147. Bukowski, M. R.; Comba, P.; Lienke, A.; Limberg, C.; Lopez de Laorden, C.; Mas-Balleste, R.; Merz, M.; Que, L., Jr. *Angew. Chem., Int. Ed.* **2006,** *45*, 3446-3449.

148. Pestovsky, O.; Stoian, S.; Bominaar, E. L.; Shan, X.; Munck, E.; Que, L., Jr.; Bakac, A. *Angew. Chem., Int. Ed.* **2005,** *44*, 6871-6874.

149. Balland, V.; Charlot, M.-F.; Banse, F.; Girerd, J.-J.; Mattioli, T. A.; Bill, E.; Bartoli, J.-F.; Battioni, P.; Mansuy, D. *Eur. J. Inorg. Chem.* **2004**, 301-308.

150. Kaizer, J.; Costas, M.; Que, L., Jr. *Angew. Chem., Int. Ed.* **2003,** *42*, 3671-3673.

151. Kim, S. O.; Sastri, C. V.; Seo, M. S.; Kim, J.; Nam, W. *J. Am. Chem. Soc.* **2005,** *127*, 4178-4179.

152. Li, F.; England, J.; Que, L., Jr. *J Am Chem Soc* **2010,** *132*, 2134-2135.

153. Kaizer, J.; Klinker, E. J.; Oh, N. Y.; Rohde, J.-U.; Song, W. J.; Stubna, A.; Kim, J.; Muenck, E.; Nam, W.; Que, L., Jr. *J. Am. Chem. Soc.* **2004,** *126*, 472-473.

154. Sastri, C. V.; Park, M. J.; Ohta, T.; Jackson, T. A.; Stubna, A.; Seo, M. S.; Lee, J.; Kim, J.; Kitagawa, T.; Muenck, E.; Que, L., Jr.; Nam, W. *J. Am. Chem. Soc.* **2005,** *127*, 12494-12495.

155. de Visser, S. P.; Oh, K.; Han, A.-R.; Nam, W. *Inorg. Chem.* **2007,** *46*, 4632-4641.

156. Oh, N. Y.; Suh, Y.; Park, M. J.; Seo, M. S.; Kim, J.; Nam, W. *Angew. Chem., Int. Ed.* **2005,** *44*, 4235-4239.

157. Sastri, C. V.; Oh, K.; Lee, Y. J.; Seo, M. S.; Shin, W.; Nam, W. *Angew. Chem., Int. Ed.* **2006,** *45*, 3992-3995.

158. Park, M. J.; Lee, J.; Suh, Y.; Kim, J.; Nam, W. *J. Am. Chem. Soc.* **2006,** *128*, 2630-2634.

159. Ekkati, A. R.; Kodanko, J. J. *J. Am. Chem. Soc.* **2007,** *129*, 12390-12391.

160. Abouelatta, A. I.; Campanali, A. A.; Ekkati, A. R.; Shamoun, M.; Kalapugama, S.; Kodanko, J. J. *Inorg. Chem.* **2009,** *48*, 7729-7739.

161. Campanali, A. A.; Kwiecien, T. D.; Hryhorczuk, L.; Kodanko, J. J. *Inorg. Chem.* **2010,** *49*, 4759-4761.

162. Stadtman, E. R. *Annu. Rev. Biochem.* **1993,** *62*, 797-821.

163. Berlett, B. S.; Stadtman, E. R. *J. Biol. Chem.* **1997,** *272*, 20313-20316.

164. Jensen, M. P.; Mehn, M. P.; Que, L., Jr. *Angew. Chem., Int. Ed.* **2003,** *42*, 4357-4360.

165. Oh, N. Y.; Seo, M. S.; Lim, M. H.; Consugar, M. B.; Park, M. J.; Rohde, J.-U.; Han, J.; Kim, K. M.; Kim, J.; Que, L., Jr.; Nam, W. *Chem. Commun.* **2005**, 5644-5646.

166. Guajardo, R. J.; Chavez, F.; Farinas, E. T.; Mascharak, P. K. *J. Am. Chem. Soc.* **1995,** *117*, 3883-3884.

167. Guajardo, R. J.; Hudson, S. E.; Brown, S. J.; Mascharak, P. K. *J. Am. Chem. Soc.* **1993,** *115*, 7971-7977.

168. Roelfes, G.; Branum, M. E.; Wang, L.; Que, L., Jr.; Feringa, B. L. *J. Am. Chem. Soc.* **2000,** *122*, 11517-11518.

169. Mialane, P.; Nivorojkine, A.; Pratviel, G.; Azema, L.; Slany, M.; Godde, F.; Simaan, A.; Banse, F.; Kargar-Grisel, T.; Bouchoux, G.; Sainton, J.; Horner, O.; Guilhem, J.; Tchertanova, L.; Meunier, B.; Girerd, J.-J. *Inorg. Chem.* **1999,** *38*, 1085-1092.

170. Walker, M. A.; Kaplita, K. P.; Chen, T.; King, D. H. *Synlett* **1997**, 169-170.

171. O'Donnell, M. J.; Polt, R. L. *J. Org. Chem.* **1982,** *47*, 2663-2666.

172. Guthikonda, R. N.; Cama, L. D.; Quesada, M.; Woods, M. F.; Salzmann, T. N.; Christensen, B. G. *J. Med. Chem.* **1987,** *30*, 871-880.

173. Chong, H.-S.; Torti, S. V.; Ma, R.; Torti, F. M.; Brechbiel, M. W. *J. Med. Chem.* **2004,** *47*, 5230-5234.

174. Clark, D. A.; Hulin, B.; Goldstein, S. W.; (Pfizer Inc., USA). Application: EP EP, 1989, p 27 pp.

175. Purchased from commercial suppliers.

176. Corey, E. J.; Xu, F.; Noe, M. C. *J. Am. Chem. Soc.* **1997,** *119*, 12414-12415.

177. Micklitsch, C. M.; Yu, Q.; Schneider, J. P. *Tetrahedron Lett.* **2006,** *47*, 6277-6280.

178. Loegers, M.; Overman, L. E.; Welmaker, G. S. *J. Am. Chem. Soc.* **1995,** *117*, 9139-9150.

179. Meng, D.; Bertinato, P.; Balog, A.; Su, D.-S.; Kamenecka, T.; Sorensen, E.; Danishefsky, S. J. *J. Am. Chem. Soc.* **1997,** *119*, 10073-10092.

180. Kodanko, J. J.; Morys, A. J.; Lippard, S. J. *Org. Lett.* **2005,** *7*, 4585-4588.

181. Miller, H. K.; Waelsch, H. *J. Am. Chem. Soc.* **1952,** *74*, 1092-1093.

182. Niklas, N.; Walter, O.; Alsfasser, R. *Eur. J. Inorg. Chem.* **2000**, 1723-1731.

183. Baffert, C.; Collomb, M.-N.; Deronzier, A.; Kjaergaard-Knudsen, S.; Latour, J.-M.; Lund, K. H.; McKenzie, C. J.; Mortensen, M.; Nielsen, L. P.; Thorup, N. *Dalton Transactions* **2003**, 1765-1772.

184. After HPLC purification, desired fractions were combined and the pH of the mixture was adjusted between 8-9 using sat. Na_2CO_3. Aqueous layer was extracted with CH_2Cl_2 (3 × 10 mL). The combined organic layer was dried over anhydrous Na_2SO_4 and concentrated to obtain the product.

185. Houghten, R. A.; Pinilla, C.; Blondelle, S. E.; Appel, J. R.; Dooley, C. T.; Cuervo, J. H. *Nature* **1991,** *354*, 84-86.

186. Dharap, S. S.; Wang, Y.; Chandna, P.; Khandare, J. J.; Qiu, B.; Gunaseelan, S.; Sinko, P. J.; Stein, S.; Farmanfarmaian, A.; Minko, T. *Proc. Natl. Acad. Sci. U. S. A.* **2005,** *102*, 12962-12967.

187. Engel, J. B.; Schally, A. V.; Dietl, J.; Rieger, L.; Hoenig, A. *Molecular Pharmaceutics* **2007,** *4*, 652-658.

188. Werle, M.; Bernkop-Schnuerch, A. *Amino Acids* **2006,** *30*, 351-367.

189. Schally, A. V.; Nagy, A. *Trends in Endocrinology and Metabolism* **2004,** *15*, 300-310.

190. Bukowski, M. R.; Zhu, S.; Koehntop, K. D.; Brennessel, W. W.; Que, L. *J. Biol. Inorg. Chem.* **2004,** *9*, 39-48.

191. Incarvito, C.; Lam, M.; Rhatigan, B.; Rheingold, A. L.; Qin, C. J.; Gavrilova, A. L.; Bosnich, B. *J. Chem. Soc., Dalton Trans.* **2001**, 3478-3488.

192. Abushanab, E.; Bindra, A. P.; Goodman, L.; Peterson, H., Jr. *J. Org. Chem.* **1973,** *38*, 2049-2052.

193. Costas, M.; Mehn, M. P.; Jensen, M. P.; Que, L. *Chemical Reviews* **2004,** *104*, 939.

194. Gebicki, J. M.; Nauser, T.; Domazou, A.; Steinmann, D.; Bounds, P. L.; Koppenol, W. H. *Amino Acids* **2010,** *39*, 1131-1137.

195. Lardinois, O. M.; Ortiz De Montellano, P. R. *J. Biol. Chem.* **2003,** *278*, 36214-36226.

196. Wilks, A.; Ortiz de Montellano, P. R. *J. Biol. Chem.* **1992,** *267*, 8827-8833.

197. Lardinois, O. M.; Ortiz de Montellano, P. R. *Biochemistry* **2004,** *43*, 4601-4610.

198. Guengerich, F. P. *J. Biol. Chem.* **1987,** *262*, 8459.

199. Blake, R. C.; Coon, M. J. *J. Biol. Chem.* **1981,** *256*, 12127.

200. Zhang, W.; Sun, H.-L.; Sato, O. *Dalton Trans.* **2011,** *40*, 2735-2743.

201. Dai, Z.; Canary, J. W. *New J. Chem.* **2007,** *31*, 1708-1718.

202. Failes, T. W.; Cullinane, C.; Diakos, C. I.; Yamamoto, N.; Lyons, J. G.; Hambley, T. W. *Chem.--Eur. J.* **2007,** *13*, 2974-2982.

203. Eroy-Reveles, A. A.; Leung, Y.; Beavers, C. M.; Olmstead, M. M.; Mascharak, P. K. *J. Am. Chem. Soc.* **2008,** *130*, 4447-4458.

204. Gonzalez, M. A.; Fry, N. L.; Burt, R.; Davda, R.; Hobbs, A.; Mascharak, P. K. *Inorg. Chem.* **2011,** *50*, 3127-3134.

205. Schatzschneider, U. *Eur. J. Inorg. Chem.* **2010**, 1451-1467.

206. Louie, A. Y.; Meade, T. J. *Chem. Rev.* **1999,** *99*, 2711-2734.

207. Jabre, N. D., Unpublished Results.

208. Kryatov, S. V.; Rybak-Akimova, E. V.; Schindler, S. *Chem. Rev.* **2005,** *105*, 2175-2226.

209. Korendovych, I. V.; Kryatov, S. V.; Rybak-Akimova, E. V. *Acc. Chem. Res.* **2007,** *40*, 510-521.

ABSTRACT

SYNTHESIS OF PEPTIDE-LIGAND CONJUGATES AND THEIR APPLICATIONS

by

NITINKUMAR DILIPKUMAR JABRE

August 2011

Advisor: Jeremy J. Kodanko, Ph.D.

Major: Chemistry

Degree: Doctor of Philosophy

Three research areas pertaining to this dissertation, (i) synthesis strategies of peptide-ligand conjugates, (ii) their applications and (iii) chemistry of ferryls were surveyed in the introduction chapter. Next, the divergent and dual divergent strategies for the synthesis of non-heme ligand-peptide conjugates were developed. Using these strategies various peptide-ligand conjugates were synthesized via solution as well as solid phase synthesis. The scope and the functional group compatibility of these strategies were also established. The utility of the dual divergent strategy has been demonstrated by synthesizing a small library of metal-binding LHRH analogues. This work showcased the ability of the dual divergent strategy to rapidly construct the diverse array of ligand structures. In another application, the synthesis and characterization of the first ferryl-peptide conjugate was presented. In this work the reactivity and the mechanistic study for this ferryl-peptide conjugate were also described. From the mechanistic studies it has been proven that the remote benzyl group controls the stability of ferryl-peptide conjugate via an intramolecular hydrogen atom transfer mechanism.

AUTOBIOGRAPHICAL STATEMENT

NITINKUMAR DILIPKUMAR JABRE

Education

2006-2011	Ph.D. in Chemistry (Major: Organic Chemistry) Wayne State University, Detroit, Michigan Advisor: Professor Jeremy J. Kodanko
2000-2002	M.Sc. in Chemistry (Major: Organic Chemistry) Maharaja Sayajirao University of Baroda, Vadodara, Gujarat, India Advisor: Professor K. B. Nair
1997-2000	B.Sc. in Chemistry Maharaja Sayajirao University of Baroda, Vadodara, Gujarat, India

Awards and Honors

- Heller fellowship for the academic year of 2010-11
- Norman A. LeBel endowed graduate award in organic chemistry (2008)
- Member of the Phi Lambda Upsilon (2007-present)
- Member of the American Chemical Society (2008-present)

Presentations

1. Incorporating tetra- and pentadentate metal-binding units into a peptide chain. **Jabre, N. D.**, Kodanko, J. J. 236th ACS national meeting at Philadelphia, Fall 2008. (Poster presentation)
2. Non-heme oxoferryl-peptide conjugates: Characterization of an intra-molecular oxidation reaction. **Jabre, N. D.**, Kodanko, J. J. 238th ACS national meeting at Washington, DC, Fall 2009. (Oral presentation)
3. Non-heme oxoferryl-peptide conjugates: Characterization of an intra-molecular oxidation reaction. **Jabre, N. D.**, Kodanko, J. J. 11th Annual graduate symposium, Wayne State University, Oct 2009. (Oral presentation)

Publications (in chronological order)

1. 2-(trichloromethyl)-1,3-bis(2,4,6-trimethylphenyl) imidazolidine. **Jabre, N. D.**, Kodanko J. J. Electronic Encyclopedia of Reagents for Organic Synthesis, 2nd Ed.
2**.** Stability of a Ferryl-Peptide Conjugate is Controlled by a Remote Substituent. **Jabre, N. D.**, Hryhorczuk, L. Kodanko, J.J. *Inorg. Chem*, **2009**, *48*, 8078-8080.
3. A Divergent Strategy for Attaching Polypyridyl Ligands to Peptides. **Jabre, N. D.**, Respondek, T., Ulku, S., Korostelova, N., Kodanko, J.J. *J. Org. Chem.* **2010**, *75*, 650-659.
4. A Highly Divergent Approach For Synthesis of Metal-Binding Peptide Libraries. **Jabre, N. D.**, Korostelova, N., Kodanko, J.J. *J. Org. Chem.* **2011**, *76*, 2273-2276.